

**Palaeoclimate and
Ice-Sheet Dynamics
in the Southern Ocean**

Inaugural-Dissertation

zur

Erlangung des Doktorgrades

der Mathematisch-Naturwissenschaftlichen Fakultät

der Universität zu Köln

vorgelegt von

Daniela Sprenk

aus Bergisch Gladbach

Köln, 2013

Berichterstatter: PD Dr. Michael E. Weber
(Gutachter)

Prof. Dr. Martin Melles

Dr. Gerhard Kuhn (AWI Bremerhaven)

Tag der mündlichen Prüfung: 18.10.2013

Abstract

For a better understanding of future climate it is inevitably to study earth history and past climate changes. The objective of this thesis was to analyse seasonal-to-millennial-scale fluctuations during the last glacial and deglacial period. Therefore, core sites located in the Atlantic Sector of the Southern Ocean providing high sedimentation rates, of up to a few metres per thousand years were investigated.

Varved sediments originating from channel-ridge systems in the southeastern Weddell Sea were analysed, including thin section and X-radiographs production, X-ray fluorescence-scanning, RADIUS particle analyses, and of course varve counting. The investigations reveal highly dynamic sedimentation in the channel-ridge systems, reflecting seasonal changes of the thermohaline current during the LGM possibly related to changes in katabatic winds and hence coastal polynya activity. Spectral analysis detected decadal-to-centennial-scale oscillations in varve thicknesses strongly correlating with the periods of solar cycles, therefore suggesting that solar cycles modulated sedimentation in the core site area during the LGM. Sedimentation in the southeastern Weddell Sea possibly also indicates multiple fluctuations of East Antarctic Ice Sheet during the LGM.

The magnetic susceptibility record of Scotia Sea cores show a one-to-one coupling with the non-sea-salt Ca^{2+} flux of East Antarctic EDML ice core, a confident atmospheric dust proxy. This clearly identifies atmospheric circulation as supplier of the magnetic susceptibility signal in the Scotia Sea, and enables the establishment of a high-resolution age model. Patagonia can be identified as major dust source during the LGM.

Biogenic opal was determined by leaching, as well as estimated using colour b^* , wet-bulk density, Si/Ti count ratios, and Fourier transform infrared spectroscopy (FTIRS). All methods can be used to detect general biogenic opal trends, thus FTIRS provides the most reliable estimation. The biogenic opal flux curve of MD07-3134 is one of the first continuous palaeoproductivity records over the last 92.5 ka for the Southern Ocean. It exhibits a relatively complicated glacial-to-interglacial pattern with large-amplitude, millennial-scale fluctuations in bioproductivity.

Kurzfassung

Um zukünftige Klimaschwankungen besser zu verstehen, ist es unabdingbar erdgeschichtliche Klimaschwankungen zu untersuchen. Das Hauptziel dieser Arbeit war die Untersuchung von dekadischen bis tausendjährigen Klimaschwankungen während der letzten Glazialen und deglazialen Periode. Deswegen wurden Kernlokalationen im Atlantischen Sektor des Südozeans mit hohen Sedimentationsraten von bis zu einigen Metern pro tausend Jahren untersucht.

Warvierte Sedimente aus Rinnen-Rücken-Systemen der südöstlichen Weddellmeeres wurden untersucht. Dafür wurden Dünnschliffe und Radiographien angefertigt, Röntgen-Fluoreszenz-Analysen und RADIUS Partikel Analysen, sowie Warven-Zählungen vorgenommen. Die Untersuchungen lassen auf hoch-dynamische Sedimentation in den Rinnen-Rücken-Systemen schließen, welche saisonale Schwankungen einer thermohalinen Strömung im Letzten Glazialen Maximum widerspiegeln. Diese stehen vermutlich in Verbindung mit Schwankungen von katabatischen Winden und damit verbundenen Küstenpolynya Aktivitäten. Spektralanalysen zeigen dekadische bis jahrhundert-jährige Oszillationen der Warven-Mächtigkeit, welche starke Ähnlichkeiten mit den Perioden von Sonnen-Zyklen zeigen, folglich wurde die Sedimentation im Arbeitsgebiet während des letzten Glazialen Maximums von zyklischen Schwankungen der Sonneneinstrahlung beeinflusst. Die Sedimentation im südöstlichen Weddellmeer deutet multiple Schwankungen des Ostantarktischen Eisschildes während des letzten Glazialen Maximums an.

Untersuchungen der magnetischen Suszeptibilität von Sedimentkernen aus dem Scotiameer zeigen eine eins-zu-eins Übereinstimmung mit nssCa^{2+} -Fluss Daten des Ostantarktischen EDML Eiskernes, welcher als sicheres Proxy für atmosphärischen Staub gilt. Diese Übereinstimmung ist also ein Indikator für atmosphärische Zirkulation als Transportmedium der magnetische Suszeptibilität, welches das Erstellen eines hoch-auflösenden Altersmodells ermöglicht. Patagonia kann als Hauptquelle von atmosphärischem Staub identifiziert werden.

Biogener Opal wurde mit Hilfe der Lösungsmethode bestimmt sowie abgeleitet von Farbkomponente b^* , Feuchtraumdichte, Si/Ti count ratios und Fourier-Transform-Infrarotspektroskopie (FTIRS). Alle Methoden spiegeln die generellen Trends der biogenen Opal Kurve wider, jedoch zeichnet sich FTIRS als zuverlässigste Ableitungsmethode aus. Die biogene Opalfloss Kurve von MD07-3134 ist einer der ersten kontinuierlichen Paläoproduktivitätsrecords des Südozeans für die letzten 92.500 Jahre. Sie zeigt eine relativ kompliziertes glazial-interglazial mit ausgeprägten jahrtausend-jährigen Schwankungen in der Bioproduktivität.

Acknowledgements

First of all, I need to thank the Deutsche Forschungsgemeinschaft (DFG; grants KU 683/9-1, WE 2039/8-1) for financially supporting my thesis, without whom this work would not have been realised. Their support also provided me the opportunity to attend some national and international conferences as well as enabled visits to the University of Umeå in Sweden, Alfred Wegener Institute Helmholtz Centre for Polar and Marine Research in Bremerhaven, and University of Bremen for scientific work.

Very special thanks to my supervisor PD Dr. M. E. Weber for giving me the opportunity to work in his research group as well as for the great support, motivation, and guidance during the last three years. I was always welcome, when I needed advice and our fruitful discussions highly improved my work.

Also I want to express my gratitude to Gerhard Kuhn from the Alfred Wegener Institute Helmholtz Centre for Polar and Marine Research in Bremerhaven for his advises and his paper contributions. Especially, I need to thank him for giving me the unique chance to go to Antarctica and visit my PhD study area, the Weddell Sea.

Additionally, I would like to thank Prof. Dr. M. Melles for being the second referee of my PhD thesis and Prof. Dr. F. Schäbitz for taking the chair of the examination committee as well as Dr. V. Wennrich for acting as assessor at my defence.

Many thanks to British Antarctic Survey for giving me the opportunity to take part in the scientific cruise JR244, thus learning much about scientific drilling and my study area. I also want to thank all JR244 participants for eight amazing weeks.

The European Science Foundation, ECORD, and PAGES are greatly acknowledged for awarding me scholarships. Without their financial support I could not have attended the Urbino summer school, the GESEP School, and the PAGES Young and Open Science Meeting in Goa.

I also want to thank my co-authors M. Frank, V. Liebetrau, M. Molina-Kescher, M. Prange, P. Rosén, M. Schulz, V. Varma, and V. Wennrich for their great collaborations and paper contributions.

Furthermore, Andreas Holzapfel is thanked for helping me with the final formatting of my thesis and of course for the great atmosphere in our tiny working group.

Special thanks go to all my colleagues at the Institute of Geology at the University of Cologne, who made my time here such a great experience on both professional and personal level. A few colleagues deserve a special thank: Armin Abitz, Raphael Conz, Till Hartmann, Johannes Jakob, Jens Karls, René Wiegand, and of course I want to thank Alexander Francke. It was always great to start a new working day with fresh coffee and egg rolls!!

Finally, I would like to thank my family, especially my parents Dagmar und Dieter Sprenk for their support and encouraging me in everything I do. I also want to express my heartfelt gratitude to Craig Brown. Even though you weren't physically here the last year, you always supported me in so many countless ways. Thank you for your patience, encouragement, and just being there for me whenever I need you.

Contents

Abstract	III
Kurzfassung	IV
Acknowledgements	V
Contents	VII
1 Introduction.....	1
1.1 General introduction.....	1
1.2 The last glacial period.....	2
1.3 Study areas	4
2 Objectives.....	6
2.1 Seasonal- to millennial-scale oscillations	6
2.2 Dust transport and palaeoproductivity.....	7
3 Seasonal changes in glacial polynya activity inferred from Weddell Sea varves	9
4 Decadal- and millennial-scale oscillations in the Weddell Sea during the LGM	35
5 Dust transport from Patagonia to Antarctica.....	60
6 Southern Ocean bioproductivity during the last glacial cycle.....	73
7 Discussion.....	100
7.1 Seasonal- to millennial-scale oscillations	100
7.2 Dust transport and palaeoproductivity.....	104
8 Conclusions and Summary	110
9 References.....	113
10 Paper contributions	121
11 Erklärung	123
12 Curriculum Vitae	124

1 Introduction

1.1 General introduction

Recently, it is becoming increasingly apparent that regional and global climate varies significantly on short, already annual- to decadal time scales. This is of great societal importance with substantial impact on global population (IPCC, 2007). Nonetheless, climate fluctuations can still not be predicted precisely, not even for the next century. For a better understanding of future climate it is inevitably to study earth history and past climate changes. Instrumental climate records exist only for a few hundred years. Therefore, it is important to study past climate changes using geological archives such as tree-rings, corals, ice cores, and sediments. Especially marine deep-sea sediments yield undisturbed records, providing valuable information about regional as well as global climate in the past. Therefore, during the last decades the deep-sea sediments have been the focus of many scientific explorations, e.g. organised by the Alfred Wegener Institute for Polar and Marine Research on a national level, or internationally by the Integrated Ocean Drilling Program (IODP).

During the Cenozoic era, the last 65 Million years (Myrs), major changes in global climate from an ice-free "greenhouse world" to an "ice-house world" took place (Zachos et al., 2008). The opening of the Drake Passage and therefore the separation between southern South America and the Antarctic Peninsula (Lagabrielle et al., 2009), led to an isolation of the Antarctic continent and enabled the formation of the Antarctic Circumpolar Current (ACC) (e.g. Barker, 2001; Barker and Burrell, 1977).

The opening of the Drake and Tasmanian passages, together with North Atlantic rift volcanism, the collision of India with the Eurasian plate and consequential Himalaya uplift, as well as closing of the circum-equatorial Panama gateway and declining atmospheric CO₂ possibly strongly influenced Cenozoic climate and led to global cooling (e.g. Livermore et al., 2005; Zachos et al., 2001). Around 35 Ma large ice sheets started to develop on East Antarctica (Zachos et al., 2001) and were more stable after around 14 Ma. The onset of the Northern hemisphere glaciation started between 3.6 and 2.7 Ma (e.g. Bartoli et al., 2011; Mudelsee and Raymo, 2005) and strongly intensified after 2.7 Ma (Haug et al., 2005).

Many studies, e.g. benthic $\delta^{18}\text{O}$ records (Lisiecki and Raymo, 2005) highlighted that ice volume varies quasi-periodically, related to changes in orbital forcing (Milankovitch, 1941). During the Middle-Pleistocene transition (MPT) from about 1.25 to 0.7 Ma (Clark et al., 2006), which timing and initiation is still discussed though (e.g. Raymo and Nisancioglu, 2003), climate changed fundamentally, shifting from a 40-kyr-obliquity cycle dominated world to a 100 kyr-world. The last 800 kyrs are strongly dominated by 100-kyr cyclic variations in ice volume (Imbrie et al., 1992) (Fig. 1). Sea-level changes during the Quaternary are primarily related to ice sheet fluctuations (Lambeck and Chappell, 2001).

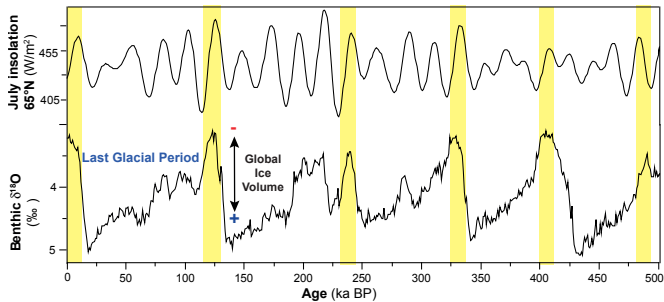


Figure 1: Climate changes dominated by 100-kyr Eccentricity solar cycle: Incoming solar radiation (Insolation) for 65°N (Berger and Loutre, 1991) and benthic $\delta^{18}\text{O}$ LR04 record (Lisiecki and Raymo, 2005) as a proxy for global ice volume. Yellow bars roughly highlight the relatively short Interglacial periods.

1.2 The last glacial period

The last glacial period was the most recent glaciation (Fig. 1) and occurred from around 110 to 14 thousand years before present (ka BP). Climate was very variable during the last glacial as well as the deglacial period with millennial-scale fluctuations in global temperature and sea level in global climate (Barker et al., 2009; Shackleton et al., 2000). Records from Greenland ice cores, e.g. NGRIP (NGRIP Members, 2004) and other archives, e.g. sediments from the North Atlantic (Bard et al., 2000; Bond et al., 1997) revealed rapid abrupt rises in temperatures within a few decades only, namely the Dansgaard-Oeschger (D/O) Events (Dansgaard et al., 1993; Oeschger et al., 1984). After the rapid temperature rise of about 8 to 15 °C (Huber et al., 2006; Siddall et al., 2010), temperatures reduced slowly, within a few hundred to thousand years, back to cold stadial conditions (Fig. 2).

Antarctic temperature changes during the last glacial period have been detected in Antarctic ice cores, e.g. EDML (EPICA Community Members, 2006), i.e. the Antarctic Isotopic Maxima (AIM). In contrast to the Greenland and North Atlantic D/O events, Antarctic temperature changes are smaller, i.e. only about 1 to 3 °C (EPICA Community Members, 2004, 2006) and more gradual (Fig. 2). Different ice core studies showed, that the events are related, although the Antarctic temperature rises were leading D/O events in Greenland (Blunier and Brook, 2001; Blunier et al., 1998), which is also visible in Figure 2. The anti-phase warming, also called "bipolar see-saw" (Broecker, 1998), seems to be related to variations in the strength of the Atlantic Meridional Overturning Circulation (AMOC) (Barker et al., 2009; Blunier and Brook, 2001) affecting the distribution of heat between North and South Atlantic. Additionally, Knutti et al. (2004) showed,

that freshwater flux into the North Atlantic has also a direct influence on Southern Ocean temperature.

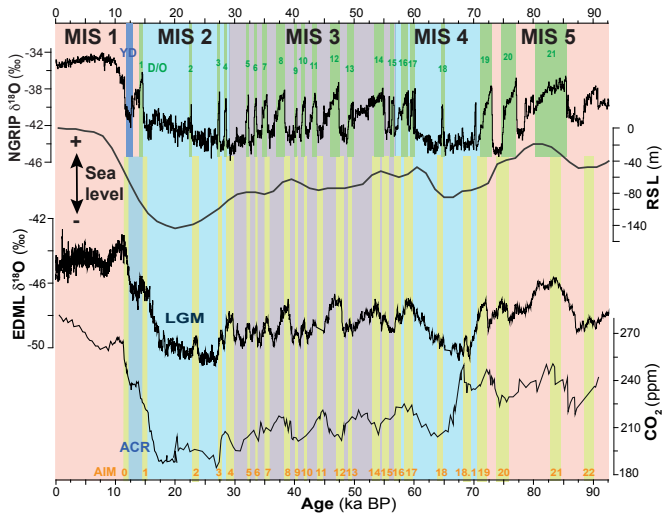


Figure 2: Millennial-scale fluctuations during the last glacial period: $\delta^{18}\text{O}$ curve determined at Northern Greenland Ice Core Project (NGRIP) (NGRIP Members, 2004) plus Dansgaard-Oeschger (D/O) events, and the Younger Dryas (YD) event (Alley, 2000) are plotted. Additionally, the reconstructed Relative Sea Level (RSL) curve (Waelbroeck et al., 2002) is included. Antarctic EPICA Dronning Maud Land (EDML) ice-core $\delta^{18}\text{O}$ record (Ruth et al., 2007) and combined CO_2 -record measured at EDC (0–20 ka; Monnin, 2006) and Byrd (20–91 ka; Ahn and Brook, 2008). Also, the Last Glacial Maximum (LGM; Clark et al., 2009) from 26.5 to 19 ka before present (BP) and the Antarctic Cold Reversal (ACR; Rahmstorf, 2002) are highlighted. Marine isotopic Stages (MIS) are plotted for reference (Lisiecki and Raymo, 2005).

During the Last Glacial Maximum (LGM) from about 26.5 to 19 ka BP northern and southern hemisphere ice sheets had their maximum extent due to decreased incoming solar radiation (insolation) in the northern hemisphere, reduced atmospheric CO_2 as well as lowered sea-surface temperatures (Clark et al., 2009). Thus, relative sea-level (Waelbroeck et al., 2002) was approximately 130 m lower than today (Fig. 2). West and East Antarctic Ice sheets were grounded and had most likely advanced close to or possibly even reached the shelf breaks, e.g. in the southern Weddell Sea (Weber et al., 2011). Northern hemisphere deglaciation was primarily triggered by an increase of northern insolation (Clark et al., 2009).

1.3 Study areas

Both study areas are located in the Atlantic sector of the Southern Ocean, which surrounds the Antarctic continent (Fig. 3). The Weddell and Scotia Sea are separated by the Southern Scotia Ridge, although even allowing deep water passing through gaps (Reid et al., 1977).



Figure 3. Overview map of Antarctica and the Southern Ocean: The study areas are located in the Atlantic Sector of the Southern Ocean. Antarctic Circumpolar Current (ACC) flows clockwise around Antarctica and connects the Atlantic, Pacific, and Indian Ocean (http://aadcm-aad.gov.au/aadc/mapcat/display_map.cfm?map_id=13438, access date 06.04.2013); Small map shows the global thermohaline circulation in the Atlantic Ocean (Rick Lumpkin; www.aoml.noaa.gov, access date 18.12.2012) with surface water (red arrows) and deep as well as bottom water (blue arrows) flow.

The Scotia Sea is located between Southern South America and the Antarctic Peninsula with an area of about $1.3 \times 10^6 \text{ km}^2$ (Maldonado et al., 2003). North and South Scotia Ridges are the northern and southern boundaries of the Scotia Sea. The Southern Sandwich-Island bow is the eastern border. In the West, the Scotia Sea reaches up to the Drake Passage. The Antarctic

Circumpolar Current (ACC) dominates ocean circulation in the Scotia Sea. With a transport volume of about 134 Sverdrup ($1 \text{ Sv} = 10^6 \text{ m}^3/\text{s}$) (Whitworth and Peterson, 1985) the ACC is the world's largest current flowing eastwards around Antarctica mainly wind-driven by the Southern Hemisphere Westerlies (Russell et al., 2006). The ACC uniquely connects the Atlantic, Pacific, and Indian Ocean, thus enabling heat, nutrient, and salt exchange between the oceans (Maldonado et al., 2003), Therefore, playing an important role in global climate control (Pugh et al., 2009).

The Weddell Sea is the southernmost part of the Atlantic sector of the Southern Ocean (Fig. 3). The Southern Scotia Ridge marks the northern boundary and in the east limited by Coats Land as well as Dronning Maud Land, where smaller ice shelves like the Brunt and Riiser-Larsen Ice Shelf are located offshore. The Filchner-Ronne Ice Shelf covers the southern Weddell Sea and in the west the Weddell Sea is bordered by the Antarctic Peninsula. As one of the major deep-water formation areas, the Weddell Sea is a key region for global thermohaline circulation (Rahmstorf, 2002; Seidov et al., 2001), also known as Conveyor Belt (e.g. Broecker, 1987, 1991). About 60 % (Orsi et al., 1999) to 70 % (Carmack and Foster, 1977) of Antarctic Bottom Water (AABW) is influenced by the bottom-water formation in the Weddell Sea, namely the Weddell Sea Deep and Bottom Waters (WSDW and WSBW) (Foldvik et al., 2004; Huhn et al., 2008). Maldonado et al. (2005) even argument that 80 % of AABW is produced in the Weddell Sea by brine rejection and supercooling. Cyclonic movement of all water masses within the Weddell Gyre dominates the Weddell Sea circulation.

2 Objectives

Research results presented in this thesis relate to sediment cores from two neighbouring study areas in the Southern Ocean, the Weddell and its northern connection, the Scotia Sea (Fig. 2). Results from the Weddell Sea focus on seasonal- to millennial-scale changes in sedimentation detected in varved sediment during the LGM. Their implications on palaeoceanography, glacial bottom-water production, and Antarctic ice-sheet dynamics are presented in chapters 3 and 4. Results from the Scotia Sea focus on decadal- to millennial-scale changes obtained throughout the last glacial cycle. Their implications on palaeoproductivity and dust transport are presented in chapters 5 and 6.

2.1 Seasonal- to millennial-scale oscillations

Chapters 3 and 4 present new details obtained from gravity cores originating from the southeastern Weddell Sea (Fig. 2), which were retrieved with R/V Polarstern (PS) in the late 1980s and early 1990s (Kuhn and Weber, 1993; Weber et al., 1994). The core sites are located in channel-ridge systems on a terrace of the continental slope in 1900 – 3000 m water depth (Michels et al., 2002). These sediments consist mostly of fine-grained siliciclastic laminated sediment deposited during the LGM and Glacial Transition (Weber et al., 2011). Some earlier studies (Weber et al., 1994; Weber et al., 2011; Weber et al., 2010a) revealed already that the laminations actually represent true varves. Due to their seasonal resolution varved sediments are ideal archives to study short-term fluctuations. Still there are many questions unsolved concerning the varves sedimentation process and climatic conditions in the Weddell Sea during the Last Glacial Period. Following questions motivated for further investigations of the varved sediments:

- What are the differences in composition of the layers?
- What causes differences in grain size and what is the triggering transportation and sedimentation process?
- Why shows the transporting current seasonal fluctuations in velocity/volume?
- How was bottom-water formed in the Weddell Sea region during LGM?
- Can the varve counting process be further improved?
- Can varve counting results improve correlating the sediment core sites among each other?
- Do the layers show any cyclic thickness variations and what are the causing processes?
- Do climate model simulations show solar forcing effects on atmospheric circulation in the Weddell Sea area?

- Can glacial short-term ice-sheet fluctuations be predicted from the varved sediment?

In chapter 3 sediment-physical and –chemical data from the newly opened sediment core PS1795 are presented. Due to the fact that each layer is only a few hundred μm up to 3 mm thick, high-resolution analyses are needed to find out more about the internal structure and elemental composition of the varves. Thin sections are an ideal tool to study varved sediments (Francus and Asikainen, 2001). Additionally, X-ray fluorescence (XRF) scanning (Croudace et al., 2006) every 0.2 mm helps to gain information about the chemical elements and their variations between individual layers. The RADIUS tool (Seelos and Sirocko, 2005) provides rapid particle analysis of digital images by ultra-high resolution scanning of thin sections. Also, coastal polynya activity and bottom-water formation under LGM conditions in the Weddell Sea is discussed.

Chapter 4 presents investigations on the sediment cores PS1599, PS1789, and PS1791. We counted varves in all laminated sections and tried to combine the counting results with AMS 14C data measured on planktonic foraminifera *Neogloboquadrina pachyderma* to correlate the sediment cores among each other. For varve counting we used the BMPix and PEAK tools (Weber et al., 2010a) and tried to improve the varve counting process. ESALab (Weber et al., 2010b) and REDFIT (Schulz and Mudelsee, 2002) programs are used for spectral analysis to analyse possible cyclicity of the thickness variations.

2.2 Dust transport and palaeoproductivity

Core sites MD07-3133 and MD07-3134 originate from the Central Scotia Sea and mainly consist of diatomaceous ooze. Thus the Scotia Sea is located between Southern South America and the Antarctic continent. Investigations of Antarctic ice cores, e.g. East Antarctic EDML ice core (Fischer et al., 2007) implemented that at least during glacial times dust mostly originated from Southern South America, e.g. Patagonia (Haberzettl et al., 2009). So, the Scotia Sea (Fig. 2) located between Southern South America and East Antarctica is an ideal location to study the dust.

For a detailed interpretation of sediment core data, it is inevitable to have a high-resolution age-depth-model. In chapters 5 and 6 we try to answer the following questions:

- Is it possible to correlate the Scotia Sea sediment cores with Antarctic ice cores?
- Can magnetic susceptibility be used as dust proxy?
- How was the atmospheric transport to Antarctica during the last glacial period?
- Which methods are useful to estimate biogenic opal content from deep-sea sediment?

- Is Fourier transform infrared spectroscopy also a useful tool to determine biogenic opal in deep-sea sediments?
- How strong is the particle flux at the core sites affected by sediment focusing?
- Can biogenic opal be used to reconstruct regional palaeoproductivity in the Scotia Sea?

Chapter 5 presents one-to-one correlations of the Scotia Sea cores magnetic susceptibility (MS) records and dust input recorded in Antarctic EDML ice core. Some earlier studies from Hofmann (1999) and Pugh et al. (2009) had also shown that MS in Southern Ocean sediment cores can be used as dust proxy. Therefore, we correlated the EDML dust record with the MS signal of the Scotia Sea cores to construct high-resolution age models for MD07-3133 and MD07-3134. The Scotia Sea cores can also help to get useful information about the dust transport since Marine Isotopic Stage (MIS) 5.

In chapter 6 different methods to determine biogenic opal and their potentials for marine sediment analyses are discussed. This is one of the first studies on biogenic opal estimations based on Fourier transform infrared spectroscopy (FTIRS) (Rosén et al., 2009; Rosén et al., 2010) for marine deep-sea sediment. It is also discussed if and to what extent biogenic opal records provide useful information about regional bioproductivity. Excess ^{230}Th normalization (e.g. Frank, 1996) is used to obtain information about possible sediment focusing in the core site area.

3 Seasonal changes in glacial polynya activity inferred from Weddell Sea varves

Journal article (in review):

D. Sprenk, M. E. Weber, G. Kuhn, V. Wennrich, T. Hartmann, and K. Seelos:
Seasonal changes in glacial polynya activity inferred from Weddell Sea varves.
Climate of the Past Discussions. Special Issue: The Past: A Compass for Future
Earth - PAGES Young Scientists Meeting 2013, submitted on 15.08.2013, in
review since 21.08.2013.

Original page numbers of the manuscript are used.

Seasonal changes in glacial polynya activity inferred from Weddell Sea varves

D. Sprenk¹, M. E. Weber¹, G. Kuhn², V. Wennrich¹, T. Hartmann¹, and K. Seelos³

[1]{University of Cologne, Institute of Geology and Mineralogy, Cologne, Germany}

[2]{Alfred-Wegener-Institut Helmholtz-Zentrum für Polar- und Meeresforschung, Bremerhaven, Germany}

[3]{Johannes Gutenberg University Mainz, Institute of Geosciences, Mainz, Germany}

Correspondence to: D. Sprenk (danielasprenk@gmail.com)

Abstract

The Weddell Sea and the associated Filchner-Ronne Ice Shelf constitute key regions for global bottom-water production today. However, little is known about bottom-water production under different climate and ice-sheet conditions. Therefore, we studied core PS1795, which consists primarily of fine-grained siliciclastic varves that were deposited on contourite ridges in the southeastern Weddell Sea during the Last Glacial Maximum (LGM). We conducted high-resolution X-ray fluorescence (XRF) analysis and grain-size measurements with the RADIUS tool (Seelos and Sirocko, 2005) using thin sections to characterize the two seasonal components of the varves at sub-mm resolution to distinguish the seasonal components of the varves.

Bright layers contain coarser grains that can mainly be identified as quartz in the medium to coarse silt grain size. They also contain higher amounts of Si, Zr, Ca, and Sr, as well as more ice-rafted debris (IRD). Dark layers, on the other hand, contain finer particles such as mica and clay minerals from the chlorite and illite groups. In addition, chemical elements, Fe, Ti, Rb, and K are elevated as well. Based on these findings as well as on previous analyses on neighbouring cores, we propose a model of glacially enhanced thermohaline convection in front of a grounded ice sheet that is supported by seasonally variable coastal polynya activity. Accordingly, katabatic (i.e. offshore blowing) winds removed sea ice from the ice edge, leading to coastal polynya formation. We suggest that glacial processes were similar to today with stronger katabatic winds and enhanced coastal polynya activity during the winter season. If this is correct, silty layers are likely glacial winter deposits, when brine rejection was increased, leading to enhanced bottom water formation and increased sediment transport. Vice versa, finer-grained clayey layers were then deposited during summer, when coastal polynya activity was likely reduced.

1 Introduction

The Weddell Sea is a key region for Earth's climate variability because it influences global thermohaline circulation (Seidov et al., 2001; Rahmstorf, 2002) as one of the major sites of deep- and bottom-water formation (Huhn et al., 2008). The present-day bottom-water formation, which is rather well known, requires flow and mixing of water masses underneath the Filchner-Rønne Ice Shelf and brine release within polynyas on the southern Weddell Sea shelf to form cold and dense water masses that can flow across the shelf and into the deep Weddell Basin (see chapter Oceanography).

However, little is known about glacial bottom-water production although Antarctica may have acted as a major supplier of deep water, i.e. Antarctic Bottom Water (AABW) during stadials (Shin et al., 2003), when production of North Atlantic Deep Water (NADW) was sluggish or even terminated (e.g. Stocker and Johnson, 2003; Knutti et al., 2004). Glacial times did not involve major floating ice shelves. Specifically during the Last Glacial Maximum (LGM) from 26.5-19 ka before present (BP) (Clark et al., 2009) most ice sheets were grounded and had advanced close to or even reached the shelf edge. In the Weddell Sea, during the LGM the ice sheet at least advanced very close, i.e. within 40 km (Larter et al., 2012) to the shelf edge and most likely even reached it (Weber et al., 2011; Elverhøi, 1984; Larter et al., 2012; Hillenbrand et al., 2012). Therefore, glacial bottom-water must have been produced very differently as ice shelf cavities required for supercooling High-Salinity Shelf Water (HSSW) to produce Ice-Shelf Water (ISW) would be inexistent (Gales et al., 2012). Here, we will provide a conceptual model of glacial brine rejection in coastal polynyas that led to intense thermohaline convection in front of a grounded ice sheet as a possible model for glacial bottom-water production.

Earlier studies (e.g. Weber et al., 1994; Weber et al., 2010; Weber et al., 2011; Spreng et al., in review) of the channel-ridge system located on a terrace of the continental slope in the southeastern Weddell Sea (Fig. 1) have revealed that the laminated deposits represent true varves formed by seasonal variations in thermohaline convection during the LGM. Recently, Spreng et al. (in review) investigated decadal-scale oscillations including a persistent 50-85-yr cycle in varve thickness data of three cores originating from the northeastern prolongation of the channel-ridge-system. Accordingly, decadal-scale fluctuations in sedimentation rates are consistent with periods of solar cycles during the LGM, e.g. the Gleissberg (Gleissberg, 1944, 1958) cycle and are therefore indirectly related to changes in total solar irradiance.

To obtain detailed information on the internal structure of the varves on a seasonal scale, we investigated gravity core PS1795 from the same channel-ridge-system and analysed sediment-physical properties. We gained detailed insight on the chemical composition and the grain size variation of the varves using high-resolution X-ray fluorescence (XRF)-scanner and RADIUS tool (Seelos and Sirocko, 2005) data every 0.2 mm.

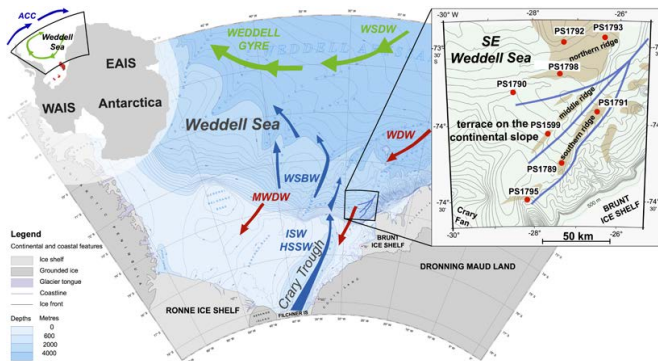


Figure 1. On the left side is an overview map showing whole Antarctica with the West (WAIS) and East (EAIS) Antarctic Ice Sheets as well as Antarctic Peninsula. The Weddell Sea (black square) is located in the southernmost part of Atlantic sector of the Southern Ocean. Additionally, the clockwise flowing Antarctic Circumpolar Current (ACC) and the Weddell Gyre (green arrows) are highlighted. The map in the centre shows a bathymetric chart of the Weddell Sea (Alfred Wegener Institute for Polar and Marine Research BCWS 1: 3 000 000; Bremerhaven, 1997). Present-days flow direction of important water masses, i.e. High Salinity Shelf Water (HSSW), Ice Shelf Water (ISW), Weddell Sea Bottom Water (WSBW), Warm Deep Water (WDW) and the through heat loss Modified WDW (MWDW) are indicated (further information see chapter 2.2). The core site area (black square) is located in the southeastern Weddell Sea close to the Brunt Ice Shelf. The small map on the right is a bathymetric map focussing on the southeastern Weddell Sea modified after (Weber et al., 1994) highlighting the Polarstern (PS) core sites referred to in this study (red dots). The core sites are located on ridges on a terrace of the continental slope. Southeast of each ridge (brown colour) runs a channel. During the LGM the thermohaline current (blue lines) was flowing towards the NE in the channels. Due to the Coriolis force most of the transported sediment is deposited NW of each channel.

During the LGM and the last glacial transition while the East Antarctic Ice Sheet advanced to the shelf break, coastal polynyas were active above the continental slope, which induced brine rejection and therefore high-salinity water production (Weber et al. 2011). These dense water masses reworked sediment and drained into the channels, depositing the material mainly northwest of each channel because of the Coriolis force, building natural levees (Michels et al., 2002). Depending on seasonal velocity changes of the thermohaline current, the transporting sediment grain size changed, leading to varved sedimentation with alternating silty-rich and more

clayey layers. Bioturbated hemipelagic mud was deposited during times, when the ice sheet was retreated from the shelf edge and sea ice was reduced. The velocity of the thermohaline current is strongly decreased, leading to significantly lower linear sedimentation rates. The final East Antarctic Ice Sheet retreat was around 16 ka, marked by a transition from laminated to bioturbated sedimentation at every core site (Weber et al., 2011).

2 Study area and regional oceanography

We study gravity cores originating from the southeastern Weddell Sea, which were retrieved with R/V Polarstern (PS) in the late 1980s and early 1990s (Fig. 1). The core sites are located in channel-ridge systems on a terrace of the continental slope in 1900–3139 m water depth. Each ridge is up to 300 m high and up to 100 km long and runs parallel, on the northwestern side of a channel (e.g. Weber et al., 1994; Kuhn and Weber, 1993).

The Weddell Sea is the southernmost part of the Atlantic sector of the Southern Ocean. The South Scotia Ridge marks the northern boundary and in the east it is limited by the Coats Land and Dronning Maud Land, where smaller ice shelves like the Brunt and Riiser-Larsen Ice Shelf are located offshore (Fig. 1). The southern Weddell Sea is covered by the Filchner-Rønne Ice Shelf. In the west the Antarctic Peninsula borders the Weddell Sea.

About 60 % (Orsi et al., 1999) to 70 % (Carmack and Foster, 1977) of the Antarctic Bottom Water (AABW) originates from the Weddell Sea, where Weddell Sea Bottom Waters (WSBW) is produced (Huhn et al., 2008; Foldvik et al., 2004). Maldonado et al. (2005) even argued that 80 % of AABW is produced in the Weddell Sea by brine rejection and supercooling. Cyclonic movement of all water masses within the Weddell Gyre dominates the Weddell Sea circulation (Fig. 1). Relatively warm Circumpolar Deep Water (CDW) is transported by the Weddell Gyre from the Antarctic Circumpolar Current (ACC) southwards along the eastern boundary into the Weddell Sea and mixes with cold surface waters generating Warm Deep Water (WDW) (e.g. Orsi et al., 1993; Gordon et al., 2010). Through heat loss and mixing primarily during winter with Winter Water (WW) while flowing further to the West along the continental margin, WDW becomes Modified Warm Deep Water (MWDW). MWDW intrudes onto the shelf and mixes with the ISW to produce WSBW (Foldvik et al., 1985). HSSW is being generated during sea ice production by brine rejection (Foldvik et al., 2004; Petty et al., 2013) and is then supercooled by circulation under the ice shelf becoming dense Ice-Shelf Water (ISW; Nicholls et al., 2009). Passive tracer experiments also point to the Filchner-Rønne Ice Shelf as the main location for bottom water production (Beckmann et al., 1999).

Bottom-water drainage is across the over-deepened Filchner Trough along the south-north running channel-ridge systems into the Weddell Basin (Fig. 1). There, it is deflected to the left due to Coriolis Force and flows clockwise along the continental slope within the Weddell Gyre

(Foldvik, 1986). Although a current meter mooring (AWI-213) in the northeastern prolongation of the channel-ridge systems investigated here, still shows a near-bottom flow underneath the Weddell Gyre with a predominant northeastern direction (Weber et al., 1994).

3 Methods

Gravity core PS1795 was opened and splitted into archive and working halves at the laboratory of the Alfred Wegener Institute in Bremerhaven. All sampling was accomplished on working halves, while sediment physical properties were measured non-destructively at 1-cm increments on full round cores and archive halves. We used the GEOTEK Multi-Sensor-Core Logger (MSCL; method see Weber et al. (1997)) for determining wet-bulk density (WBD), compression wave velocity (Vp) as well as magnetic susceptibility (MS). For MS measurements a Bartington point sensor (MS2F) was used and the data was volume-corrected. Also L*, a*, and b* colour components (Weber, 1998) were measured, using a Minolta spectrophotometer CM-2002. L* gives information about the sediment lightness, colour a* reflects the amount of green-red, and colour b* is the blue-yellow component.

Water content was estimated on sediment samples every 5 cm by freeze-drying. Information about the geochemical composition was gained by analysing bulk samples with an element analyser. Contents of total carbon (TC), inorganic carbon (TIC), and organic carbon (TOC; TIC subtracted from TC), as well as total nitrogen (TN) and total sulphur (TS) were measured. We also determined biogenic opal contents by leaching with 1M NaOH-solution according to the method see Müller and Schneider (1993). All resulting bulk data have been corrected for the containing amount of sea salt in the pore fluid (35 ‰).

To analyse sediment fabric, we cut out 1-cm thick, 10-cm wide, and 25-cm long plates from the centre of each core using a double-bladed saw. The plates were exposed for 3 to 5 minutes to a HP 43855 X-Ray System. After scanning the negatives at 300 dots per inch (dpi) resolution, we adjusted brightness and contrast to enable a better distinction of dark and bright layers, which are only a few millimetres thick.

Additionally we counted all grains >1 mm and >2 mm in diameter, reflecting ice-rafted debris (IRD). To do that, we used the scanned X-radiographs and place a semi-transparent 1x1 mm grid onto it; for further information on the method see Grobe (1987).

To obtain information on the distribution of chemical elements we measured the sediment cores non-destructively at 1-cm resolution using an Avaatech XRF core scanner (Jansen et al., 1998) at the Alfred Wegener Institute in Bremerhaven. For high-resolution element analysis, XRF-scanning was carried out every 0.2 mm on three consecutive split sediment core sections (197 – 499 cm) of PS1795 using a 3.0 kW Molybdenum tube. For these measurements, the ITRAX XRF-scanner (Cox Analytical, Sweden), a multi-function instrument for non-destructive optical,

radiographic, and chemical elemental sediment core analyses (Croudace et al., 2006), was used at the Cologne University laboratory. We also used the ITRAX scanner equipped with a 1.9 kW Chromium tube, to produce X-radiographs of the archive halves.

For accelerator mass spectrometry (AMS) radiocarbon dating we used well-preserved carbonate shell material originating from planktonic foraminifera *Neogloboquadrina pachyderma* (sinistral). Beforehand, H₂O₂ was added to each sample to remove the organic material. All measurements were conducted at the ETH laboratory of Ion Beam Physics in Zurich. AMS ¹⁴C ages were reservoir corrected (1.215 ± 30 years; see Weber et al. (2011)), based on age dating of carbonate shell material from a living bryozoa from neighbouring Site PS1418-1 (Melles, 1991). Clam version 2.1 (Blaauw, 2010) and Marine09 calibration curve (Reimer et al., 2011) were applied to calibrate the AMS ¹⁴C of PS1795 and calculate calendar ages (Table 1). We used a cubic spline age-depth model with the weighted average of 10000 iterations with 95 % confidence range.

We also produced two overlapping thin sections (PS1795: 354.6-373.2 cm; 371.5-381.2 cm) for a detailed analysis of individual layers. Therefore, aluminium boxes were pressed into the sediment and then sliced with a fishing line. After carefully removing the sediment slabs from the core half, samples were immediately flash-frozen in liquid nitrogen and then freeze-dried. Slabs were then embedded in epoxy resin under vacuum and cured afterwards. For more details on the method see Cook et al. (2009) and Francus and Asikainen (2001). To obtain thin sections, the dried epoxy-impregnated sediment slabs were cut, grinded, and polished to a thickness of only a few millimetres. The thin sections were also scanned using the ITRAX system at the University of Cologne at 0.2-mm-resolution as well as scanned with a flatbed scanner for negative transparency scanning.

Additionally, we applied the RADIUS tool, providing rapid particle analysis of digital images by ultra-high resolution scanning of thin sections (Seelos and Sirocko, 2005), which uses the commercial image processing software analySIS (Soft Imaging System GmbH) controlled by three macro-scripts by Seelos (2004). Thin sections were therefore scanned on a fully-automatic polarization microscope in combination with a digital microscope camera at the University of Mainz. The scripts derive mineral-specific particle-size distributions that cover grain sizes from medium silt to coarse sand. The RADIUS tool was used on the thin sections (PS1795: 354.6-373.2 cm; 371.5-381.2 cm) at 100- μ m-resolution.

For automatic layer recognition and counting we used the BMPix and PEAK tool (Weber et al., 2010). First, grey values were extracted from the scanned X-radiographs using the BMPix tool. Then, the PEAK tool was used to count every maximum, i.e. bright layers, every minimum, i.e. dark layers, or every transition of the grey scale curve. For more precise counting results we manually examined and revised all counting results generated by the PEAK tool. See Spreng et al.

(in review) for further information about the counting method, its uncertainties, and discrepancy estimations.

4 Results

4.1 Sediment-physical data

The 8.99 m long gravity core PS1795 (74°30'S, 28°11'W, 1884 meter water depth) is located southwest of the southern sediment ridge (Fig. 1). Sediments are relatively homogenous grey to brown (Fig. 2A), only the uppermost 23 cm are yellow to orange-brown due to oxidation. Analyses of the coarse grain fraction ($>63 \mu\text{m}$) of PS1795 every five centimetres shows that the main components of the coarse grains are quartz (80 % on average), but also feldspars, biotite, and hornblende make up 3 – 5 % each. Overall, maxima in MS (Fig. 2C) correlate with high high IRD counts (Fig. 2B).

From 2.15 m to the bottom of the core at 8.99 m, sediment is mostly laminated, consisting of alternating clayey and silty layers, each only up to a few millimetre thick. Laminated sediment consists mainly of terrigenous material with only 2 – 6 % biogenic opal, less than 0.2 % TIC/TOC, and about 0.04 % TN. WBD vary only slightly from 1.8 to 2.0 g/cm^3 . IRD content shows relatively strong fluctuations in the laminated sediment and varies between 0–18 grains/cm^2 (Fig. 2).

Between 6.42 – 6.87 m the sediment is nearly structureless, showing no bioturbation or laminations and contains only few IRD (Fig. 2B). Sediment-physical properties, e.g. MS, water content, and WBD of the 45-cm long section show only marginal fluctuations, suggesting a very homogenous composition.

A 3-cm thick coarse sand layer is intercalated into laminated sediment at 6.21 m, which is also reflected in sediment-physical properties. The coarse sand layer shows maxima in MS, IRD content, and WBD as well as minima in water content, TN, biogenic opal, Si, and Fe (Fig. 2).

The uppermost 2.15 m of PS1795 are characterized by highly bioturbated mud with varying IRD-content. The transition from laminated to bioturbated sediment is clearly documented in all parameters (Fig. 2). Water contents rise significantly from about 30 % to 40 %, colour a^* drops slightly, and WBD decreases to $\sim 1.6 \text{ g/cm}^3$. Overall, bioturbated sediment shows higher TOC, TIC, TN, and biogenic opal values than laminated sediment, indicating higher bioproductivity. Between 0.37 – 0.48 m bioturbated sediment contains high amount of IRD as well as the highest TOC contents and the lowest biogenic opal values.

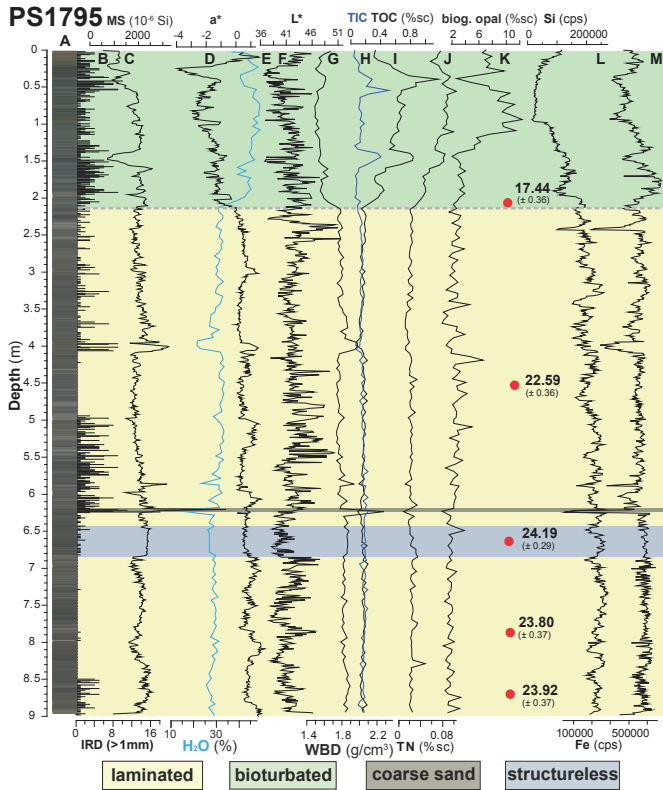


Figure 2. Sediment-physical data from sediment core PS1795: A shows the red/green/blue (RGB) colour pattern; B shows the amounts of grains >1 mm, representing iceberg-rafted debris (IRD; method see Grobe (1987)); C is magnetic susceptibility (MS) record; D is colour a^* (green-red component); E shows the water content of the sediment; F gives lightness (L^*); G is wet-bulk density (WBD); H to K are sea-salt corrected (sc) total organic and inorganic carbon (TIC/TOC), biogenic opal, and total Nitrogen (TN); L and M show chemical elements Silicon (Si), and Iron (Fe) determined with a X-ray fluorescence-scanner. AMS ^{14}C ages (marked with red dots) measured on planktonic foraminifera *Neogloboquadrina pachyderma* are given in ka cal before present. The grey line at 2.15 m depth marks a possible hiatus (see chapter 4.2).

To form bioturbated sediment requires low sedimentation rates and at least partly open-water conditions (reduced sea-ice cover). Accordingly, bioturbated sediment was most likely deposited during times, when the ice sheet was retreated from the shelf edge (e.g. Weber et al., 1994; Weber et al., 2011). Therefore, the dense water masses are formed on the southern Weddell Sea shelf as today (see Oceanography chapter). Accordingly, due to the retreated ice sheet less ice-transported sediment was deposited on the upper slope.

4.2 Chronology

Using sediment slices up to 25-cm thick and labour-intense microscopic analysis, we managed to collect enough intact shell material from planktonic foraminifera *Neogloboquadrina pachyderma* for six AMS ^{14}C analyses (Table 1). Three samples have less than 0.3 mg C, which is close to the detection limit of radiocarbon dating possible at ETH Zurich. Two of those samples show slight age reversals relative to those with greater amounts of C, and are therefore not included in the final age models. Nonetheless, the error range of AMS ^{14}C age of 24.19 ± 0.29 ka at 6.68 m depth lies within the age range of the age-depth-models and is possibly caused by high linear sedimentation rates of about 1.1 – 1.6 m/kyr (Fig. 6).

We constructed two different age-depth-models for the sediment core PS1795. One age-model for undisturbed sedimentation relying only on the AMS ^{14}C ages plus an age-depth-model, which includes a hiatus at a core depth of about 2.15 m. The X-radiograph highlights an erosive contact between laminated and bioturbated sediment at 2.15 m (Fig. 2) and also the varve counting results lead to the assumption that sedimentation is disturbed at the base of the bioturbated section. However, it is not possible to count the varves accurately between 2.15 and 2.57 m due to the low quality of the X-radiographs, the material can be identified as varved sediment. Nonetheless, based on the visually detectable faint lamination, the material can be considered varves. Using an estimated LSR of approximately 1.1– 1.6 m/kyr the varved sediment possibly includes about 260–380 varves, which gives an age for the top of the varved sediments between 21.8 and 22.4 ka. The topmost 2.15 m, cover about the last 17 – 18 kyrs as the AMS ^{14}C age of 17.44 ± 0.36 ka close to the base of the bioturbated section reveals. This reflects linear sedimentation rates of only 0.12 m/kyr for the bioturbated sediment. Accordingly, the combination of varve counting and radiocarbon dating strongly suggests incomplete sedimentation, with a hiatus of approximately 3 to 4 kyr (Fig. 2).

Table 1. Accelerator mass spectrometry (AMS) ^{14}C ages measured on planktonic foraminifera *Neogloboquadrina pachyderma* shells at the ETH laboratory of Ion Beam Physics in Zurich. Also the amount of C used for each measurement is included in the table. AMS ^{14}C ages were reservoir corrected (1215 ± 30 years), based on age dating of carbonate shell material from a living bryozoa

from neighbouring Site PS1418-1 (Melles, 1991). Clam 2.1 (Blaauw, 2010) and the Marine09 calibration curve (Reimer et al., 2011) were used to calculate calendar years before present (cal yrs BP). For all ages also the estimated error of the dating method is given.

Laboratory code	Sample depth (cm)	Amount C (mg)	Uncalibrated ^{14}C age (yrs BP) \pm error	Age min (cal yrs BP)	Age max (cal yrs BP)	Probability (%)
ETH-48371	210-215	0,23*	15947 \pm 77	17087	17797	95
ETH-48372	390-415	0,38*	22211 \pm 86	24304	24946	95
ETH-48373	450	0,87	20501 \pm 60	22221	22678	83.9
ETH-48373	450	0,87	20501 \pm 60	22764	22950	8
ETH-48373	450	0,87	20501 \pm 60	23140	23229	3.1
ETH-48374	655-680	0,31*	21912 \pm 90	23903	24474	95
ETH-48375	775-795	0,42	21546 \pm 80	23437	24170	95
ETH-48376	865-880	0,54	21643 \pm 77	23558	24289	95

4.3 Varves

The varve character of the laminations has been established in earlier studies (Weber et al. (1994, 2010a, 2011; Sprenk et al., in review). The most convincing argument is provided by core PS1789 (location see Fig. 1), which yields the visually most complete record of LGM variation. Two horizons at 199 cm and 1211 cm core depth date to 19,223 and 22,476 ka, respectively. Over this age difference of 3253 years (\pm 529 years), we counted 3329 laminae couplets (see Fig. 8 of Weber et al., 2010) – a very convincing and robust indication of the seasonal nature of the lamination. The AMS ^{14}C ages and varve counting results of PS1795 of this study also approve the seasonal sedimentation (see following chapters).

In this study, analyses concentrate on laminated sections of newly opened core PS1795. Accordingly, the density of the coarser layers is slightly higher, leading to less darkening of the X-ray film (Axelsson, 1983), therefore X-radiographs have been successfully used for varve counting on sediment cores PS1599, PS1789, and PS1791 (Sprenk et al., in review). Although, the varved sections of PS1795 have similar average grain sizes as the cores studied previously, the seasonal differences are subdued, the X-radiographs do not show the differences accordingly (Fig. a) and the layers cannot always be adequately counted. To obtain more information on the texture and composition of the individual layers as well as to better understand the seasonal sedimentation process, we produced thin sections of the varved sediment.

4.3.1 Thin sections

Figure 4 shows that the scanned images of the thin sections provide more detailed information of the internal structure and composition of the varves. Strong thickness variations can be noticed both in the brown-coloured clayey layers and the light-coloured silty layers (Fig. 3), with thicknesses of only few hundred μm up to 3 mm. There are only smaller variations in grain size and no erosional or sharp bases. Both findings argue against turbiditic deposition and favour varve formation (Fig. 3A). Sand and coarse-silt contents may vary significantly between individual layers. However, some parts of the record reveal very little difference in grain size so that individual layers are hardly recognisable in thin sections (Fig. 3) and cannot be distinguished on X-radiographs (Fig. 4) at all. Some layers are completely IRD-free (Fig. 3B), while others contain high amounts of sand-size grains (Fig. 3C). IRD appears to be mainly embedded in the lighter silty layers. Fig. 4D shows some large IRD – up to 2 mm in diameter – deforming the underlying layers. This is a clear indication that either icebergs or sea ice transported the IRD and deposited it by dropping onto the sea floor.

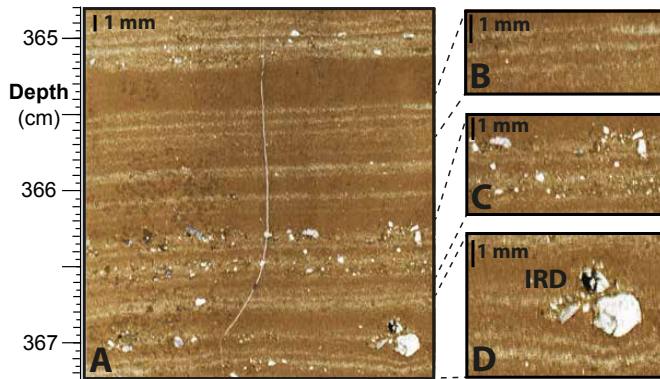


Figure 3. Detailed images of a scanned thin section of PS1795. A gives an overview of the varved sediment and the thickness variation of silty (light-coloured) and clayey (brown-coloured) layers. On the right side are three zoomed-in photos: Regular silty-clayey-layers (B); sand-rich silty layers with some ice-rafted debris (IRD) (C); D shows some individual large IRD, deposited by deforming the sediment below.

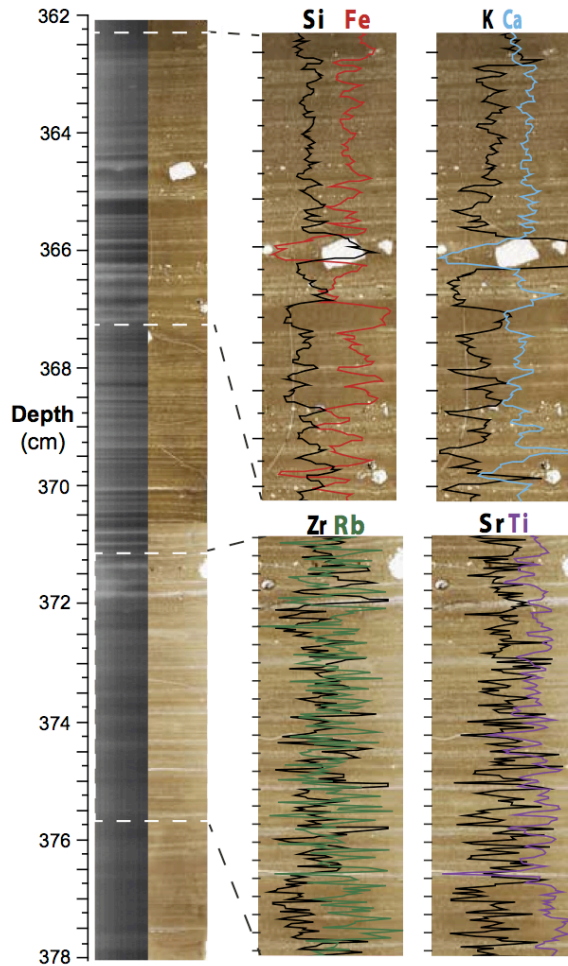


Figure 4. High-resolution element composition of a varved sediment section of core PS1795 (362 – 378 cm). The left side shows X-radiographs, generated using a X-ray fluorescence (XRF) scanner and scanned images of the thin sections. On the right side are zoomed-in images of the thin sections plus XRF-scanner element counts every 0.2 mm of the sediment slabs, from which the thin sections were produced.

4.3.2 Element composition

To investigate elemental composition changes, we scanned the sediment slabs prepared for thin sections (see Methods) every 0.2 mm (Fig. 4). Additionally, three archive halves were scanned for XRF at high resolution. Due to the fact that the varves are not exactly horizontally orientated and the radiographs, taken from a different part of the sediment as the XRF-scanner data were measured, both data sets do not reflect the same position in the sediment at the same depth. Therefore, we shifted the complete XRF-data curves a few millimetres (Fig. 5) in order to align them. Accordingly, most parts of Fig. 5 show a good correlation between XRF-derived elemental counts and the grey value curve estimated from X-radiographs, roughly reflecting density changes of the material. The most meaningful variation of elements in varved sediment are displayed in Figs. 4 and 5 and described in the following chapters. Characteristics of the clayey and silty layers are also highlighted in Table 2.

Si can either be of detrital or biogenic origin, i.e. bounded in biogenic opal (Sprenk et al., 2013). Given that the biogenic opal content of the glacial varves (Fig. 2K; chapter 4.1) of PS1795 is less than 5 %, with a mean of 2.2 %, Si is mostly of detrital origin. Analyses of the coarse-grained fraction also revealed that, on average, about 80 % of the particles coarser than 63 μm are actually quartz grains. The combination of thin sections and XRF-data (Fig. 4) highlights that Si counts are relatively enriched in coarser, light-coloured layers relative to brownish clayey layers. This indicates that Si counts every 0.2 mm can be an ideal additional tool for detrital varve counting. Figure 5 shows that the overall amount of Si also correlates to grey values derived from radiographs, which are positively correlated to sediment density (see methods). Si counts are also a good indicator for facies changes (see Fig. 2). Si counts are significantly lower in bioturbated sections relative to varved sections, due to increased water content of the sediment.

Potassium (K), iron (Fe), and titanium (Ti) show strong positive correlation, which is reflected in the Ti/Fe ratio of $r^2=0.84$ and K/Ti ratio of $r^2=0.90$. This suggests that K, Fe, and Ti are mainly bounded in clay minerals such as the chlorite and illite groups as well as mica biotite. Figure 4 highlights that K, Fe, and Ti show maxima in brownish coloured clayey layers.

Rubidium (Rb) has a similar ionic radius as K. Therefore, it commonly replaces it and can often be detected in K-feldspars, mica, and clay minerals (Chang et al., in press). Cu, Zn, Rb, Cs, Ba, and Sn are generally related to clay minerals (Vital and Stattegger, 2000). Fine-grained sediments show typically high Rb counts (Dypvik and Harris, 2001), which is also documented in varved sections of PS1795, where Rb is like K, Fe, and Ti enriched in clayey layers (Fig. 4).

Strontium (Sr) has an atomic radius similar to calcium (Ca) and can therefore replace it easily. Both elements are slightly enriched in siltier layers (Fig. 4). Ca and Si show a good correlation with a coefficient of $r^2=0.78$.

Zirconium (Zr) is comparatively immobile, mainly residing in heavy minerals, e.g. zircon, resistant to chemical as well as physical weathering (Wayne Nesbitt and Markovics, 1997; Alfonso

et al., 2006). Thus Zr is mainly transported with coarser particles (Vogel et al., 2010). Zr shows maxima mainly in coarser silty layers. Comparing the scanned thin sections and the Zr counts (Fig. 4), reveals that especially thicker and coarser silty layers have maxima in Zr counts.

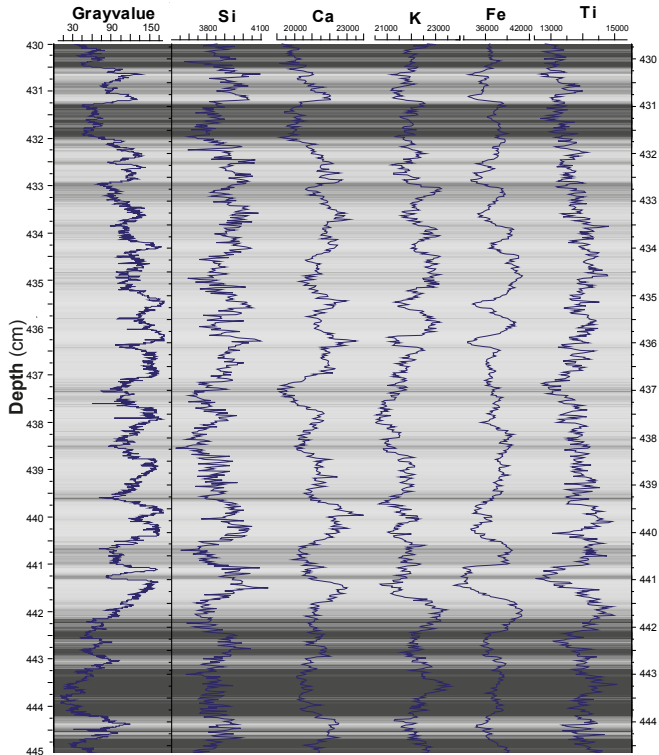


Figure 5. Seasonal-scale changes in chemical element composition: high-resolution X-ray fluorescence scanner data (area counts) every 0.2 mm of PS1795 core section (430 – 445 cm). Additionally, the estimated grey scale value curve estimated from scanned X-radiograph using the BMPix tool (Weber et al., 2010) was added.

4.3.3 RADIUS tool

To gain more information on the particles and their size distribution in varved layers, we applied the particle analysing RADIUS tool (Seelos, 2004) on high-resolution, scanned thin sections. The RADIUS tool differentiates between (i) bright particles, i.e. mainly quartz, and light feldspars, (ii) dark particles, i.e. opaque minerals, and (iii) carbonates (Seelos and Sirocko, 2005). Carbonate particles are neglected in Fig. 6 given that the values are extremely low and not significant, which is also reflected in the low TIC content of varved sediment (Fig. 2).

Figure 6 shows the percentage of detected bright and dark particles in the grain size fraction 20 – 63 μm , i.e. medium to coarse silt, of total grains (i.e. of all classified grains up to 200 μm in diameter). In lighter layers, bright silt-sized particles have local maxima and are accounting for up to 10 % of the total grains. Also, the mean size of the bright particles is mostly higher in lighter layers than in brown layers (Fig. 6). Although, single IRD, e.g. at 385.5 or 369 cm, strongly influence the mean particle size. The median size of bright particles is about 34 μm . In contrast to that, dark particles have only median sizes of about 22 μm . This is also reflected in the overall low content of dark particles in the medium to coarse silt fraction with only up to 1.2 % of all classified grains and yet in some parts even no detected dark particles. The correlation of the silt-sized dark particles and the sediment layers is not as striking as for the bright particles (Fig. 6). However, many lighter layers also show increased amounts in silt-sized as well as higher mean size of dark particles.

5 Discussion

5.1 Seasonal sedimentation changes

Our age model relying on AMS ^{14}C dates and varve counting reveals that the varved sediment was deposited during the LGM, when the ice sheets in the Weddell Sea area had most likely advanced to the shelf break (e.g. Weber et al., 2011; Hillenbrand et al., 2012). The estimated linear sedimentation rate of about 1.1 – 1.6 m/kyrs for the varved sediment of PS1795 (e.g. Fig. 6), is somewhat lower than established for core sites farther downslope on the same channel-ridge system. Sprenk et al. (in review) calculated mean linear sedimentation rates from varve counting varying between 2.2 and 5.3 m/kyr for the cores PS1599, PS1789, and PS1791 (Fig. 1). The differences in sedimentation rates are possibly related to the location of the core sites. In contrast to the earlier investigated core sites located on the sediment ridges NW of the channels, PS1795 originates from a shallower position farther southwest outside the channel, on a steeper part of the continental slope (Fig. 1) where the channel-ridge system starts to develop.

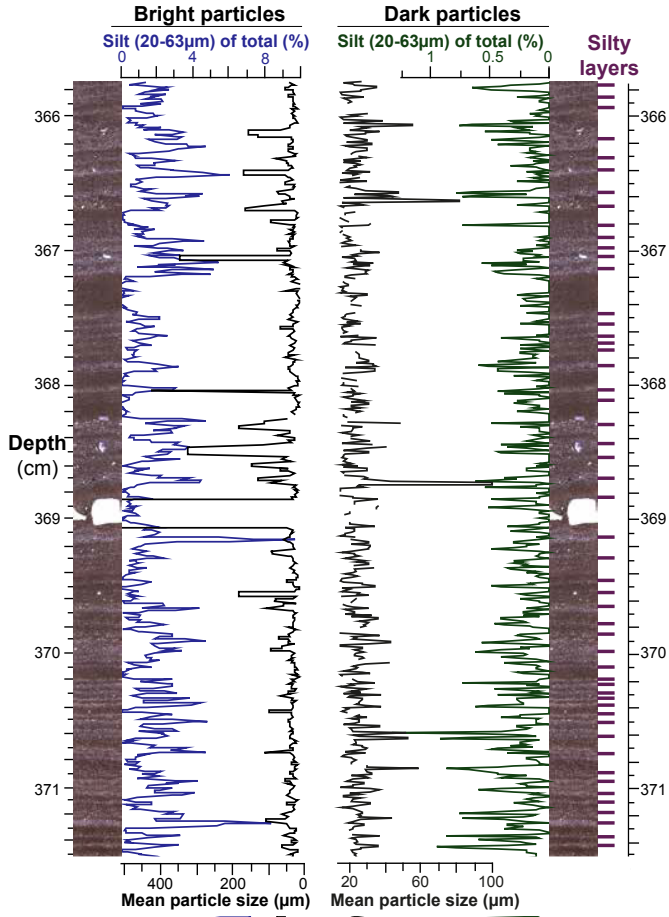


Figure 6. Detailed particle analysis of the varved sediment section 365.8-371.5 cm with the RADIUS tool (Seelos and Sirocko, 2005) applied on high-resolution scans of the thin sections. Total refers to all analysed particles up to 200 µm size. Purple bars mark the 52 counted light-coloured silty layers with a resultant linear sedimentation rate of about 1.1 m/kyrs.

The main differences of the layers come from seasonal changes in grain size and related changes in element and mineral composition (Table 2). The lighter-coloured layers show maxima in the amount of bright particles, mainly quartz in the medium to coarse silt grain size (Fig. 6), which is also reflected in Si count maxima (Figs 4,5). The lighter-coloured layers shows also slightly increased amounts of silt-sized dark particles. Enriched Zr counts in the silty layers also allude to coarser grain-sized material besides higher densities indicated by less darkening of the X-ray film (Fig. 4). Interestingly, most of the IRD is included in the lighter layers (Fig. 3). The brownish-coloured layers are characterized by predominant clay-sized particles and related minerals like mica, clay minerals like e.g. chlorite and illite group members, also indicated by maxima in Fe, Ti, Rb, and K counts (Figs 4,5).

Table 2. Characteristics of seasonally deposited clayey and silty layers. Elements were measured using ITRAX X-ray fluorescence scanner (see also Figs 4-6).

Characteristics	Clayey layer	Silty layer
Colour	brown	light-coloured
Si, Ca, Sr, Zr	low	high
K, Ti, Fe, Rb	high	low
Grey value	low	high
Silt-sized bright particles	low	high
Silt/fine sand content	low	high
Ice-rafted debris	low	high
Bottom current velocity	low	high

5.2 Modern and LGM polynyas and their relation to bottom-water production in the Weddell Sea

Today, Antarctic coastal polynyas are very important areas for AABW production and therefore, polynyas also contribute to the maintenance of the overturning circulation in the oceans (Morales Maqueda et al., 2004). Offshore blowing katabatic winds remove sea ice from coastal areas or the shelf-ice edge and often implement the development of coastal polynyas (Kern, 2009; Williams et al., 2007). Open water areas form where heat from the ocean can be released to the cold atmosphere and sea-ice production is intensified leading to brine rejection and thus dense water formation (Tamura et al., 2008). Haid and Timmermann (2013) identified the Brunt Ice Shelf, which is close to the core sites (Fig. 1), together with the Ronne Ice Shelf (e.g. Hollands et

al., 2013) and southern regions of Antarctic Peninsula as important polynya areas and highlighted that ice production is 9 – 14 times higher in these areas compared to neighbouring regions with the highest mean heat flux during the winter months July and August. Today, coastal polynyas are pervasive around Antarctica during winter (Kern, 2009) and considered as the areas of highest ice production in winter (Morales Maqueda et al., 2004). Tamura et al. (2008) estimated that 10 % of all sea ice in the Southern Ocean and about 6 % in the Weddell Sea (Renfrew et al., 2002) is produced in Antarctic coastal polynyas. In the Weddell Sea, investigations showed that years with large coastal polynya areas are in accordance with maxima in total ice extent (Comiso and Gordon, 1998). Renfrew et al. (2002) highlighted that the inter-annual variations in coastal polynya activity and area seem to be related to katabatic winds, cyclones, as well as barrier winds.

Heinemann et al. (2013) studied coastal polynyas in the Weddell Sea area and showed that in the area of Coats Land, in front of the Brunt Ice Shelf (Fig. 1), the offshore winds are mainly driven by katabatic winds, due to the steepness and length of the slope. However, for glacial conditions, there is still little knowledge on katabatic winds and coastal polynya activity as well as their seasonal changes in the southeastern Weddell Sea. Due to the fact that ice sheets covered the continental shelf in the Weddell Sea, the bottom-water formation must have deviated from today, where dense bottom waters are formed on the continental shelf under the ice shelves (e.g. Haid and Timmermann, 2013). LGM simulations by Shin et al. (2003) showed that around 80 % of the AABW could have been formed by increased brine release in the sea-ice production zones in the Southern Ocean. Coastal polynyas in front of the grounded ice sheet above the continental slope might have played a major role in the bottom water formation during the LGM. Earlier studies (e.g. Weber et al. (1994); Weber et al. (2011); Spreng et al. (in review)) indicated that during the LGM intensified katabatic winds likely drove coastal polynya formation in the southeastern Weddell Sea. Smith et al. (2010) also pointed out that during the last glacial, off-blowing katabatic winds in front of the grounded Antarctica Peninsula Ice Sheet formed coastal polynyas in the Western Weddell Sea.

The Weddell Sea varves were deposited only during glacial times when the grounded ice sheet had very likely advanced to the shelf break (e.g. Hillenbrand et al., 2012). Based on earlier (e.g. Weber et al., 1994; Kuhn and Weber, 1993; Spreng et al., in review) as well as on this study, we favour the following scenario of glacial sedimentation: during the LGM, plumes of cold and dense water were generated in front of the grounded East Antarctic Ice Sheet above the upper slope by coastal polynya, i.e. operated by strong offshore blowing (i.e. katabatic) winds enhancing sea-ice formation and thus brine release. The resulting dense water mass moved down the continental slope and was canalized into the channel-ridge systems northeast of Cary Fan (Fig. 1), producing cold and saline WSBW. Apparently, this flow oscillated seasonally with a stronger salt injection during glacial winter due to increased brine release by more intense coastal polynya. We should note that spaces of open water, which were generated by the katabatic winds and led to glacial polynyas did likely not stay open for long because of the low temperatures. Rapid freezing

and associated intense brine rejection should therefore be a major difference to present-day polynyas, which may stay open for longer and do therefore not invoke major brine rejection. The resulting glacial thermohaline current flowed underneath and against the probably weakened Weddell Gyre. The clayey layer would hence have to be interpreted as a summer signal, resulting from less intense katabatic winds, hence less sea-ice transport away from the coast, reduced brine rejection in front of the ice sheet that led to reduced thermohaline convection, lower current velocities in the channels, and less overspilling on the ridges. Vice versa, coarser-grained silty layer should represent a winter signal as a result of enhanced katabatic winds that carried sea ice away from the continent more effectively, inducing rapid freezing processes at the surface that spurred thermohaline convection, led higher velocities in the channels and higher overspilling on the ridges. As a whole, the seasonally variable thermohaline convection produced large volumes of bottom water and transported vast amounts of sediment into the deeper environment that have originally been delivered by meltwater channels from the grounded ice sheet and/or by gravitational processes (Anderson et al., 1986), leaving its trace in form of varved sediment on the ridges (Figs. 3-5). In a coupled climate model, Justino and Peltier (2006) demonstrated that the seasonal cycle in the Southern Ocean was likely much stronger during LGM than it is today with a very pronounced winter season. Since coastal polynya formation is mainly driven by the intensity of the katabatic winds, sea-ice was moved away from the continent and/or thinned close to the coast in glacial winter, allowing for a more intense transport of icebergs counterclockwise around Antarctica within the Antarctic Coastal Current. This could explain why coarser-grained (winter) layers occur preferentially with higher amounts of IRD.

Alternatively, coarser layers could have been deposited during summer, when ice melt occurred more likely. This interpretation could be supported by the fact that the silty layers contain higher IRD contents resulting from ice melt. Ice melt could occur either through direct surface melt, although modelling of atmospheric teleconnections from sea-surface temperature variations from equatorial Pacific (Weber et al., 2011) show that increasing temperatures would not lead to a negative ice mass balance under LGM conditions. Meltwater could also be delivered by meltwater channels directly from the ice sheet. That process, however would only deliver fresh water that is not dense enough to sink down and move across the shelf and onto the continental slope and into the channels that accompany the ridges because the surrounding brines are much denser. Also, seasonal deposition on the ridges requires a continuous flow of a dense water mass at varying volume (velocity) in the channels that is deflected to the left due to the influence of Coriolis Force, and overspills the channels on their northwestern side. This process can most likely only be sustained by a seasonally variable thermohaline convection resulting from polynya formation in front of the ice edge. Nonetheless, there is no definitive interpretation possible at the current stage as to which season produced which layer.

6 Conclusions

We presented high-resolution sediment-physical and geochemical data of the newly opened sediment core PS1795 from a channel-ridge system located on a terrace of the continental slope of the southeastern Weddell Sea. AMS ^{14}C ages and varve counting results for PS1795 underline earlier studies that laminations represent true varves and are therefore seasonally deposited during the LGM with sedimentation rates of about 1.1 – 1.6 m/kyr. Thin sections, XRF-scanning at 0.2 mm resolution, as well as RADIUS tool analysis reveal detailed information on the internal varve composition. Individual layers have thicknesses of only few hundred μm up to 3 mm. The facts that laminae couplets show only small variations in grain size and there are no erosional or sharp surfaces argues against turbiditic sedimentation and favours varve formation. In fact, grain-size variability of some parts is so low that layers are hardly be distinguishable in thin sections cannot be recognised on X-radiographs at all. Analyses of thin sections show that IRD is mainly embedded in the lighter, silty layers with some large debris – up to 2 mm in diameter – deforming the underlying layers. This is a clear indication of transport by either icebergs or sea ice, and deposition by dropping onto the sea floor.

Our results reveal seasonal changes in grain size and related changes in element and mineral composition. Lighter-coloured layers contain higher amounts of silt-sized particles, mostly quartz grains, which is also shown by maxima in Si counts. Light layers are also enriched in Zr, reveal coarser grain sizes and show higher densities as indicated by less darkening of the X-ray film. Finer grained layers are of darker colour, contain mainly clay-sized particles as well as maxima in K, Fe, Ti, and Rb, i.e. typical trace elements for clay minerals such as chlorite and illite as well as mica such as biotite.

Consequently, sedimentation in the channel-ridge-system was highly dynamic during the LGM, reflecting seasonal velocity changes of the thermohaline current that transporting sediment from the upper slope downslope to the core sites. Sediments were deposited when the grounded ice sheet had advanced to the Weddell Sea shelf edge. Offshore blowing katabatic winds removed sea ice from the ice edge and coastal polynyas developed. We suggest that glacial coastal polynya processes were in general similar to today inasmuch as stronger katabatic winds and enhanced coastal polynya activity occurred during the winter season. However, that does not imply the spaces of open water may have existed for long. Following this concept, silty layers are likely glacial winter deposits, when brine release was increased leading to intensified bottom water formation and increased sediment transport. Vice versa, finer-grained clayey layers were deposited during summer, when coastal polynya activity was possibly reduced.

Nonetheless, there is currently no concluding interpretation as to which season produced which layer. Coarser layers could also have been deposited during glacial summer by meltwater channels or when more sea ice melted, which might also explain the higher IRD content in silty

layers. However, the density of melted freshwater would have been too low to sink down the continental slope and initiate the required thermohaline circulation.

Acknowledgements

The authors are grateful for financial support from the Deutsche Forschungsgemeinschaft (DFG; grants RI 525/17-1, KU 683/9-1, WE2039/8-1) and the DFG-Priority Programme Antarctic Research 1158. Our study was part of the Alfred Wegener Institute research program “Polar Regions and Coasts in a changing Earth System” (PACES), Topic 3 “Lessons from the Past”. We thank Irka Hajdas from the Laboratory of Ion Beam at the ETH Zurich for the AMS ^{14}C measurements as well as Ralf Baeumler and Jens Karls from the University of Cologne for helping with the thin sections. Supplementary data to this paper are available at (doi will be implemented soon).

References

- Alfonso, J. A., Martínez, M., Flores, S., and Benzo, Z.: Distribution of Trace Elements in Offshore Sediments of the Orinoco Delta, *Journal of Coastal Research*, 502-510, 10.2112/03-0142.1, 2006.
- Anderson, J. B., Wright, R., and Andrews, B.: Weddell Fan and Associated Abyssal Plain, Antarctica: Morphology, Sediment Processes, and Factors Influencing Sediment Supply, *Geo-Marine Letters*, 121-129, 1986.
- Axelsson, V.: The use of X-ray radiographic methods in studying sedimentary properties and rates of sediment accumulation, *Hydrobiologia*, 103, 65-69, 1983.
- Beckmann, A., Hellmer, H. H., and Timmermann, R.: A numerical model of the Weddell Sea: Large-scale circulation and water mass distribution, *Journal of Geophysical Research: Oceans*, 104, 23375-23391, 10.1029/1999JC900194, 1999.
- Blaauw, M.: Methods and code for ‘classical’ age-modelling of radiocarbon sequences, *Quaternary Geochronology*, 5, 512-518, 10.1016/j.quageo.2010.01.002, 2010.
- Carmack, E. C., and Foster, T. D.: Water masses and circulation in the Weddell Sea, edited by: Dumkar, M. J., 151-165 pp., 1977.
- Chang, H., An, Z., Wu, F., Jin, Z., Liu, W., and Song, Y.: A Rb/Sr record of the weathering response to environmental changes in westerly winds across the Tarim Basin in the late Miocene to the early Pleistocene, *Palaeogeography, Palaeoclimatology, Palaeoecology*, 10.1016/j.palaeo.2013.06.006, in press.
- Clark, P. U., Dyke, A. S., Shakun, J. D., Carlson, A. E., Clark, J., Wohlfarth, B., Mitrovica, J. X., Hostetler, S. W., and McCabe, A. M.: The Last Glacial Maximum, *Science*, 325, 710-714, 10.1126/science.1172873, 2009.
- Comiso, J. C., and Gordon, A. L.: Interannual variability in summer sea ice minimum, coastal polynyas and bottom water formation in the Weddell Sea, *Antarctic Research Series*, 74, 293-315, 1998.
- Cook, T., Bradley, R., Stoner, J., and Francus, P.: Five thousand years of sediment transfer in a high arctic watershed recorded in annually laminated sediments from Lower Murray Lake, Ellesmere Island, Nunavut, Canada, *Journal of Paleolimnology*, 41, 77-94-94, 10.1007/s10933-008-9252-0, 2009.

- Croudace, I. W., Rindby, A., and Rothwell, R. G.: ITRAX: description and evaluation of a new multi-function X-ray core scanner, Geological Society, London, Special Publications, 267, 51-63, 2006.
- Dypvik, H., and Harris, N. B.: Geochemical facies analysis of fine-grained siliciclastics using Th/U, Zr/Rb and (Zr+Rb)/Sr ratios, *Chemical Geology*, 181, 131-146, 10.1016/S0009-2541(01)00278-9, 2001.
- Elverhøi, A.: Glacigenic and associated marine sediments in the Weddell Sea, fjords of Spitsbergen and the Barents Sea: A review, *Marine Geology*, 57, 53-88, 10.1016/0025-3227(84)90195-6, 1984.
- Foldvik, A., Gammelsrød, T., and Tørresen, T.: Circulation and water masses on the southern Weddell Sea shelf, in: *Oceanology of the Antarctic Continental Shelf*, Antarct. Res. Ser., AGU, Washington, DC, 5-20, 1985.
- Foldvik, A.: Oceanographic research during Nare-84/85, *Oceanogr. Res.*, 107-109, 1986.
- Foldvik, A., Gammelsrød, T., Østerhus, S., Fahrbach, E., Rohardt, G. M., S., Nicholls, K. W., Padman, L., and Woodgate, R. A.: Ice shelf water overflow and bottom water formation in the southern Weddell Sea, *Journal of Geophysical Research*, 109, 10.1029/2003JC002008, 2004.
- Francus, P., and Asikainen, C. A.: Sub-sampling unconsolidated sediments: A solution for the preparation of undisturbed thin-sections from clay-rich sediments, *Journal of Paleolimnology*, 26, 323-326, 10.1023/A:1017572602692, 2001.
- Gales, J. A., Larter, R. D., Mitchell, N. C., Hillenbrand, C. D., Østerhus, S., and Shoosmith, D. R.: Southern Weddell Sea shelf edge geomorphology: Implications for gully formation by the overflow of high-salinity water, *Journal of Geophysical Research*, 117, F04021, 10.1029/2012JF002357, 2012.
- Gleissberg, W.: A table of secular variations of the solar cycle, *Terr. Magn. Atmos. Electr.*, 49, 243-244, 1944.
- Gleissberg, W.: The eighty-year sunspot cycle, *J. Br. Astron. Assoc.*, 68, 148-152, 1958.
- Gordon, A. L., Huber, B., McKee, D., and Visbeck, M.: A seasonal cycle in the export of bottom water from the Weddell Sea, *nature geoscience*, 3, 551-556, doi:10.1038/NGE0916, 2010.
- Grobe, H.: A simple method for the determination of ice-rafted debris in sediment cores, *Polarforschung*, 57, 123-126, 1987.
- Haid, V., and Timmermann, R.: Simulated heat flux and sea ice production at coastal polynyas in the southwestern Weddell Sea, *Journal of Geophysical Research: Oceans*, n/a-n/a, 10.1002/jgrc.20133, 2013.
- Heinemann, G., Ebner, L., Haid, V., and Timmermann, R.: Katabatic winds and polynya dynamics in the Weddell Sea region (Antarctica), *EGU General Assembly 2013*, Vienna, 2013.
- Hillenbrand, C.-D., Melles, M., Kuhn, G., and Larter, R. D.: Marine geological constraints for the grounding-line position of the Antarctic Ice Sheet on the southern Weddell Sea shelf at the Last Glacial Maximum, *Quaternary Science Reviews*, 32, 25-47, 10.1016/j.quascirev.2011.11.017, 2012.
- Hollands, T., Haid, V., Dierking, W., Timmermann, R., and Ebner, L.: Sea ice motion and open water area at the Ronne Polynya, Antarctica: Synthetic aperture radar observations versus model results, *Journal of Geophysical Research: Oceans*, 118, 1940-1954, 10.1002/jgrc.20158, 2013.
- Huhn, O., Hellmer, H. H., Rhein, M., Rodehacke, C., Roether, W., Schodlok, M. P., and Schroeder, M.: Evidence of deep- and bottom-water formation in the western Weddell Sea, *Deep-Sea Research Part II*, 55, 1098-1116, doi:10.1016/j.dsr2.2007.12.015, 2008.
- Jansen, J. H. F., Van der Gaast, S. J., Koster, B., and Vaars, A. J.: CORTEX, a shipboard XRF-scanner for element analyses in split sediment cores, *Marine Geology*, 151, 143-153, 10.1016/S0025-3227(98)00074-7, 1998.

- Justino, F., and Peltier, W. R.: Influence of present day and glacial surface conditions on the Antarctic Oscillation/Southern Annular Mode, *Geophysical Research Letters*, 33, L22702, 10.1029/2006GL027001, 2006.
- Kern, S.: Wintertime Antarctic coastal polynya area: 1992–2008, *Geophysical Research Letters*, 36, L14501, doi:10.1029/2009GL038062, 2009.
- Knutti, R., Flückiger, J., Stocker, T. F., and Timmermann, A.: Strong hemispheric coupling of glacial climate through freshwater discharge and ocean circulation, *Nature*, 430, 851-856, 2004.
- Kuhn, G., and Weber, M. E.: Acoustical characterization of sediments by Parasound and 3.5 kHz systems: Related sedimentary processes on the southeastern Weddell Sea continental slope, Antarctica, *Marine Geology*, 113, 201-217, 1993.
- Larter, R. D., Graham, A. G. C., Hillenbrand, C.-D., Smith, J. A., and Gales, J. A.: Late Quaternary grounded ice extent in the Filchner Trough, Weddell Sea, Antarctica: new marine geophysical evidence, *Quaternary Science Reviews*, 53, 111-122, 10.1016/j.quascirev.2012.08.006, 2012.
- Maldonado, A., Barnolas, A., Bohoyo, F., Escutia, C., Galindo-Zaldívar, J., Hernández-Molina, J., Jabaloy, A., Lobo, F. J., Nelson, C. H., Rodríguez-Fernández, J., Somoza, L., and Vázquez, J.-T.: Miocene to Recent contourite drifts development in the northern Weddell Sea (Antarctica), *Global and Planetary Change*, 45, 99-129, doi:10.1016/j.gloplacha.2004.09.013, 2005.
- Melles, M.: Paläoglazologie und Paläozeanographie im Spätquartär am Kontinentalrand des südlichen Weddellmeeres, Antarktis, *Ber. Polarforsch.*, 1991.
- Michels, K. H., Kuhn, G., Hillenbrand, C.-D., Diekmann, B., Fütterer, D. K., Grobe, H., and Uenzelmann-Neben, G.: The southern Weddell Sea: combined contourite-turbidite sedimentation at the southeastern margin of the Weddell Gyre, *Geological Society Memoirs*, 22, 305-323, 2002.
- Morales Maqueda, M. A., Willmott, A. J., and Biggs, N. R. T.: Polynya dynamics: A review of observations and modeling, *Review of Geophysics*, 42, RG1004, doi:10.1029/2002RG000116, 2004.
- Müller, P. J., and Schneider, R.: An automated leaching method for the determination of opal in sediments and particulate matter, *Deep-Sea Research I*, 425-444, 1993.
- Nicholls, K. W., Østerhus, S., Makinson, K., Gammelsrød, T., and Fahrback, E.: Ice-ocean processes over the continental shelf of the southern Weddell Sea, Antarctica: A review, *Reviews of Geophysics*, 47, RG3003, 10.1029/2007RG000250, 2009.
- Orsi, A. H., Nowlin jr, W. D., and Whitworth III, T.: On the circulation and stratification of the Weddell Gyre, *Deep-Sea Research I*, 40, 169-203, 1993.
- Orsi, A. H., Johnson, G. C., and Bullister, J. L.: Circulation, mixing, and production of Antarctic Bottom Water, *Progress in Oceanography*, 43, 55-109, doi:10.1016/s0079-6611(99)00004-x, 1999.
- Petty, A. A., Feltham, D. L., and Holland, P. R.: Impact of Atmospheric Forcing on Antarctic Continental Shelf Water Masses, *Journal of Physical Oceanography*, 43, 920-940, 10.1175/JPO-D-12-0172.1, 2013.
- Rahmstorf, S.: Ocean circulation and climate during the past 120,000 years, *Nature*, 419, 207-214, 2002.
- Reimer, P. J., Baillie, M. G. L., Bard, E., Bayliss, A., Beck, J. W., Blackwell, P. G., Ramsey, C. B., Buck, C. E., Burr, G. S., Edwards, R. L., Friedrich, M., Grootes, P. M., Guilderson, T. P., Hajdas, I., Heaton, T. J., Hogg, A. G., Hughen, K. A., Kaiser, K. F., Kromer, B., McCormac, F. G., Manning, S. W., Reimer, R. W., Richards, D. A., Southon, J. R., Talamo, S., Turney, C. S. M., van der Plicht, J., and Weyhenmeyer, C. E.: *IntCal09 and Marine09 Radiocarbon Age Calibration Curves, 0-50,000 Years cal BP*, 2011, 2011.
- Renfrew, I. A., King, J. C., and Markus, T.: Coastal polynyas in the southern Weddell Sea: Variability of the surface energy budget, *J. Geophys. Res.*, 107, 3063, 10.1029/2000jc000720, 2002.

- Seelos, K.: Entwicklung einer numerischen Partikelanalyse-Methode auf Basis digitaler Dünnschliffaufnahmen und Anwendung der Routine auf die ELSA-HL2- Kernsequenz 66-41 m, Doktor, Institut für Geowissenschaften, Johannes Gutenberg-Universität, Mainz, 1-171 pp., 2004.
- Seelos, K., and Sirocko, F.: RADIUS – rapid particle analysis of digital images by ultra-high-resolution scanning of thin sections, *Sedimentology*, 52, 669-681, 2005.
- Seidov, D., Barron, E., and Haupt, B. J.: Meltwater and the global ocean conveyor: northern versus southern connections, *Global and Planetary Change*, 30, 257-270, 2001.
- Shin, S.-I., Liu, Z., Otto-Bliesner, B. L., Kutzbach, J. E., and Vavrus, S. J.: Southern Ocean sea-ice control of the glacial North Atlantic thermohaline circulation, *Geophysical Research Letters*, 30, 68:61-68:64, 10.1029/2002GL015513, 2003.
- Smith, J. A., Hillenbrand, C.-D., Pudsey, C. J., Allen, C. S., and Graham, A. G. C.: The presence of polynyas in the Weddell Sea during the Last Glacial Period with implications for the reconstruction of sea-ice limits and ice sheet history, *Earth and Planetary Science Letters*, 296, 287-298, 10.1016/j.epsl.2010.05.008, 2010.
- Sprenk, D., Weber, M. E., Kuhn, G., Rosén, P., Frank, M., Molina-Kescher, M., Liebetrau, V., and Röhlhng, H.-G.: Southern Ocean bioproductivity during the last glacial cycle – new decadal-scale insight from the Scotia Sea, *Geological Society, London, Special Publications*, 381, 10.1144/SP381.17, 2013.
- Sprenk, D., Weber, M. E., Kuhn, G., Prange, M., Varma, V., and Schulz, M.: Decadal- to millennial-scale oscillations in the Weddell Sea during the Last Glacial Maximum, *Quaternary Science Reviews*, in review.
- Stocker, T. F., and Johnson, S. J.: A minimum thermodynamic model for the bipolar seesaw, *Paleoceanography*, 18, 1087-1095, 2003.
- Tamura, T., Ohshima, K. I., and Nihashi, S.: Mapping of sea ice production for Antarctic coastal polynyas, *Geophysical Research Letters*, 35, L07606, doi:10.1029/2007GL032903, 2008.
- Vital, H., and Stattegger, K.: Major and trace elements of stream sediments from the lowermost Amazon River, *Chemical Geology*, 168, 151-168, 10.1016/S0009-2541(00)00191-1, 2000.
- Vogel, H., Wagner, B., Zanchetta, G., Sulpizio, R., and Rosén, P.: A paleoclimate record with tephrochronological age control for the last glacial-interglacial cycle from Lake Ohrid, Albania and Macedonia, *Journal of Paleolimnology*, 44, 295-310, 2010.
- Wayne Nesbitt, H., and Markovics, G.: Weathering of granodioritic crust, long-term storage of elements in weathering profiles, and petrogenesis of siliciclastic sediments, *Geochimica et Cosmochimica Acta*, 61, 1653-1670, 10.1016/S0016-7037(97)00031-8, 1997.
- Weber, M. E., Bonani, G., and Fütterer, K. D.: Sedimentation processes within channel-ridge systems, southeastern Wedell Sea, Antarctica, *Paleoceanography*, 9, 1027-1048, 1994.
- Weber, M. E., Niessen, F., Kuhn, G., and Wiedicke, M.: Calibration and application of marine sedimentary physical properties using a multi-sensor core logger, *Marine Geology*, 136, 151-172, 10.1016/S0025-3227(96)00071-0, 1997.
- Weber, M. E.: Estimation of biogenic carbonate and opal by continuous non-destructive measurements in deep-sea sediments: application to the eastern Equatorial Pacific, *Deep-Sea Research* 1, 45, 1955-1975, 10.1016/S0967-0637(98)00028-4, 1998.
- Weber, M. E., Reichelt, L., Kuhn, G., Pfeiffer, M., Korff, B., Thurov, J., and Ricken, W.: BMPix and PEAK tools: New methods for automated laminae recognition and counting—Application to glacial varves from Antarctic marine sediment, *Geochemistry Geophysics Geosystems*, 11, 1-18, 10.1029/2009GC002611, 2010.
- Weber, M. E., Clark, P. U., Ricken, W., Mitrovica, J. X., Hostetler, S. W., and Kuhn, G.: Interhemispheric Ice-Sheet Synchronicity During the Last Glacial Maximum, *Science*, 334, 1265-1269, 10.1126/science.1209299 2011.

Williams, W. J., Carmack, E. C., and Ingram, R. G.: Chapter 2 Physical Oceanography of Polynyas, in: Elsevier Oceanography Series, edited by: Smith, W. O., and Barber, D. G., Elsevier, 55-85, 2007.

4 Decadal- and millennial-scale oscillations in the Weddell Sea during the LGM

Journal article (in review):

D. Sprenk, M. E. Weber, G. Kuhn, M. Prange, V. Varma, and M. Schulz: Decadal- and millennial-scale oscillations in the Weddell Sea during the Last Glacial Maximum. *Quaternary Science Reviews*, submitted on 25.04.2013, required reviews completed on 20.08.2013.

Original page numbers of the manuscript are used.

Decadal- to millennial-scale oscillations in the Weddell Sea during the Last Glacial Maximum

D. Sprenk^{a*}, M. E. Weber^a, G. Kuhn^b, M. Prange^c, V. Varma^c, and M. Schulz^c

^aInstitute of Geology and Mineralogy, University of Cologne, Zuelpicher Str. 49a, 50674 Cologne, Germany

^bAlfred-Wegener-Institut Helmholtz-Zentrum für Polar- und Meeresforschung, Am Alten Hafen 26, 27568 Bremerhaven, Germany

^cMARUM-Center for Marine Environmental Sciences and Department of Geosciences, University of Bremen, Klagenfurter Straße, 28359 Bremen, Germany

*Corresponding author at: University of Cologne, Institute of Geology and Mineralogy, Zuelpicher Straße 49a, D-50674 Cologne. Tel.: +49221 4706152

E-mail address: dsprenk@uni-koeln.de

Keywords: Southern Ocean, Weddell Sea, varved sediment, Last Glacial Maximum (LGM), spectral analysis, decadal-scale oscillations, Atlantic Multidecadal Oscillation (AMO), solar cycles, Gleissberg cycle, Schwabe cycle, ice-sheet fluctuations

Abstract

High-resolution sediment records from the Southern Ocean providing detailed insight into the Last Glacial Maximum (LGM) are very rare. We present a varved-based chronology for glacial sediment from the Southern Ocean. These three sediment cores originate from a channel-ridge system on the continental slope of the southeastern Weddell Sea. Most of the sediment consists of fine-grained siliciclastic varves, whose accumulation is related to seasonal velocity changes of a contour current.

A high-resolution correlation for the sediment cores based on the combination of ¹⁴C dating and varve counting, reveals that facies changes from lamination to bioturbation and vice versa occurred simultaneously in the core site area around 25, 23, 21.5, 20, and 19 ka. The duration of the non-laminated, mainly bioturbated periods that interrupted varve accumulation, was only a couple of centuries up to a millennium, and presumably associated with ice-sheet retreat from the shelf, an inactive contour current on the slope, and at least partially open water

conditions above the sites. We therefore suggest multiple fluctuations of the East Antarctic Ice Sheet during the LGM.

The thickness of the varves varies quite strongly between the different core sites and time. We conducted bulk and evolutionary spectral analyses revealing decadal-to-centennial-scale variations. Most dominant is a 50-85-yr cycle, which seems to have been very robust during the LGM. Detected (multi-) decadal-scale frequencies are consistent with the periods of the Schwabe, lower and upper Gleissberg cycles. In addition to solar forcing, internal atmosphere-ocean variability such as the Atlantic Multidecadal Oscillation (AMO) may have influenced the sedimentation processes at the multi-decadal timescale. Climate model experiments support the inference that solar-forced anomalies in atmospheric circulation over the Weddell Sea promoted coastal polynya formation during periods of high solar activity, enhancing brine formation and influencing the sedimentation process at our core sites.

1 Introduction

Recently it has become more and more obvious that regional and global climate varies significantly also on short-term, i.e. annual- to decadal scales. Instrumental climate records are only available for up to a few hundred years, therefore high-resolution archives, e.g. tree rings, corals, and varved sediments, are essential for studying short-term past climate fluctuations to learn more about these oscillations and their possible forcing mechanisms. Unfortunately, climate records with annual-resolution and covering a long time period are relatively rare, thus there are still many open questions about the mechanisms of decadal-to-centennial-scale climate oscillations. Until now, there is only insufficient knowledge available if (multi-) decadal cycles also occurred during glacial times.

As the Weddell Sea is a major deep-water formation area, it is one of the key regions for the global thermohaline circulation. Unfortunately, most marine records from the Weddell Sea exhibit only low accumulation rates. We study sediment cores from the southeastern Weddell Sea that consist of long laminated sections that are only interrupted by short bioturbated intervals. Earlier studies (e.g. Weber et al., 1994; Weber et al., 2011) revealed that the lamination is due to seasonal variations in thermohaline convection during the Last Glacial Maximum (LGM) and are therefore true varves. Varved sediment consists of seasonally deposited layers and is therefore an ideal high-resolution climate archive (Ojala et al., 2012). Therefore investigating these varved sediments from the Weddell Sea is very promising to gain information about possible decadal-scale climate fluctuations during the last Glacial Maximum and their mechanisms.

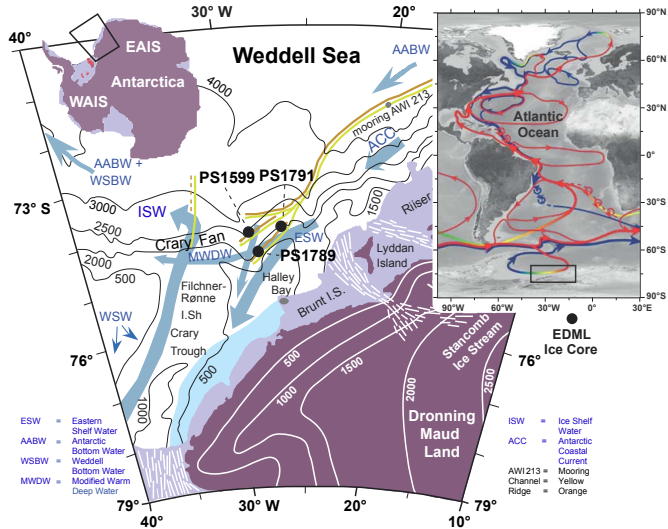


Figure 1. The map shows the southeastern Weddell Sea (Weber et al., 2011) highlighting the Polarstern (PS) core sites referred to in this study (for more information see Table 1); The core sites are located on ridges (orange lines) on a terrace of the continental slope. Southeast of each ridge runs a channel (yellow lines); Deep purple area refers to the continental ice sheets; Ice-shelf areas are in light purple colour; blue arrows indicate the flow direction of major water masses; Small map shows the global thermohaline circulation in the Atlantic Ocean (Rick Lumpkin; www.aoml.noaa.gov, access date 18.12.2012) with surface water (red arrows) and deep as well as bottom water (blue arrows) flow; The core site area (black square) is located in the southernmost part of the Atlantic sector of the Southern Ocean, where 60 (Orsi et al., 1999) to 80 % (Maldonado et al., 2005) of the Antarctic Bottom Water (AABW) is formed by brine rejection and supercooling.

2 Study area and ocean circulation

2.1 Study area

The Weddell Sea is the southernmost part of the Atlantic sector of the Southern Ocean. The northern border is the South Scotia Ridge and in the east it is limited by the Coats Land and Dronning Maud Land, where smaller ice shelves like the Brunt and Riiser-Larsen Ice Shelf are

located offshore (Fig 1.). In the south it is covered by the Ronne and Filchner Ice shelves and in the west the Antarctic Peninsula border the Weddell Sea. Our study sites are located in the southeastern part of the Weddell Sea on a terrace of the continental slope. Each ridge is up to 300 m high and up to 100 km long and runs parallel on the northwestern side of a channel (e.g. Weber et al., 1994; Kuhn and Weber, 1993).

During the LGM and the Last Glacial Transition while the East Antarctic Ice Sheet advanced to the shelf break, coastal polynyas were active above the continental slope, which induced brine rejection and therefore high-salinity water production (Weber et al. 2011). These dense water masses reworked sediment and drained into the channels, depositing the material mainly northwest of each channel (Fig. 1) because of the Coriolis force, building natural levees (Michels et al., 2002). Depending on seasonal velocity changes of the thermohaline current, the transported sediment grain size changed, leading to varved sedimentation with alternating silt-rich and more clayey layers. Bioturbated hemipelagic mud was deposited during times, when the polynya was inactive and less sediment was transported to the core sites. The final East Antarctic Ice Sheet retreat was around 16 ka, marked by a transition from laminated to bioturbated sedimentation at the core sites (Weber et al., 2011).

2.2 Ocean circulation

The Weddell Sea circulation is dominated by the cyclonic movement of all water masses within the Weddell Gyre. The Weddell Gyre transports relatively warm Circumpolar Deep Water (CDW) from the Antarctic Circumpolar Current (ACC) southwards, which modifies to the cooler Warm Deep Water (WDW) (e.g. Orsi et al., 1993; Gordon et al., 2010; Hillenbrand et al., 2012). Through heat loss and mixing with Winter Water (WW) while flowing further to the West along the continental margin, the WDW becomes the Modified Warm Deep Water (MWDW), which is together with the High Salinity Shelf Water (HSSW) and the Ice-shelf water (ISW), both originating from the southern Weddell Sea shelf, a major contributor to the bottom-water formation in this area (Hillenbrand et al., 2012). About 60 % (Orsi et al., 1999) to 70 % (Carmack and Foster, 1977) of the Antarctic Bottom Water (AABW) is influenced by the bottom-water formation in the Weddell Sea, namely the Weddell Sea Deep and Bottom Waters (WSDW and WSBW) (Huhn et al., 2008; Foldvik et al., 2004). Maldonado et al. (2005) even argue that 80 % of AABW is produced in the Weddell Sea by super-cooling and brine rejection related to intensive sea-ice production in coastal polynyas (Tamura et al., 2008). Together with the Ross Sea and the northern North Atlantic, where the North Atlantic Deep Water (NADW) is formed (Orsi et al., 1999), the Weddell Sea is the major deep-water formation area (Huhn et al., 2008). Therefore, these areas are key regions for the global thermohaline circulation (Seidov et al., 2001; Rahmstorf, 2002), also known as Conveyor Belt (Gordon, 1986; e.g. Broecker, 1987) (Fig. 1, small map).

3 Material and methods

3.1 Material

We study gravity cores originating from the southeastern Weddell Sea, which were retrieved with R/V Polarstern (PS) in the late 1980s and early 1990s (Fig. 1). The core sites are located on sediment ridges on a terrace of the continental slope at 1900 – 2900 m water depth (Table 1). The sediment cores mainly consist of terrigenous components and only minor amount of biogenic material. Most sections of the sediment cores are varved. Each varve consists of a layer couplet. The layers show only minor differences in grain size with varying amounts of silt-sized and clay-sized particles. Therefore, it is not easy to distinguish individual layers by visual examination of the core or surface photos thereof. However, coarser layers have higher densities, which leads to less darkening of the X-ray film (Axelsson, 1983). Therefore, we used X-radiographs for layer recognition and counting (Fig. 2).

Table 1 Information on Weddell Sea core sites referred to in this study, including the water depth and the gravity core length.

Core site	Latitude	Longitude	Water depth (m)	Core length (m)
PS1599	74° 04' S	27° 42' W	2487	11,32
PS1789	74° 14' S	27° 18' W	2411	14,19
PS1791	73° 55' S	26° 32' W	2894	12,89

3.2 Methods

For accelerator mass spectrometry (AMS) ^{14}C dating we used well-preserved carbonate shell material originating from planktonic foraminifera *Neogloboquadrina pachyderma* (sinistral). Beforehand, H_2O_2 was added to each sample to remove the organic material. All the measurements were done at the ETH laboratory of Ion Beam Physics in Zurich. The AMS ^{14}C ages were reservoir corrected (1.215 ± 30 years), based on age dating of carbonate shell material from a living bryozoa from neighbouring Site PS1418-1 (Melles, 1991). Calib 6.0 (<http://calib.qub.ac.uk/calib/>) was used for calculation from conventional radiocarbon ages into calendar ages.

To analyse sediment fabric, we cut out 1-cm thick, 10-cm wide, and 25-cm long plates from the centre of each core using a double-bladed saw. The plates were exposed for 3 to 5 minutes to a HP 43855 X-Ray System. After scanning the negatives at 300 dots per inch (dpi) resolution, we adjusted brightness and contrast to enable a better distinction of dark and bright layers, which are just a few millimetres thick.

We then used BMPix and PEAK tool (Weber et al., 2010a) software packages for automatic layer recognition and counting. First, grey values were extracted from the scanned X-

radiographs with the BMPix tool (Figs. 2 and 3). We used a line width of 30 pixel over which the measurement is integrated perpendicular to the scanning direction from one measurement to the next. Over 25 cm length, we generated approximately 3000 grey values, translating into 12 measurements/mm, or in other words, a sample resolution of 85 μm .

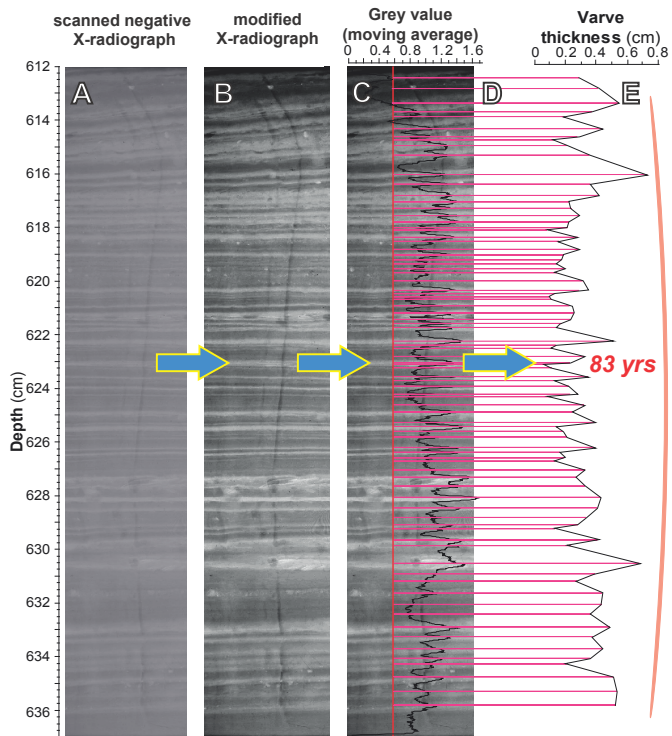


Figure 2. Method to count the siliciclastic varves and determine the varve thickness variation: A is the negative of the 25-cm long X-radiograph from core site PS1791 scanned at 300 dpi; B shows the X-radiograph displayed in A with adjusted brightness/contrast; C is the moving average of the grey value curve determined by using the BMPix software (Weber et al., 2010a); D shows the grey value maxima (pink lines) counted with the PEAK tool. E shows the amount (red number) and thickness variation in centimetre of the counted varves.

We took advantage of the software's ability to count laminations in five different ways, which also helped to reduce the overall count error. Annual counts were achieved by counting every maximum (max count; bright layers) and every minimum (min count; dark layers) of an annual layer couplet. Seasonal counts were achieved by counting every transition from dark to bright layers (up crossings) and from bright to dark layers (down crossings) as well as halfway passage (zero crossings) of the grey scale curve (Fig. 2). In order to optimize the counting results quickly and iteratively, the user can adjust three basic settings, the full width half maximum of the Gaussian smoothing, the minimum cycle length, and the minimum amplitude (details see Weber et al. (2010a)).

Finally, we evaluated counting errors by comparing manual counts conducted by two individuals and automated counts achieved with the PEAK (Table 2). Accordingly, two candidates counted all minima, maxima, up crossings, down crossings, and zero crossings manually for two selected varved sections (for Site PS1789 at 689-717 cm, and for Site PS1791 at 612-637 cm core depth). Then, both candidates counted the same properties using the PEAK tool. For manual counts potential sources of error include individual misjudgement, inconsistent layer treatment, and miscalculations. For automated counts differences may arise from the adjustment of the three basic settings and the width of the line, over which the BMPix software integrates the grey value perpendicular to the counting direction.

Table 2 Error estimation for the layer counting was achieved by counting two representative X-radiographs (PS1789, 689-717 cm and PS1791, 612-637 cm). Displayed are the amounts of maxima, minima, transitions into bright (up crossings) and dark layers (down crossings) as well as zero crossings counted by 2 individuals manually. Additionally, the layers were counted by both persons using the BMPix and PEAK software (Weber et al., 2010a). While using the software the person operating the software needs to adjust different settings (e.g. counting position, minimum grey value peak height, width, and area). For more information on the counting see methods chapter and Fig. 2. The mean of the different counting results (e.g. maxima, minima) and their discrepancy in per cent are included in the table.

Counting method	Mimima	Maxima	Up crossings	Down crossings	Zero crossings
PEAK tool person 1	205	209	212	214	408 (2x204)
PEAK tool person 2	206	205	204	202	412 (2x206)
Manually person 1	209	211	212	202	396 (2x198)
Manually person 2	200	203	204	199	404 (2x202)
Mean of counting	204,5	207	208	206,5	404 (2x202)
Discrepancy (%)	±2,2	±1,9	±1,9	±3,6	±2,0

However, the counting results for both candidates and the five methods applied are fairly similar (Table 2). Between 198 and 214 peaks were counted, which reflects a total discrepancy of $\pm 3,9$ %. Depending on the counted feature, the discrepancy varies between $\pm 1,9$ and $\pm 3,6$ %. Maxima and up crossing counts show the lowest discrepancies ($\pm 1,9$ %). This is due to the fact that, at least for the glacial varves from the Antarctic continental slope, bright layers – and the transitions into bright layers (up crossings) are the most distinct features that produce the most reliable counting results.

So we used the maxima counting results for the further analyses. We also suggest that a combination of both methods leads to the most accurate counting result. Therefore, in a last iteration step, we further reduced the counting error by manually examining and revising, if necessary, the automated counting results generated by PEAK tool.

Table 3 Varve counting results and estimated mean sedimentation rates (mm/yr i.e. m/kyr) for the varved sediment sections. For additional information on the varve counting see methods and Figs. 2 and 3.

Core Site	Section (cm)	Section length (cm)	Counted years	Mean sed. rate (mm/yr)
PS1599	184-239	55	130	4,23
PS1599	260-372	112	257	4,36
PS1599	400-552	152	482	3,15
PS1599	600-895	295	1167	2,53
PS1599	968-1127	159	720	2,21
PS1789	132-182	50	95	5,26
PS1789	198-471	273	756	3,61
PS1789	488-872	384	1392	2,76
PS1789	897-1263	366	1331	2,75
PS1789	1280-1419	139	348	3,99
PS1791	112-160	48	64	7,5
PS1791	173-352	179	390	4,59
PS1791	355-575	220	706	3,12
PS1791	587-836	249	859	2,9
PS1791	842-1284	442	1462	3,02

To conduct bulk and evolutionary spectral analysis on the varve thickness variability data we used the ESALAB (Weber et al., 2010b) and REDFIT (Schulz and Mudelsee, 2002) software. Both programs rely on the (Lomb, 1976) and (Scargle, 1982, 1989) algorithms, providing an estimation of the spectrum by fitting harmonic sine and cosine components to the data set. This enables the use of unevenly spaced input data and leads to robust and high resolution resulting

spectra (Weber et al., 2010b). For all spectral analysis estimations raw, i.e. unsmoothed varve thickness data was used. Additionally, to extract chronological variability of only selected periods and thereby omitted undesirable frequency bands from the data analysis (Kern et al., 2012), we applied a Gaussian bandpass filter to the layer and varve thickness dataset using AnalySeries2.0.4.2 (Paillard et al., 1996).

4 Results and discussion

4.1 Chronology & stratigraphic correlation

The contourite ridges range among the very few Antarctic archives with carbonate shell preservation. Although scarce, it allows for the implementation of a sound and reliable low-resolution chronology relative to those obtained from dating the bulk acid insoluble organic carbon fraction, which usually contains old, reworked organic matter (e.g. Domack et al., 1999). Our AMS ^{14}C dates give a minimum age for the beginning of the LGM at ca. 25.7 ka (Weber et al., 2010a) and allow for the identification of common key points of Antarctic glacial retreat detected at all sites around 19 ka (Weber et al., 2011; Weber et al., 1994), synchronous to the onset of deglaciation of Northern Hemisphere ice sheets (Clark et al., 2009), and final ice-sheet retreat, at least for the Weddell Sea part of the East Antarctic Ice Sheet, around 16 ka (Weber et al., 2011).

However, given the rather large error of glacial AMS ^{14}C ages and the scarceness of carbonate shells, any high-resolution correlation among the sites based on AMS ^{14}C remains ambitious. Only three to five AMS ^{14}C ages have been determined for sites PS1599, PS1789 and PS1791, respectively (Weber et al., 2011) using planktonic foraminifera *Neogloboquadrina pachyderma* (Fig. 3). In addition, no ash layers have been found in the sediment so far. Therefore, varve-counting results are very helpful to correlate the sites at higher resolution, to gain further information about changes in sedimentation processes, facies, and sedimentation rates.

Varve thickness shows strong variability between individual core sections and between sites (Fig. 3), with mean thicknesses of 0.3 – 0.75 cm, documenting unusually high mean sedimentation rates of 3 – 7.5 m/kyr (Table 3). However, the total mean sedimentation rates of varved sections for each core are very similar with values of 3.1 m/kyr (PS1599), 3.15 m/kyr (PS1789), and 3.15 m/kyr (PS1791), pointing to a common formation mechanism.

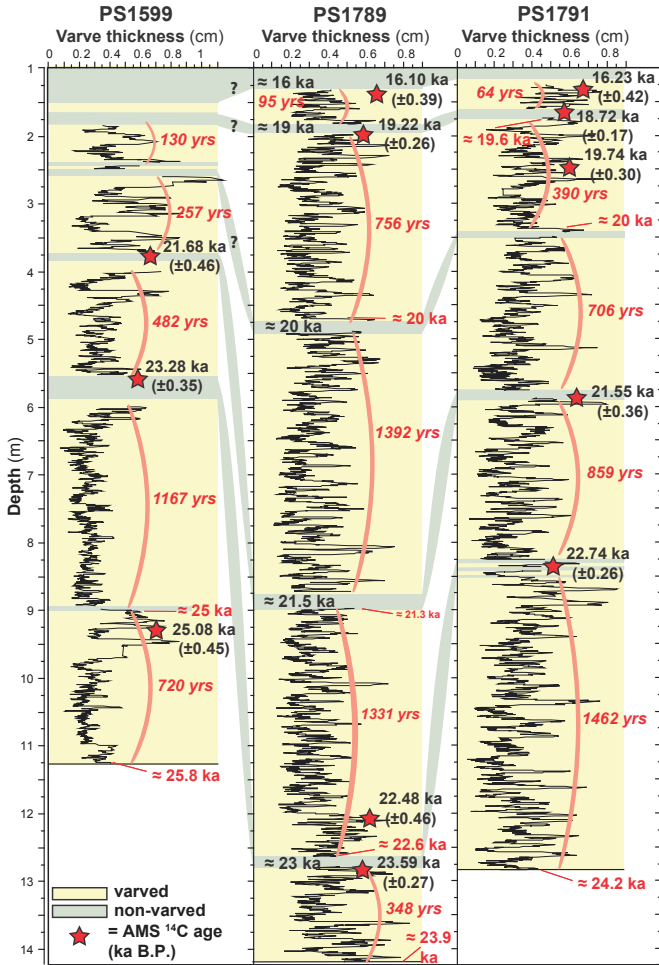


Figure 3. Centennial- to millennial-scale cycle in the Weddell Sea sediment: The correlation of the non-varved, mostly bioturbated sections (green bars) interrupting the varved (yellow bars) sediment occurred roughly at the same time (around 25, 23, 21.5, 20, 19, and finally at 16 ka; green bars) with a pacing of approximately 1000 to 2000 years. Accelerator mass spectrometry (AMS) ¹⁴C-ages (red stars) of *Neoglobobadrina pachyderma* were used to correlate the core sites

(Weber et al., 2011). Varve thickness (red italic number) was estimated using the excel macros BMPix and PEAK tools (Weber et al., 2010a) to generate a greyscale curve from X-radiograph and maxima counting (for more information see Fig. 2). The resulting varve thickness data were smoothed with a 5-point moving average filter (AnalySeries2.0.4.2; Paillard et al., 1996) for graphical reasons to highlight the decadal-scale fluctuations, but raw data was used for all further analysing.

4.2 Millennial-scale variability in glacial Weddell Sea sediment

We combined the few AMS ^{14}C ages and varve counts to correlate the cores (Fig. 3). Given the uncertainties described above, we conclude that facies changes from lamination to bioturbation and vice versa occurred simultaneously around 25, 23, 21.5, 20, and 19 ka (Fig. 3), with a millennial-scale (1000 – 2000 years) pacing. According to Weber et al. (2011), bioturbated sediment is associated with ice-sheet retreat from the shelf, an inactive contour current on the slope, and at least partially open water conditions above the sites. The duration of the non-laminated periods that interrupted varve accumulation, based on the combination of AMS ^{14}C dating and varve counting, was a couple of centuries up to a millennium. The upper 4 m of PS1599 (Fig. 3) likely include hiatuses that complicate the correlation to the other sites. PS1599 is located on a sediment ridge further northwest (Fig. 1), whereas sites PS1789 and PS1791 originate from the southernmost ridge and show good agreement (Fig. 3).

The facies changes described above are only noticeable in glacial sediment sections. After the final ice-sheet recession from the outer shelf around 16 ka (Weber et al., 2011) the contour current became inactive, and non-laminated (hemipelagic) mud was deposited at low sedimentation rates of only about 0.06 (PS1791) to 0.08 m/kyr (PS1789-1) providing further indication for centennial-scale duration of glacially non-laminated sections.

Facies changes associated with varve interruption occur every few centuries to approximately 2000 years in our record (Fig. 3), suggesting multiple fluctuations of the East Antarctic Ice Sheet during the LGM. These recurrence time period bears some similarity to the typical timescale of abrupt climate events in the North Atlantic during the last glacial period (Grootes and Stuiver, 1997; Schulz, 2002).

4.3 Spectral analysis

To gain more insight into cyclic sedimentation during the LGM and varve thickness variation, we performed bulk and evolutionary spectral analysis. The spectral analysis measurements were made individually on the raw varve thickness data on all laminated sections

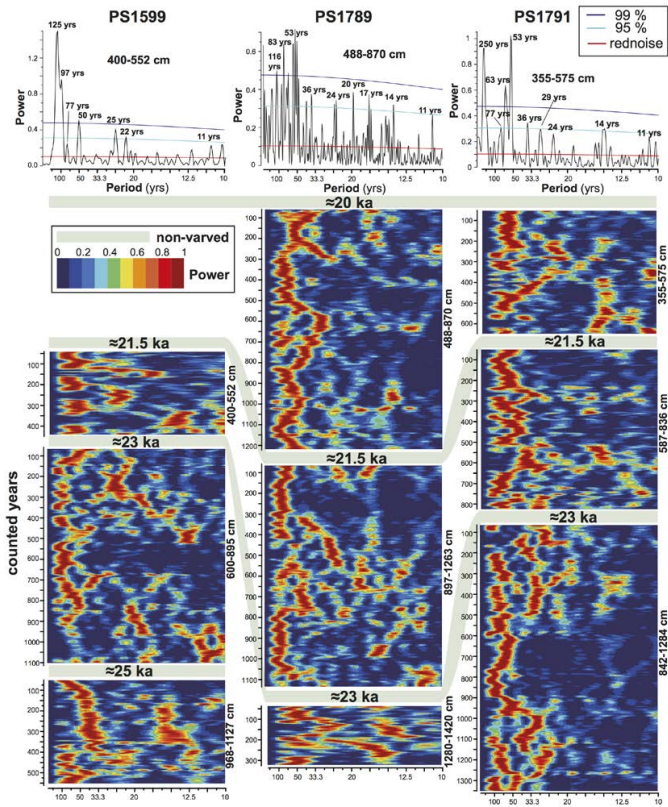


Figure 4. Bulk and evolutionary spectra performed on the varve thickness data determined with the ESALAB tool (Weber et al., 2010b) of southeastern Weddell Sea cores. Accelerator mass spectrometry (AMS) ^{14}C -ages of *Neogloboquadrina pachyderma* and varve counting results (see Fig. 3) were used to correlate the core sites (Weber et al., 2011). Varve thickness was estimated using the excel macros BMPix and PEAK tools (Weber et al., 2010a).

number of similar peaks exceeding the 99 % confidence level. Note that the bulk spectra at the top of Figure 4 give only a representation of one specific section from each core. The most common spectral feature identifiable in all cores is enhanced power concentration between 50 and 83 yr. For example, sites PS1789 and PS1791 share a distinct peak at 53 yr. At PS1599 a 50-yr peak is noticeable. Some peaks, e.g. 90-97-yr, 116-125-yr, and 250-yr periods, are also exceeding the 99 % confidence level in most of the analysed core sections. Additionally, a few higher-frequency cycles exceeding the 96 % confidence level, e.g. 11-yr, 14-yr, 17-yr, 20-29-yr, as well as 36-yr (Fig. 4), can be noticed in most of the bulk spectra.

The evolutionary spectra of all three cores reveal an overall persistent and powerful 50-85-yr-oscillation band, which seems to have been a robust feature during the LGM (Fig. 4). Other frequencies are only pronounced temporarily in the evolutionary spectra rather than being persistent LGM features. For example, the 14-yr cycle is quite powerful in the 355-575 cm core section of PS1791.

4.4 Potential causes of multi-decadal variability in sedimentation during the LGM

Our high-resolution study of Weddell Sea sediment revealed multi-decadal-scale changes in sedimentation, which seem to have been persistent during the LGM. For an in-depth investigation of the cyclic varve thickness variation, we also conducted spectral analysis on the summer and winter layer thicknesses separately. Their bulk and evolutionary spectra show the same decadal-scale cyclic fluctuations as already described above for an annual layer couplet. Maxima in the thickness of summer layers mostly coincide with winter layer maxima and vice versa (Fig. 5A, B). This leads us to the conclusion that the driving mechanism influenced and modulated the sedimentation process throughout the year, overprinting the seasonal sedimentation changes.

On the one hand grain size and amount of material deposited in the core site area is controlled by the availability and supply of sediment material on the upper slope (Michels et al., 2002). This quartz-rich material originates from the shelf and is transported in suspension by ice-shelf water (Diekmann and Kuhn, 1999) onto the slope. On the other hand the contour current reworking this material and transporting it to the core sites also influences the sedimentation process. The current velocity is mainly dependent on the amount of brine release, thus being controlled by coastal polynya activity. Heinemann et al. (2013) investigated coastal polynyas in the Weddell Sea area and showed that in the area of Coats Land, in front of the Brunt Ice Shelf (Fig. 1), the offshore winds are mainly driven by katabatic winds, due to the steepness and length of the slope. Possible indirect or direct driving mechanisms of the (multi-) decadal-scale

sedimentation changes in the Weddell Sea could therefore involve external forcing by variations in solar irradiance and/or internal climate variability through atmosphere-ocean interactions.

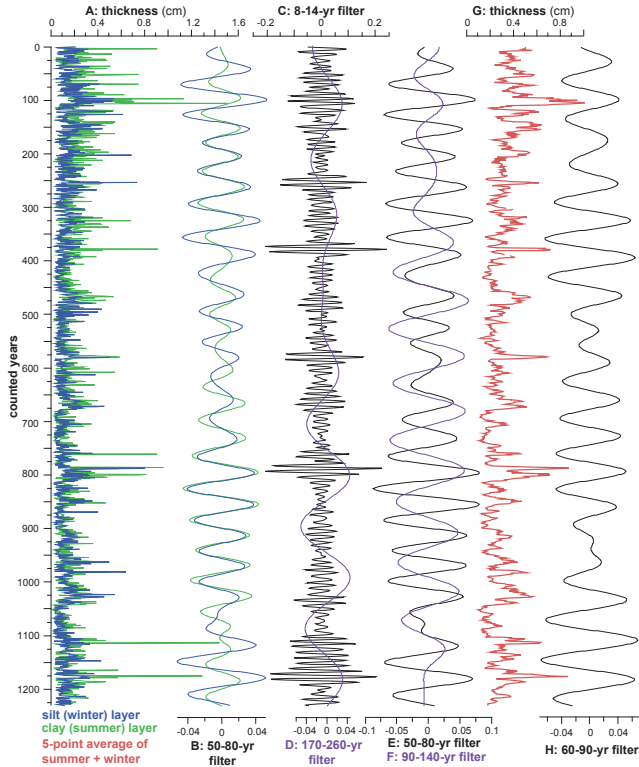


Figure 5. Gaussian band pass filtering of varve and layer thickness data (PS1789; 488 – 872 cm; see Figs. 3 and 4) around the length of solar cycles and Atlantic Multidecadal Oscillation (AMO): A shows raw thickness data of the silty (winter) and clayey (summer) layers; B refers to the 50-80-yr period (lower Gleissberg cycle) filtered from the unsmoothed summer (green curve) and winter (blue curve) layer thickness data (A). C to F are filtered from the raw varve thickness data: C: 8-14-yr (Schwabe), D and E: 50-80-yr and 90-140-yr (lower and upper Gleissberg) as well as F: 170-260-yr (De Vries/Suess) solar cycles (Ogurtsov et al., 2002). G shows a 5-point moving average of the varve (summer plus winter layer (A)) thickness for comparison. H is the result of filtering the 60-90-yr period band of the AMO (e.g. Kerr, 2000) from the varve thickness data. For all the

filtering a Gaussian bandpass filter (AnalySeries2.0.4.2; Paillard, 1996) was used. Automated layer recognition and counting were performed using the BMPix and PEAK tools (Weber et al., 2010a) (see methods and Fig. 2).

4.4.1 Solar Origin

Minor changes in total solar irradiance, e.g. 0.07 % variation in 11 years (Gray et al., 2010), seem to have direct or indirect impact on the global climate. Solar cycles have been detected in a number of climate archives (e.g. Beer et al., 2000; Gray et al., 2010; Versteegh, 2005) including marine and lake sediment (Kern et al., 2013), ice cores (e.g. Steinhilber et al., 2012; Grootes and Stuiver, 1997), tree rings (e.g. Breitenmoser et al., 2012), and speleothems (e.g. Knudsen et al., 2012; Wang et al., 2005). Seidenglanz et al. (2012) noticed in a comprehensive global climate model that a 90-yr solar forcing leads to responses in water temperatures especially in deep-water masses of the South Atlantic.

Recently, Ogurtsov et al. (2002) showed that the 87-yr Gleissberg cycle (Gleissberg, 1944) is indeed a complex 50-140-yr solar cycle with two oscillation modes, i.e. the lower 50-80-yr and upper 90-140-yr Gleissberg cycles. The multi-decadal-scale sedimentation changes in our Weddell Sea cores correspond remarkably to the 50-80-yr cycle of the lower Gleissberg solar oscillation. The 90-140-yr upper Gleissberg cycle also occurs in most of the spectra, e.g. 97-yr as well as 125-yr (PS1599) and 83-yr as well as 116-yr (PS1789) power peaks in the bulk spectra (Fig. 4).

A 250-yr power peak noticeable in some bulk spectra, e.g. PS1791 section 355-575 cm (Fig. 4) could be related to the 210-yr DeVries/Suess cycle (Wagner et al., 2001), also described as 170-260-yr solar band (Ogurtsov et al., 2002). The higher frequency cycles dominant in the bulk spectra (Fig. 4) are possibly related to the 11-yr Schwabe cycle (Schwabe, 1844), recently described as 8-14-yr solar band (Ogurtsov et al., 2002), and the 22-yr Hale cycle (Mursula et al., 2002).

The accordance of prominent solar cycles with the oscillation frequencies found in our sediment records strongly suggests a solar influence on the sedimentation most likely associated with coastal polynya formation and brine release in the southern Weddell Sea. Climate model simulations (Varma et al., 2011) support the notion of a solar forcing effect on the atmospheric circulation and hence sea-ice dynamics in the Weddell Sea region. Figure 6 shows the seasonal mean response in sea-level pressure anomalies and surface wind anomalies in response to a 70-yr lasting reduction in total solar irradiance of 2 W/m^2 (i.e. 0.15%) for different seasons as simulated by the fully-coupled comprehensive global climate model CCSM3 (Community Climate System Model version 3). The sea-level pressure response exhibits a rather annular pattern in southern mid- to high latitudes associated with an overall meridional shift of the southern westerlies, which is poleward during austral winter (i.e. June, July, and August) and equatorward during the other

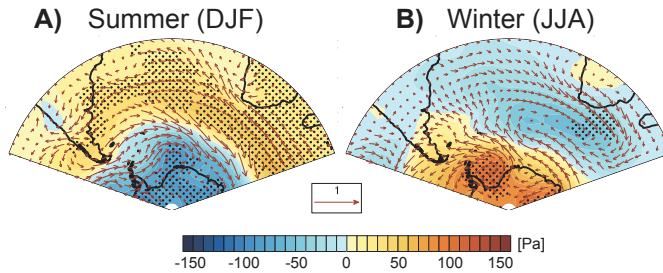


Figure 6. Summer (i.e. December, January, and February; DJF) and winter (i.e. June, July, and August; JJA) mean surface wind (m/s) anomalies and sea-level pressure (Pa) anomalies (high minus low total solar irradiance) in response to a 70-year lasting reduction in total solar irradiance of 2 W/m^2 as simulated by CCSM3. Three solar sensitivity runs (ensemble) with reduced irradiance (1363 W/m^2) were branched off from a pre-industrial control run with greater solar output (1365 W/m^2). Shown is the ensemble mean response, where each ensemble member was averaged over the entire 70-year interval of the sensitivity experiment. Stippling indicates significance of the sea-level pressure anomaly at the 0.05 level (applying a Student's t-test). For details on the model setup and experimental design the reader is referred to Varma et al. (2011).

seasons. In fact, the southern mid- to high latitude wind changes constitute the strongest dynamic response to solar irradiance changes worldwide in the model simulation (not shown), which may be attributed to feedbacks involving atmospheric eddy momentum fluxes (Lorenz and Hartmann, 2001) as well as ocean and sea-ice dynamics (Varma et al., 2011). Similar responses in southern hemisphere surface winds, albeit with a larger magnitude, were simulated with a climate model that includes the effect of solar-induced stratospheric ozone variations (Varma et al., 2012). The dynamic response to solar forcing also comprises significant surface wind anomalies over the Weddell Sea during summer (i.e. December, January, and February) and winter (i.e. June, July, and August), whereas the surface response in that area is not statistically significant ($p > 0.05$ in sea-level pressure) during autumn (i.e. March, April, and May) and spring (i.e. September, October, and November) and therefore is not included in Figure 6 and not further discussed. Surface wind anomalies during both summer (Fig. 6A) and winter (Fig. 6B) are southwesterly over the eastern Weddell Sea, in response to solar maxima. Consequently, during solar maxima stronger offshore blowing winds would favour coastal polynya and hence brine formation, thus leading to intensified sedimentation in the core site area. By contrast, during solar minima the surface wind anomalies are northeasterly over the eastern Weddell Sea. These wind anomalies push sea ice towards the margin of the southeastern Weddell Sea, counteracting the formation of coastal polynyas. Therefore less brine release and lower velocities of the contour current would lead to

lower sedimentation in the core site area during solar minima. The simulation suggests that slight changes in total solar irradiance lead to a significant response in surface winds over the eastern Weddell Sea, likely affecting contour current and sedimentation dynamics in the region of our core sites.

4.4.2 Internal atmosphere-ocean variability

Also, the 50–85-yr cyclic varve thickness variation could be related to the AMO (Delworth and Mann, 2000; Kerr, 2000), recurring changes in North Atlantic sea-surface temperature with a pacing of 60-90 years. The origin of the AMO though is still not fully understood, it seems to be related to changes in Atlantic meridional overturning circulation (AMOC; e.g. Knight et al., 2006). Zhang et al. (2011) highlighted that the North Brazil Current connecting the Northern and Southern Atlantic Ocean also shows decadal-scale oscillations being linked to AMO as well as AMOC.

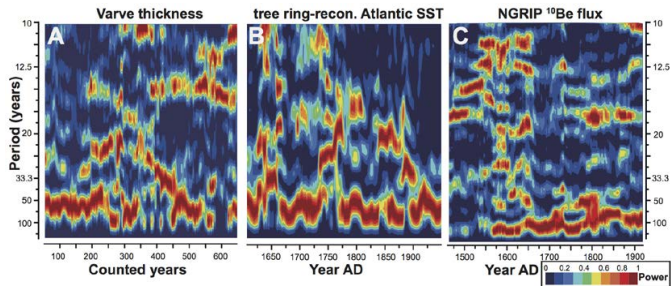


Figure 7. Comparison between evolutionary spectra of the Weddell Sea sediment and records reflecting the Atlantic Multidecadal Oscillation (AMO) as well as solar activity: A is an evolutionary spectrum of the varve thickness variability during the Last Glacial Maximum determined in Weddell Sea sediment (PS1791: 355-575 cm; see Fig. 4); B shows the evolutionary spectrum of a tree ring-reconstructed Atlantic sea-surface temperature (SST) record for 1567-1990 AD, mainly reflecting the AMO (Gray et al., 2004); C is an evolutionary spectrum of the annual ^{10}Be flux record measured in the NGRIP ice core from Greenland covering 1389-1994 AD, reflecting solar activity changes like the 11-yr Schwabe and the Gleissberg solar cycles (Berggren et al., 2009). All evolutionary spectra were determined using the ESALAB program (Weber et al., 2010b).

Until now, the AMO has only been detected in Holocene records. There is no consistent information available if the AMO also existed during the LGM. As already mentioned above the AMO might be related to changes in AMOC. Recently, Ritz et al. (2013) estimated that the AMOC strength in the LGM was indistinguishable from its recent strength, but was reduced during cooling events, e.g. Younger Dryas and Heinrich event 1.

Knudsen et al. (2011) found 55-70-yr long oscillations during the last 8 kyrs linked to the internal ocean-atmosphere variability of the AMO. Until now, the AMO has been mainly detected in Northern Hemisphere marine and lacustrine sediment archives, Greenland ice core records (e.g. GISP2 ice core, Knudsen et al., 2011) as well as speleothems (Winter et al., 2011). In addition, coral data from the Caribbean show that regional sea-surface temperature variations are possibly related to the AMO (Hetzinger et al., 2008) as well as the number of northern tropical Atlantic hurricanes (Hetzinger et al., 2008; Goldenberg et al., 2001) and North American droughts (e.g. Nigam et al., 2011; Oglesby et al., 2012) as well as US rainfall and river flow (Enfield et al., 2001). Recently, different Caribbean stalagmite records reflecting rainfall variability show typical cyclic multi-decadal variations during at least the last 1.3 kyr (Winter et al., 2011; Fensterer et al., 2012). Wyatt et al. (2012) showed that the AMO influences the Northern Hemisphere, and consequently also global climate. Evidence for an influence of the AMO on Antarctic temperatures indeed exists (Chylek et al., 2010) such that an effect of multi-decadal internal climate variability on sea-ice/ocean processes in the Weddell Sea and hence on our sedimentary records cannot be ruled out. Also it is still discussed if the AMO itself is related to and therefore reflects solar irradiance changes, as mentioned in earlier studies (e.g. Ólafsdóttir et al., 2013).

The similar oscillation band of multi-decadal-scale solar cycles and the AMO complicates the differentiation. The most prominent 50-85-yr cycle in our Weddell Sea cores lies in the range of the lower Gleissberg solar cycle (50-80-yr) as well as the 60-90-yr cyclic AMO band. Therefore, we extracted oscillation bands typical for the decadal-scale solar cycles as well as the AMO by using a Gaussian bandpass filter (Fig. 5). The filtering was done exemplarily on the varve thickness data of the PS1791 section 488-872 cm covering around 1200 years during the LGM. The signal of the lower Gleissberg cycle (Fig. 5E) seems to be slightly more prominent than the signal of the AMO cycle (Fig. 5H). The Gaussian bandpass filtering also reveals strong variations of the 8-14-yr cycle (Fig. 5C) in the varve thickness, possibly related to the Schwabe cycle, whereby strongest signals are related to thickest varves, i.e. highest sedimentation rates (Fig. 5G).

Additionally, we compared an evolutionary spectrum of the varve thickness variation in the Weddell Sea cores (Fig. 7A) with evolutionary spectra of data sets, which record the AMO (Fig. 7B) and solar activity changes (Fig. 7C). The spectra represent different time periods, due to the rareness of LGM records with annual resolution. To get comparable spectra, we used the same settings in ESALAB (Weber et al., 2010b) for the estimating. Figure 7B shows the spectrum of a tree ring-reconstructed Atlantic sea-surface temperature (SST) record for 1567-1990 AD mainly

reflecting the AMO (Gray et al., 2004). Figure 7C is an evolutionary spectrum of the annual ^{10}Be flux record measured in the NGRIP ice core from Greenland covering 1389-1994 AD, reflecting solar activity changes like the 11-yr Schwabe and the Gleissberg solar cycles (Berggren et al., 2009).

5 Conclusions

A high-resolution correlation for the sediment cores based on the combination of ^{14}C dating and varve counting, reveals that facies changes from lamination to bioturbation and vice versa occurred simultaneously in the core site area around 25, 23, 21.5, 20, and 19 ka. The duration of the non-laminated, mainly bioturbated periods that interrupted varve accumulation, was only a couple of centuries up to a millennium, and presumably associated with ice-sheet retreat from the shelf, an inactive contour current on the slope, and at least partially open water conditions above the sites. We therefore suggest multiple fluctuations of the East Antarctic Ice Sheet during the LGM.

The Weddell Sea sediment cores show decadal-to-centennial-scale varve thickness variations, reflecting sedimentation changes during the LGM. Several cycles, e.g. 11-yr, 14-yr, 17-yr, 20-29-yr, 36-yr, 90-yr, and 116-yr, exceeding the 96 and even the 99 % confidence level could be detected in the bulk spectra. Most dominant is a 50-85-yr oscillation band, which is noticeable in the evolutionary spectra of all analysed core sections, and therefore seems to have been a robust feature during the LGM. Maxima in the thickness of summer layers coincide with winter layer maxima and vice versa. This leads us to the conclusion that the driving mechanism influenced and modulated the sedimentation process throughout the year, overprinting the seasonal sedimentation changes.

To our knowledge this is one of the first studies showing (multi-) decadal-scale oscillations in varved marine sediment during glacial times. As the cycles are consistent with the periods of the Schwabe, lower and upper Gleissberg solar cycles, we conclude that solar cycles likely have been modulating the sedimentation in the core site area during the LGM. Climate model experiments support the inference that solar-forced anomalies in atmospheric circulation over the Weddell Sea promoted coastal polynya formation during periods of high solar activity, enhancing brine formation and influencing the sedimentation process at our core sites. In addition to solar forcing, internal atmosphere-ocean variability such as the AMO may have also influenced the sedimentation processes at the multi-decadal timescale.

Acknowledgements

The authors are grateful for financial support from the Deutsche Forschungsgemeinschaft (DFG; grants RI 525/17-1, KU 683/9-1, WE2039/8-1) and the DFG-Priority Programmes Antarctic Research 1158 and INTERDYNAMIC 1266. Our study was part of the Alfred-Wegener-Institut research program “Polar Regions and Coasts in a changing Earth System” (PACES), Topic 3 “Lessons from the Past”. Supplementary data to this paper are available at (doi will be implemented).

References

- Axelsson, V.: The use of X-ray radiographic methods in studying sedimentary properties and rates of sediment accumulation, *Hydrobiologia*, 103, 65-69, 1983.
- Beer, J., Mende, W., and Stellmacher, R.: The role of the sun in climate forcing, *Quaternary Science Reviews*, 19, 403-415, 2000.
- Berggren, A.-M., Beer, J., Possnert, G., Aldahan, A., Kubik, P., Christl, M., Johnson, S. J., Abreu, J., and Vinther, B. M.: A 600-year annual 10Be record from the NGRIP ice core, Greenland, *Geophysical Research Letters*, 36, L11801, doi:10.1029/2009GL038004, 2009.
- Breitenmoser, P., Beer, J., Broennimann, S., Frank, D., Steinhilber, F., and Wanner, H.: Solar and volcanic fingerprints in tree-ring chronologies over the past 2000 years, *Palaeogeography, Palaeoclimatology, Palaeoecology*, 313–314, 127-139, doi:10.1016/j.palaeo.2011.10.014, 2012.
- Broecker, W. S.: The biggest chill, *Natural History Magazine*, 96, 74-82, 1987.
- Carmack, E. C., and Foster, T. D.: Water masses and circulation in the Weddell Sea, edited by: Dumkar, M. J., 151-165 pp., 1977.
- Chylek, P., Folland, C. K., Lesins, G., and Dubey, M. K.: Twentieth century bipolar seesaw of the Arctic and Antarctic surface air temperatures, *Geophysical Research Letters*, 37, L08703, doi:10.1029/2010GL042793, 2010.
- Clark, P. U., Dyke, A. S., Shakun, J. D., Carlson, A. E., Clark, J., Wohlfarth, B., Mitrovica, J. X., Hostetler, S. W., and McCabe, A. M.: The Last Glacial Maximum, *Science*, 325, 710-714, 10.1126/science.1172873, 2009.
- Delworth, T. L., and Mann, M. E.: Observed and simulated multidecadal variability in the Northern Hemisphere, *Climate Dynamics*, 16, 661-676, 2000.
- Diekmann, B., and Kuhn, G.: Provenance and dispersal of glacial-marine surface sediments in the Weddell Sea and adjoining areas, Antarctica: ice-rafting versus current transport, *Mar. Geol.*, 209-231, 1999.
- Domack, E. W., Taviani, M., and Rodriguez, A.: Recent sediment remolding on a deep shelf, Ross Sea: implications for radiocarbon dating of Antarctic marine sediments, *Quaternary Science Reviews*, 18, 1445-1451, 1999.
- Enfield, D. B., Mestas-Nunez, A. M., and Trimble, P. J.: The Atlantic multidecadal oscillation and its relation to rainfall and river flows in the continental U.S., *Geophysical Research Letters*, 28, 2077-2080, 2001.
- Fensterer, C., Scholz, D., Hoffmann, D., Spötl, C., Pajón, J. M., and Mangini, A.: Cuban stalagmite suggests relationship between Caribbean precipitation and the Atlantic Multidecadal Oscillation during the past 1.3 ka, *The Holocene*, 22, 1405-1412, doi:10.1177/0959683612449759, 2012.

- Foldvik, A., Gammelsrød, T., Østerhus, S., Fahrback, E., Rohardt, G., Schroeder, M., Nicholls, K. W., Padman, L., and Woodgate, R. A.: Ice shelf water overflow and bottom water formation in the southern Weddell Sea, *Journal of Geophysical Research*, 109, 1-15, doi:10.1029/2003JC002008, 2004.
- Gleissberg, W.: A table of secular variations of the solar cycle, *Terr. Magn. Atmos. Electr.*, 49, 243-244, 1944.
- Goldenberg, S. B., Landsea, C. W., Mestas-Nunez, A. M., and Gray, W. M.: The Recent Increase in Atlantic Hurricane Activity: Causes and Implications, *Science*, 293, 474-479, doi:10.1126/science.1060040, 2001.
- Gordon, A. L.: Inter-ocean Exchange of Thermocline Water, *Journal of Geophysical Research*, 91, 5037-5046, 1986.
- Gordon, A. L., Huber, B., McKee, D., and Visbeck, M.: A seasonal cycle in the export of bottom water from the Weddell Sea, *nature geoscience*, 3, 551-556, doi:10.1038/NGEO916, 2010.
- Gray, L. J., Beer, J., Geller, M., Haigh, J. D., Lockwood, M., Matthes, K., Cubasch, U., van Geel, B., and White, W.: Solar influences on climate, *Reviews of Geophysics*, 48, 1-53, doi:10.1029/2009RG000282, 2010.
- Gray, S. T., Graumlich, L. J., Betancourt, J. L., and Pederson, G. T.: A tree-ring based reconstruction of the Atlantic Multidecadal Oscillation since 1567 A.D, *Geophysical Research Letters*, 31, L12205, doi:10.1029/2004GL019932, 2004.
- Groote, P. M., and Stuiver, M.: Oxygen 18/16 variability in Greenland snow and ice with 10–3- to 105-year time resolution, *Journal of Geophysical Research: Oceans*, 102, 26455-26470, doi:10.1029/97JC00880, 1997.
- Heinemann, G., Ebner, L., Haid, V., and Timmermann, R.: Katabatic winds and polynya dynamics in the Weddell Sea region (Antarctica), *EGU General Assembly 2013*, Vienna, 2013.
- Hetzinger, S., Pfeiffer, M., Dullo, W.-C., Keenlyside, N., Latif, M., and Zinke, J.: Caribbean coral tracks Atlantic Multidecadal Oscillation and past hurricane activity, *Geology*, 36, 11-14, doi:10.1130/G24321A.1, 2008.
- Hillenbrand, C.-D., Melles, M., Kuhn, G., and Larter, R. D.: Marine geological constraints for the grounding-line position of the Antarctic Ice Sheet on the southern Weddell Sea shelf at the Last Glacial Maximum, *Quaternary Science Reviews*, 32, 25-47, 10.1016/j.quascirev.2011.11.017, 2012.
- Huhn, O., Hellmer, H. H., Rhein, M., Rodehacke, C., Roether, W., Schodlok, M. P., and Schroeder, M.: Evidence of deep- and bottom-water formation in the western Weddell Sea, *Deep-Sea Research Part II*, 55, 1098-1116, doi:10.1016/j.dsr2.2007.12.015, 2008.
- Kern, A. K., Harzhauser, M., Piller, W. E., Mandic, O., and Soliman, A.: Strong evidence for the influence of solar cycles on a Late Miocene lake system revealed by biotic and abiotic proxies, *Palaeogeography, Palaeoclimatology, Palaeoecology*, 329-330, 124-136, doi:10.1016/j.palaeo.2012.02.023, 2012.
- Kern, A. K., Harzhauser, M., Soliman, A., Piller, W. E., and Mandic, O.: High-resolution analysis of upper Miocene lake deposits: Evidence for the influence of Gleissberg-band solar forcing, *Palaeogeography, Palaeoclimatology, Palaeoecology*, 370, 167-183, doi:10.1016/j.palaeo.2012.12.005, 2013.
- Kerr, R. A.: A North Atlantic Climate Pacemaker for the Centuries, *Science*, 288, 1984-1985, 10.1126/science.288.5473.1984 2000.
- Knight, J. R., Folland, C. K., and Scaife, A. A.: Climate impacts of the Atlantic Multidecadal Oscillation, *Geophysical Research Letters*, 33, n/a-n/a, 10.1029/2006GL026242, 2006.
- Knudsen, M. F., Seidenkrantz, M.-S., Jacobsen, B. H., and Kuijpers, A.: Tracking the Atlantic Multidecadal Oscillation through the last 8,000 years, *nature communications*, doi:10.1038/ncomms1186, 2011.

- Knudsen, M. F., Jacobsen, B. H., Riisager, P., Olsen, S., and Seidenkrantz, M.-S.: Evidence of Suess solar-cycle bursts in subtropical Holocene speleothem $\delta^{18}O$ records, *The Holocene*, 22, 597-602, doi:10.1177/0959683611427331, 2012.
- Kuhn, G., and Weber, M. E.: Acoustical characterization of sediments by Parasound and 3.5 kHz systems: Related sedimentary processes on the southeastern Weddell Sea continental slope, Antarctica, *Marine Geology*, 113, 201-217, 1993.
- Lomb, N. R.: Least-squares frequency analysis of unequally spaced data, *Astrophysics and Space Science*, 39, 447-462, 1976.
- Lorenz, D. J., and Hartmann, D. L.: Eddy-Zonal Flow Feedback in the Southern Hemisphere, *Journal of the Atmospheric Sciences*, 58, 3312-3327, 10.1175/1520-0469(2001)058<3312:EZFFIT>2.0.CO;2, 2001.
- Maldonado, A., Barnolas, A., Bohoyo, F., Escutia, C., Galindo-Zaldívar, J., Hernández-Molina, J., Jabaloy, A., Lobo, F. J., Nelson, C. H., Rodríguez-Fernández, J., Somoza, L., and Vázquez, J.-T.: Miocene to Recent contourite drifts development in the northern Weddell Sea (Antarctica), *Global and Planetary Change*, 45, 99-129, doi:10.1016/j.gloplacha.2004.09.013, 2005.
- Melles, M.: Paläoglazologie und Paläozeanographie im Spätquartär am Kontinentalrand des südlichen Weddellmeeres, Antarktis, *Ber. Polarforsch.*, 1991.
- Michels, K. H., Kuhn, G., Hillenbrand, C.-D., Diekmann, B., Fütterer, D. K., Grobe, H., and Uenzelmann-Neben, G.: The southern Weddell Sea: combined contourite-turbidite sedimentation at the southeastern margin of the Weddell Gyre, *Geological Society Memoirs*, 22, 305-323, 2002.
- Mursula, K., Usoskin, I. G., and Kovaltsov, G. A.: A 22-year cycle in sunspot activity, *Advances in Space Research*, 29, 1979-1984, 2002.
- Nigam, S., Guan, B., and Ruiz-Barradas, A.: Key role of the Atlantic Multidecadal Oscillation in 20th century drought and wet periods over the Great Plains, *Geophysical Research Letters*, 38, n/a-n/a, doi:10.1029/2011GL048650, 2011.
- Oglesby, R., Feng, S., Hu, Q., and Rowe, C.: The role of the Atlantic Multidecadal Oscillation on medieval drought in North America: Synthesizing results from proxy data and climate models, *Global and Planetary Change*, 84-85, 56-65, doi:10.1016/j.gloplacha.2011.07.005, 2012.
- Ogurtsov, M. G., Nagovitsyn, Y. A., Kocharov, G. E., and Jungner, H.: Long-Period Cycles of the Sun's Activity Recorded in Direct Solar Data and Proxies, *Solar Physics*, 211, 371-394, doi:10.1023/A:1022411209257, 2002.
- Ojala, A. E. K., Francus, P., Zolitschka, B., Besonen, M., and Lamoureux, S. F.: Characteristics of sedimentary varve chronologies - A review, *Quaternary Science Reviews*, 43, 45-60, doi:10.1016/j.quascirev.2012.04.006, 2012.
- Ólafsdóttir, K. B., Geirsdóttir, Á., Miller, G. H., and Larsen, D. J.: Evolution of NAO and AMO strength and cyclicity derived from a 3-ka varve-thickness record from Iceland, *Quaternary Science Reviews*, 69, 142-154, 10.1016/j.quascirev.2013.03.009, 2013.
- Orsi, A. H., Nowlin jr, W. D., and Whitworth III, T.: On the circulation and stratification of the Weddell Gyre, *Deep-Sea Research I*, 40, 169-203, 1993.
- Orsi, A. H., Johnson, G. C., and Bullister, J. L.: Circulation, mixing, and production of Antarctic Bottom Water, *Progress in Oceanography*, 43, 55-109, doi:10.1016/s0079-6611(99)00004-x, 1999.
- Paillard, D.: Macintosh Program Performs Time-Series Analysis, in: *EOS*, 77(39), 1996.
- Paillard, D., Labeyrie, L., and Yiou, P.: Macintosh Program performs time-series analysis, *EOS Transactions*, 77, 379-379, doi:10.1029/96eo00259, 1996.
- Rahmstorf, S.: Ocean circulation and climate during the past 120,000 years, *Nature*, 419, 207-214, 2002.
- Ritz, S. P., Stocker, T. F., Grimalt, J. O., Menviel, L., and Timmermann, A.: Estimated strength of the Atlantic overturning circulation during the last deglaciation, *Nature Geoscience*, 6, 208-212, doi:10.1038/NCEO1723, 2013.

- Scargle, J. D.: Studies in astronomical time series analysis. II. Statistical aspects of spectral analysis of unevenly spaced data, *The Astrophysical Journal*, 263, 835-853, 1982.
- Scargle, J. D.: Studies in astronomical time series analysis. III. Fourier transforms, autocorrelation functions, and cross-correlation functions of unevenly spaced data, *The Astrophysical Journal*, 343, 874-887, 1989.
- Schulz, M.: On the 1470-year pacing of Dansgaard-Oeschger warm events, *Paleoceanography*, 17, 2002.
- Schulz, M., and Mudelsee, M.: REDFIT: estimation red-noise spectra directly from unevenly spaced paleoclimatic time series, *Computer & Geosciences*, 28, 421-426, 2002.
- Schwabe, H.: Sonnen-Beobachtungen im Jahre 1843, *Astronomische Nachrichten*, 495, 233-236, 1844.
- Seidenglanz, A., Prange, M., Varma, V., and Schulz, M.: Ocean temperature response to idealized Gleissberg and de Vries solar cycles in a comprehensive climate model, *Geophysical Research Letters*, 39, 1-6, doi:10.1029/2012GL053624, 2012.
- Seidov, D., Barron, E., and Haupt, B. J.: Meltwater and the global ocean conveyor: northern versus southern connections, *Global and Planetary Change*, 30, 257-270, 2001.
- Steinhilber, F., Abreu, J. A., Beer, J., Brunner, I., Christl, M., Fischer, H., Heikkilä, U., Kubik, P. W., Mann, M., McCracken, K. G., Miller, H., Miyahara, H., Oerter, H., and Wilhelms, F.: 9,400 years of cosmic radiation and solar activity from ice cores and tree rings, *Proceedings of the National Academy of Sciences*, 109, 5967-5971, 2012.
- Tamura, T., Ohshima, K. I., and Nihashi, S.: Mapping of sea ice production for Antarctic coastal polynyas, *Geophysical Research Letters*, 35, L07606, doi:10.1029/2007GL032903, 2008.
- Varma, V., Prange, M., Lamy, F., Merkel, U., and Schulz, M.: Solar-forced shifts of the Southern Hemisphere Westerlies during the Holocene, *Climate of the Past*, 7, 339-347, doi:10.5194/cp-7-339-2011, 2011.
- Varma, V., Prange, M., Spanghel, T., Lamy, F., Cubasch, U., and Schulz, M.: Impact of solar-induced stratospheric ozone decline on Southern Hemisphere westerlies during the Late Maunder Minimum, *Geophysical Research Letters*, 39, L20704, doi:10.1029/2012GL053403, 2012.
- Versteegh, G. J. M.: Solar Forcing of Climate. 2: Evidence from the Past, *Space Science Reviews*, 120, 243-286, doi:10.1007/s11214-005-7047-4, 2005.
- Wagner, G., Beer, J., Masarik, J., Muscheler, R., Kubik, P. W., Mende, W., Laj, C., Raisbeck, G. M., and Yiou, F.: Presence of the solar de Vries cycle (~205 years) during last ice age, *Geophysical Research Letters*, 28, 303-306, 2001.
- Wang, Y. J., Cheng, H., Edwards, R. L., He, Y., Kong, X., An, Z., Wu, J., Kelly, M. J., Dykoski, C. A., and Li, X.: The Holocene Asian Monsoon: Links to Solar Changes and North Atlantic Climate, *Science*, 308, 854-857, 2005.
- Weber, M. E., Bonani, G., and Fütterer, K. D.: Sedimentation processes within channel-ridge systems, southeastern Wedell Sea, Antarctica, *Paleoceanography*, 9, 1027-1048, 1994.
- Weber, M. E., Reichelt, L., Kuhn, G., Pfeiffer, M., Korff, B., Thurow, J., and Ricken, W.: BMPix and PEAK tools: New methods for automated laminae recognition and counting—Application to glacial varves from Antarctic marine sediment, *Geochemistry Geophysics Geosystems*, 11, 1-18, doi:10.1029/2009GC002611, 2010a.
- Weber, M. E., Tougiannis, N., Kleineder, M., Bertram, N., Ricken, W., Rolf, C., Reinsch, T., and Antoniadis, P.: Lacustrine sediments document millennial-scale climate variability in northern Greece prior to the onset of the northern hemisphere glaciation, *Palaeogeography, Palaeoclimatology, Palaeoecology*, 291, 360-370, doi:10.1016/j.palaeo.2010.03.007, 2010b.
- Weber, M. E., Clark, P. U., Ricken, W., Mitrovica, J. X., Hostetler, S. W., and Kuhn, G.: Interhemispheric Ice-Sheet Synchronicity During the Last Glacial Maximum, *Science*, 334, 1265-1269, doi:10.1126/science.1209299, 2011.

Winter, A., Miller, T., Kushnir, Y., Sinha, A., Timmermann, A., Jury, M. R., Gallup, C., Cheng, H., and Edwards, R. L.: Evidence for 800 years of North Atlantic multi-decadal variability from a Puerto Rican speleothem, *Earth and Planetary Science Letters*, 308, 23-28, doi:10.1016/j.epsl.2011.05.028, 2011.

Wyatt, M. G., Kravtsov, S., and Tsonis, A. A.: Atlantic Multidecadal Oscillation and Northern Hemisphere's climate variability, *Climate Dynamics*, 38, 929-949, doi:10.1007/s00382-011-1071-8, 2012.

Zhang, D., Msadek, R., McPhaden, M. J., and Delworth, T.: Multidecadal variability of the North Brazil Current and its connection to the Atlantic meridional overturning circulation, *Journal of Geophysical Research: Oceans*, 116, n/a-n/a, 10.1029/2010JC006812, 2011.

5 Dust transport from Patagonia to Antarctica

Journal article (published):

M. E. Weber, G. Kuhn, D. Sprenk, C. Rolf, C. Ohlwein, and W. Ricken (2012):
Dust transport from Patagonia to Antarctica – a new stratigraphic approach from
the Scotia Sea and its implications for the last glacial cycle. *Quaternary Science
Reviews*, 36, 177-188

Permission to reuse in PhD thesis from Elsevier provided by Copyright Clearance
Center (License number: 3185381413302).

Original page numbers of the published article are used.



Dust transport from Patagonia to Antarctica – A new stratigraphic approach from the Scotia Sea and its implications for the last glacial cycle

M.E. Weber^{a,*}, G. Kuhn^b, D. Sprenk^a, C. Rolf^c, C. Ohlwein^d, W. Ricken^a

^a Institute of Geology and Mineralogy, University of Cologne, Zulpicher Str. 49a, 50674 Cologne, Germany

^b Alfred Wegener Institute for Polar and Marine Research (AWI), Helmholtz Association, Am Alten Hafen 26, 27568 Bremerhaven, Germany

^c Leibniz Institute for Applied Geophysics, Stilleweg 2, 30655 Hannover, Germany

^d Meteorological Institute, University of Bonn, Auf dem Hügel 20, 53121 Bonn, Germany

ARTICLE INFO

Article history:

Received 26 June 2011
Received in revised form
28 November 2011
Accepted 11 January 2012
Available online 14 February 2012

Keywords:

Dust
Magnetic susceptibility
Atmospheric circulation
Chronology
Paleoclimate
Last glacial cycle
Southern Ocean
Scotia Sea
Patagonia
Antarctica

ABSTRACT

We studied two deep-sea cores from the Scotia Sea to reconstruct past atmospheric circulation in the southern hemisphere and to resolve a long-standing debate on the interpretation of magnetic susceptibility (MS) records in Southern Ocean (SO) sediment. High-sedimentation sites MD07-3134 (0.2–1.2 m/kyr) and MD07-3133 (0.3–2.1 m/kyr) cover the last 92.5 kyr and 36 kyr, respectively. Both exhibit a one-to-one coupling of the MS and Ca^{2+} signal to the non-sea salt (nss) Ca^{2+} signal of the EDML ice core, clearly identifying atmospheric circulation as means of distribution. Comparison of additional proxies also excludes major influence by volcanic sources, sea-ice, icebergs, or oceanic current transport. The close resemblance of the dust proxies over the last glacial cycle, in turn, allows for the establishment of an age model of unprecedented resolution and precision for SO deep-sea sediment because atmospheric transport involves no major leads or lags. This is of particular importance because MS is routinely measured on deep-sea cores in the SO but the sediments usually lack biogenic carbonate and therefore had only limited stratigraphic control so far.

Southern South America (SSA) is the likely source of eolian material because Site MD07-3133, located closer to the continent, has slightly higher MS values than Site MD07-3134, and also the MS record of Patagonian Site SALSA shows comparable variability. Patagonia was the dust source for both the Scotia Sea and East Antarctica. Dust fluxes were several times higher during glacial times, when atmospheric circulation was either stronger or shifted in latitude, sea level was lowered, shelf surfaces were exposed, and environmental conditions in SSA were dominated by glaciers and extended outwash plains. Hence, MS records of SO deep-sea sediment are reliable tracers of atmospheric circulation, allowing for chronologically-constrained reconstructions of the circum Antarctic paleoclimate history.

© 2012 Elsevier Ltd. All rights reserved.

1. Introduction (Rationale)

Reliable proxies for past atmospheric transport are crucial for paleoclimate studies because aerosol nuclei blown over long distances affect oceanic bioproductivity and cloud cover (Fischer et al., 2007). The amount of wind-blown material also helps identifying potential source regions and reconstructing the intensity of past atmospheric circulation. The long-range transport may also allow for the correlation of sites over large distances, thereby providing a powerful stratigraphic tool. Dust records of Antarctic ice cores yield important information on past atmospheric circulation in the Southern Hemisphere. They are used to evaluate global

circulation models and to infer the paleoenvironmental conditions of the surrounding continents. East Antarctic ice cores (e.g., the European Project for Ice Coring in Antarctica; EPICA Dronning Maud Land; EDML) indicate SSA as a major source of dust during glacial stages of the last glacial cycle (EPICA Community Members, 2006). There, the cold periods provided drier conditions with increased physical weathering and intensified glacial erosion in combination with a more persistent westerly circulation.

Marine sites located in the SO opal belt and close to the Antarctic continent often lack biogenic carbonate because they are located below the relatively shallow carbonate compensation depth (CCD) (e.g., Hillenbrand et al., 2003). Also, dating the bulk insoluble organic carbon closer to the continent is problematic because it may contain old, reworked material (Domack et al., 1999). In addition, the injection of carbon dioxide with low radiocarbon activity from oceanic abyssal reservoirs that were isolated from the atmosphere

* Corresponding author. Tel.: +49 221 470 7316; fax: +49 221 470 1663.
E-mail address: michael.weber@uni-koeln.de (M.E. Weber).

for several thousand years may alter reservoir corrections for ^{14}C ages (Skinner et al., 2010). These stratigraphic problems obstruct paleoclimate reconstruction in SO marine sediment so far.

Accordingly, only a limited number of lower-resolution marine cores indicated dust proxies in SO deep-sea sediment (e.g., Pugh et al., 2009). However, no study has been able to provide a high-resolution chronology showing a one-to-one coupling of signals, thereby ultimately proving the validity of this proxy assignment. We investigated two high-resolution deep-sea cores from the Scotia Sea (sedimentation rates are 0.2–2.1 m/kyr), showing a one-to-one coupling of MS, sampled at decadal resolution, and atmospheric dust over the last glacial cycle.

2. Core location and setting

We retrieved two deep-sea sediment cores from the Scotia Sea during Marion Dufresne (MD) II cruise 160 in March 2007, which are located between the presumed source area of the Patagonian loess (e.g., Haberzettl et al., 2009) and East Antarctica (e.g., the EDML ice core, EPICA Community Members, 2006) to study the dust transport history along the trajectory to the Antarctic continent (Fig. 1) along the Atlantic side of the SO. Sediment sites MD07-3133 (57°26' S, 43°27' W; 3101 m water depth; 32.8 m core length) and MD07-3134 (59°25' S, 41°28' W; 3663 m water depth; 58.2 m core length) from the southern part of the central Scotia Sea belong to the northern end of Dove Basin and Pirie Bank, respectively (Fig. 1). The sites are situated in the prolongation of the so-called "iceberg alley" (Anderson and Andrews, 1999), a zone where

icebergs calving from the margins of the Weddell Sea and further east merge with icebergs coming from the West, follow the cyclonic, wind-driven movement of all water masses (Carmack and Foster, 1977; Gordon et al., 1981). Most of the icebergs exit the Weddell Sea to the north (Pudsey and Howe, 1998) along with deep-water passing through gaps into the South Scotia Ridge (Reid et al., 1977).

The Antarctic Circumpolar Current (ACC) dominates oceanic circulation in the Scotia Sea. With a transport volume of roughly 140 Sverdrup ($1 \text{ Sv} = 10^6 \text{ m}^3/\text{s}$) it is the largest current on the planet (Pugh et al., 2009) and the only one connecting the Atlantic, Indic, and Pacific (Maldonado et al., 2003), thereby allowing for an exchange of salt and nutrients among the oceans. The main water mass of the ACC is Circumpolar Deep Water (CDW), a mixture of North Atlantic Deep Water (NADW), Antarctic Bottom Water (AABW), and Antarctic Intermediate Water (AAIW) (e.g., Mantyla and Reid, 1983). The ACC flows west to east and is mainly wind-driven between 45 and 55° S. Therefore, it provides a major oceanic atmospheric link which exhibits global teleconnections (Anderson et al., 2009).

Atmospheric circulation in the Scotia Sea is dominated by cyclonic transport within the Southern Hemisphere Westerlies (SHW), which cover a wide latitudinal range from 40 to 70° S and show highest wind speeds between 45 and 50° S (Toggweiler and Russell, 2008). Towards Antarctica, polar easterlies prevail with anti-cyclonic atmospheric circulation (Iriondo, 2000). For Antarctic ice cores dust particle concentration as well as nssCa^{2+} flux are used to trace atmospheric circulation (Lambert et al., 2011).

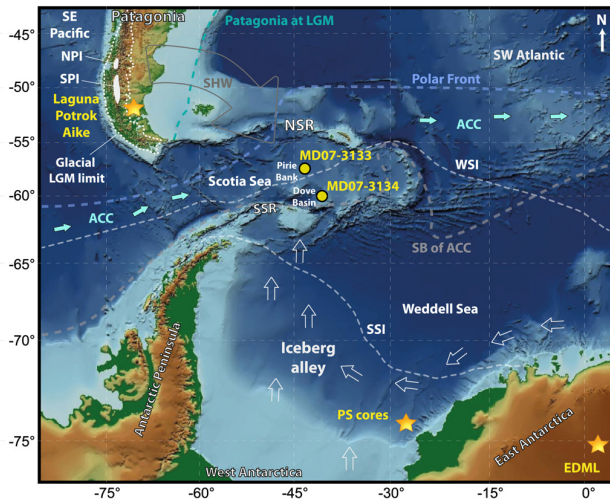


Fig. 1. Location map. Sites MD07-3133 and MD07-3134 are located in the central Scotia Sea. White arrows refer to "iceberg alley" of Anderson and Andrews (1999). Laguna Potrok Aike refers to Patagonian lake record (Haberzettl et al., 2009). Gray arrow indicates the main wind direction of Southern Hemisphere Westerlies (SHW). Turquoise dashed line shows the extent of Patagonia at the last glacial maximum (LGM) (Iriondo, 2000). White dotted line indicates the limit of Patagonian ice sheet during the LGM (Hein et al., 2010). Polar Front (PF) is shown by blue dashed line and Southern Boundary of Antarctic Circumpolar Current (SB of ACC) is indicated by gray dashed line (Diekmann et al., 2000). The white lines describe the winter (WSI) and summer (SSI) sea-ice extent (Gersonde et al., 2005). PS cores refer to studies of Weber et al. (1994, 2010). NPI and SPI are Northern and Southern Patagonian icefield; NSR and SSR are North and South Scotia Ridge. (For interpretation of the references to color in this figure legend, the reader is referred to the web version of this article.)

3. Analytical methods

Sediment physical properties were measured non-destructively at 1-cm increments on whole and split cores using a Multi-Sensor-Core Logger (MSCL; method see Weber et al., 1997). We determined wet-bulk density (WBD), compressional wave velocity (V_p), and MS (kappa volume specific, with C and F sensor). Using an iteration procedure described in Weber et al. (1997), we calculated water content, porosity, and dry bulk density (DBD) by applying specific mass attenuation coefficients to each measurement to account for varying water content and grain densities. We also corrected the density measurements for the salinity of the interstitial fluid to reduce the error in calculating DBD to less than 2%.

We also determined the distribution of chemical elements non-destructively using an AVAATECH X-ray Fluorescence Core Scanner (XRF-CS) (Jansen et al., 1998). In this paper, we concentrate on Ca elemental XRF peak area intensities measured in total counts per second (cps). Following the methods of Richter et al. (2006), we performed the analysis using a sample spot of 1 by 1 cm in size at 1-cm increments.

To obtain further stratigraphic information, we used a pass-through cryogenic magnetometer from 2-G Enterprises (Rolf, 2000) with an embedded AF demagnetizer (max. 30 mT) to determine the natural remanent magnetization (NRM) at the magnetic laboratory of the Leibniz Institute for Applied Geophysics (LIAG) in Einbeck (Grubenhagen, Germany), where we also measured MS at 0.5-cm increments by employing a long core susceptibility logger from Magnon GmbH (Germany).

As demonstrated by several publications (Tauxe, 1993; Kissel and Laj, 2004; Yamazaki and Kanamatsu, 2007; Hambach et al., 2008), under suitable conditions (e.g. homogeneity of rock magnetic parameters) sediments can preserve continuous records of paleointensity variations. The magnetization intensity of sediments is not only proportional to the concentration of magnetic particles but also to their degree of alignment with the ambient geomagnetic field (Nowaczyk and Frederichs, 1999). Therefore, normalizing the NRM intensity after demagnetization (to eliminate viscous overprints) by concentration-dependent parameters such as MS, should lead to records that reflect essentially the variation of the intensity of the geomagnetic field. This assumption is only true if the grain size of the magnetic effective minerals throughout the sediment is almost homogenous because MS does not only depend on concentration but also on grain-size. We measured relative paleointensities at 1-cm increments and used it as a further means of stratigraphic control.

We also used a Minolta spectrophotometer CM-2002 to measure L^* , a^* , and b^* color components (method see Weber, 1998) at 1-cm increments. In addition, we determined the amount of biogenic opal (BSi), using the leaching method of Müller and Schneider (1993), and correcting the primary results of biogenic silicon by adding 10 wt % H_2O to account for the water bound in the amorphous opal skeleton ($BSi = BSi_{MMS} + 10\% H_2O$). A correction of the mass % due to the high salt concentration in the freeze-dried samples was applied as well. Since this method is time-consuming and expensive, we used it only on specific sections that exhibit large-amplitude fluctuations. Finally, we counted all particles >1 mm in diameter on x-radiographs on a 1 by 1 cm grid (principal method see Grobe, 1987) as an indicator of the content of ice-rafted debris (IRD).

High-resolution paleoclimate proxies were then obtained through a combination of traditional analytical means and state-of-the-art core logging techniques of physical (MSCL) and optical (spectrophotometer) measurements (Weber, 1998). We used AnalySeries software (Paillard, 1996) to perform tuning experiments and to construct high-resolution age–depth models. Also, we

calculated orbital insolation values, using the solutions provided by Laskar et al. (2004).

4. Sediment composition and ground-truth stratigraphy

Sediment composition strongly varies with climate conditions (Weber and Piasas, 1999). Deep-sea sediments can be considered a three-component system, consisting primarily of biogenic carbonate, BSi and detrital components (e.g., clay minerals, quartz, etc.). Scotia Sea Sites MD07-3133 and MD07-3134 are located well below the CCD, i.e., the sediments are more or less carbonate free and consist primarily of BSi (mainly diatoms) and detrital material.

BSi-rich, unconsolidated sediments exhibit extremely high porosities because interstitial fluid rests both within the shells (intragranular) and in the pore space (intergranular). Accordingly, water contents are also very high, whereas WBD and DBD are extremely low, also because BSi has lower grain densities than detrital material (Weber et al., 1997). The negative correlation between WBD and BSi follows sediment-physical laws and is hence generally valid. For the Scotia Sea sites it is so striking ($r = 0.9$) that 90% of the variability documented for BSi can be expressed by changes in WBD. In addition, WBD and V_p are negatively correlated. Low-density, high-velocity sections are also indicative for high amounts of BSi, an observation that has been made globally for non-compacted ocean sediments (Weber et al., 1997). Also, the b^* value of sediment color shows a positive linear correlation to BSi ($r = 0.85$), i.e., the yellower the sediment, the higher the amount of BSi. Since opal leaching measurements are very time consuming, we restricted initial measurements to some major transitions in the record and used WBD and color b^* as high-resolution BSi proxies.

The production of BSi and the related carbon sink is an important part of the climate system and 50–75% of the global burial occurs in the “opal belt” of the SO (Nelson et al., 1995). Although the mechanisms are not fully understood, sedimentary cycles in the SO are dominated by changes in BSi on glacial-to-interglacial time scales (Diekmann, 2007). South of the Antarctic Polar Front (APF), sediments show higher interglacial and lower glacial contents (Pudsey and Howe, 1998). Glacial to interglacial changes in the SO are associated with latitudinal shifts of the frontal systems (Toggweiler, 2009), leading to substantial changes in the upwelling associated with BSi-rich waters (Anderson et al., 2009).

We used these major changes to apply a first, low-resolution age model to the BSi proxy (WBD and color b^*) records of Site MD07-3134 (Fig. 2), containing the MIS boundaries of the orbital time scale according to Lisiecki and Raymo (2005). As a result, Marine Isotopic Stage (MIS) boundaries 5/4 (71 ka), 4/3 (57 ka), 3/2 (29 ka), and 2/1 (14 ka) comply with 46, 38.5, 16.5, and 11 m core depth, respectively. This stratigraphic assignment is also reflected in fundamental changes in sediment facies, which, in turn, is documented by changing proportions of BSi and detrital material. Warm climatic periods (MIS 5 and 1) show homogenous, olive gray to yellowish diatomaceous ooze, cold periods (MIS 4 and 2) indicate gray to blue–gray diatom-bearing mud, and MIS 3 mostly reveals olive-gray diatomaceous mud.

Relative paleointensity of Site MD07-3134 is generally low with a poor signal-to-noise ratio, specifically in the lowermost and uppermost parts of the record. This is due to the poor signal preservation in diatom-rich sediment since the carrier of the MS signal is usually fine-grained detrital material. However, comparison to the global paleointensity stack (GLOPIIS, Laj et al., 2004) over the last 75 kyr, reveals some common trends despite the difference that the GLOPIIS record contains higher amplitudes and more structured long-term trends (Fig. 2). One specific drop around 24 m

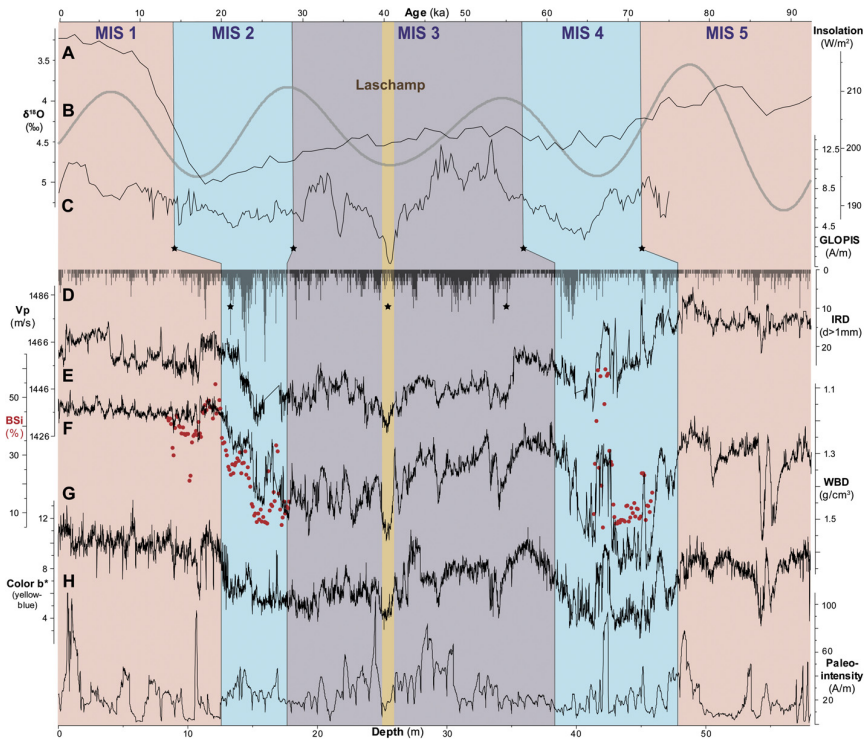


Fig. 2. Ground-truth chronology of Site MD07-3134 displayed versus sediment depth. Upper panel shows global $\delta^{18}\text{O}$ record (A) of Lisiecki and Raymo (2005); spring (September) insolation at 59°S (B) (Laskar et al., 2004); and GLOPIS (C) paleointensity stack (Laj et al., 2004) vs age for the last 92.5 kyr. Lower panel gives content of ice-rafted debris (D; IRD $>1\text{ mm}$; gray histogram lines); Biogenic opal (BSi) proxies p-wave velocity (Vp; E), wet-bulk density (WBD; F), and sediment color b^* (G); measured BSi (red dots); and relative paleointensity (H). Note that assignment to Marine Isotopic Stages (MIS) relies on WBD and color b^* changes relative to global $\delta^{18}\text{O}$ changes. The Laschamp event (Guillou et al., 2004) is indicated as a significant drop in relative paleointensity (orange bar). Black stars refer to ground-truth data points used to develop the age model (see text for details). Underlain color pattern refers to MIS. (For interpretation of the references to color in this figure legend, the reader is referred to the web version of this article.)

is considered the Laschamp Event ($40.4 \pm 1.1\text{ ka}$; Guillou et al., 2004). This age control point was added to the low-resolution age model of Site MD07-3134.

Further stratigraphic evidence comes from volcanic ashes. We detected rather massive layers rich in IRD, e.g., at Site MD07-3134 in 8.9, 13.36, 34.17, and 43.88 m core depth. Kanfoush et al. (2000) dated such layers, correlated them across the Southern Atlantic (SA), and named them SA0 (ca 14–15 ka) to SA6 (ca 55 ka). Nielsen et al. (2007) demonstrated that the material was of volcanic origin. For Site MD07-3134, volcanic layers SA0 and SA6 were found in 13.36 and 34.17 m core depth, respectively. The detection of these two layers further supports the independent MIS ground-truth assignment based on BSi changes because SA6 is just a little younger than MIS boundary 4/3, and SA0 is exactly as old as MIS boundary 2/1.

5. Tuned chronology and high-resolution age model

Using the seven control points of the ground-truth age model (four MIS boundary control points, the Laschamp Event, and two ash layer ages), we converted the depth scale of Site MD07-3134 into an age scale. For reasons explained in Chapter 7, our tuning target is the nssCa^{2+} flux record of the EDML ice core (Fischer, 2008), a confident indicator of atmospheric dust transport. The close resemblance of the nssCa^{2+} flux record and the MS record of Site MD07-3134 on this preliminary time scale is striking and provides further evidence for the validity of the ground-truth stratigraphy. It documents, with slight temporal shifts, a one-to-one reproduction of virtually every single increase during the last glacial cycle. This strong correlation allows for further fine-tuning of the record to nssCa^{2+} flux within the boundaries given by the ground-truth stratigraphy. We applied three

stratigraphic approaches to produce a tuned, high-resolution age model, evaluate its quality, and provide error estimates: (i) manual picking of tie points, (ii) an automated pattern-matching algorithm, and (iii) a smoothing spline regression using the manual tie points.

For the first and basic approach, we used AnalySeries (version 2.0.4.2.; Paillard, 1996), a highly iterative software that displays four windows, to perform tuning experiments. Window 1 is used to manually pick tie points from the graphical display of the record (MD07-3134; displayed versus depth) that correlate best with the target (EDML; displayed versus age). The remaining windows calculate, in real time, various statistics and display them graphically with updates every time new tie points are selected. Window 2 displays the record curve on top of the target curve versus age.

Hence, the graphical correlation is immediately visualized and can be changed iteratively for optimization. Windows 3 and 4 display the depth–age structure and the development of sedimentation rates throughout the record, respectively, and are also helpful for evaluating the legitimacy of the tuning procedure. After carefully optimizing the visual fit by using all (and only) significant correlations (either minima or maxima in the records), we established 48 confident age control points (Fig. 3) for the last 92.5 kyr that provide the best fit between record and target.

The very close match of record and target proves a common mechanism of formation. The resulting correlation coefficient from manually assigned tie points is $r > 0.9$ for elevated signals, and $r = 0.85$ for the entire record. Accordingly, the correlation is very

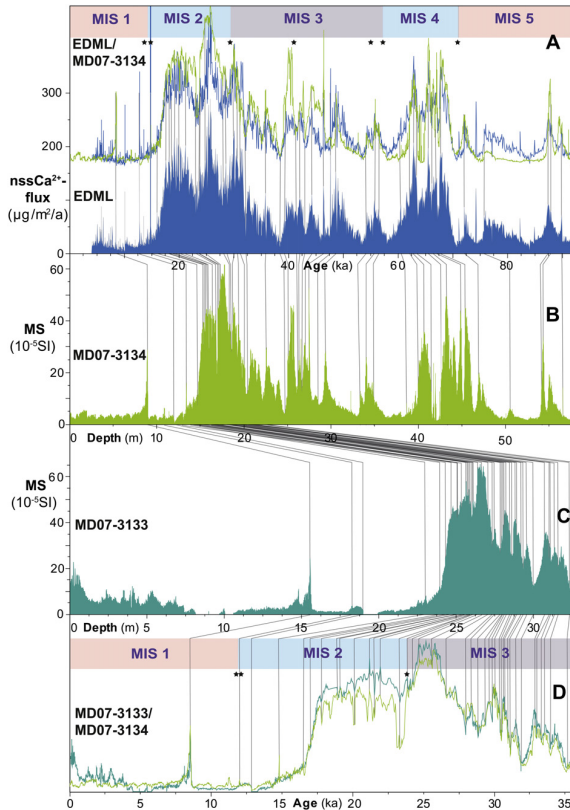


Fig. 3. Correlation of (A) EDML $nssCa^{2+}$ -flux (Fischer, 2008) on EDML1/EDC3 time scale (Parrenin et al., 2007; Ruth et al., 2007) and magnetic susceptibility (MS) records of Sites MD07-3134 and MD07-3133. Correlation lines mark tuned tie points to convert sediment depth of Sites MD07-3134 (B) and MD07-3133 (C) to calendar ages using AnalySeries 2.0.4.2 (Paillard, 1996). (D) shows correlation of MS records of Sites MD07-3133 and MD07-3134. Black stars refer to ground-truth data points (see text for details). Underlain color pattern refers to Marine Isotopic Stages (MIS). (For interpretation of the references to color in this figure legend, the reader is referred to the web version of this article.)

robust for higher contents and usually, these intervals display closer-spaced age control points. However, when both signals decrease, the correlation becomes less striking.

The second approach follows the idea of evaluating the chronology by independent measures in order to test for common traps and circularities of (manual) tuning. Common tools are dynamic time wrapping (DTW) algorithms (e.g., Giorgino, 2009), which compute a time axis stretch and map two time series optimally by minimizing the cumulative distance. Since these methods are built for various, mostly technical applications, matching high-resolution time series of MS and $nssCa^{2+}$ flux requires a detailed setup of windowing functions, step patterns, etc. Here, we used a Rabiner–Juang step pattern and LOESS smoothing with a span (degree of smoothing) of 0.025 in order to remove minor subscale noise that deterministic DTW algorithms cannot handle. Results coincide with manually picked tie points throughout most parts of the record and with only slight deviations at 10–15 ka and at 75–85 ka (Fig. 4A), which can be seen as independent verification of the tuning procedure. However, the DTW algorithm still

represents a deterministic point of view and the results strongly depend on the various options that have to be set a priori. Since this is clearly a limiting factor, the final age–depth model is therefore built on a more robust approach that also accounts for uncertainties.

The third approach applies a cubic smoothing spline (e.g., Hastie and Tibshirani, 1990) to the age control points (Fig. 3) that were picked manually. It overcomes the problem of traditional splines, which may produce extreme outliers and artefacts due to the fact that the observations are treated deterministic, i.e. without error. The smoothing factor has been set to 0.25, which allows for (partial) leads and lags between the two time series, albeit not for an overall bias. In order to estimate the uncertainty in this model, especially the identification of tie points, we generated 500 replicates by ordinary non-parametric bootstrap re-sampling (Efron and Tibshirani, 1994). Fig. 4A shows the resulting age–depth model in terms of median, interquartile range, and 0.05/0.95 quantiles. The bootstrap correlation for the time series of MS and $nssCa^{2+}$ flux is 0.843 for the median and within a 95% uncertainty range of [0.821,

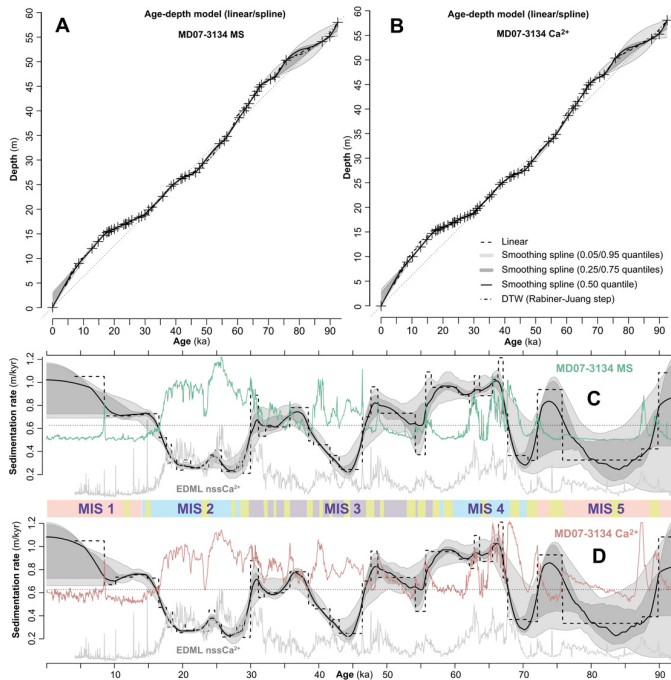


Fig. 4. Top shows age–depth models based on the correlation of EDML $nssCa^{2+}$ flux to MD07-3134 MS (A) and to MD07-3134 Ca^{2+} (B) using a smoothing spline (solid) with bootstrap estimates of uncertainty (gray shading). Tie points (+) as well as results from a stepwise linear model (dashed) and from a dynamic time wrapping (DTW) algorithm (dash-dot) are shown for comparison. Age plots underneath give sedimentation rates for MD07-3134 MS (C) and MD07-3134 Ca^{2+} (D), corresponding to the different age–depth models provided by A and B. Solid line shows median. Gray areas mark uncertainties in terms of quantile ranges as obtained from bootstrap re-sampling. Background curves are shown for reference only. They represent MD07-3134 records of MS (green) and Ca^{2+} (red) at the top and EDML $nssCa^{2+}$ flux (gray) (Fischer, 2008) at the bottom (in relative units). Underlain color pattern is explained in Fig. 5. (For interpretation of the references to color in this figure legend, the reader is referred to the web version of this article.)

0.856]. However, the correlation coefficient should be interpreted carefully when matching time series since it neither accounts for autocorrelation in both time series nor for the reduced degrees of freedom due to the definition of tie points.

The corresponding sedimentation rates vary from approximately 0.2 m/kyr to 1.2 m/kyr (Fig. 5E). Note that the uncertainty ranges are narrow compared to the temporal variation in most parts of the time series and naturally become wider in sections with fewer tie points (usually those with MS and nssCa^{2+} flux values), indicating a more uncertain definition of the sedimentation rate.

Finally, the question arises if the robustness of the technique could be evaluated by using different records. Therefore, we also applied the three approaches described above to the Ca^{2+} record of site MD07-3134 that has been generated by XRF scanning techniques, instead of the MS record, and the nssCa^{2+} flux record of the EDML ice core. For Site MD07-3134, MS and Ca^{2+} records show a correlation coefficient of $r = 0.88$. The resulting age–depth relation and the sedimentation rates including their uncertainty

estimates are almost identical relative to those given by the MS tuning, whereas the bootstrap correlation slightly drops to 0.806 for the median with 95% uncertainty ranges of [0.706,0.827]. As a conclusion, we summarize that both age–depth model and sedimentation rates are well defined by the smoothing spline approach, with uncertainties given in Fig. 4.

From the various supply mechanisms proposed for the MS signal (a detailed analysis will follow in Chapter 7), only atmospheric circulation remains (a thorough discussion of this conclusion will follow in Chapter 8), which also has significant implications for the quality and reliability of the age model. The fact that we more or less phase-lock nssCa^{2+} flux with both the MS and Ca^{2+} signals during this procedure is therefore reasonable because dust transport from Patagonia to Antarctica takes only about a week (Li et al., 2010). Therefore, no major leads or lags should be involved for atmospheric transport. Accordingly, our chronology provides a precise and high-resolution age model of unprecedented confidence and resolution for SO deep-sea sediment.

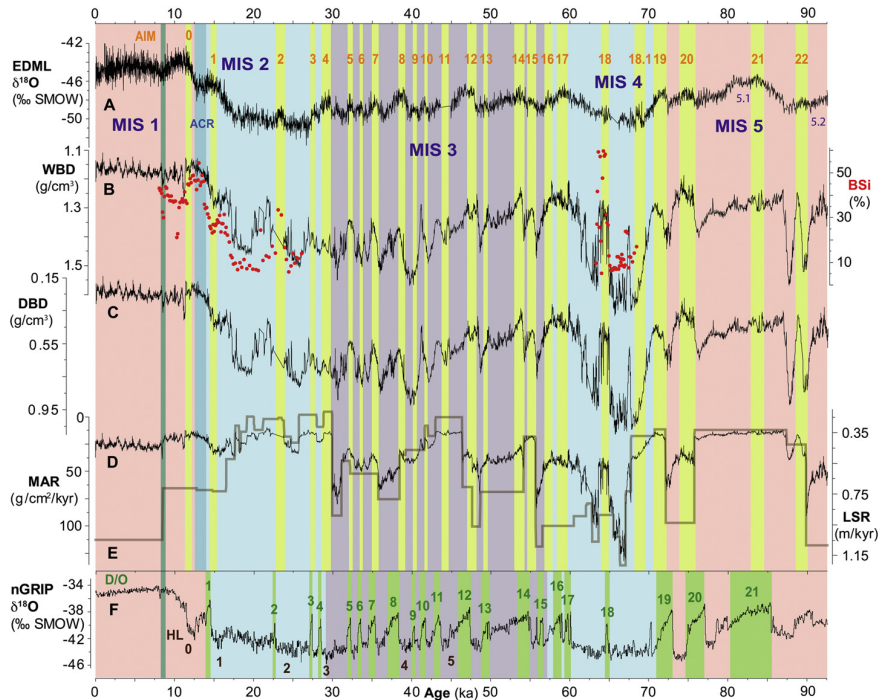


Fig. 5. Paleoclimate records at site MD07-3134 for the last 92.5 kyr. A is EDML $\delta^{18}\text{O}$ (EPICA Community Members, 2006). B–E are records of Site MD07-3134; B is wet-bulk density (WBD) and measured biogenic opal (BSi) (red circles); C shows dry-bulk density (DBD); D is mass accumulation rate (MAR; black plotted on top of E (linear sedimentation rate; LSR; bold brown); F refers to Northern Hemisphere nGRIP $\delta^{18}\text{O}$ (NGRIP Members, 2004) for comparison. The underlain pattern consists of Marine Isotopic Stages (MIS) 5–1 (Lisiecki and Raymo, 2005), Antarctic Isotopic Maxima (AIM; yellow) 22–0 (EPICA Community Members, 2006), Antarctic Cold Reversal (ACR; dark blue), Heinrich Layers (HL; brown) (Rahmstorf, 2002), Dansgaard–Oeschger–Cycles (D/O; green) (Blunier and Brook, 2001), and 8.2 event (turquoise) (Roehling and Pälike, 2005). (For interpretation of the references to color in this figure legend, the reader is referred to the web version of this article.)

In a last step, we applied the same stratigraphic approaches to Site MD07-3133 and fine-tuned the MS record to the one of Site MD07-3134 implementing 48 age control points for the last 36 kyr (Fig. 3). High-resolution time series could have been obtained from BSI proxy records (WBD and Vp). These proxies show a pattern that contains characteristics of the $\delta^{18}\text{O}$ time series from EDMIL (EPICA Community Members, 2006) and nGRIP (nGRIP Members, 2004), both on orbital and suborbital time scales (Fig. 5). Nonetheless, the resemblance is not as striking as for MS and nssCa^{2+} flux, and the two $\delta^{18}\text{O}$ time series from the polar ice sheets are phase-shifted, probably related to temporal changes in oceanic heat transport between the hemispheres (EPICA Community Members, 2006). Because of these uncertainties on millennial time scales, we abandoned the option to use BSI as a tuning record. However, these ambiguities are not given for MS and nssCa^{2+} flux (see discussion in Chapter 7).

We calculated mass accumulation rates (MAR; $\text{g}/\text{cm}^2/\text{kyr}$) by multiplying LSR (cm/kyr) with DBD (g/cm^3). Average LSR are high, ranging from 0.2 to 1.2 m/kyr and from 0.3 to 2.1 m/kyr for Sites MD07-3134 and MD07-3133, translating into MAR of 10–120 $\text{g}/\text{cm}^2/\text{kyr}$ and 15–170 $\text{g}/\text{cm}^2/\text{kyr}$, and into sample resolution of 50–8 years and 33–5 years (given a sample increment of 1 cm), respectively. The detailed LSR and MAR structure of Site MD07-3134 (Fig. 5) shows a complicated pattern with intermediate values during MIS 5, high values during late MIS 4 and early MIS 3, lowest values during late MIS 3 and early MIS 2, and high values again during the Holocene. There is no linear relationship with orbital-scale variations, e.g., the Holocene shows high values, whereas MIS 5 indicates low values. Also, MAR are highest during MIS 4 and lowest during MIS 2. Although MIS 1 sections of Sites MD07-3133 and MD07-3134 have high LSR and visually appear as diatom oozes (with BSI contents $\geq 40\%$), their DBD are extremely low and hence Holocene MAR are not higher than those during MIS 4 and early MIS 3, where DBD are much higher.

6. Supply mechanism for magnetic susceptibility

In order to evaluate the possible supply mechanisms for the MS signal, we have to consider iceberg transport, oceanic circulation, volcanic sources, sea-ice distribution, and atmospheric circulation. We used IRD as an indicator for iceberg transport. One has to be careful when adopting this approach. For instance, Kanfoush et al. (2000) used IRD to deduce Antarctic ice-sheet instability during the last glacial cycle from deep-sea cores across the Polar Frontal Zone. However, Nielsen et al. (2007) demonstrated that the IRD material was of volcanic origin, probably from the South Sandwich Islands, and concluded that sea-ice transported it. We also detected some of these IRD-rich layers (e.g., at Site MD07-3134 in 8.9 m, 13.36 m (layer SA0 according to Kanfoush et al., 2000), 34.17 m (layer SA6), and 43.88 m depth; see also above discussion on the age model), but they are distinct and massive, whereas the IRD curve that we have produced consists mainly of small grains (1–3 mm in size) in a dispersed, diatom- or clay-rich matrix. Therefore, we are confident that the IRD records of Sites MD07-3133 and MD07-3134 can be used as a reliable tracer of long-lasting (centuries to millennia) phases of enhanced iceberg fluxes from the Antarctic Ice Sheet.

This interpretation is corroborated by the fact that the central Scotia Sea is located in the prolongation of the so-called “iceberg alley” (Anderson and Andrews, 1999), a zone where icebergs calving from the margins of the Weddell Sea merge and follow the cyclonic, wind-driven movement of all water masses (Carmack and Foster, 1977; Gordon et al., 1981). Most of the icebergs exit the Weddell Sea to the north (Pudsey and Howe, 1998) along with deep-water passing through gaps into the South Scotia Ridge (Reid et al., 1977), before they reach Sites MD07-3133 and MD07-3134. Therefore, the Antarctic Ice Sheet can be considered the primary source of IRD.

The temporal distribution of IRD displays a complicated pattern of enhanced phases of iceberg transport of unequal length and amplitude (Fig. 6). Some of the major amplitudes are concentrated on deglaciation periods during the later half of MIS 4 and MIS 2. Also, some longer stadial intervals during MIS 3 contain higher values, whereas interglacial periods MIS 5 and MIS 1 show lower contents. However, the IRD pattern shows virtually no resemblance to the MS curve, i.e. icebergs can be excluded as a primary means of transporting and delivering the MS signal.

Besides icebergs, **oceanic circulation** could be important. Earlier studies (Diekmann et al., 2000) emphasized that current transport was mainly responsible for dispersal of the MS signal. However, Hofmann (1999) found comparable MS pattern in cores from different current regimes. In addition, the Scotia Sea is isolated from major sediment sources of the continental margins – only the western part is located in the supply areas of SSA and the Antarctic Peninsula (Maldonado et al., 2003). Therefore, oceanic circulation is also unlikely the major supplier of the MS signal. Nonetheless, it might serve as a secondary means of redistribution (Pugh et al., 2009). The MS carrier would most likely be the detrital fraction (mainly clay minerals), whereas biogenic sediment components (mainly carbonate and BSI) unlikely stored, but potentially diluted the signal (Florindo et al., 2003). However, Pugh et al. (2009) showed, by calculating the flux of the specific MS of the detrital component, that signal alteration of kappa was minor in Scotia Sea sediment. Northern hemisphere Heinrich events, for instance, were mostly detected by negative excursions of the MS signal in deep-sea cores, because icebergs released from the Laurentide Ice Sheet carried detrital carbonates from the region off Hudson Strait (e.g., Hemming, 2004). Accordingly, sediment composition will influence the MS record, but not necessarily point to the mechanism of transport.

Another potential transport agent is **sea-ice**. Here, two processes are capable of incorporating and re-locating material. First, turbulent outflow of fine-grained material in high-energy systems such as glacial outwash plains or delta systems can re-suspend material. In case of rapid cooling, this hypopycnal sediment lobe would be incorporated into the freezing sea-ice (frazil ice). Also, due to turbulence, sinking ice particles can incorporate material from the bottom of shallow shelf areas (Reimnitz et al., 1987). This process, often promoted by strong winds, is well known from the Arctic region (Kempema et al., 1989). However, Antarctica lacks large shelf areas that are fed by river suspension and therefore frazil ice formation through supercooling of surface waters did likely not include large quantities of fine-grained sediment.

During times of intense sea-ice coverage, however, material delivered by atmospheric processes will first be deposited on the sea-ice. Forced by wind and oceanic circulation, it will drift away from the Patagonian source region along the ACC and eventually rain out into the deep sea in areas of melting (e.g., Nielsen et al., 2007). Since sea-ice in the Antarctic realm only carries material delivered by eolian processes, both sea-ice transport and atmospheric circulation carry the same source material. Therefore, sea-ice formation can be considered a secondary source of sediment transport, although it could only have a minor impact on the Scotia Sea, because there is virtually no correlation between the MS record and the ssNa^+ flux record of the EDMIL ice core, a sea-ice indicator (Fischer et al., 2007) (Fig. 6). We should note that volcanic eruptions also deliver ashes as eolian fallout that will be carried by both atmospheric winds and sea-ice.

7. Magnetic susceptibility as dust indicator

Dust particle concentration records provide direct information on atmospheric transport activity and sediment sources. Unfortunately, these records are hard to decipher in ocean sediment and

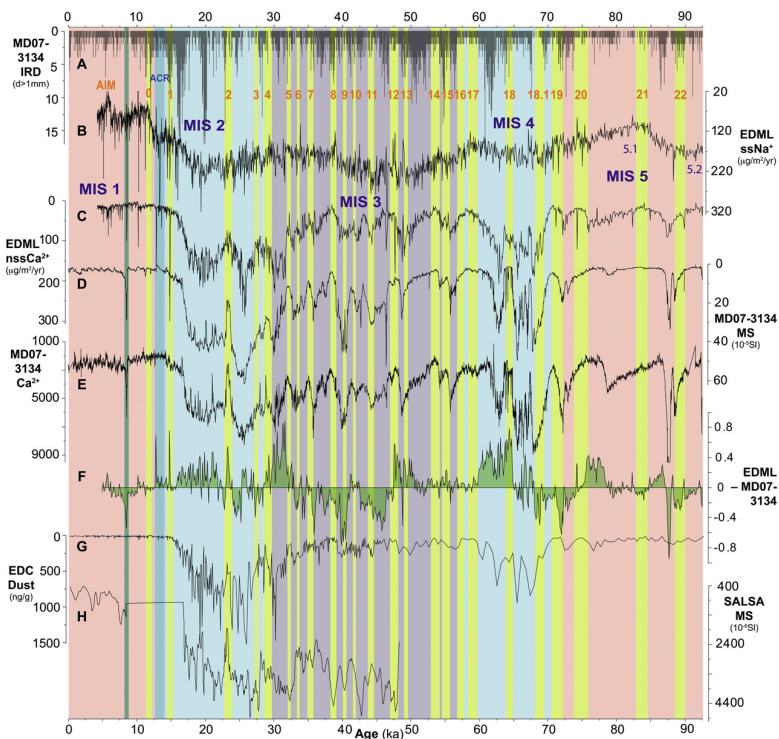


Fig. 6. Atmospheric dust proxies in the Southern Ocean during the last glacial cycle (92.5 ka to present). A shows ice-rafted debris (IRD) (>1 mm; gray histogram lines) content of Site MD07-3134; B and C are EDML ssNa⁺- and nssCa²⁺-flux (Fischer, 2008) on EDML1/EDC3 time scale (Parrenin et al., 2007; Ruth et al., 2007); D and E are records of Site MD07-3134; D is magnetic susceptibility (MS) and E is calcium concentration (Ca²⁺-XRF-CS spectral peak area counts); F shows the residual curve calculated by subtracting normalized MD07-3134 records MS and Ca²⁺ from twice the EDML nssCa²⁺ flux; G displays dust particle concentration of the EDC ice core (Lambert et al., 2011); H refers to MS record of Patagonian maar lake Laguna Potrok Aike (Haberzettl et al., 2009). See Fig. 5 for explanation of underlain pattern.

only available for a limited number of Antarctic ice cores. Fig. 6 displays the dust particle concentration for Epica Dome C (EDC; Lambert et al., 2008), the record with the highest resolution available so far. Ice-core records of nssCa²⁺ flux are confident and well-established indicators for atmospheric dust (e.g., Röthlisberger et al., 2004), specifically during glacial times (Lambert et al., 2011). Also, they are available at very high resolution for a number of Antarctic ice cores.

The close resemble of the MS signal of the deep Scotia Sea Basin and the nssCa²⁺ flux of the EDML ice core (Fig. 3) clearly favors **atmospheric circulation** as the major mechanism of supply. Accordingly, a significant influence through ocean currents, icebergs, and sea-ice (see Chapter 6), can be excluded for the Scotia Sea sites.

Comparison of MS and nssCa²⁺ flux records shows that atmospheric signals documented for the Scotia Sea mostly reached the EDML site (Fig. 6). There were times when amplitudes decreased

significantly along the transport path (e.g., at 46.3, 42.6, and 41–39 ka), and not all signals reached the EDC site (e.g., at 46.4, 32.8 ka). Also, during deglaciation, Scotia Sea and EDML share two spikes that are important for the age model (at 14.8 and 8.5 ka) that do not appear at EDC. These similarities support our effort of tuning the Scotia Sea sites to EDML rather than to a more distant ice core.

The XRF-CS determined Ca²⁺ record of the Scotia Sea cores also resembles the EDML nssCa²⁺ flux record (Fig. 6). Virtually every single increase in the Scotia Sea Ca²⁺ record has counterparts in the nssCa²⁺ flux record from the East Antarctic Ice Sheet (EAIS). The fact that the same chemical element replicates in both archives is another strong argument for atmospheric transport of Ca²⁺. It is also the reason why we conducted tuning experiments using Ca²⁺ (see Chapter 5) in addition to MS. Both Ca²⁺ and MS originate from the carbonate-free detrital sediment fraction (mostly from feldspars) since biogenic carbonate is not present because the Scotia Sea sites are located underneath the CCD.

This finding supports an original concept of Hofmann (1999) who also used MS to infer atmospheric dust transport. It also corroborates the assumption of Pugh et al. (2009) that MS can be used as dust indicator in SO deep-sea sediment that is more or less carbonate free. They inferred the link of MS and Antarctic dust for more than ten lower-sedimentation sites from the Scotia Sea (in the vicinity of Sites MD07-3133 and MD07-3134) on glacial-to-interglacial time scales.

Therefore, one of our main conclusions is that the MS record of our high-resolution sites is a very powerful tool for detailed chronostratigraphic correlation over long distances under the given circumstances, specifically on millennial time scales. Phase-locking nssCa^{2+} flux and MS is reasonable because both signals are atmospheric and, hence, no major leads or lags should be involved. Accordingly, chronologies relying on this atmospheric correlation provide precise and high-resolution age models, allowing for detailed comparison of climate signals (see above, and Figs. 5 and 6). This is of particular importance because deep-sea sites in the SO usually lack biogenic carbonate and therefore had only limited stratigraphic control so far.

Dust transport is closely coupled to climatic conditions. Generally, cold periods provide higher temperature gradients between equator and poles, leading to intensified atmospheric circulation (Toggweiler and Russell, 2008). Indeed, our inferred dust input into the Scotia Sea was significantly higher during glacial than during interglacials – up to 10 times during parts of MIS 4 and 2 (also at the end of MIS 3), relative to MIS 5 and 1 (Fig. 6). Dust input into Antarctic ice cores followed the same pattern with higher fluxes during glacial periods (Fischer et al., 2007; Lambert et al., 2008). The same co-variance is documented for millennial-scale variability. Colder phases between Antarctic Isotopic Maxima (AIM) indicate elevated contents, whereas most AIM show reduced dust concentrations (specifically AIM 20, 18, 14, 12, 8, 7, 5, 3, and 1; Fig. 6).

Site MD07-3133 has, on average, higher amplitudes of variability with elevated contents during glacial stages relative to Site MD07-3134 because it is located closer to the Patagonian source area. We examined the difference between the Scotia Sea and the EAIS by re-sampling the EDML nssCa^{2+} flux and MD07-3134 MS and Ca^{2+} records at 0.1 kyr increments, scaling each record to unit variance, and subtracting the two Scotia Sea records from twice the EAIS record (see Fig. 6F). The residual curve does not exhibit any long-term trend, thus the mean difference of atmospheric transport remained constant over glacial-to-interglacial cycles between the two areas. A constant dust source was also inferred by Basile et al. (1997) and Delmonte et al. (2010) for several glacial cycles. There is no systematic assignment of lows and highs to AIM; however there seems to be a common trend with higher relative EAIS dust contents (positive values) toward the end of MIS 5 and 3, declining to strongly negative values (higher relative dust in the Scotia Sea) at the beginning of MIS 4 and 2, and switching back to positive values for the remaining parts of glacial MIS 4 and 2, respectively. There are also a few distinct events that may be unrelated to atmospheric transport, e.g., clear Scotia Sea signals around 88 ka and in the vicinity of the Laschamp Event (around 40 ka), and higher EAIS contents around 32–30 ka.

8. Patagonia as dust supplier during the last glacial Cycle

SSA is the only large southern landmass within the dominating SHW. It is therefore natural to assume that Patagonia is the source for Antarctic dust. According to Iriondo (2000), cyclonic winds reaching Patagonia will rise several km on the western side of the Andes, lose their moisture, and carry large amounts of fine-grained sand and silt to the dry East Patagonian low lands (humidity is $\leq 5\%$). These high-pressure cyclonic systems in the

upper troposphere move east and southeast, with possible influence as far as 80° S. They are compensated by Antarctic anticyclonic movement, which sinks air and aerosols to the surface on the Antarctic continent.

Li et al. (2010) conducted trajectory studies and identified two Patagonian dust sources with the southernmost area around San Julian's Great Depression as the dominant dust source. Transport to East Antarctica takes about 7 days and is driven by eastward moving low-pressure systems. Since the Scotia Sea sites are located in the trajectory of atmospheric transport from SSA to East Antarctica, we see strong evidence that the eolian record of Sites MD07-3133 and MD07-3134 also originated from Patagonia. This interpretation is corroborated by the fact that MD07-3133, which is located a couple of hundred km closer to the presumed source area, has slightly higher MS contents than Site MD07-3134 (Fig. 3). Hofmann (1999) found similar indications for Scotia Sea sites. Also, Fischer et al. (2007) attributed the threefold higher dust content of EDML relative to EDC to the smaller distance to the SSA source region. The MS records from Site MD07-3134 and Patagonian lake Laguna Potrok Aike (Haberzettl et al., 2009) show common features during deglaciation. For that period, commonalities are also evident relative to the dust content of EDC (Fig. 6). However, the glacial part of the lake record indicates that probably additional processes influence the Patagonian record. Furthermore, their glacial chronology is less constrained (Haberzettl et al., 2009).

Kaiser and Lamy (2010) studied the terrigenous supply at ODP Site 1233 located off southern Chile. They argue that dust fluctuations were largely controlled by environmental changes in SSA. From the study of glacial outwash plains in Patagonia, Sugden et al. (2009) also conclude that the amount of atmospheric dust depends on the glacial conditions. During the sea-level low stand of the last glacial maximum (LGM), when sea level was about 130 m lower than today (Huybrechts, 2002), large portions of the Argentine Shelf were exposed, in fact, the Patagonian land area had almost doubled (Iriondo, 2000) in size (see also Fig. 1). Physical weathering (e.g., frost wedging) prevailed on the ice-free glacial outwash plains that received the debris of the Andes, and large loess areas formed. Accordingly, dry and cold climate, strong west winds, and large areas of fine-grained sediment made the East Patagonian low lands an ideal source area for atmospheric dust (Sugden et al., 2009). Vice versa, during sea-level high stands, the source area for dust supply was significantly reduced. This would explain the strong dependence of atmospheric dust concentration in the SO on Milankovitch forcing, primarily on the 100-kyr eccentricity cycle. The availability (or unavailability) of pro-glacial lakes could also provide an on/off switch for some of the higher-amplitude dust peaks on millennial time scales detected at Site MD07-3134 (e.g., around 25, 30, 36, 40, 44, 46, 49, 56, 63, 66, 67, 68, 72, 87, and 89 ka).

Using atmospheric modeling, Toggweiler et al. (2006) postulate that the SHW shifted north by as much as $7-10^\circ$ during cold climatic periods. This would imply that the strongest westerlies were located over Patagonia only during glacial times. Around 17 ka, SHW started to shift south during the early part of deglaciation (Toggweiler et al., 2006; Lamy et al., 2007; Toggweiler, 2009), so Patagonia was no longer in the center of high wind speeds. Dust concentrations also dropped substantially to interglacial levels at 17–16 ka, both in the Scotia Sea and over East Antarctica. This change occurred during a time of enhanced temperature rise documented for East Antarctic ice cores (EPICA Community Members, 2006) and was probably associated with the redistribution of heat between the hemispheres caused by a reduction in the Atlantic meridional overturning circulation (Stocker and Johnson, 2003; Weber et al., 2011). Also, glaciers in Patagonia started to retreat rapidly at 16.5–15 ka (Hein et al., 2010). The shift of the SHW probably involved upwelling of CO_2 -rich deep water that accompanied atmospheric warming (Andersen

et al., 2009). These major environmental and climatic changes reduced the availability of dust in the Patagonian source areas.

Dust provenance studies from East Antarctic ice cores indicate Patagonia as the main dust supplier through the last glacial cycle (EPICA Community Members, 2006) and through the last 800 kyr (Delmonte et al., 2010). Delmonte et al. (2004) report a 10–30 times higher dust flux during the LGM relative to the Holocene for Antarctic ice cores. Accordingly, for warm climatic periods atmospheric dust contents were significantly lower. For these times, the correlation of MS and nssCa^{2+} flux in our Scotia Sea sites is rather insignificant and the dust source might be much more debatable. Based on magnetic studies, Lanci et al. (2008) propose changing dust provenances between glacial and interglacials. Revel-Rolland et al. (2006) call for Australia as the dominant dust source for interglacials using isotopic composition changes, whereas Gabrielli et al. (2010) argue, based on rare earth element analysis, for a combination of various dust source areas (SSA, Australia, New Zealand, and South Africa).

On the other hand, Lunt and Valdes (2001) argue, based on modeling (trajectory) studies, that dust transport efficiency for particles in East Antarctica is currently higher than it has been during the LGM. This again implies that higher glacial dust concentrations are primarily caused by changing environmental conditions in the source area rather than by changes in atmospheric circulation. Accordingly, they claim Patagonia as dust source during both glacial and interglacial times. In addition, the fact that the SHW did not change direction during glacial and interglacial cycles, argues for dust transport from Patagonia to the Scotia Sea also in recent times.

9. Summary and conclusions

Identification of reliable proxies for past atmospheric transport is crucial for paleoclimate studies in many ways. In this paper, we concentrate on two aspects: the identification of MS as a reliable dust tracer in SO deep-sea cores, and the use of the signal as a powerful stratigraphic tool. Two high-sedimentation sites from the Scotia Sea (MD07-3133 and MD07-3134; sedimentation rates vary 0.3–2.1 m/kyr and 0.2–1.2 m/kyr, respectively) show a one-to-one coupling of the MS and the nssCa^{2+} flux signal of the EDML ice core, clearly identifying atmospheric circulation as means of distribution, and excluding major influence by sea-ice, iceberg, or oceanic current transport. The fact that the same chemical element (Ca^{2+}) also co-varies in Antarctic ice cores and in the Scotia Sea provides a further, strong argument for atmospheric transport. This interpretation has significant implications for the quality and reliability of the age model because atmospheric transport involves no leads or lags on millennial time scales. Accordingly, phase locking of nssCa^{2+} flux with MS and Ca^{2+} is reasonable and the detailed structure of variability allows for the establishment of an age model of unprecedented resolution and confidence for SO deep-sea sediment. This is of particular importance because MS is a standard property measured on most marine sediment cores. Even more importantly, deep-sea sites in the SO usually lack biogenic carbonate and therefore had only limited stratigraphic control so far.

The tight coupling of the two signals over the last glacial cycle shows that both the Scotia Sea and East Antarctica were affected by the same atmospheric circulation system. The resemblance to sites located in Patagonia and the decrease of MS values further away from the continent, favors SSA as the major dust source for the Scotia Sea, specifically during glacial periods, when dust fluxes were much higher during times of low sea-level stands, shelf surfaces were exposed and more glacial environmental conditions existed in SSA. Accordingly, MS records of SO deep-sea sites are reliable tracers of atmospheric circulation that can be used to

confidently establish circum Antarctic teleconnections and study paleoclimate change at both orbital and millennial-scale resolution.

Acknowledgments

We are grateful for financial support from the Deutsche Forschungsgemeinschaft (DFG; grants RI 525/17-1, KU 683/9-1) and the suggestions from three anonymous reviewers. Our study was part of the Southern Ocean Initiative of the International Marine Past Global Change Study (IMAGES) program and the AWI research program “Polar Regions and Coasts in a changing Earth System” (PACES), Topic 3 “Lessons from the Past”. Supplementary data to this paper are available at doi:10.1594/PANGAEA.717904 (<http://doi.pangaea.de/10.1594/PANGAEA.717904>).

References

- Anderson, J.B., Andrews, J.T., 1999. Radiocarbon constraints on ice sheet advance and retreat in the Weddell Sea. *Antarctic Geology* 27, 179–182.
- Anderson, R.F., Ali, S., Bradtmiller, L.L., Nielsen, S.H.H., Fleisher, M.Q., Anderson, B.E., Burckle, L.H., 2009. Wind-driven upwelling in the Southern Ocean and the deglacial rise in atmospheric CO_2 . *Science* 323, 1443–1448.
- Basile, I., Grousset, F.E., Revel, M., Petit, J.R., Biscaye, P.E., Barlow, N.J., 1997. Patagonian origin of glacial dust deposited in East Antarctica (Vostok and Dome C) during glacial stages 2.4 and 6. *Earth and Planetary Science Letters* 146, 573–589.
- Blunier, T., Brook, E.J., 2001. Timing of millennial-scale climate change in Antarctica and Greenland during the last glacial period. *Science* 291, 109–112.
- Carmack, E.C., Foster, T.D., 1977. Water Masses and Circulation in the Weddell Sea. *Delmonte, B., Andersson, P.S., Schöberg, H., Hansson, M., Petit, J.R., Delmas, R., Gaillardet, D.M., Maggi, V., Frezzotti, M.*, 2010. Geographical provenance of aeolian dust in East Antarctica during Pleistocene glaciations: preliminary results from Talos Dome and comparison with East Antarctic and new Andean ice core data. *Quaternary Science Reviews* 29, 256–264.
- Delmonte, B., Petit, J.R., Andersen, K.K., Basile-Doelsch, I., Maggi, V., Ya Lipenkov, V., 2004. Dust size evidence for opposite regional atmospheric circulation changes over east Antarctica during the last climatic transition. *Climate Dynamics* 23, 427–438.
- Diekmann, B., 2007. Sedimentary patterns in the late Quaternary Southern Ocean. *Deep Sea Research Part II: Topical Studies in Oceanography* 54, 2350–2366.
- Diekmann, B., Kuhn, G., Rachold, V., Abelmann, A., Brathauer, U., Fütterer, D.K., Gersonde, R., Grobe, H., 2000. Terrigenous sediment supply in the Scotia Sea (Southern Ocean): response to Late Quaternary ice dynamics in Patagonia and on the Antarctic Peninsula. *Palaeogeography, Palaeoclimatology, Palaeoecology* 162, 357–387.
- Domack, E.W., Taviani, M., Rodriguez, A., 1999. Recent sediment remodeling on a deep shelf, Ross Sea: implications for radiocarbon dating of Antarctic marine sediments. *Quaternary Science Reviews* 18, 1445–1451.
- Efron, B., Tibshirani, R.J., 1994. *An Introduction to the Bootstrap* (Chapman & Hall/CRC Monographs on Statistics & Applied Probability). Chapman and Hall/CRC.
- EPICA Community Members, 2006. One-to-one coupling of glacial climate variability in Greenland and Antarctica. *Nature* 444, 195–198.
- Fischer, H., 2008. EPICA EDML Chemical Concentrations and Fluxes.
- Fischer, H., Fundel, E., Ruth, U., Twarloh, B., Wegner, A., Udisti, R., Becagli, S., Castellano, E., Morganti, A., Severi, M., Wolff, E., Littot, G., Röhrlingsberger, R., Mulvaney, R., Hutterli, M.A., Kaufmann, P., Federer, U., Lambert, F., Bigler, M., Hansson, M., Jonsell, U., de Angelis, M., Boutron, C., Siggaard-Andersen, M.-L., Steffensen, J.P., Barbante, C., Gaspari, V., Gabrielli, P., Wagenbach, D., 2007. Reconstruction of millennial changes in dust emission, transport and regional sea ice coverage using the deep EPICA ice cores from the Atlantic and Indian Ocean sector of Antarctica. *Earth and Planetary Science Letters* 260, 340–354.
- Florindo, F., Roberts, A.P., Palmer, M.R., 2003. Magnetite dissolution in siliceous sediments. *Geochemistry Geophysics Geosystems* 4, 1053.
- Gabrielli, P., Wegner, A., Petit, J.R., Delmonte, B., De Deckker, P., Gaspari, V., Fischer, H., Ruth, U., Kriewas, M., Boutron, C., Cescon, P., Barbante, C., 2010. A major glacial-interglacial change in aeolian dust composition inferred from Rare Earth Elements in Antarctic ice. *Quaternary Science Reviews* 29, 265–273.
- Gersonde, R., Crosta, X., Abelmann, A., Armand, L., 2005. Sea-surface temperature and sea ice distribution of the Southern Ocean at the EPIC Last Glacial Maximum—a circum-Antarctic view based on siliceous microfossil records. *Quaternary Science Reviews* 24, 869–896.
- Giorgino, T., 2009. Computing and visualizing dynamic time warping alignments in R: the dtw package. *Journal of Statistical Software* 31, 1–24.
- Gordon, A.L., Martinson, D.G., Taylor, H.W., 1981. The wind-driven circulation in the Weddell-Endeavour Basin. *Deep-Sea Research A*, 151–163.
- Grobe, H., 1987. A simple method for the determination of ice-rafted debris in sediment cores. *Polarforschung* 57, 123–126.
- Guillou, H., Singer, B.S., Laj, C., Kissel, C., Scaillet, S., Jicha, B.R., 2004. On the age of the Laschamp geomagnetic excursion. *Earth and Planetary Science Letters* 227, 331–343.

- Hauberzertl, T., Anselmetti, F.S., Bowen, S.W., Fey, M., Mayr, C., Zolitschka, B., Ariztegui, D., Mauz, B., Ohlendörfer, C., Kastner, S., Lücke, A., Schätzl, F., Wille, M., 2009. Late Pleistocene dust deposition in the Patagonian steppe – extending and refining the paleoenvironmental and tephrochronological record from Laguna Potrok Aike back to 55 ka. *Quaternary Science Reviews*, 29, 2927–2939.
- Hambach, U., Rolf, C., Schnepf, E., 2008. Magnetic dating of Quaternary sediments, volcanics and archaeological material: an overview. *Eiszeitalter und Gegenwart Quaternary Science Journal* 57, 25–51.
- Hastie, T.J., Tibshirani, R.J., 1990. *Generalized Additive Models*. Taylor and Francis.
- Hein, A.S., Hulton, N.R.J., Dunai, T.J., Sugden, D.E., Kaplan, M.R., Xu, S., 2010. The chronology of the Last Glacial Maximum and deglacial events in central Argentine Patagonia. *Quaternary Science Reviews* 29, 1212–1227.
- Hemming, S.R., 2004. Heinrich events: massive late Pleistocene detritus layers of the North Atlantic and their global climate imprint. *Reviews of Geophysics* 42, RC1005.
- Hillenbrand, C.-D., Grobe, H., Diekmann, B., Kuhn, G., Fütterer, D.K., 2003. Distribution of clay minerals and proxies for productivity in surface sediments of the Bellingshausen and Amundsen seas (West Antarctica) – relation to modern environmental conditions. *Marine Geology* 193, 253–271.
- Hofmann, A., 1999. Kurzfristige Klimaschwankungen im Scotiaemeer und Ergebnisse zur Kalbungsgeschichte der Antarktis während der letzten 200 000 Jahre – Rapid climate oscillations in the Scotia Sea and results of the calving history of Antarctica during the last 200 000 years. *Geowissenschaften. Universität Bremen*, Bremen, 178 p.
- Huybrechts, P., 2002. Sea-level changes at the LGM from ice-dynamic reconstructions of the Greenland and Antarctic ice sheets during the glacial cycles. *Quaternary Science Reviews* 21, 203–231.
- Iriondo, M., 2000. Patagonian dust in Antarctica. *Quaternary International* 68, 83–86.
- Jansen, J.H.F., Van der Gaast, S.J., Koster, B., Vaars, A.J., 1998. CORTEX, a shipboard XRF-scanner for element analyses in split sediment cores. *Marine Geology* 151, 143–153.
- Kaiser, J., Lamy, F., 2010. Links between Patagonian Ice Sheet fluctuations and Antarctic dust variability during the last glacial period (MIS 4–2). *Quaternary Science Reviews* 29, 1464–1471.
- Kanfoush, S.L., Hodell, D.A., Charles, C.D., Guilderson, T.P., Mortyn, P.G., Ninnemann, U.S., 2000. Millennial-scale instability of the Antarctic Ice Sheet during the Last Glaciation. *Science* 288, 1815–1818.
- Kempema, E.W., Reimnitz, E., Barnes, P.W., 1989. Sea ice sediment entrainment and rafting in the Arctic. *Journal of Sedimentary Research* 59, 308–317.
- Kissel, C., Lai, C., 2004. Improvements in procedure and paleointensity selection criteria (PICRT-03) for Thellier and Thellier determinations: application to Hawaiian basaltic long cores. *Physics of the Earth and Planetary Interiors* 147, 155–169.
- Lai, C., Kissel, C., Beer, J., 2004. High resolution global paleointensity stack since 75 kyr (GLOPIS-75) calibrated to absolute values. In: Channell, J., Kent, D., Lowrie, W., Meert, J. (Eds.), *Timescales of the Paleomagnetic Field*. American Geophysical Union, Washington, D.C., pp. 255–265.
- Lambert, F., Delmonte, B., Petit, J.R., Bigler, M., Kaufmann, P.R., Hutterli, M.A., Stocker, T.F., Ruth, U., Steffensen, J.P., Maggi, V., 2008. Dust – climate couplings over the past 800,000 years from the EPICA Dome C ice core. *Nature* 452, 616–619.
- Lambert, F., Bigler, M., Steffensen, J.P., Hutterli, M., Fischer, H., 2011. The calcium–dust relationship in high-resolution data from Dome C, Antarctica. *Climate of the Past Discussions* 7, 1113–1137.
- Lamy, F., Kaiser, J., Arz, H.W., Hebbeln, D., Ninnemann, U., Timm, O., Timmermann, A., Toggweiler, J.R., 2007. Modulation of the bipolar seesaw in the Southeast Pacific during Termination 1. *Earth and Planetary Science Letters* 259, 400–413.
- Lancei, L., Delmonte, B., Maggi, V., Petit, J.R., Kent, D.V., 2008. Ice magnetization in the EPICA-Dome C ice core: implication for dust sources during glacial and interglacial periods. *Journal of Geophysical Research* 113, D14207.
- Laskar, J., Robutel, P., Joutel, F., Gastineau, M., Correia, A.C.M., Levrard, B., 2004. A long-term numerical solution for the insolation quantities of the Earth. *Astronomy and Astrophysics* 428, 261–285.
- Li, F., Ginoux, P., Ramaswamy, V., 2010. Transport of Patagonian dust to Antarctica. *Journal of Geophysical Research* 115.
- Lisiecki, L.E., Raymo, M.E., 2005. A Pliocene–Pleistocene stack of 57 globally distributed benthic $\delta^{18}O$ records. *Paleoceanography* 20, PA1003.
- Lunt, D.J., Valdes, P.J., 2001. Dust transport to Dome C Antarctica at the Last Glacial Maximum and present day. *Geophysical Research Letters* 28, 295–298.
- Maldonado, A., Barnolas, A., Bohoyeva, F., Galindo-Zaldívar, J., Hernández-Molina, J., Lobo, F., Rodríguez-Fernández, J., Somoza, L., Vázquez, J.T., 2003. Contourite deposits in the central Scotia Sea: the importance of the Antarctic Circumpolar Current and the Weddell Gyre flows. *Paleogeography, Palaeoclimatology, Paleoecology* 198, 187–221.
- Mantyla, A.W., Reid, J.L., 1983. Abyssal characteristics of the World Ocean Waters. Deep-Sea Research Part A: Oceanographic Research Papers 30, 805–833.
- Müller, P.J., Schneider, R., 1993. An automated leaching method for the determination of opal in sediments and particulate matter. *Deep-Sea Research* 4, 425–444.
- Nelson, D.M., Tréguer, P., Brzezinski, M.A., Laybarr, A., Quéguiner, B., 1995. Production and dissolution of biogenic silica in the ocean: revised global estimates, comparison with regional data, and relationship to biogenic sedimentation. *Global Biogeochemical Cycles* 9, 359–372.
- NGRIP Members, 2004. High-resolution record of Northern Hemisphere climate extending into the last interglacial period. *Nature* 431, 147–151.
- Nielsen, S.H.H., Hodell, D.A., Kamenov, G., Guilderson, T., Perfit, M.R., 2007. Origin and significance of ice-rafted detritus in the Atlantic sector of the Southern Ocean. *Geochemistry Geophysics Geosystems* 8, 1–23.
- Nowaczyk, M.R., Fredericks, T.W., 1999. Geomagnetic events and relative paleointensity variations during the past 300 ka as recorded in Kolbeinsey Ridge sediments, Iceland Sea: indication for a strongly variable geomagnetic field. *International Journal of Earth Sciences* 88, 116–131.
- Paillard, D., 1996. *Macintosh Program Performs Time-Series Analysis*. EOS.
- Parrenin, F., Barnola, J.-M., Beer, J., Blunier, T., Castellano, E., Chappellaz, J., Dreyfus, G., Fischer, H., Fujita, S., Jouzel, J., Kawamura, K., Lemieux-Dudon, B., Lougoué, L., Masson-Delmotte, V., Narcisi, B., Petit, J.R., Raisbeck, C., Raynaud, D., Ruth, U., Schwander, J., Severi, M., Spahni, R., Steffensen, J.P., Svensson, A., Udisti, R., Waelbroeck, C., Wolff, E., 2007. The ED3 chronology for the EPICA Dome C ice core. *Climate of the Past* 3, 485–497.
- Pudsey, C.J., Howe, J.A., 1998. Quaternary history of the Antarctic Circumpolar Current: evidence from the Scotia Sea. *Marine Geology* 148, 83–112.
- Pugh, R.S., McCave, I.N., Hillenbrand, C.D., Kuhn, G., 2009. Circum-Antarctic ice modelling of Quaternary marine cores under the Antarctic Circumpolar Current: ice-core dust–magnetic correlation. *Earth and Planetary Science Letters* 284, 113–123.
- Rahmstorf, S., 2002. Ocean circulation and climate during the last 200,000 years. *Nature* 419, 207–214.
- Reid, J.L., Nowlin, J.W.D., Patzert, W.C., 1977. On the characteristics and circulation of the southwestern Atlantic Ocean. *Journal of Physical Oceanography* 7, 62–91.
- Reimnitz, E., Kempema, E.W., Barnes, P.W., 1987. Anchor ice, seabed freezing, and sediment dynamics in shallow Arctic Seas. *Journal of Geophysical Research* 92, 14671–14678.
- Revel-Rolland, M., De Deckker, P., Delmonte, B., Hesse, P.P., Magee, J.W., Basille-Doelsch, I., Grousset, F., Bosch, D., 2006. Eastern Australia: a possible source of dust in East Antarctica interglacial ice. *Earth and Planetary Science Letters* 249, 1–13.
- Richter, T.O., van der Gaast, S., Koster, B., Vaars, A., Gieles, R., de Stigter, H.C., De Haas, H., van Weering, T.C.E., 2006. The Aavaetch XRF Core Scanner: Technical Description and Applications to NE Atlantic Sediments. In: *Geological Society, London, Special Publications*, vol. 267, 39–50 pp.
- Rohling, E.J., Pliśke, H., 2005. Centennial-scale climate cooling with a sudden cold event around 8200 years ago. *Nature* 434, 975–979.
- Rolf, C., 2000. Das Kryogenmagnetometer im Magnetiklabor Grubenhagen. *Geologisches Jahrbuch* 152, 161–188.
- Röthlisberger, R., Bigler, M., Wolff, E.W., Joos, F., Monnin, E., Hutterli, M.A., 2004. Ice core evidence for the extent of past atmospheric CO₂ change due to iron fertilisation. *Geophysical Research Letters* 31, L16207.
- Ruth, U., Barnola, J.-M., Beer, J., Bigler, M., Blunier, T., Castellano, E., Fischer, H., Fundel, F., Huybrechts, P., Kaufmann, P., Kipfthuhl, J., Lambrecht, A., Morganti, A., Oerter, H., Parrenin, F., Rybak, O., Severi, M., Udisti, R., Wilhelm, F., Wolff, E., 2007. “EDML1”: a chronology for the EPICA deep ice core from Dronning Maud Land, Antarctica, over the last 150 000 years. *Climate of the Past* 3, 475–484.
- Skinner, L.C., Fallon, S., Waelbroeck, C., Michel, E., Barker, S., 2010. Ventilation of the deep Southern Ocean and deglacial CO₂ rise. *Science* 328, 1147–1151.
- Stocker, T.F., Johnson, S.J., 2003. A minimum thermodynamic model for the bipolar seesaw. *Paleoceanography* 18, 1087–1095.
- Sugden, D.E., McCulloch, R.D., Bory, A.J.-M., Hein, A.S., 2009. Influence of Patagonian glaciers on Antarctic dust deposition during the last glacial period. *Nature Geoscience* 2, 281–285.
- Tauxe, L., 1993. Sedimentary records of relative paleointensity of the geomagnetic field in sediments: theory and practice. *Reviews of Geophysics* 31, 319–354.
- Toggweiler, J.R., 2009. Shifting westerlies. *Science* 323, 1434–1435.
- Toggweiler, J.R., Russell, J., 2008. Ocean circulation in a warming climate. *Nature* 451, 286–288.
- Toggweiler, J.R., Russell, J.L., Carson, S.R., 2006. Midlatitude westerlies, atmospheric CO₂, and climate change during the ice ages. *Paleoceanography* 21, PA2005.
- Weber, M.E., 1998. Estimation of biogenic carbonate and opal by continuous non-destructive measurements in deep-sea sediments: application to the eastern Equatorial Pacific. *Deep-Sea Research* 45, 1955–1975.
- Weber, M.E., Bonani, G., Fütterer, K.D., 1994. Sedimentation processes within channel-ridge systems, southeastern Weddell Sea, Antarctica. *Paleoceanography* 9, 1027–1048.
- Weber, M.E., Clark, P.U., Ricken, W., Mitrovica, J.X., Hostetler, S.W., Kuhn, G., 2011. Interhemispheric ice-sheet synchronicity during the Last Glacial Maximum. *Science* 334, 1265–1269.
- Weber, M.E., Niessen, F., Kuhn, G., Wiedicke, M., 1997. Calibration and application of marine sedimentary physical properties using a multi-sensor core logger. *Marine Geology* 151–172.
- Weber, M.E., Piasis, N.C., 1999. Spatial and temporal distribution of biogenic carbonate and opal in deep-sea sediments from the eastern equatorial Pacific: implications for ocean history since 1.3 Ma. *Earth and Planetary Science Letters* 174, 59–73.
- Weber, M.E., Reichelt, L., Kuhn, G., Pfeiffer, M., Korff, B., Thurow, J., Ricken, W., 2010. BMPX and PFAK tools: new methods for automated laminae recognition and counting—application to glacial varves from Antarctic marine sediment. *Geochemistry Geophysics Geosystems* 11, 1–18.
- Yamazaki, T., Kanamatsu, T., 2007. A relative paleointensity record of the geomagnetic field since 1.6 Ma from the North Pacific. *Earth, Planets and Space* 59, 785–794.

6 Southern Ocean bioproductivity during the last glacial cycle

Journal article (published):

D. Sprenk, M. E. Weber, G. Kuhn, P. Rosén, M. Frank, M. Molina-Kescher, V. Liebetrau, and H.-G. Röhling (2013):

Southern Ocean bioproductivity during the last glacial cycle - a new detection method and decadal-scale insight from the Scotia Sea. *Antarctic Palaeoenvironments and Earth-Surface Processes*. Geological Society, London, Special Publications, Volume 381.

The Geological Society of London allows the reuse of the accepted, but not typeset version of the article in the PhD thesis. The published article can be purchased at:

<http://sp.lyellcollection.org/content/early/2013/07/25/SP381.17.full.pdf+html>

Original page numbers of the accepted article are used.

Southern Ocean bioproductivity during the last glacial cycle – new detection method and decadal-scale insight from the Scotia Sea

*D. Sprenk¹, M. E. Weber¹, G. Kuhn², P. Rosén³, M. Frank⁴, M. Molina-Kescher⁴, V. Liebetrau⁴, H.-G. Röhlings⁵

¹Institute of Geology and Mineralogy, University of Cologne, Zulpicher Str. 49a, D-50674 Cologne

²Alfred-Wegener-Institut Helmholtz-Zentrum für Polar und Meeresforschung, Am Alten Hafen 26, D-27568 Bremerhaven

³Climate Impacts Research Centre (CIRC), Umeå University, SE-981 07 Abisko

⁴GEOMAR Helmholtz Centre for Ocean Research Kiel, Wischhofstr. 1-3, D-24148 Kiel

⁵LBEG Landesamt für Bergbau, Energie und Geologie, Stilleweg 2, D-30655 Hannover

*Corresponding author (e-mail: dsprenk@uni-koeln.de)

Accepted version: -11700 words, 92 references, 5 figures

Abbreviated title: Last glacial Southern Ocean productivity

Abstract

We present biogenic opal flux records from two deep-sea sites in the Scotia Sea (MD07-3133 and MD07-3134) at decadal-scale resolution, covering the last glacial cycle. In addition to conventional and time-consuming biogenic opal measuring methods, we introduce new biogenic opal estimation methods derived from sediment colour b^* , wet bulk density, Si/Ti-count ratio, and Fourier transform infrared spectroscopy (FTIRS). All methods capture the biogenic opal amplitude, however, FTIRS – a novel method for marine sediment – yields the most reliable results. ²³⁰Th normalization data show strong differences in sediment focusing with intensified sediment focusing during glacial times. At MD07-3134 ²³⁰Th normalized biogenic opal fluxes vary between 0.2 and 2.5 g/cm²/kyr. Our biogenic opal flux records indicate bioproductivity changes in the Southern Ocean, strongly influenced by sea ice distribution and also summer sea surface temperature changes. South of the Antarctic Polar Front, lowest bioproductivity occurred during the Last Glacial Maximum when upwelling of mid-depth water was reduced and sea ice cover intensified. Around 17 ka, bioproductivity increased abruptly, corresponding to rising atmospheric CO₂ and decreasing seasonal sea ice coverage.

Keywords: biogenic opal flux; bioproductivity; Southern Ocean; Scotia Sea; Fourier transform infrared spectroscopy; last glacial cycle; upwelling; sediment focusing, ²³⁰Th normalization

The Southern Ocean plays an important role in transferring carbon dioxide (CO₂) via wind-induced upwelling from the deep sea to the atmosphere (Toggweiler et al. 2006; Anderson et al. 2009) and is therefore one of the key regions from which to study climate change. Bioproductivity in the Southern Ocean is mainly controlled by the rate of upwelling of cold nutrient- and silica-rich water masses, the extent of sea ice coverage, and the availability of light and micronutrients (Dezileau et al. 2003; de Baar et al. 2005; Stenni et al. 2010). Thus, bioproductivity in the Southern Ocean is mainly coupled to local climate change. Biogenic opal is an important nutrient that fuels biological production in the surface waters around Antarctica. Recent investigations (Pondaven et al. 2000; Chase et al. 2003; Bradtmiller et al. 2007; Anderson et al. 2009) revealed that biogenic opal flux in the Southern Ocean primarily reflects variations in bioproductivity rather than changes in preservation, which enables its use for studying palaeoenvironmental changes during the last glacial cycle. Anderson et al. (2009) also identified biogenic opal as an upwelling proxy because south of the Polar Frontal Zone in the Southern Ocean, its production is ultimately limited by the supply of dissolved Si from the deep ocean. Horn et al. (2011) argued that biogenic opal flux might not be a direct upwelling proxy, but could also indicate major changes in nutrient demand such as iron. Until now, high-resolution and continuous biogenic opal flux records from the Southern Ocean extending back to the last interglacial, are rare (e.g. Anderson et al. 2009) and therefore only limited knowledge exists on how Southern Ocean bioproductivity changed in the past.

We studied two deep-sea cores from the Scotia Sea, with linear sedimentation rates of up to 1.2 m/kyr (MD07-3134) and 1.8 m/kyr (MD07-3133). As biogenic opal analysis using the leaching method by Müller & Schneider (1993) is very time-consuming and expensive we additionally tested several biogenic opal estimation methods, e.g. Si/Ti-count ratio, wet bulk density, colour b* and Fourier transform infrared spectroscopy (FTIRS), and compared the results to conventionally-measured biogenic opal. FTIRS has been successfully used to determine biogenic opal quantitatively in lacustrine sediment (Vogel et al. 2008). We present one of the first studies to assess biogenic opal from FTIRS in marine sediment. Our goal is to provide a high-resolution biogenic opal accumulation rate record, giving the opportunity to study bioproductivity changes at decadal-scale resolution in the Southern Ocean over the last glacial cycle (92.5 ka to present; note that all ages mentioned are calendar ages).

Core Material

Sediment cores used in this study originate from the central Scotia Sea (Fig. 1) and were drilled with a Calypso II piston corer during the Marion Dufresne (MD) II cruise 160 in March 2007. Core sites MD07-3133 (57°26' S, 43°27' W, 3101 m water depth, 32.8 m core recovery) and MD07-3134 (59°25' S, 41°28' W, 3663 m water depth, 58.2 m core recovery) are located approximately 450 km apart. Both core sites lie below the carbonate compensation depth. Therefore, the core material is virtually free of biogenic carbonate and consists of varying amounts

of lithogenic material and biogenic opal. Homogenous, olive grey to yellow diatomaceous oozes were deposited during warm climatic periods (Marine Isotopic Stages (MIS) 5 and 1), grey to blue-grey diatom-bearing mud during cold periods (MIS 4 and 2), and mostly olive-grey diatomaceous mud during MIS 3.

Chronology

The chronology of Sites MD07-3133 and MD07-3134 is detailed in Weber et al. (2012). It relies on seven ground-truth data points obtained at Site MD07-3134. Accordingly, MIS boundaries 5/4 (71 ka), 4/3 (57 ka), 3/2 (29 ka), and 2/1 (14 ka) comply with 46, 38.5, 16.5, and 11 m core depth, respectively. Relative palaeointensity data indicates a significant drop at approximately 24 m in the core that is considered to represent the Laschamp Event (40.4 ± 1.1 ka; Guillou et al. 2004). Furthermore, volcanic ashes also rich in ice-rafted detritus (e.g. Site MD07-3134 at 8.9, 13.36, 34.17, and 43.88 m core depth) have been dated and correlated across the Southern Atlantic as layers SA0 (ca. 14 – 15 ka) to SA6 (ca. 55 ka) (Kanfoush et al. 2000; Nielsen et al. 2007). For Site MD07-3134, volcanic layers SA0 and SA6 were found at 13.36 and 34.17 m in the core, respectively. The detection of these two layers further supports the independent MIS ground-truth assignment because SA6 is just slightly younger than MIS boundary 4/3, and SA0 is exactly as old as MIS boundary 2/1.

Weber et al. (2012) provided convincing arguments that from the various supply mechanisms proposed for magnetic susceptibility and Ca^{2+} concentrations, i.e. icebergs, ocean circulation, atmospheric circulation, volcanic sources, and sea ice, only atmospheric circulation remains for the Scotia Sea sites. Hence, they correlated both signals to the non-sea-salt Ca^{2+} flux of the European Project for Ice Coring in Antarctica (EPICA) Dronning Maud Land (EDML) record (Fischer et al. 2007a) to increase the resolution of their age model for Site MD07-3134. They applied three stratigraphic approaches to produce a tuned, high-resolution age model, evaluate its quality, and provide error estimates: (i) manual picking of tie points, (ii) an automated pattern-matching algorithm, and (iii) a smoothing spline regression using the manual tie points.

As a result, Weber et al. (2012) established 48 confident age control points for the last 92.5 kyr. Average linear sedimentation rates are high, ranging from 0.2 – 1.2 m/kyr and from 0.3 – 1.8 m/kyr for Sites MD07-3134 and MD07-3133, translating into mass accumulation rates (calculated by multiplying linear sedimentation rate with dry bulk densities) of 10 – 130 g/cm²/kyr and 9 – 100 g/cm²/kyr, and into sample resolution of 50 – 8 years and 33 – 5 years (given a sample increment of 1 cm), respectively.

Tuning magnetic susceptibility to the non-sea-salt Ca^{2+} flux has significant implications for the quality and reliability of the age model. The fact that the two signals are more or less phase-locked during this procedure is reasonable because dust transport from Patagonia to Antarctica takes only approximately a week (Li et al. 2010). Therefore, no major leads or lags should be involved for atmospheric transport. Accordingly, the chronology of our two sites provides a precise and high-resolution age model for Southern Ocean deep-sea sediment.

Setting

The Scotia Sea is located in the Atlantic Sector of the Southern Ocean where the Antarctic Circumpolar Current dominates oceanic circulation. It is the world's largest current with a transport volume of approximately 134 Sverdrup ($1 \text{ Sv} = 10^6 \text{ m}^3/\text{s}$) (Whitworth & Peterson 1985) flowing eastward around the Antarctic continent. The Antarctic Circumpolar Current includes, in most regions, water masses from the seafloor to the surface. Its velocity generally decreases with depth but is also severely influenced by local seabed topography (Pugh et al. 2009). Uniquely connecting the Atlantic, Indian, and Pacific, the Antarctic Circumpolar Current allows for heat, nutrient, and salt exchange between the oceans (Maldonado et al. 2003); accordingly, playing an important role in global climate control (Pugh et al. 2009). It is mainly wind-driven by the Southern Hemisphere Westerlies between 45° and 55°S . These westerlies are also responsible for transporting surface waters away from Antarctica through Ekman transport, leading to upwelling of mid-depth water (2 to 3 km) south of the current, a unique process restricted to the Southern Ocean (Berger & Loutre 1991).

In the Scotia Sea, the Antarctic Circumpolar Current flows between the Subtropical Front and Southern Antarctic Circumpolar Current Front (Fig. 1). Its flow is concentrated in circumpolar, vertically-coherent, seafloor-reaching fronts: the Subantarctic Front, Antarctic Polar Front, and Southern Antarctic Circumpolar Current Front (Orsi et al. 1995). The Antarctic Polar Front is the northern limit of wind-driven, nutrient-rich deep-water upwelling because of northward Ekman transport. It therefore forms an ecological and physical water-mass boundary to colder, more silicate-rich and less saline water masses south of it (Pondaven et al. 2000; Dezileau et al. 2003; Cassar et al. 2007; Diekmann 2007), where both core sites are located (Fig. 1). The area between the Antarctic Polar Front and northern limit of seasonal sea ice is known as the Circum-Antarctic Opal Belt with high biosiliceous production rates (Geibert et al. 2005; Diekmann 2007). The southern boundary of siliceous deposits corresponds well to the Southern Antarctic Circumpolar Current Front in the Atlantic Sector of the Southern Ocean (Geibert et al. 2005).

Methods

We used a Minolta spectrophotometer CM-2002 to measure L^* , a^* , and b^* colour components at 1 cm intervals (Weber 1998). To obtain information on chemical element distribution (e.g. for Si, Ti), every centimetre of sediment was analysed according to the method of Richter et al. (2006) using an Avaatech X-ray Fluorescence Core Scanner (XRF-CS) (Jansen et al. 1998).

Sediment physical properties such as wet bulk density and magnetic susceptibility ($kappa$ volume specific) were measured non-destructively every centimetre with a Geotek Multi-Sensor Core Logger (Weber et al. 1997). Dry bulk densities, which are required for the calculation of mass accumulation rates, were calculated from wet bulk densities using an iteration procedure described in Weber et al. (1997), by applying specific mass attenuation coefficients to each

measurement to account for fluctuating water content and grain density. To check its accuracy we also compared the non-destructive data to dry bulk densities determined on freeze-dried samples.

Besides measuring biogenic opal on specific samples we implemented several strategies to estimate it at high spatial resolution. We first analysed biogenic opal by leaching the sediment in 1M NaOH-solution according to the method of Müller & Schneider (1993). The initial values for biogenic silicon were corrected by adding 10 wt% H₂O for the water bound in the amorphous opal skeleton (biogenic opal = biogenic opal_{M&S}+10% H₂O). All resulting data needed to be corrected for the sea salt content of the pore fluid (35‰). As this leaching method is relatively expensive and time-consuming, measurements were restricted to 10 cm intervals of specific sections that exhibit large-amplitude variations (MD07-3133: 1655 – 2785 cm, 112 samples; MD07-3134: 745 – 1785 cm, 4135 – 4585 cm; 141 samples).

Biogenic opal-rich, unconsolidated sediments exhibit extremely high porosities because interstitial fluid rests both within the shells (intragranular) and in the pore space (intergranular). The high sediment water contents as well as the lower grain densities of biogenic opal in contrast to detrital material and biogenic carbonate, cause the extremely low wet and dry bulk densities of biogenic opal-rich sediments. Therefore, wet bulk densities are negatively correlated to biogenic opal (Weber 1998) for diatom-rich deep-sea sediments well below the carbonate compensation depth and hence biogenic opal can be estimated from wet bulk densities using linear correlation coefficients (Fig. 2 A).

Another striking correlation is given for colour b* and biogenic opal in diatom-rich sediment (Weber 1998), i.e. the more yellow the sediment, the higher the amount of biogenic opal, whereas more bluish colours indicate low biogenic opal. Accordingly, we derived linear correlation coefficients to estimate the amount of biogenic opal from colour b* for Scotia Sea Sites MD07-3133 and MD07-3134 (Fig. 2 B).

Also, we used the ratio of Si and Ti XRF-counts to obtain information on biogenic opal changes. Si originates from either detrital siliciclastics or from biogenic, mostly diatom sources. Because Ti reflects only clastic input (Murray et al. 1993), the XRF Si/Ti ratio should only represent changes in biogenic opal (Francus et al. 2009; Balascio et al. 2011). Because XRF core-scanner measurements were made at higher resolution than some other proxies (1 cm increments), we implemented a 9-point moving average to smooth the data (using AnalySeries 2.0.4.2.; Paillard et al. 1996). Then we used the linear correlation between the Si/Ti XRF-count ratio and leached biogenic opal to calculate biogenic opal values, depending on Si/Ti-count ratios (Fig. 2 C).

Furthermore, we implemented FTIRS to obtain high-resolution information on biogenic opal and other biogeochemical sediment components. FTIRS is a fast and relatively inexpensive technique, which requires only 11 mg of sample material (Rosén et al. 2011). It was therefore employed at 10 cm intervals over the entire core lengths of Sites MD07-3133 and MD07-3134 (316 and 575 samples, respectively) at the Climate Impacts Research Centre in Umeå, Sweden. Until now FTIRS was successfully used to determine, quantitatively, total inorganic and organic carbon, and biogenic opal in lacustrine sediment (Vogel et al. 2008). Here, we present one of the

first studies to assess these sediment properties quantitatively for marine sediment. Samples were first freeze-dried and grounded to $< 63 \mu\text{m}$ using a swing mill. In addition, 500 mg of oven-dried (80 °C) potassium bromide (KBr, Merck), which is transparent in the infrared band, was added to each sample. This is necessary to avoid very high absorbances (> 2), which are released by low intensities of infrared light that would otherwise reach the detector and produce higher noise levels in the data and spectral distortions (Griffiths & De Haseth 1986). The samples were measured using a FTIR spectrometer (Bruker Vertex 70) equipped with a diffuse reflectance accessory. Each sample was scanned 128 times and data were collected every 2 cm^{-1} (reciprocal centimetres). The measurement resolution was 4 cm^{-1} for wavenumbers between 3750 and 400 cm^{-1} , which equals wavelengths from 2666 to 25000 nm , thus yielding 1735 data points per sample. To avoid variations caused by temperature, all samples were placed in the same temperature-controlled laboratory ($25 \pm 0.2 \text{ }^\circ\text{C}$) as the FTIRS device for at least five hours prior to analysis. Multiple scatter correction and baseline correction were used to linearize spectra and remove variation in spectra caused by noise (Geladi et al. 1985; Rosén et al. 2010). Baseline correction performs a linear correction of the spectra so that two points (3750 and $2210\text{--}2200 \text{ cm}^{-1}$) equals zero. Multiple scatter correction removes spectral variation arising from different effective path lengths and particle sizes (Geladi et al. 1985). Partial least squares regression was used to develop quantitative calibration models between FTIR spectra of sediment and conventionally measured sediment properties (Martens & Naes 1989). An internal calibration model based on 253 samples from MD07-3133 and MD07-3134 were regressed on 253 conventionally determined sea salt corrected mass percentage biogenic opal contents using the leaching technique (Müller & Schneider 1993; Vogel et al. 2008). Wavenumbers between 450 and 1320 cm^{-1} were used in the partial least squares regression model, i.e. a region where different types of silicates absorb. Although different silicates absorb in the FTIRS wavenumber region between 1050 and 1250 cm^{-1} , it is not necessary to subtract spectra as the curve's shape shows characteristic differences for, e.g. quartz and biogenic opal. The predictive performance of the partial least squares regression calibration model was assessed by 10% cross-validation. This means that the calibration model was developed using 90% of data of the calibration samples with the remaining 10% used to test the predictions. This process was repeated a total of ten times as each group, in turn, was set aside. Root mean squared error of cross validation was used as an estimate of prediction error. All primary sediment properties were square root transformed prior to the analysis. SIMCA-P 11.5 (Umetrics AB, SE-907 19 Umeå, Sweden) was used for all multivariate data analyses.

Correction of sediment focusing using $^{230}\text{Th}_x$ normalization

The extremely high sedimentation rates of up to 1.8 m/kyr clearly indicate that the sediments of this site have been subject to massive sediment focusing induced by bottom currents. This is observed at many locations in the Southern Ocean and results in completely erroneous mass accumulation rates, which can be off by a factor of 12 (Frank et al. 1999) or even more (this study). For the calculation of realistic mass accumulation rates (rain rates) of biogenic opal and

other components, the effects of sediment focusing have to be quantified and be corrected for applying excess ^{230}Th ($^{230}\text{Th}_{\text{ex}}$) normalization (Kumar et al. 1995; Frank et al. 1996; Frank et al. 2000; Francois et al. 2004). This method is based on the constant production of ^{230}Th from its global homogeneously distributed radioactive parent ^{234}U . In contrast to U, Th is highly particle reactive resulting in essentially the entire amount of locally produced ^{230}Th being deposited in the sediments below. This means that the mass accumulation rate of ^{230}Th in the sediments should match its production in the overlying water column. Given that ^{230}Th can only be advectively transported in solution over very short distances as a consequence of its particle reactivity, any significant increases over the expected ^{230}Th -mass accumulation rate must be a result of sediment focusing and can be quantitatively corrected for by relating it to the expected flux at any particular location.

For the determination of the activities of ^{230}Th , ^{232}Th , ^{234}U , and ^{238}U , between 50 and 90 mg of sediment were weighed and spiked with $^{229}\text{Th}/^{233}\text{U}/^{236}\text{U}$ in the laboratory of GEOMAR in Kiel. The samples were first treated with aqua regia and were then subjected to total dissolution in a mixture of concentrated nitric, hydrofluoric, and perchloric acid. Subsequently U and Th were separated from each other and from disturbing matrix elements via ion exchange chromatography using an Uteva resin (Eichrom). The activities of the U and Th isotopes were determined on an Agilent 7500 quadrupole mass spectrometer. The precision of the measurements was better than 1% (2 standard errors) for the respective U isotopes and better than 2% (2 standard errors) for the Th isotopes. For the calculation of $^{230}\text{Th}_{\text{ex}}$ activities see Frank et al. (1996).

Results

Correlation coefficients of $r=0.95$ and 0.83 indicate that wet bulk density changes at Sites MD07-3133 and MD07-3134 are mainly caused by fluctuations in biogenic opal content (Fig. 2 A). Also colour b^* changes predominantly reflect fluctuations in biogenic opal content (Fig. 2 B), although their relation is, with correlation coefficients of $r=0.91$ and 0.79 , not as striking as for wet bulk density. The generally good correlation coefficients (≥ 0.79) let us assume that both wet bulk density and colour b^* can be used to estimate realistic biogenic opal contents (within the given errors).

Additionally, XRF-measured Si/Ti-count ratios provide, to some extent, rough information about biogenic opal fluctuations. The correlation coefficient for Si/Ti and biogenic opal is $r=0.58$ and 0.62 for Sites MD07-3133 and MD07-3134 (Fig. 2 C). However, its use as a biogenic opal proxy is questionable due to uncertainties associated with Ti values (see discussion for further explanation).

The most promising estimation method is FTIRS (Fig. 2 D) with correlation coefficients of $r=0.99$ and $r=0.93$ for Sites MD07-3133 and MD07-3134. The models of leached and FTIRS-estimated biogenic opal show good statistical performance, with cross-validated root mean squared errors of 4.8% (MD07-3133), respectively 8.7% (MD07-3134) of the gradient. FTIRS

provides the closest similarities of all estimation methods to the reference method of conventional leaching.

We then calculated biogenic opal contents from the various proxy data sets for Sites MD07-3133 and MD07-3134 (Fig. 3), using the linear regression lines discussed above (Fig. 2). In general, the same overall trend is recognizable for all biogenic opal estimation curves, however, the amplitude varies significantly for some parts of the cores. Higher linear sedimentation rates lead to higher-resolution data for Site MD07-3133 relative to Site MD07-3134, specifically for the Holocene section. However, both cores share the same overall trend and principal features. As expected from the correlation coefficients FTIRS-estimated and leached biogenic opal share the most commonalities. Biogenic opal contents estimated from colour b^* capture the glacial to interglacial transition; however, colour b^* overestimates biogenic opal contents for the uppermost and lowermost core sections of Site MD07-3133. In fact, for the upper 12 m of MD07-3133, estimates from colour b^* , wet bulk density, and the Si/Ti-count ratio show substantial discrepancies relative to FTIRS estimates (Fig. 3).

On average, highest biogenic opal contents occur during interglacial MIS 5 and 1, confirming results of earlier studies on deep-sea sediment in the Atlantic sector (e.g. Charles et al. 1991; Mortlock et al. 1991; Pudsey & Howe 1998; Diekmann 2007), the Indian Sector (Bareille et al. 1998), and the Pacific Sector (Chase et al. 2003) of the Southern Ocean, south of the Antarctic Polar Front. Interglacial MIS 3 shows intermediate contents of biogenic opal with an overall decreasing trend towards MIS 2. During glacial MIS 4 and 2, absolute minima in biogenic opal contents are noticeable (Fig. 3). Surprisingly, maximum biogenic opal contents occur during glacial MIS 4 (Site MD07-3134). These extraordinary high values seem robust (i.e. not caused by analytical errors), as five data points scatter around 60% biogenic opal in less than 1 m of sediment core. This section also shows low densities and yellower sediment colour, corresponding to substantially elevated biogenic opal contents. FTIRS also indicates high biogenic opal values for this section, whereas the highest FTIRS-estimated biogenic opal values (~ 67%) occur at the end of MIS 5. MIS 5 and 4 show high-amplitude and high-frequency changes in biogenic opal, whereas during MIS 2 and 1 biogenic opal contents were relatively stable showing only low-amplitude fluctuations.

To better understand the biogenic opal sedimentation changes through time, we calculated mass accumulation rates for FTIRS-estimated biogenic opal contents (Fig. 4 E), which we consider the most precise estimation method (see methods; Fig. 2). This was done by multiplying the biogenic opal content as a percentage with the mass accumulation rate, i.e. the product of sedimentation rate and dry bulk density (Fig. 4 A, B). Instead of linear sedimentation rates, we used sedimentation rates estimated from a cubic smoothing spline age-model (Weber et al. 2012) (Fig. 4 A, grey lines). This overcomes the problems of normal splines, which don't include errors and so might produce outliers and artefacts, hence, representing more realistic sedimentation rates. Both cores exhibit extremely high sedimentation rates in some sections with values up to 1.8 and 1.2 m/kyr for Sites MD07-3133 and MD07-3134. Warmer periods (MIS 3 and 1) show

approximately 1.5 – 2 times increased sedimentation rates at Sites MD07-3133 relative to Site MD07-3134, whereas during MIS 2 nearly identical rates occur at both core sites (Fig. 4 A). The sedimentation rates and biogenic opal mass accumulation rates show a relatively complicated glacial-to-interglacial pattern with large-amplitude changes. While biogenic opal mass accumulation rate reaches its minimum during the Last Glacial Maximum with values of approximately 3 g/cm²/kyr at both core sites, up to 10 times higher rates are observed during MIS 4 (Fig. 4 E).

²³⁰Th-normalization data for MD07-3134 show that sediment focusing was very high, ranging from 5 (minimum value at 84.3 ka) to 29 (maximum value at 55.9 ka). During the interglacials the focusing factor ranged between 5 and 13, meaning that 5 to 13 times more sediment was added laterally to the core site via focusing than vertically through the water column. In the last glacial, in particular MIS 3, the focusing factors were generally even higher and ranged between 11 and 29. Strictly speaking, the ²³⁰Th-normalized fluxes can only be applied for the 10 samples on which ²³⁰Th was measured because there is no control over changes in sediment focusing between the depths of the measured ²³⁰Th-normalized values. We are aware of this limitation and the interpolated ²³⁰Th-normalized rain rates are just provided as an approximation for illustrative purposes until we have additional ²³⁰Th-normalized data.

The interpolated rain rate for MD07-3134 (Fig 4. D) varies between 2 and 4.3 g/cm²/kyr, with maximum values around 67 ka resulting from intermediate dry bulk densities (Fig. 4 B), a focusing factor of 10, and a relatively high linear sedimentation rate (Fig. 4 A). In order to achieve a more realistic record of the biogenic opal flux we multiplied ²³⁰Th-normalized rain rates and FTIRS-estimated biogenic opal amount to get ²³⁰Th-normalized biogenic opal flux (Fig. 4 C). The calculated ²³⁰Th-normalized biogenic opal flux varies from 0.2 to 2.5 g/cm²/kyr. Maxima occur during interglacials, with mean values of 1 (MIS 1) and 1.4 (MIS 5) g/cm²/kyr, whereas glacial MIS 2 and 3 were generally characterized by lower values near 0.5 g/cm²/kyr. MIS 4 shows large short-term fluctuations, which, however, would need to be confirmed by additional ²³⁰Th_{res} measurements at higher resolution. In general, the ²³⁰Th-normalized biogenic opal flux data (Fig. 4 C) show a similar pattern over the past 92.5 kyr compared with the uncorrected biogenic opal accumulation rates (Fig. 4 D) albeit with realistic numbers when compared to other sites in the Atlantic sector of the Southern Ocean (Kumar et al. 1995; Frank et al. 2000). As we have no ²³⁰Th-normalization data for MD07-3133, we can only suggest that the sediment focusing was analogous and maybe even higher than at the MD07-3134 core site, as the linear sedimentation rate shows a similar trend, but higher values (Fig. 4 A).

Discussion

To what extent are biogenic opal estimation methods reliable?

Biogenic opal can be analysed and estimated using various techniques, but no standardized determination methodology exists because each method has advantages and drawbacks. As deduced from Figure 3, the main biogenic opal fluctuations are captured by all estimation

methods; so all methods can be used to decipher general biogenic opal trends; however, there are some strong discrepancies. Leaching according to Müller & Schneider (1993) is one of the most commonly used methods because of its simplicity and robustness (Swann 2010). However, samples with $\leq 10\%$ biogenic opal might be affected by the pH value of the leaching solution (Schlüter & Rickert 1998).

XRF Si/Ti ratio is often used to indicate biogenic opal content changes in sediments (e.g. Francus et al. 2009; Balascio et al. 2011; Johnson et al. 2011). Nonetheless, Tjallingii et al. (2007) found reduced XRF-element intensities for light elements such as Si and Al of wet material relative to dried material, which they relate to differences in water contents. Accordingly, this can lead to misinterpretations of wet-measured samples. Our Si/Ti-count ratios reflect roughly the main biogenic opal fluctuations, especially at MD07-3134 (Fig. 3), but they should be only seen as rough estimations because of the given measurement uncertainties. Colour b^* can also be a useful parameter to estimate biogenic opal content of carbonate-free sediments that mainly contain varying amounts of biogenic opal, quartz and clay minerals. Our estimation shows that wet bulk density is also useful to roughly estimate biogenic opal content. It would also yield reliable results for sediments containing biogenic carbonate because biogenic opal has significantly lower densities ($\sim 2.2 \text{ g/cm}^3$) than biogenic carbonate ($\sim 2.8 \text{ g/cm}^3$) or detrital material ($\sim 2.6 \text{ g/cm}^3$). However, greater amounts of organic carbon (density of $\sim 1.4 \text{ g/cm}^3$) would lead to misinterpretations (Weber 1998).

Estimates from colour b^* , wet bulk density, and the Si/Ti-count ratio for the upper 12 m of MD07-3133 show substantial discrepancies relative to FTIRS estimates (Fig. 3). This may be due to a combination of coring effect and sediment facies, i.e. the upper parts of core MD07-3133 were partially supersaturated with water. These sections leaked pore water when they were cut into 1-m sections because of missing cohesive forces typical for the fabric of diatomaceous oozes. Accordingly, scanning techniques such as the Multi-Sensor Core Logger and the XRF-scanner measured false values in the uppermost core section, because they rely on completely filled core liners as well as smooth and even surfaces. So these estimations have limitations if sediments are supersaturated with water or show uneven surfaces.

A number of studies (e.g. Vogel et al. 2008; Rosén et al. 2011) show that FTIRS can be used to gain high-resolution and high-quality geochemical information on lacustrine sediment consisting of varying amounts of inorganic and organic components. Our results (Figs. 2 D and 3) also indicate that FTIRS is a very promising and useful tool for studying marine sediment composition. Correlation coefficients of $r=0.99$ (MD07-3133) and $r=0.93$ (MD07-3134) and an all-gradient accordance (Fig. 2 D) underline our suggestion that FTIRS seems to be the most reliable estimation method, and hence can be used successfully for deep-sea sediment analysis. Therefore, we used the FTIRS results for all further discussions and comparisons (Figs. 4 and 5).

Biogenic opal flux as a bioproductivity proxy

There is a strong debate on the reliability of biogenic opal flux data for indicating bioproductivity. It is still not entirely clear whether biogenic opal preservation is consistent over longer time periods and how the silicon cycle is coupled with the carbon biogeochemical cycle during interglacials (e.g. Pondaven et al. 2000; Ragueneau et al. 2000; Dezileau et al. 2003). However, in recent years, a number of studies indicate that biogenic opal flux can be used as bioproductivity proxy. Chase et al. (2003) and Bradtmiller et al. (2007) argued that biogenic opal flux reflects variations in diatom productivity and not changes in biogenic opal preservation. For the Indian sector Pondaven et al. (2000) found that local differences in biogenic opal preservation, apparent in the polar frontal zone and south of it, have only a modulating but no primary effect on biogenic opal flux fluctuations. The good correlation of Sites MD07-3133 and MD07-3134 biogenic opal mass accumulation rate records (Fig. 5 E), which are approximately 450 km apart (Fig. 1), indicates that this argument is also true for the central Scotia Sea.

Presently, the $^{231}\text{Pa}/^{230}\text{Th}$ ratio is the most accurate and most commonly used proxy for analysing particle and water mass transport in the Southern Ocean, e.g. past opal fluxes (Kretschmer et al. 2011). Also Anderson et al. (2009) found strong correlation between the biogenic opal flux (i.e. mass accumulation rate) and $^{231}\text{Pa}/^{230}\text{Th}$ ratios, which are not altered by biogenic material loss during early diagenesis (Chase et al. 2003) in Southern Ocean sediment. This led them to the conclusion that biogenic opal flux variations reflect changes in biogenic opal production and silicon supply, rather than changes in preservation.

Estimated mean sedimentation rates are extremely high at both core sites: mean linear sedimentation rate for MIS 1 is 0.9 (MD07-3134) and 1.6 (MD07-3133) m/kyr, approximately 0.5 m/kyr (MD07-3133 and MD07-3134) for MIS 2, 0.7 m/kyr (MD07-3134) for MIS 3 as well as MIS 5, and 0.9 m/kyr (MD07-3134) for MIS 4. Our values are more than 10 to 30 times higher than reported in previous studies, where rates of less than 5 cm/kyr for interglacials, and more than 5 cm/kyr for glacial times in the Scotia Sea were estimated (Pudsey & Howe 1998; Diekmann et al. 2000; Pugh et al. 2009). Accordingly, we conclude that both core sites are strongly influenced by sediment focusing, which is also reflected in the ^{230}Th normalized data of MD07-3134 (Fig. 4 C and D), showing quite strong variability in sediment focusing with average interglacial values of 8 and average glacial values of 20. To our knowledge, these are some of the highest focusing factors ever determined with this method. The calculated ^{230}Th normalized rain rates (Fig. 4 D) now correspond very well to other Southern Ocean sites, for instance, neighbouring core PS2319-1 (Francois et al. 2004). However, the ^{230}Th normalized biogenic opal flux overall shows the same trend as our estimated biogenic opal mass accumulation rate (Fig. 4 E) for MD07-3134.

High sediment focusing of course is an indicator for bottom currents affecting an area, but these currents obviously did not vary so dynamically that they destroyed the dust related signal (Pugh et al. 2009; Weber et al. 2012) within the decadal resolution. In contrast they collected the sediments from an upstream mostly shallower region and focused the material deposition to the core sites thereby enhancing time resolution of the sedimentary record. By increasing the focusing

factor from 8 to 20 during glacials this sediment advection acted like a slow motion frame. The Antarctic Circumpolar Current has a significant effect on sea floor sedimentation in that area (Pudsey & Howe 1998). As a mainly wind-driven current (Maldonado et al. 2003) we assume that it resulted in decadal and centennial variations, which are comparable to dust climate signals, e.g. Antarctic EDML non-sea-salt Ca^{2+} flux (Fischer et al. 2007a).

In regions such as the Antarctic Zone, where nutrient concentration is constantly high, iron availability strongly influences bioproductivity (Martínez-García et al. 2011). Different iron fertilization experiments (e.g. Martin et al. 1990; Boyd et al. 2000) showed that Southern Ocean productivity is limited by Fe-deficiency. Coastal sediments, aerosols, upwelling, ice melting, and vertical mixing, can supply iron to the Southern Ocean (Cassar et al. 2007), however today the major nutrient and iron supply originates from upwelling water masses or lateral advection (Meskhidze et al. 2007; Martínez-García et al. 2011). The influence of dust-transported aeolian iron on bioproductivity is still debated. Erickson et al. (2003) suggested that bioproductivity in the Antarctic Circumpolar Current region is mainly controlled by atmospheric dust-Fe, mostly from Patagonia, whereas Kaufmann et al. (2010) argued that dust flux variations had no major influence on Southern Ocean productivity over the last 150 ka. Further, modelling studies suggest that upwelling delivers approximately 99% of micronutrients to the Southern Ocean rather than dust (Lefèvre & Watson 1999). At Sites MD07-3133 and MD07-3134 dust-indicator magnetic susceptibility exhibits mostly minima when biogenic opal mass accumulation rate is high and vice versa (Fig. 4 E, F). During the Last Glacial Maximum, dust transport was significantly intensified and led to 10–30 times higher concentrations in Antarctic ice cores (Delmonte et al. 2004) and in the Scotia Sea (Sites MD07-3133 and MD07-3134; Weber et al. 2012), whereas biogenic opal mass accumulation rates were extremely low during that period. Accordingly, we believe that iron-fertilization via dust-transport is not the main driver of bioproductivity changes in the Scotia Sea. In addition, iron released from melting icebergs (Raiswell 2011), i.e. Fe either from terrigenous material or aeolian dust (Lin et al. 2011), might have a minor affect on bioproductivity, as both sediment core sites are within the so-called “iceberg alley” (Anderson & Andrews 1999; Stuart & Long 2011).

Biogenic opal export increase at the end of the last glacial could reflect higher nutrient content in upwelling waters or just intensified upwelling, more fractional utilization of nutrients, or, to a lesser extent, better preservation of sinking biogenic opal (Horn et al. 2011). Allen et al. (2011) conclude that reduced surface water productivity and/or export in the Scotia Sea during the Last Glacial Maximum, caused by enhanced sea ice cover, lower sea surface temperatures, and therefore shorter growing seasons, and not changes in dissolution processes, are more likely to explain the lower abundance of diatoms in sediment cores during the Last Glacial Maximum.

Bioproductivity changes since the last interglacial

Given the above arguments, we believe that the Scotia Sea biogenic opal mass accumulation rates at Sites MD07-3133 and MD07-3134 mainly provide records of changing bioproductivity

since the last interglacial. Interestingly, a relatively complicated glacial-to-interglacial pattern is noticeable (Fig. 5 E-G). Large amplitude millennial-scale fluctuations occur in the Scotia Sea records, which exhibit decadal-scale sample resolution. We estimate the lowest bioproductivity for the Last Glacial Maximum, while Southern Hemisphere Westerlies seem to have been located approximately 7 to 10° latitude north of their present position (e.g. Moreno et al. 1999; Toggweiler et al. 2006). During that time upwelling of silica- and CO₂-rich, relatively warm mid-depth water to the sea surface was reduced significantly – approximately 30% relative to today (Horn et al. 2011), which led to low-temperature and low-salinity surface waters that supported sea ice formation in the Southern Ocean (Toggweiler et al. 2006). Also, micronutrient availability in the Scotia Sea was at a minimum during the Last Glacial Maximum (Hendry et al. 2011). As shown in Figure 5, low biogenic opal mass accumulation rates at the Last Glacial Maximum correspond to (i) low $\delta^{18}\text{O}$ values of the EDML ice core (Fig. 5 A), which provide a local ice sheet temperature indicator (EPICA Community Members 2006) and (ii) to high sea-salt Na⁺ fluxes of the EDML ice core (Fig. 5 B; Fischer et al. 2007b), which reflect intense sea ice cover. During MIS 2, decreased biogenic opal mass accumulation rates were estimated by Diekmann (2007) for the southern parts of Antarctic Circumpolar Current in all Southern Ocean sectors. Also Frank et al. (2000), Chase et al. (2003), Dezileau et al. (2003), and Bradtmiller et al. (2009) found lower biogenic opal accumulation rates south of the Antarctic Polar Front during MIS 2 relative to MIS 1, thereby suggesting less diatom productivity during MIS 2.

Around 17 ka, atmospheric CO₂ increased rapidly and the Southern Hemisphere Westerlies probably shifted south (Toggweiler 2009). It remains unclear whether the shift in Southern Hemisphere Westerlies caused the rise in CO₂ or if the shift was a result of rising CO₂. Denton et al. (2010) show that reorganization of ocean circulation, induced by intensified cooling as a result of large meltwater pulses in the Northern Hemisphere, weakened the Atlantic Meridional Overturning Circulation. This consequently led to a poleward shift of the Southern Hemisphere Westerlies, intensified upwelling of CO₂-rich mid-depth water, and therefore the warming of Antarctica (Toggweiler & Russell 2008; Toggweiler & Lea 2010). Banderas et al. (2012), Burke & Robinson (2012), and Kwon et al. (2012) support this theory by inferring increased deep-water mixing and less stratification of the water column in the Southern Ocean during the deglacial period. Anderson et al. (2009) also interpreted biogenic opal flux as an upwelling proxy because biogenic opal production is ultimately limited by dissolved Si supply, explaining its direct, but not necessarily linear connection. Biogenic opal mass accumulation rate rose abruptly at MD07-3133 and still also the ²³⁰Th-normalized biogenic opal flux record of MD07-3134 (Fig. 5 E, G, grey vertical bar) rose around 17 ka, thus representing probable increases in bioproductivity and upwelling. The rise is followed by a maximum around 15 ka in biogenic opal accumulation rate at MD07-3133, which was also detected at other core sites in the Southern Ocean (Atlantic, Indian, and Pacific sectors) (Anderson et al. 2009), and coincides with Antarctic Isotopic Maximum 1.

During the Antarctic Cold Reversal (14.54 - 12.76 ka; Putnam et al. 2010) biogenic opal mass accumulation rates at MD07-3133 and MD07-3134 (Fig. 5 E) are only slightly reduced and

remain high. Also EDML ice core data show only a minor reduction in $\delta^{18}\text{O}$ and rise in sea-salt Na^+ flux (Fig. 5 A, B) according to regional differences. This is slightly different from the observation of Anderson et al. (2009) of strongly decreased biogenic opal flux (Fig. 5 G) indicating reduced Southern Ocean upwelling during that time. The Antarctic Cold Reversal is followed by the Antarctic Isotopic Maximum 0, an abrupt rise in temperature and CO_2 , as well as sea ice decrease, also the biogenic opal content rose at both core sites during that time.

Linear sedimentation rate and biogenic opal mass accumulation rate were equivalent for both Scotia Sea sites during the Last Glacial Maximum but increased by a factor of 1.5 to 2 at Site MD07-3133 during MIS 3, the Antarctic Cold Reversal, and MIS 1 (Fig. 4 A, E). Higher amplitudes further north could be related to an approximately 5° shift in latitude of the Antarctic Circumpolar Current fronts (and associated opal belt) to the north during the Last Glacial Maximum (Gersonde et al. 2003). Also, Allen et al. (2011) observed a shift of the winter sea ice limit of at least 5° northwards during the Last Glacial Maximum, so that it remained north of the Scotia Sea. Accordingly, at that time, both core sites would have been within the winter sea ice limit, explaining the similarly reduced biogenic opal mass accumulation and linear sedimentation rates. Today, MD07-3133 which is located approximately 450 km northwest of MD07-3134 (Fig. 1) lies north of the winter sea ice limit with significantly elevated biogenic opal mass accumulation and linear sedimentation rates, while MD07-3134 is within the winter sea ice limit and exhibits reduced biogenic opal mass accumulation and linear sedimentation rates. Therefore, we suggest that the distribution of sea ice has a strong influence on bioproductivity and can be the reason for pronounced regional differences in the Southern Ocean.

The last glacial period was characterized by abrupt millennial-scale climate fluctuations (e.g. Blunier & Brook 2001; Ahn & Brook 2008), which have been detected worldwide, e.g. in stalagmites in southeast China (Cosford et al. 2008), in Antarctic ice cores (e.g. EDML; EPICA Community Members 2006; Fig. 5 A, B), and in Greenland ice cores (nGRIP; NGRIP Members 2004; Fig. 5 H). Also in marine sediments (ODP site 1089, Cortese & Abelmann (2002); Fig. 5 D) in the Atlantic Sector summer sea surface temperature record shows large millennial-scale temperature changes during the last glacial, and correlates relatively well with our biogenic opal percentages, and to a lesser extent also with the biogenic opal mass accumulation rate records. During periods with high summer sea surface temperature, maxima in biogenic opal percentages can also be recognized. Around 65 ka in MIS 4 the MD07-3134 data shows an absolute maximum in biogenic opal percentages, which is also observed in the ^{230}Th -normalized biogenic opal flux (Fig. 5 G). At this time, summer sea surface temperature at ODP site 1089 (Cortese & Abelmann 2002; Fig 5 D), in the Atlantic Sector, also rose about 4°C .

The precise and detailed chronology of Sites MD07-3133 and MD07-3134 in combination with the decadal-scale resolution of biogenic opal determinations provides the opportunity to study regional bioproductivity changes in the Southern Ocean relative to the timing of individual Antarctic Isotopic Maxima. Strong high-frequency fluctuations are also noticeable in the biogenic opal content record (Fig. 5 G) and to a lesser extent in biogenic opal mass accumulation rate (Fig.

5 E). At Site MD07-3134, biogenic opal peaks, representing enhanced bioproductivity, occurred during the relatively warm phases in Antarctica, i.e. during Antarctic Isotopic Maxima 5, 7, 8, 10, 12, 13, 14, 16, 17, and 19, while less sea ice occurred (Fig. 5 B). Extremely large spikes are documented for Antarctic Isotopic Maxima 15, 18, 20, and 22, when biogenic opal mass accumulation rate in the central Scotia Sea increases up to more than 20 g/cm²/kyr, at times when the sea ice cover was only marginally reduced and Antarctic atmospheric temperatures and CO₂ concentration elevated only slightly. These fluxes are, however, clearly biased by sediment focusing as stated by the ²³⁰Th normalization results (Fig. 4 C and D), but still showing the same incline. In general, biogenic opal content and mass accumulation rates show the same trend as atmospheric CO₂ concentration (Fig. 5 C); biogenic opal rises correspond well to increasing CO₂ concentration, while during low CO₂ biogenic opal is also mainly at minima. In addition, Anderson et al. (2009) also found an increase in upwelling at each phase of rising CO₂ during MIS 3, illustrated by higher biogenic opal flux in the Southern Ocean (Fig. 5 G, blue and grey curve), which corresponds quite well with the ²³⁰Th normalized biogenic opal flux from MD07-3134 (Fig. 5 G, black curve). Our investigations show that variations in biogenic opal flux reflect bioproductivity changes and strongly correlate to sea ice cover, summer sea surface temperature as well as atmospheric CO₂ variations.

Summary and Conclusions

Silica is an important nutrient that fuels biological production in the Southern Ocean. We investigated two long deep-sea sediment cores from the central Scotia Sea south of the present Antarctic Polar Front, that exhibit exceptionally high sedimentation rates (up to 1.8 and 1.2 m/kyr for Sites MD07-3133 and MD07-3134, respectively) to gain detailed (decadal-scale) insight into past biogenic opal flux variations.

In a first step, we measured biogenic opal conventionally by leaching 253 samples from core sections providing large-amplitude variations according to the method of Müller & Schneider (1993). Then, we estimated biogenic opal by testing three methods that rely on ~9100 non-destructive measurements (at 1-cm increments) of sediment colour b*, wet bulk density, and Si/Ti-count ratios. Finally, we determined biogenic opal using FTIRS on 891 samples at 10-cm increments.

One interesting result is that all methods can be used to decipher general biogenic opal trends. However, FTIRS – a novel method for marine sediment – provides the most reliable estimation relative to the conventional leaching method. It is rather inexpensive and requires only a small portion (11 mg) of sample material.

Biogenic opal flux records in the Southern Ocean are only marginally affected by preservation changes and therefore provide valid information on past bioproductivity changes. We provide the first decadal-scale resolution continuous bioproductivity record for the Southern Ocean over the last 92.5 kyr. The biogenic opal mass accumulation rate records of the central

Scotia Sea exhibit a relatively complicated glacial-to-interglacial pattern with large-amplitude, millennial-scale fluctuations in bioproductivity.

South of the Antarctic Polar Front, lowest bioproductivity levels deduced from biogenic opal fluxes occurred during the Last Glacial Maximum, when upwelling of mid-depth water was reduced and sea ice cover intensified. ^{230}Th normalized biogenic opal fluxes in core MD07-3134 show a similar pattern albeit at realistic values of between 1 and 1.5 $\text{g/cm}^2/\text{kyr}$ during interglacials, whereas glacial MIS 2 and 3 were generally characterized by lower values near 0.5 $\text{g/cm}^2/\text{kyr}$. These numbers are comparable to other records in the Atlantic sector of the Southern Ocean. Around 17 ka, bioproductivity increased abruptly, corresponding to rising atmospheric CO_2 and decreasing seasonal sea ice coverage. Distribution of sea ice strongly influences bioproductivity and may be the reason for pronounced regional differences in the Southern Ocean. Also summer sea surface temperature changes are strongly correlated to the biogenic opal flux changes in the central Scotia Sea.

We are grateful for financial support from the Deutsche Forschungsgemeinschaft (DFG; grants RI 525/17-1, KU 683/9-1, WE2039/8-1) and the DFG-Priority Programme Antarctic Research 1158. Thanks are also due to Carin Olofsson and Carsten Meyer-Jacob for assisting the FTIRS measurements at Climate Impacts Research Centre in Umeå, Sweden. Ana Kolevica is thanked for the U-series isotope measurements on the quadrupole ICPMS at GEOMAR, Kiel. Finally, we thank the reviewers Robert Anderson and Xavier Crosta, who greatly helped to improve the manuscript. Our study was part of the Southern Ocean Initiative of the International Marine Past Global Change Study (IMAGES) program and the AWI research program "Polar Regions and Coasts in a changing Earth System" (PACES), Topic 3 "Lessons from the Past". Supplementary data to this paper are available at doi:10.1594/PANGAEA.789348 (<http://doi.pangaea.de/10.1594/PANGAEA.789348>).

Reference list

- AHN, J. & BROOK, E. J. 2008. Atmospheric CO_2 and Climate on Millennial Time Scales During the Last Glacial Period. *Science*, 322, 83-85.
- ALLEN, C. S., PIKE, J. & PUDSEY, C. J. 2011. Last glacial-interglacial sea-ice cover in the SW Atlantic and its potential role in global deglaciation. *Quaternary Science Reviews*, 30, 2446-2458.
- ANDERSON, J. B. & ANDREWS, J. T. 1999. Radiocarbon constraints on ice sheet advance and retreat in the Weddell Sea, Antarctica. *Geology*, 27, 179-182.
- ANDERSON, R. F., ALI, S., BRADTMILLER, L. I., NIELSEN, S. H. H., FLEISHER, M. Q., ANDERSON, B. E. & BURCKLE, L. H. 2009. Wind-Driven Upwelling in the Southern Ocean and the Deglacial Rise in Atmospheric CO_2 . *Science*, 323, 1443-1448.
- BALASCIO, N. L., ZHANG, Z., BRADLEY, R. S., PERREN, B., DAHL, S. O. & BAKKE, J. 2011. A multi-proxy approach to assessing isolation basin stratigraphy from the Lofoten Islands, Norway. *Quaternary Research*, 75, 288-300.
- BANDERAS, R., ÁLVAREZ-SOLAS, J. & MONTOYA, M. 2012. Role of CO_2 and Southern Ocean winds in glacial abrupt climate change. *Climate of the Past*, 8, 1011-1021.

- BAREILLE, G., LABRACHERIE, M., BERTRAND, P., LABEYRIE, L., LAVAUX, G. & DIGNAN, M. 1998. Glacial-interglacial changes in the accumulation rates of major biogenic components in Southern Indian Ocean sediments. *Journal of Marine Systems*, 17, 527-539.
- BERGER, A. & LOUTRE, M. F. 1991. Insolation values for the climate of the last 10 million years. *Quaternary Science Reviews*, 10, 297-317.
- BLUNIER, T. & BROOK, E. J. 2001. Timing of Millennial-Scale: Climate Change in Antarctica and Greenland During the Last Glacial Period. *Science*, 291, 109-112.
- BOYD, P. W., WATSON, A. J., LAW, C. S., ABRAHAM, E. R., TRULL, T., MURDOCH, R., BAKKER, D. C. E., BOWIE, A. R., BUESSELER, K. O., CHANG, H., CHARETTE, M., CROOT, P., DOWNING, K., FREW, R., GALL, M., HADFIELD, M., HALL, J., HARVEY, M., JAMESON, G., LAROCHE, J., LIDDICOAT, M., LING, R., MALDONADO, M. T., MCKAY, R. M., NODDER, S., PICKMERE, S., PRIDMORE, R., RINTOUL, S., SAFI, K., SUTTON, P., STRZEPEK, R., TANNEBERGER, K., TURNER, S., WAITE, A. & ZELDIS, J. 2000. A mesoscale phytoplankton bloom in the polar Southern Ocean stimulated by iron fertilization. *Nature*, 407, 695-702.
- BRADTMILLER, L. I., ANDERSON, R. F., FLEISHER, M. Q. & BURCKLE, L. H. 2009. Comparing glacial and Holocene opal fluxes in the Pacific sector of the Southern Ocean. *Palaeoceanography*, 24, PA2214, doi:10.1029/2008PA001693.
- BRADTMILLER, L. I., ANDERSON, R. F., FLEISHER, M. Q. & BURCKLE, L. H. 2007. Opal burial in the equatorial Atlantic Ocean over the last 30 ka: Implications for glacial-interglacial changes in the ocean silicon cycle. *Paleoceanography*, 22, PA4216, doi:10.1029/2007PA001443.
- BURKE, A. & ROBINSON, L. F. 2012. The Southern Ocean's Role in Carbon Exchange During the Last Deglaciation. *Science*, 335, 557-561.
- CASSAR, N., BENDER, M. L., BARNETT, B. A., FAN, S., MOXIM, W. J., LEVY II, H. & TILBROOK, B. 2007. The Southern Ocean Biological Response to Aeolian Iron Deposition. *Science*, 317, 1067-1070.
- CHARLES, C. D., FROELICH, P. N., ZIBELLO, M. A., MORTLOCK, R. A. & MORLEY, J. J. 1991. Biogenic opal in southern ocean sediments over the last 450,000 years: implications for surface water chemistry and circulation. *Paleoceanography*, 6, 697-728, doi:10.1029/91PA02477
- CHASE, Z., ANDERSON, R. F., FLEISHER, M. Q. & KUBIK, P. W. 2003. Accumulation of biogenic and lithogenic material in the Pacific sector of the Southern Ocean during the past 40,000 years. *Deep-Sea Research II*, 50, 799-832.
- CORTESE, G. & ABELMANN, A. 2002. Radiolarian-based paleotemperatures during the last 160 kyr at ODP Site 1089 (Southern Ocean, Atlantic Sector). *Palaeogeography, Palaeoclimatology, Palaeoecology*, 182, 259-286.
- COSFORD, J., QING, H., YUAN, D., ZHANG, M., HOLMDEN, C., PATTERSON, W. & HAI, C. 2008. Millennial-scale variability in the Asian monsoon: Evidence from oxygen isotope records from stalagmites in southeastern China. *Palaeogeography, Palaeoclimatology, Palaeoecology*, 266, 3-12.
- DE BAAR, H. J. W., BOYD, P. W., COALE, K. H., LANDRY, M. R., TSUDA, A., ASSMY, P., BAKKER, D. C. E., BOZEC, Y., BARBER, R. T., BRZEZINSKI, M. A., BUESSELER, K. O., BOYÉ, M., CROOT, P. L., GERVAIS, F., GORBUNOV, M. Y., HARRISON, P. J., HISCOCK, W. T., LAAN, P., LANCELOT, C., LAW, C. S., LEVASSEUR, M., MARCHETTI, A., MILLERO, F. J., NISHIOKA, J., NOJIRI, Y., VAN OIJEN, T., RIEBESELL, U., RIJKENBERG, M. J. A., SAITO, H., TAKEDA, S., TIMMERMANS, K. R., VELDHUIS, M. J. W., WAITE, A. M. & WONG, C.-S. 2005. Synthesis of iron fertilization experiments: From the Iron Age in the Age of Enlightenment. *Journal of Geophysical Research: Oceans*, 110, C9, C09S16, doi:10.1029/2004jc002601.
- DELMONTE, B., PETTIT, J. R., ANDERSEN, K. K., BASILE-DOELSCH, I., MAGGI, V. & YA LIPENKOV, V. 2004. Dust size evidence for opposite regional atmospheric circulation changes over east Antarctica during the last climatic transition. *Climate Dynamics*, 23, 427-438.
- DENTON, G. H., ANDERSON, R. F., TOGGWEILER, J. R., EDWARDS, R. L., SCHAEFER, J. M. & PUTNAM, A. E. 2010. The Last Glacial Termination. *Science*, 328, 1652-1656.

- DEZILEAU, L., REYSS, J. L. & LEMOINE, F. 2003. Late Quaternary changes in biogenic opal fluxes in the Southern Indian Ocean. *Marine Geology*, 202, 143-158.
- DIEKMANN, B. 2007. Sedimentary patterns in the late Quaternary Southern Ocean. *Deep-Sea Research II*, 54, 2350-2366.
- DIEKMANN, B., KUHN, G., RACHOLD, V., ABELMANN, A., BRATHAUER, U., FÜTTERER, D. K., GERSONDE, R. & GROBE, H. 2000. Terrigenous sediment supply in the Scotia Sea (Southern Ocean): response to Late Quaternary ice dynamics in Patagonia and on the Antarctic Peninsula. *Palaeogeography, Palaeoclimatology, Palaeoecology*, 162, 357-387.
- EPICA COMMUNITY MEMBERS 2004. Eight glacial cycles from an Antarctic ice core. *Nature*, 429, 623-628.
- EPICA COMMUNITY MEMBERS 2006. One-to-one coupling of glacial climate variability in Greenland and Antarctica. *Nature*, 444, 195-198.
- ERICKSON, D. J., HERNANDEZ, J. L., GINOUX, P., GREGG, W. W., MCCLAIN, C. & CHRISTIAN, J. 2003. Atmospheric iron delivery and surface ocean biological activity in the Southern Ocean and Patagonian region. *Geophysical Research Letters*, 30, 12, 1609, doi:10.1029/2003GL017241.
- FISCHER, H., FUNDEL, F., RUTH, U., TWARLOH, B., WEGNER, A., UDISTI, R., BECAGLI, S., CASTELLANO, E., MORGANTI, A., SEVERI, M., WOLFF, E., LITTOT, G., RÖTHLISBERGER, R., MULVANEY, R., HUTTERLI, M. A., KAUFMANN, P., FEDERER, U., LAMBERT, F., BIGLER, M., HANSSON, M., JONSELL, U., DE ANGELIS, M., BOUTRON, C., SIGGAARD-ANDERSEN, M.-L., STEFFENSEN, J. P., BARBANTE, C., GASPARI, V., GABRIELLI, P. & WAGENBACH, D. 2007a. EPICA EDML chemical concentrations and fluxes. doi:10.1594/PANGAEA.683642.
- FISCHER, H., FUNDEL, F., RUTH, U., TWARLOH, B., WEGNER, A., UDISTI, R., BECAGLI, S., CASTELLANO, E., MORGANTI, A., SEVERI, M., WOLFF, E., LITTOT, G., RÖTHLISBERGER, R., MULVANEY, R., HUTTERLI, M. A., KAUFMANN, P., FEDERER, U., LAMBERT, F., BIGLER, M., HANSSON, M., JONSELL, U., DE ANGELIS, M., BOUTRON, C., SIGGAARD-ANDERSEN, M.-L., STEFFENSEN, J. P., BARBANTE, C., GASPARI, V., GABRIELLI, P. & WAGENBACH, D. 2007b. Reconstruction of millennial changes in dust emission, transport and regional sea ice coverage using the deep EPICA ice cores from the Atlantic and Indian Ocean sector of Antarctica. *Earth and Planetary Science Letters*, 260, 340-354.
- FRANCOIS, R., FRANK, M., RUTGERS VAN DER LOEFF, M. M. & BACON, M. P. 2004. 230Th normalization: An essential tool for interpreting sedimentary fluxes during the late Quaternary. *Paleoceanography*, 19, PA1018, doi:10.1029/2003PA000939.
- FRANCUS, P., LAMB, H., NAKAGAWA, T., MARSHALL, M., BROWN, E. & MEMBERS, S. P. 2009. The potential of high-resolution X-ray fluorescence core scanning: Applications in paleolimnology. *PAGES news*, 17, 93-95.
- FRANK, M., GERSONDE, R. & MANGINI, A. 1999. Sediment redistribution, 230Th-normalization and implications for the reconstruction of particle flux and export paleoproductivity. In: Fischer, G. & Wefer, G. (eds) *Use of Proxies in Paleoceanography: Examples from the South Atlantic*. Springer, New York, 409-426.
- FRANK, M., GERSONDE, R., RUTGERS VAN DER LOEFF, M. M., KUHN, G. & MANGINI, A. 1996. Late Quaternary sediment dating and quantification of lateral sediment redistribution applying 230Th: A study from the eastern Atlantic sector of the Southern Ocean. *Geologische Rundschau*, 85, 554-566.
- FRANK, M., GERSONDE, R., VAN DER LOEFF, M. R., BOHRMANN, G., NÜRNBERG, C. C., KUBIK, P. W., SUTER, M. & MANGINI, A. 2000. Similar glacial and interglacial export bioproductivity in the Atlantic sector of the Southern Ocean: Multiproxy evidence and implications for glacial atmospheric CO₂. *Paleoceanography*, 15, 642-658, doi:10.1029/2000PA000497.
- GEIBERT, W., VAN DER LOEFF, M. M. R., USBECK, R., GERSONDE, R., KUHN, G. & SEEBERG-ELVERFELDT, J. 2005. Quantifying the opal belt in the Atlantic and southeast Pacific sector of the Southern Ocean by means of ²³⁰Th normalization. *Global Biogeochemical Cycles*, 19, GB4001, doi:10.1029/2005GB002465.
- GELADI, P., MACDOUGALL, D. & MARTENS, H. 1985. Linearization and Scatter-Correction for Near-Infrared Reflectance Spectra of Meat. *Applied Spectroscopy*, 39, 491-500.

- GERSONDE, R., ABELMANN, A., BRATHAUER, U., BECQUEY, S., BIANCHI, C., CORTESE, G., GROBE, H., KUHN, G., NIEBLER, H.-S., SEGL, M., SIEGER, R., U. Z. & FÜTTERER, D. K. 2003. Last glacial sea surface temperatures and sea-ice extent in the Southern Ocean (Atlantic-Indian sector): A multiproxy approach. *Paleoceanography*, 18(3), 1061, doi:10.1029/2002PA000809.
- GERSONDE, R., CROSTA, X., ABELMANN, A. & ARMAND, L. 2005. Sea-surface temperature and sea ice distribution of the Southern Ocean at the EPILOG Last Glacial Maximum—a circum-Antarctic view based on siliceous microfossil records. *Quaternary Science Reviews*, 24, 869-896.
- GRIFFITHS, P. R. & DE HASETH, J. A. 1986. *Fourier transform infrared spectrometry*. Wiley, New York.
- GUILLOU, H., SINGER, B. S., LAJ, C., KISSEL, C., SCAILLET, S. & JICHA, B. R. 2004. On the age of the Laschamp geomagnetic excursion. *Earth and Planetary Science Letters*, 227, 331-343.
- HENDRY, K. R., RICKABY, R. E. M. & ALLEN, C. S. 2011. Changes in micronutrient supply to the surface Southern Ocean (Atlantic sector) across the glacial termination. *Geochemistry Geophysics Geosystems*, 12, Q09007, doi:10.1029/2011gc003691.
- HORN, M. G., BEUCHER, C. P., ROBINSON, R. S. & BRZEZINSKI, M. A. 2011. Southern ocean nitrogen and silicon dynamics during the last deglaciation. *Earth and Planetary Science Letters*, 310, 334-339.
- JANSEN, J. H. F., VAN DER GAAST, S. J., KOSTER, B. & VAARS, A. J. 1998. CORTEX, a shipboard XRF-scanner for element analyses in split sediment cores. *Marine Geology*, 151, 143-153.
- JOHNSON, C. M., BROWN, E. T. & SHI, J. 2011. Biogenic silica deposition in Lake Malawi, East Africa over the past 150,000 years. *Palaeogeography, Palaeoclimatology, Palaeoecology*, 303, 103-109.
- KANFOUSH, S. L., HODELL, D. A., CHARLES, C. D., GUILDERTSON, T. P., MORTYN, P. G. & NINEMANN, U. S. 2000. Millennial-Scale Instability of the Antarctic Ice Sheet During the Last Glaciation. *Science*, 288, 1815-1818.
- KAUFMANN, P., FUNDEL, F., FISCHER, H., BIGLER, M., RÜTH, U., UDISTI, R., HANSSON, M., DE ANGELIS, M., BARBANTE, C., WOLFF, E. W., HUTTERLI, M. & WAGENBACH, D. 2010. Ammonium and non-sea salt sulfate in the EPICA ice cores as indicator of biological activity in the Southern Ocean. *Quaternary Science Reviews*, 29, 313-323.
- KRETSCHMER, S., GEIBERT, W., RUTGERS VAN DER LOEFF, M. M., SCHNABEL, C., XU, S. & MOLLENHAUER, G. 2011. Fractionation of ²³⁰Th, ²³¹Pa, and ¹⁰Be induced by particle size and composition within an opal-rich sediment of the Atlantic Southern Ocean. *Geochimica et Cosmochimica Acta*, 75, 6971-6987.
- KUMAR, N., ANDERSON, R. F., MORTLOCK, R. A., FROELICH, P. N., KUBIK, P., DITTRICH-HANNEN, B. & SUTER, M. 1995. Increased biological productivity and export production in the glacial Southern Ocean. *Nature*, 378, 675-680.
- KWON, E. Y., HAIN, M. P., SIGMAN, D. M., GALBRAITH, E. D., SARMIENTO, J. L. & TOGGWEILER, J. R. 2012. North Atlantic ventilation of "southern-sourced" deep water in the glacial ocean. *Paleoceanography*, 27, PA2208, doi:10.1029/2011pa002211.
- LEFÈVRE, N. & WATSON, A. J. 1999. Modeling the geochemical cycle of iron in the oceans and its impact on atmospheric CO₂ concentrations. *Global Biogeochemical Cycles*, 13, 727-736, doi:10.1029/1999GB900034.
- LI, F., GINOUX, P. & RAMASWAMY, V. 2010. Transport of Patagonian dust to Antarctica. *Journal of Geophysical Research*, 115, D18217, doi:10.1029/2009jd012356.
- LIN, H., RAUSCHENBERG, S., HEXEL, C. R., SHAW, T. J. & TWINING, B. S. 2011. Free-drifting icebergs as sources of iron to the Weddell Sea. *Deep Sea Research Part II*, 58, 1392-1406.
- LISIECKI, L. E. & RAYMO, M. E. 2005. A Pliocene-Pleistocene stack of 57 globally distributed benthic $\delta^{18}O$ records. *Paleoceanography*, 20, PA1003, doi:10.1029/2004pa001071.
- MALDONADO, A., BARNOLAS, A., BOHOYOA, F., GALINDO-ZALDÍVAR, J., HERNÁNDEZ-MOLINA, J., LOBO, F., RODRÍGUEZ-FERNÁNDEZ, J., SOMOZA, L. & VÁZQUEZ, J. T. 2003. Contourite deposits in the central Scotia Sea: the importance of

- the Antarctic Circumpolar Current and the Weddell Gyre flows. *Palaeogeography, Palaeoclimatology, Palaeoecology*, 198, 187-221.
- MARTENS, H. & NAES, T. 1989. *Multivariate calibration*. John Wiley & Sons, New York.
- MARTIN, J. H., GORDON, R. M. & FITZWATER, S. E. 1990. Iron in Antarctic waters. *Nature*, 345, 156-158.
- MARTÍNEZ-GARCÍA, A., ROSELL-MELE, A., JACCARD, S. L., GEIBERT, W., SIGMAN, D. M. & HAUG, G. H. 2011. Southern Ocean dust-climate coupling over the past four million years. *Nature*, 476, 312-315.
- MESKHIDZE, N., NENES, A., CHAMEIDES, W. L., LUO, C. & MAHOWALD, N. 2007. Atlantic Southern Ocean productivity: Fertilization from above or below? *Global Biogeochemical Cycles*, 21, GB2006, doi:10.1029/2006GB002711.
- MONNIN, E. 2006. EPICA Dome C high resolution carbon dioxide concentrations. doi:10.1594/PANGAEA.472488.
- MORENO, P. I., LOWELL, T. V., JACOBSON JR, G. L. & DENTON, G. H. 1999. Abrupt Vegetation and Climate Changes During the Last Glacial Maximum and Last Termination in The Chilean Lake District: A Case Study from Canal De La Puntilla (41°S). *Geografiska Annaler: Series A, Physical Geography*, 81, 285-311.
- MORTLOCK, R. A., CHARLES, C. D., FROELICH, P. N., ZIBELLO, M. A., SALTZMAN, J., HAYS, J. D. & BURCKLE, L. H. 1991. Evidence for lower productivity in the Antarctic Ocean during the last glaciation. *Nature*, 351, 220-223.
- MÜLLER, P. J. & SCHNEIDER, R. 1993. An automated leaching method for the determination of opal in sediments and particulate matter. *Deep-Sea Research I*, 40, 425-444.
- MURRAY, R. W., LEINEN, M. & ISERN, A. R. 1993. Biogenic flux of Al to sediment in the central equatorial Pacific Ocean: evidence for increased productivity during glacial periods. *Paleoceanography*, 8, 651-670, doi:10.1029/93PA02195.
- NGRIP MEMBERS 2004. High-resolution record of Northern Hemisphere climate extending into the last interglacial period. *Nature*, 431, 147-151.
- NIELSEN, S. H. H., HODELL, D. A., KAMENOV, G., GUILDERTSON, T. & PERFIT, M. R. 2007. Origin and significance of ice-rafted detritus in the Atlantic sector of the Southern Ocean. *Geochemistry, Geophysics, Geosystems*, 8, Q12005, doi:10.1029/2007GC001618
- ORSI, A. H., WHITWORTH III, T. & NOWLIN JR, W. D. 1995. On the meridional extent and fronts of the Antarctic Circumpolar Current. *Deep-Sea Research I*, 42, 641-673.
- PAILLARD, D., LABEYRIE, L. & YIOU, P. 1996. Macintosh Program performs time-series analysis. *EOS Transactions*, 77, 379-379, doi:10.1029/96eo00259.
- PONDAVEN, P., RAGUENEAU, O., TREGUER, P., HAUVEPRE, A., DEZILEAU, L. & REYSS, J. L. 2000. Resolving the 'opal paradox' in the Southern Ocean. *Nature*, 405, 168-172.
- PUDSEY, C. J. & HOWE, J. A. 1998. Quaternary history of the Antarctic Circumpolar Current: evidence from the Scotia Sea. *Marine Geology*, 148, 83-112.
- PUGH, R. S., MCCAIVE, I. N., HILLENBRAND, C. D. & KUHN, G. 2009. Circum-Antarctic age modelling of Quaternary marine cores under the Antarctic Circumpolar Current: Ice-core dust-magnetic correlation. *Earth and Planetary Science Letters*, 284, 113-123.
- PUTNAM, A. E., DENTON, G. H., SCHAEFER, J. M., BARRELL, D. J. A., ANDERSEN, B. G., FINKEL, R. C., SCHWARTZ, R., DOUGHTY, A. M., KAPLAN, M. R. & SCHLUCHTER, C. 2010. Glacier advance in southern middle-latitudes during the Antarctic Cold Reversal. *Nature Geoscience*, 3, 700-704.
- RAGUENEAU, O., TREGUER, P., LEYNAERT, A., ERSON, R. F., BRZEZINSKI, M. A., DEMASTER, D. J., DUGDALE, R. C., DYMOND, J., FISCHER, G., FRANCOIS, R., HEINZE, C., MAIER-REIMER, E., MARTIN-JEZEQUEL, V., NELSON, D. M. & QUEGUINER, B. 2000. A review of the Si cycle in the modern ocean: recent progress and missing gaps in the application of biogenic opal as a paleoproductivity proxy. *Global and Planetary Change*, 317-365.
- RAHMSTORF, S. 2002. Ocean circulation and climate during the past 120,000 years. *Nature*, 419, 207-214.
- RAISWELL, R. 2011. Iceberg-hosted nanoparticulate Fe in the Southern Ocean: Mineralogy, origin, dissolution kinetics and source of bioavailable Fe. *Deep Sea Research Part II*, 58, 1364-1375.

- RICHTER, T. O., VAN DER GAAST, S., KOSTER, B., VAARS, A., GIELES, R., DE STIGTER, H. C., DE HAAS, H. & VAN WEERING, T. C. E. 2006. The Avaatech XRF Core Scanner: technical description and applications to NE Atlantic sediments. Geological Society, London, Special Publications, 267, 39-50.
- ROSEN, P., VOGEL, H., CUNNINGHAM, L., HAHN, A., HAUSMANN, S., PIENITZ, R., ZOLITSCHKA, B., WAGNER, B. & PERSSON, P. 2011. Universally Applicable Model for the Quantitative Determination of Lake Sediment Composition Using Fourier Transform Infrared Spectroscopy. *Environmental Science & Technology*, 45, 8858-8865.
- ROSEN, P., VOGEL, H., CUNNINGHAM, L., REUSS, N., CONLEY, D. J. & PERSSON, P. 2010. Fourier transform infrared spectroscopy, a new method for rapid determination of total organic and inorganic carbon and biogenic silica concentration in lake sediments. *Journal of Paleolimnology*, 43, 247-259.
- SCHLÜTER, M. & RICKERT, D. 1998. Effect of pH on the measurement of biogenic silica. *Marine Chemistry*, 63, 81-93.
- STENNI, B., MASSON-DELMOTTE, V., SELMO, E., OERTER, H., MEYER, H., RÖHLISBERGER, R., JOUZEL, J., CATTANI, O., FALOURD, S., FISCHER, H., HOFFMANN, G., IACUMIN, P., JOHNSEN, S. J., MINSTER, B. & UDIŠTI, R. 2010. The deuterium excess records of EPICA Dome C and Dronning Maud Land ice cores (East Antarctica). *Quaternary Science Reviews*, 29, 146-159.
- STUART, K. M. & LONG, D. G. 2011. Tracking large tabular icebergs using the SeaWinds Ku-band microwave scatterometer. *Deep Sea Research Part II*, 58, 1285-1300.
- SWANN, G. 2010. A comparison of the Si/Al and Si/time wet-alkaline digestion methods for measurement of biogenic silica in lake sediments. *Journal of Paleolimnology*, 44, 375-385.
- TJALLINGII, R., RÖHL, U., KÖLLING, M. & BICKERT, T. 2007. Influence of the water content on X-ray fluorescence core-scanning measurements in soft marine sediments. *Geochemistry, Geophysics, Geosystems*, 8, Q02004, doi:10.1029/2006GC001393.
- TOGGWEILER, J. R. 2009. Shifting Westerlies. *Science*, 323, 1434-1435.
- TOGGWEILER, J. R. & LEA, D. W. 2010. Temperature differences between the hemispheres and ice age climate variability. *Paleoceanography*, 25, PA2212, doi:10.1029/2009pa001758.
- TOGGWEILER, J. R. & RUSSELL, J. 2008. Ocean circulation in a warming climate. *Nature*, 451, 286-288.
- TOGGWEILER, J. R., RUSSELL, J. L. & CARSON, S. R. 2006. Midlatitude westerlies, atmospheric CO₂, and climate change during the ice ages. *Paleoceanography*, 21, 15 pp, doi:10.1029/2005pa001154.
- VOGEL, H., ROSEN, P., WAGNER, B., MELLES, M. & PERSSON, P. 2008. Fourier transform infrared spectroscopy, a new cost-effective tool for quantitative analysis of biogeochemical properties in long sediment records. *Journal of Paleolimnology*, 40, 689-702.
- WEBER, M. E. 1998. Estimation of biogenic carbonate and opal by continuous non-destructive measurements in deep-sea sediments: application to the eastern Equatorial Pacific. *Deep-Sea Research I*, 45, 1955-1975.
- WEBER, M. E., KUHN, G., SPRENK, D., ROLF, C., OHLWEIN, C. & RICKEN, W. 2012. Dust transport from Patagonia to Antarctica - A new stratigraphic approach from the Scotia Sea and its implications for the last glacial cycle. *Quaternary Science Reviews*, 36, 177-188.
- WEBER, M. E., NIESSEN, F., KUHN, G. & WIEDICKE, M. 1997. Calibration and application of marine sedimentary physical properties using a multi-sensor core logger. *Marine Geology*, 136, 151-172.
- WHITWORTH, T. & PETERSON, R. G. 1985. Volume Transport of the Antarctic Circumpolar Current from Bottom Pressure Measurements. *Journal of Physical Oceanography*, 15, 810-816.

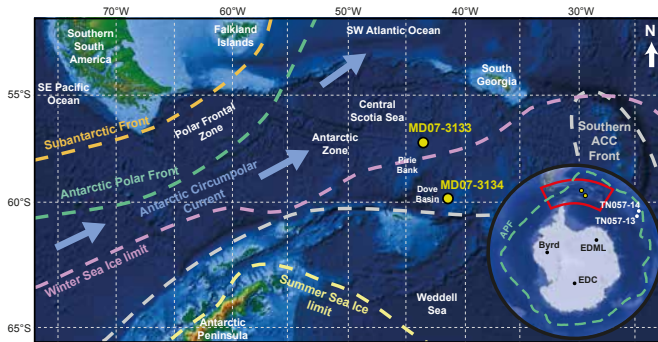


Figure 1: Location map showing the MD07-3133 and MDQ7-3134 core sites referred to in this study; Subantarctic Front, Antarctic Polar Front, Southern Antarctic Circumpolar Current Front, limits modified from Gersonde et al. (2005). Additionally, the positions of Winter and Summer Sea Ice limits today (Gersonde et al. 2005; Allen et al. 2011) are shown. Also, the direction of Antarctic Circumpolar Current is highlighted. Underlying map originates from <http://maps.ngdc.noaa.gov/viewers/bathymetry/> (access date: 20.10.2011). TN core sites are from Anderson et al. (2009); BYRD (Ahn & Brook 2008), EPICA Dronning Maud Land (EDML; EPICA Community Members 2006), and EPICA Dome C (EDC, EPICA Community Members 2004) refer to Antarctic ice cores (for details see text).

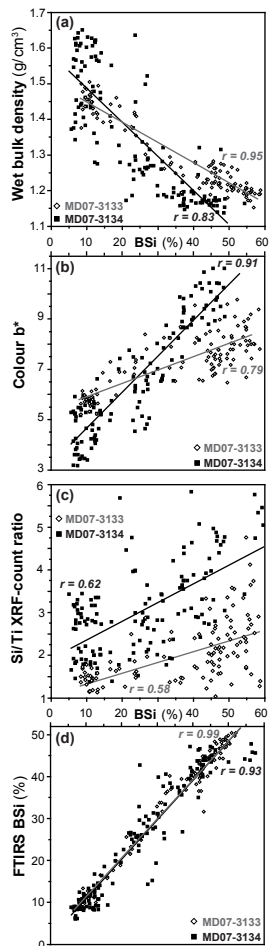


Figure 2: Scatter plots illustrating linear correlations for conventionally leached biogenic opal (BSi) values (method see Müller & Schneider 1993) and BSi content estimated from wet bulk density (a), colour b* (b), XRF-core-scanner measured Si/Ti-count ratio (c), and Fourier transform infrared spectroscopy (FTIRS) (d; method see Rosén et al. 2010). White diamonds and grey lines refer to Site MD07-3133, black squares and black lines indicate data from Site MD07-3134.

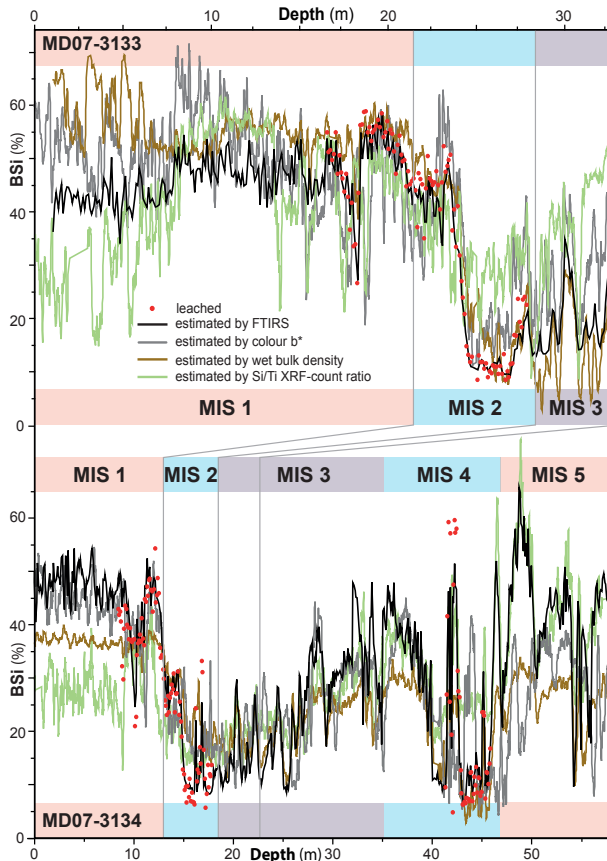


Figure 3: Comparison of biogenic opal (BSi) contents evaluated with different methods for sites MD07-3133 (top) and MD07-3134 (bottom): conventionally (leached; data points highlighted as red dots; method see Müller & Schneider 1993); and BSi estimated from wet bulk density (brown curve), colour b^* (grey curve), Fourier transform infrared spectroscopy (FTIRS; black curve; method see Rosén et al. 2010), and XRF-core-scanner measured Si/Ti-count ratio (green curve; method see Balascio et al. 2011). Marine Isotopic Stages (MIS) 1 to 5 are plotted for reference (Lisiecki & Raymo 2005).

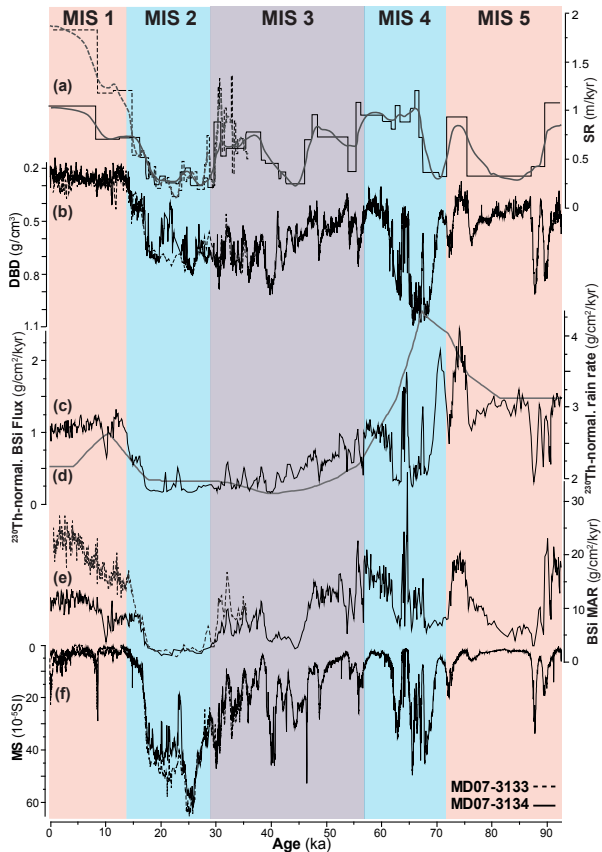


Figure 4: Sites MD07-3133 (dashed lines) and MD07-3134 (solid lines) records: (a) Linear sedimentation rate (LSR) (black lines) and sedimentation rates (SR) estimated from a cubic smoothing spline age-model (grey lines; Weber et al. 2012); (b) Dry bulk density (DBD); (c) ^{230}Th -normalized biogenic opal (BSi) flux evaluated by using the Fourier transform infrared spectroscopy (FTIRS) estimated biogenic opal values (for method see Rosén et al. 2010); (d) ^{230}Th -normalized average rain rate; (e) BSi mass accumulation rate (MAR) evaluated using FTIRS estimated BSi values multiplied by SR from a cubic smoothing spline age-model (a) and DBD (b); (f) Magnetic susceptibility (MS) records as dust proxy (Weber et al. 2012). Marine Isotopic Stages (MIS) 1 to 5 are plotted for reference (Lisiecki & Raymo 2005).

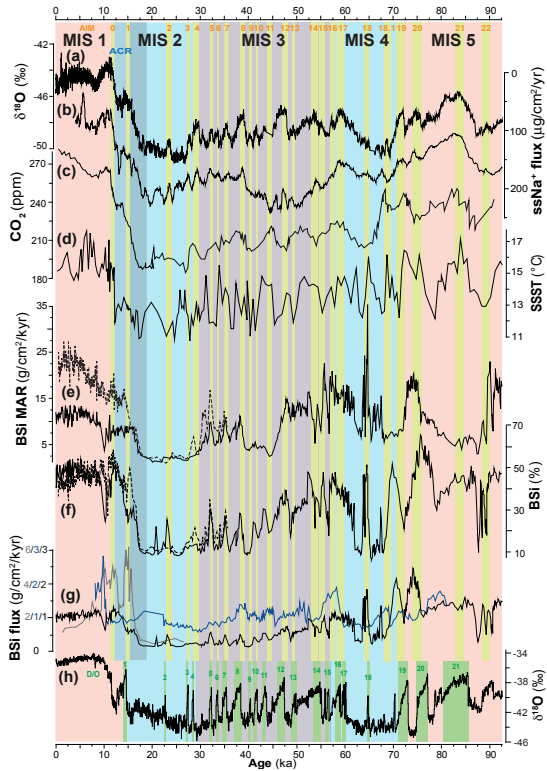


Figure 5: Palaeoclimate and palaeoproductivity records for the last 92.5 kyr highlighting millennial-scale climate fluctuations during the last glacial: (a and b) EDML ice core $\delta^{18}\text{O}$ (EPICA Community Members 2006) as local ice sheet temperature indicator and ssNa^+ flux (Fischer et al. 2007a) as sea ice proxy; (c) combined record of CO_2 measured at EDC (0 – 20 ka; Monnin 2006) and Byrd ice core (20 – 91 ka; Ahn & Brook 2008); (d) radiolarian-based summer sea-surface temperature (SSST) reconstruction derived at ODP site 1089 (Cortese & Abelmann 2002) in the Atlantic sector of the Southern Ocean; (e) biogenic opal mass accumulation rates (BSi MAR) for MD07-3133 (dashed line) and MD07-3134 (solid line) core sites calculated from multiplying FTIRS-estimated BSi (method see Rosén et al. 2010) and sedimentation rates estimated from a cubic smoothing spline age-model (Weber et al. 2012); (f) MD07-3133 and MD07-3134 BSi content as percentages estimated with FTIRS; (g) ^{230}Th -normalized BSi flux from sediment cores MD07-3134 (black line), TN057-13PC (grey line) and TN057-14PC (blue line; Anderson et al. 2009) from the SE Atlantic Sector of the Southern Ocean (Fig. 1); (h) is Northern Hemisphere NGRIP ice core $\delta^{15}\text{O}$ (NGRIP Members 2004). Marine Isotopic Stages (MIS) 1 to 5 are plotted for reference (Lisiecki & Raymo 2005), as well as Antarctic Isotopic Maxima (AIM; EPICA Community Members 2006; Stenni et al. 2010), Antarctic Cold Reversal (ACR; Rahmstorf 2002), and Dansgaard-Oeschger-Cycles (D/O; Blunier & Brook 2001).

7 Discussion

7.1 Seasonal- to millennial-scale oscillations

Glacial bottom-water formation is still discussed, while North Atlantic Deep Water (NADW) production was sluggish or maybe even terminated (Knutti et al., 2004; Stocker and Johnson, 2003), Antarctica was maybe the main supplier of deep water, namely the Antarctic Bottom Water (AABW) (Shin et al., 2003). During the Last Glacial Maximum (LGM), the ice sheet in the Southern Weddell Sea had at least advanced very close, i.e. within 40 km (Larter et al., 2012) or most likely even reached the shelf break (e.g. Hillenbrand et al., 2012; Larter et al., 2012; Weber et al., 2011). Today, High-Salinity Shelf Water (HSSW) is generated during sea ice production by brine rejection (Foldvik et al., 2004; Petty et al., 2013) and then supercooled by circulation under the ice shelf becoming dense Ice-Shelf Water (ISW). Modified warm deep water (MWDW) intruding on the shelf mixes with ISW producing WSBW. Due to the fact that ice sheet covered the continental shelf, glacial bottom-water formation in the Weddell Sea must have been produced different as ice shelf cavities required for supercooling HSSW to produce ISW would be inexistent (Gales et al., 2012).

Coastal polynyas might have played an important role in deep-water formation during the LGM (Sprenk et al., in review-a; Sprenk et al., in review-b). Offshore blowing katabatic winds remove sea ice from coastal areas or ice edges, which often implements the development of coastal polynya (Kern, 2009; Williams et al., 2007). Coastal polynyas are open water areas induced from off-shore blowing winds, where heat from the ocean can be released to the cold atmosphere and sea-ice production is intensified leading to brine rejection and thus dense water formation (Tamura et al., 2008). The Brunt Ice Shelf, close to the Weddell Sea cores (Sprenk et al., in review-b) has been identified as important polynya area, where sea ice production is 9 – 14 times higher compared to neighbouring regions with the highest mean heat flux during winter months July and August (Haid and Timmermann, 2013). Today, about 10 % of all sea ice in the Southern Ocean is produced in Antarctic coastal polynyas (Tamura et al., 2008) with a major amount of 6 % alone in the Weddell Sea (Renfrew et al., 2002). In the Weddell Sea investigations showed that years with large coastal polynya areas are in accordance with maxima in total sea ice extent (Comiso and Gordon, 1998). The inter-annual variations in coastal polynya activity and area seem to be related to katabatic winds, cyclones, as well as barrier winds (Renfrew et al., 2002).

Heinemann et al. (2013) studies on coastal polynyas in the Weddell Sea revealed that in the area of Coats Land, in front of the Brunt Ice Shelf, offshore winds are mainly driven by katabatic winds, due to the steepness and length of the slope. Different studies (Sprenk et al., in review-a; Weber et al., 2011; Weber et al., 2010a) indicated that during the LGM intensified katabatic winds likely drove coastal polynya formation in the southeastern Weddell Sea. In the western Weddell Sea, Smith et al. (2010) also indicated that katabatic winds in front of the Antarctic Peninsula Ice Sheet formed coastal polynyas.

Sprenk et al. (in review-b) investigations including AMS¹⁴C ages and varve counting results of the newly opened sediment core PS1795 from the southeastern Weddell Sea revealed that the varved sediment was deposited during the LGM, matching results from earlier studies (Weber et al., 2011; Weber et al., 2010a) of varved sediment cores located close by. Although, the estimated linear sedimentation rates of about 1.1 – 1.6 m/kyr are slightly lower than the sedimentation rates calculated for sediment cores PS1599, PS1789, and PS1791, which are varying between 2.2 and 5.3 m/kyr (Sprenk et al., in review-a). These differences in sedimentation rates are possibly related to the location of the sediment cores. PS1795 originates from shallower water depth, southwest outside the southernmost channel, on a slightly steeper part of the continental slope, where the channel-ridge system starts to develop, in contrast to the other cores, which are located on the ridges NW of each channel.

For the first time, analyses on thin sections of the varves are presented in Sprenk et al. (in review-b) showing only small variations in grain size and no erosional or sharp bases of the layers, which argue against turbiditic deposition and favour varve formation. Main differences of the layers are seasonally related fluctuations in grain size and related changes in element and mineral composition. High-resolution XRF-scanner data on the thin sections show that the lighter-coloured layers have maxima in Si, Sr, Ca, and Zr counts. The comparatively immobile Zr primarily resides in heavy minerals like zircon, thus resistant to chemical and physical weathering (Alfonso et al., 2006; Wayne Nesbitt and Markovics, 1997), therefore mainly transported with coarser particles. Furthermore, RADIUS tool (Seelos and Sirocko, 2005) analysis reveal, that lighter-coloured layers contain more medium- to coarse silt-sized quartz grains and have a higher mean grain size than the brown layers. The brownish-coloured layers are characterized by predominant clay-sized particles and maxima in Fe, Ti, Rb, and K counts, generally related to minerals like mica and clay minerals (Dypvik and Harris, 2001; Vital and Statterger, 2000), e.g. chlorite and illite group members.

The seasonally related changes in grain size and elements described above, led Sprenk et al. (in review-b) discuss the following two scenarios of glacial sedimentation: during the LGM, plumes of cold and dense water were generated in front of the grounded East Antarctic Ice Sheet above the upper slope by coastal polynya, i.e. operated by strong offshore blowing katabatic winds enhancing sea-ice formation and thus brine release. The resulting dense water mass moved down the continental slope and was canalized into the channel-ridge systems northeast of Cray Fan, producing cold and saline WSBW. Apparently, this flow oscillated seasonally with a stronger salt injection during glacial winter due to increased brine release by more intense coastal polynya. We should note that spaces of open water, which were generated by the katabatic winds and led to glacial polynyas did likely not stay open for long because of the low temperatures, causing rapid freezing and associated intense brine release. The resulting glacial thermohaline current flowed underneath and against the probably weakened Weddell Gyre. The clayey layer would hence have be interpreted as a summer signal, resulting from less intense katabatic winds, hence less sea-ice transport away from the coast, reduced brine rejection in front of the ice sheet that led to reduced thermohaline convection, lower current velocities in the channels, and less overspilling

on the ridges. Vice versa, coarser-grained silty layer should represent a winter signal as a result of enhanced katabatic winds that carried sea ice away from the continent more effectively, inducing rapid freezing processes at the surface that spurred thermohaline convection, led higher velocities in the channels and higher overspilling on the ridges. As a whole, the seasonally variable thermohaline convection produced large volumes of bottom water and transported vast amounts of sediment into the deeper environment that have originally been delivered by meltwater channels from the grounded ice sheet and/or by gravitational processes (Anderson et al., 1986) leaving its trace in form of varved sediment on the ridges. In a coupled climate model, Justino and Peltier (2006) demonstrated that the seasonal cycle in the Southern Ocean was likely much stronger during LGM than it is today with a very pronounced winter season. Since coastal polynya formation is mainly driven by the intensity of the katabatic winds, sea ice was moved away from the continent and/or thinned close to the coast in glacial winter, allowing for a more intense transport of icebergs counter-clockwise around Antarctica within the Antarctic Coastal Current. This could explain why coarser-grained (winter) layers occur preferentially with higher amounts of iceberg-rafted debris (IRD).

Alternatively, coarser layers could have been deposited during summer, when ice melt occurred more likely. This interpretation could be supported by the fact that the silty layers contain higher IRD contents resulting from ice melt. Ice melt could occur either through direct surface melt, although modelling of atmospheric teleconnections from sea-surface temperature variations from equatorial Pacific (Weber et al., 2011) show that increasing temperatures would not lead to a negative ice mass balance under LGM conditions. Meltwater also could have been delivered by meltwater channels directly from the ice sheet. That process, however would only deliver fresh water that is not dense enough to sink down and move across the shelf and onto the continental slope and into the channels that accompany the ridges because the surrounding brines are much denser. Also, seasonal deposition on the ridges requires a continuous flow of a dense water mass at varying volume and velocity in the channels that is deflected to the left due to the influence of Coriolis Force, and overflows the channels on their northwestern side. This process can most likely only be sustained by a seasonally variable thermohaline convection resulting from polynya formation in front of the ice edge. Nonetheless, there is no definitive interpretation possible at the current stage as to which season produced which layer.

In chapter 4 varve counting results from sediment cores PS1599, PS1789, and PS1791 are presented. Combined varve counting results and AMS¹⁴C ages reveal that facies changes from lamination to bioturbation occurred simultaneously at the core sites around 25, 23, 21.5, 20, and 19 ka with a millennial-scale pacing (Sprenk et al., in review-a). These facies changes are only noticeable in the glacial sediment sections and are associated with varve interruption every few centuries to approximately 2000 years and are possibly related to ice-sheet retreats from the shelf edge, strongly reduced thermohaline current flow in the channels on the continental slope and at least partly open water conditions. Therefore, suggesting multiple fluctuations of the ice sheet in

the Weddell Sea during the LGM. These recurrence time period bears some similarities to the typical timescale of abrupt climate events in the North Atlantic during the last glacial period (Grootes and Stuiver, 1997; Schulz, 2002). After the final ice-sheet retreat from the shelf area around 16 ka (Weber et al., 2011) hemipelagic mud was deposited at low sedimentation rates of only 0.06 (PS1791) to 0.08 m/kyr (PS1789) and is highly bioturbated.

Strong cyclic changes in varve thickness are detectable in all varved sections of PS1599, PS1789, and PS1791 (Sprenk et al., in review-a). Bulk and evolutionary spectral analysis reveal decadal-to centennial variations in varve thickness with a dominating 50-85-yr cycle, which seems to be robust during the LGM. For an in-depth investigation of the cyclic varve thickness variation also the summer and winter layer thicknesses were analysed individually. Their bulk and evolutionary spectra show overall the same decadal-scale fluctuations as described for an annual layer couplet. Therefore, concluding that the driving mechanism influenced and modulated the sedimentation process throughout the year, overprinting the seasonal sedimentation changes.

Minor changes in total solar irradiance, e.g. 0.07 % variation in 11 years (Gray et al., 2010) seem to have direct or indirect impact on the global climate. Solar cycles have been detected in a number of climate archives (Beer et al., 2000) including marine and lake sediment (Kern et al., 2013), ice cores (Steinhilber et al., 2012), tree rings and speleothems (e.g. Breitenmoser et al., 2012). A comprehensive global climate model indicated that a 90-yr solar forcing leads to responses in water temperatures especially in deep-water masses of the South Atlantic (Seidenglanz et al., 2012).

Ogurtsov et al. (2002) revealed that the 87-yr Gleissberg cycle (Gleissberg, 1944) is indeed a complex solar cycle with two oscillation modes, i.e. the lower 50-80-yr and the upper 90-140-yr Gleissberg cycle. The multi-decadal scale sedimentation changes in the Weddell Sea cores correspond remarkably to the 50-80-yr cycle of the lower Gleissberg oscillation. Frequencies similar to the 90-140-yr upper Gleissberg cycle also occur in most spectra. High frequency cycles dominant in the bulk spectra are possibly related to the 11-yr Schwabe (Schwabe, 1844) cycle, recently described as 8-14-yr solar band (Ogurtsov et al., 2002), and the 22-yr Hale cycle (Mursula et al., 2002).

The accordance of prominent solar cycles with the oscillation frequencies found in the varved sediment records strongly suggest a solar influence on the sedimentation most likely associated with coastal polynya activity and brine release in the southern Weddell Sea. Climate model simulations (Varma et al., 2011) support the notion of a solar forcing effect on the atmospheric circulation and hence sea-ice dynamics in the Weddell Sea region. Climate model experiments presented in Sprenk et al. (in review-a) support the inference that solar-forced anomalies in atmospheric circulation over the Weddell Sea promoted coastal polynya formation during periods of high solar activity, enhancing brine formation and influencing the sedimentation process in the channel-ridge system.

Although, the decadal-scale varve thickness changes could also be related to the Atlantic Multidecadal Oscillation (AMO), recurring changes in North Atlantic sea-surface temperature

with a pacing of 60-90 years (Delworth and Mann, 2000; Kerr, 2000) influencing the Northern Hemisphere (Wyatt et al., 2012), and consequently also global climate. The origin of AMO is still not fully understood, although it seems to be related to changes in Atlantic meridional overturning circulation (AMOC; Knight et al., 2006). Ritz et al. (2013) indicated that also the North Brazil Current connecting the Northern and Southern Atlantic also shows decadal-scale oscillations linked to AMO as well as AMOC. Until now, the AMO has been only detected in Holocene records and there is no consistent information available if the AMO also existed during the LGM. Recently, Ritz et al. (2013) estimated that the AMOC strength in the LGM was indistinguishable from its recent strength, but reduced during cooling events like the Younger Dryas. Evidence for an influence of the AMO on Antarctic temperatures during the 20th century exist, and are anti-phase to the Arctic (Chylek et al., 2010). An effect of AMO also on sea-ice/ocean processes in the Weddell Sea during the LGM cannot be ruled out, particularly because it is still discussed if AMO itself is related to and therefore reflects solar irradiance changes (e.g. Ólafsdóttir et al., 2013). Simulations by Park and Latif (2008) using the Kiel Climate Model, suggest that decadal-scale AMOC variations originate in the North Atlantic, while multi-centennial changes are driven in the Southern Ocean, thus both are related to fluctuations in sea-ice extent. Although, they also considered decadal-scale variations in the Southern Annular Mode (SAM; Thompson and Wallace, 2000). Recent climate model analyses revealed decadal-to-centennial-scale changes in SAM in the Southern Ocean also during the LGM, showing teleconnections in sea-surface temperature, AMOC, and atmospheric circulation (Sprenk and Lohmann, unpublished).

7.2 Dust transport and palaeoproductivity

Interpretation of the magnetic susceptibility signal in Southern Ocean sediments is still debated. Possible supply mechanisms could be iceberg transport, oceanic circulation, volcanic sources, sea-ice distribution, and atmospheric circulation. The Scotia Sea is located in the prolongation of the so-called "Iceberg Alley" (Anderson and Andrews, 1999). Large amounts of Antarctic calved icebergs are transported by the Antarctic Coastal Current counter-clockwise around Antarctica into the Weddell Sea (Stuart and Long, 2011), which are then entrapped in the clockwise flowing Weddell Gyre. Most of the icebergs exit through gaps in the South Scotia Ridge into the Scotia Sea (Pudsey and Howe, 1998). A recent study (Weber et al., in review) highlights that the IRD records of MD07-3133 and MD07-3134 from the Central Scotia Sea record a spatially integrated signal of Antarctic Ice Sheet variability. Weber et al. (2012) present magnetic susceptibility records from these sediment cores, showing no accordance with the counted IRD in the sediment, thus ruling out that icebergs are transporting the magnetic susceptibility signal.

Ocean circulation is also a potential supply mechanism, Diekmann et al. (2000) assumed that current transport is mainly responsible for transporting the magnetic susceptibility signal. However, Hofmann (1999) investigated comparable magnetic susceptibility records from different current regimes. The Scotia Sea is isolated from major sediment sources of continental margins

with only the western part being in the supply areas of southern South America and the Antarctic Peninsula (Maldonado et al., 2003), also pointing against ocean currents as main supplier of magnetic susceptibility. Although, oceanic circulation might be responsible for secondary redistribution (Pugh et al., 2009). ^{230}Th -normalization data for MD07-3134 reveal strong differences in sediment focusing with intensified sediment focusing during glacial times, so Sprenk et al. (2013) assumed that bottom currents collected the sediment from an upstream shallower region and focused the material composition to the core sites, thereby enhancing time resolution of the record. By increasing the focusing factor from 8 to 20 during the last glacial period, this sediment advection acted like a slow motion frame.

Another possible transport mechanism for the magnetic susceptibility signal is sea ice, which can incorporate and re-locate material. In contrast to Arctic regions (Kempema et al., 1989), Antarctica lacks large shelf areas fed by river suspension, so frazil ice formation through supercooling of surface waters possibly did not include high amounts of fine-sized particles. Although, during times with large sea-ice cover, material transported by atmospheric circulation is first deposited on the sea ice, then acting as a secondary transport process. However, Weber et al. (2012) found no agreement between magnetic susceptibility record of the Scotia Sea cores with the EDML sea-ice indicator, i.e. sea-salt Na^+ flux (Fischer et al., 2007).

Atmospheric circulation is most likely the primary supply mechanism for magnetic susceptibility. Weber et al. (2012) present a striking correlation of the magnetic susceptibility record of the Scotia Sea cores with non-sea-salt Ca^{2+} -flux of EDML ice core (Fischer et al., 2007), a confident atmospheric dust proxy (Lambert et al., 2011; Röthlisberger et al., 2004). Earlier studies (Hofmann, 1999; Pugh et al., 2009) already showed that the magnetic susceptibility signal is linked to Antarctic dust supply on interglacial-glacial timescales.

Southern South America is the only large land mass within the Southern Hemisphere Westerlies dominated region and Patagonia has been identified as main East Antarctic dust supplier during glacial cycles of the last 800 kyrs (Delmonte et al., 2010). Also indicated by dust provenance studies from East Antarctic ice cores (EPICA Community Members, 2006). Weber et al. (2012) investigated that MD07-3133, i.e. located closer to Southern South America shows higher magnetic susceptibility values than MD07-3134, thus also indicating South America as dust source during the last glacial period. Similar investigations had also revealed Hofmann (1999). The Scotia Sea cores and Patagonian Laguna Potrok Aike maar lake (Haberzettl et al., 2009) magnetic susceptibility records show the same trends during MIS 2, also promoting Patagonia as glacial dust source. Although, (Lanci et al., 2008) promote different dust sources for glacial and interglacial times. (Revel-Rolland et al., 2006) analyses on isotope composition changes reveal Australia as dominant dust source for interglacials. (Gabielli et al., 2010) even suggest a combination of southern South America, Australia, New Zealand, and South Africa as dust supplier. Modelling studies by Lunt and Valdes (2001) indicate that dust transport efficiency for particles in East Antarctica is even higher today than during the LGM, thus implying that higher glacial dust concentrations are primarily caused by changing environmental conditions in the

source area rather than by changes in atmospheric circulation. Consequently, Lunt and Valdes (2001) predict Patagonia as glacial and interglacial dust source, which is also supported by the fact, that the direct of the Southern Hemisphere Westerlies did not vary.

During glacial times a higher temperature gradient between poles and equator existed, leading to intensified atmospheric circulation (Toggweiler and Russell, 2008). Antarctic dust input was significantly higher during glacial times (Fischer et al., 2007; Lambert et al., 2008) with about 10 to 30 times higher dust flux during the LGM compared to the Holocene (Delmonte et al., 2004). Antarctic dust input shows millennial-scale fluctuations with reduced dust input (Fischer et al., 2007) during Antarctic Isotopic Maxima (AIM), also noticeable in magnetic susceptibility minima in the Scotia Sea sites (Weber et al., 2012), possibly due to decreased aridity and/or reduced wind speeds in Patagonia (Fischer et al., 2007). Studies on glacial outwash plains in Patagonia, led Sugden et al. (2009) conclude that the atmospheric dust amount is controlled by glacial conditions. When sea level was around 130 m lower during the LGM than today (Huybrechts, 2002), large parts of the Argentine Shelf were exposed, thus the area of Patagonia had nearly doubled (Iriondo, 2000). Physical weathering prevailed on the ice-free glacial outwash plains, which received material from the Andes, and large loess areas formed. Therefore, the East Patagonian low lands were the ideal dust source area, due to dry and cold conditions, strong west winds, and large areas of fine-grained material (Sugden et al., 2009).

The Southern Hemisphere Westerlies had shifted around 7–10 °C north of their recent position during the LGM (Moreno et al., 1999), implying that the strongest westerlies were only then located over Patagonia. During that time upwelling of silica- and CO₂-rich, relatively warm mid-depth water to the sea surface water was reduced significantly, i.e. approximately 30 % relative to today (Horn et al., 2011), also reflected in strongly reduced biogenic opal flux rates (Anderson et al., 2009; Sprenk et al., 2013).

Circulation model results (Toggweiler et al., 2006) predict, that after the LGM, around 17 ka the westerlies shifted south again, therefore Patagonia was no longer in the centre of winds. Dust input in the Scotia Sea (Weber et al., 2012) and East Antarctica (Fischer et al., 2007) strongly decreased around 17 to 16 ka, while enhanced temperature rises are recorded in East Antarctic ice cores (EPICA Community Members, 2006). Also, Patagonian glaciers retreated rapidly at 16.5–15 ka (Hein et al., 2010). It remains unclear whether the shift in Southern Hemisphere Westerlies caused the rise in CO₂ or vice versa. Reorganization of ocean circulation, induced by intensified cooling as a result of large meltwater pulses in the Northern Hemisphere, weakened the Atlantic Meridional Overturning Circulation (Denton et al., 2010). Consequently, leading to a poleward shift of the Southern Hemisphere Westerlies, intensified upwelling of CO₂-rich mid-depth water, and therefore the warming of Antarctica (Toggweiler and Lea, 2010; Toggweiler and Russell, 2008). Inferring increased deep-water mixing and less stratification of the water column in the Southern Ocean during the deglacial period (Banderas et al., 2012; Burke and Robinson, 2012; Kwon et al., 2012) supports this theory. Anderson et al. (2009) also interpreted biogenic opal flux as an upwelling proxy because biogenic opal production is ultimately limited by dissolved Si

supply, explaining its direct, but not necessarily linear connection. Until now, high-resolution and continuous biogenic opal flux records from the Southern Ocean for the last glacial and deglacial period are rare, and therefore limited knowledge exists about Southern Ocean bioproductivity changes in the past. Bioproductivity in the Southern Ocean is mainly controlled by the rate of upwelling of cold nutrient- and silica rich water masses, the extent of sea-ice cover as well as the availability of light and micronutrients (de Baar et al., 2005; Dezileau et al., 2003). The reliability of biogenic opal flux as indicator for bioproductivity is still debated, because it is still not entirely clear whether biogenic opal preservation is consistent over longer time periods. Chase et al. (2003) and Bradtmiller et al. (2007) argued that biogenic opal flux reflects variations in diatom productivity and not changes in biogenic opal preservation. For the Indian sector of the Southern Ocean local differences in biogenic opal preservation, apparent in the polar frontal zone and south of it, have a modulating but not a primary effect on biogenic opal flux fluctuations (Pondaven et al., 2000). The good correlation of sites MD07-3133 and MD07-3134, which are approximately 450 km apart, indicates that this is also true for the central Scotia Sea (Sprenk et al., 2013).

Sprenk et al. (2013) determined biogenic opal using the conventional and very time-consuming leaching method of Müller and Schneider (1993), still it is one of the most commonly used methods due to its simplicity and robustness (Swann, 2010). However, samples with less than 10 % biogenic opal might be affected by the pH value of the leaching solution (Schlüter and Rickert, 1998). Additionally, biogenic opal was estimated from sediment colour b^* , wet-bulk density, Si/Ti-count ratios and Fourier transform infrared spectroscopy (FTIRS; Rosén et al., 2009). Colour b^* is useful parameter to estimate biogenic opal content (Weber, 1998), as both core sites are located below the carbonate compensation depth (CCD), i.e. carbonate-free and contain mainly biogenic opal, quartz, and clay minerals. All methods capture the main biogenic opal fluctuations in the Scotia Sea cores. A number of studies (e.g. Rosén et al., 2009; Rosén et al., 2010; Vogel et al., 2008) showed that FTIRS can be used to gain high-resolution geochemical information on lacustrine sediment. Sprenk et al. (2013) indicate that FTIRS is also a very promising and useful tool for analysing marine deep-sea sediments.

Sprenk et al. (2013) presented extremely high sedimentation rates of up to 1.8 m/kyr with mean sedimentation rates of 1.6 m/kyr (MD07-3133) and 0.9 m/kyr (MD07-3134) for MIS 1 and about 0.5 m/kyr (MD07-3133 and MD07-3134) for MIS 2. These values are more than 10 – 30 times higher than reported in previous studies (e.g. Pudsey and Howe, 1998) estimating rates of less than 5 cm/kyr for interglacials, and more than 5 cm/kyr for glacial times in the Scotia Sea. It clearly indicated that sedimentation in the core site area was strongly influenced by massive sediment focusing induced by bottom currents. Presently, the $^{231}\text{Pa}/^{230}\text{Th}$ ratio is the most accurate and most commonly used proxy for analysing particle and water mass transport in the Southern Ocean, e.g. past opal fluxes (Kretschmer et al., 2011). Anderson et al. (2009) revealed a strong correlation between biogenic opal flux and $^{231}\text{Pa}/^{230}\text{Th}$ ratios, which are not altered by biogenic material loss during early diagenesis (Chase et al., 2003) in Southern Ocean sediment. This led

Anderson et al. (2009) conclude that biogenic opal flux variations reflect changes in biogenic opal production and silicon supply, rather than changes in preservation.

Nutrient concentration is constantly high in regions such as the Antarctic Zone, so iron availability strongly influences bioproductivity (Martínez-García et al., 2011). Different iron fertilization experiments (e.g. Boyd et al., 2000; Martin et al., 1990) showed that Southern Ocean productivity is limited by Fe-deficiency. Coastal sediments, aerosols, upwelling, ice melting, and vertical mixing, can supply iron to the Southern Ocean (Cassar et al., 2007), however today the major nutrient and iron supply originates from upwelling water masses or lateral advection (Martínez-García et al., 2011; Meskhidze et al., 2007). The influence of dust-transported aeolian iron on bioproductivity is still debated. Erickson et al. (2003) suggested that bioproductivity in the Antarctic Circumpolar Current region is mainly controlled by atmospheric dust-Fe, mostly from Patagonia, whereas Kaufmann et al. (2010) argued that dust flux variations had no major influence on Southern Ocean productivity over the last 150 ka. Further, modelling studies suggest that upwelling delivers approximately 99 % of micronutrients to the Southern Ocean rather than dust (Lefèvre and Watson, 1999). At Sites MD07-3133 and MD07-3134 dust-indicator magnetic susceptibility (Weber et al., 2012), exhibits mostly minima when biogenic opal mass accumulation rate is high and vice versa (Sprenk et al., 2013). During the LGM, dust transport was significantly intensified and led to 10 – 30 times higher concentrations in East Antarctic ice cores (Delmonte et al., 2004) and in the Scotia Sea (Weber et al., 2012), whereas biogenic opal mass accumulation rate was extremely low during that period. Accordingly, we believe that iron-fertilization via dust-transport is not the main driver of bioproductivity changes in the Scotia Sea. In addition, iron released from melting icebergs (Raiswell, 2011), i.e. Fe either from terrigenous material or aeolian dust (Lin et al., 2011), might have a minor affect on bioproductivity, as both sediment core sites.

Biogenic opal export increase at the end of the last glacial could reflect higher nutrient content in upwelling waters or just intensified upwelling, more fractional utilization of nutrients, or, to a lesser extent, better preservation of sinking biogenic opal (Horn et al., 2011). Allen et al. (2011) concluded that reduced surface water productivity and/or export in the Scotia Sea during the LGM, caused by enhanced sea ice cover, lower sea surface temperatures, and therefore shorter growing seasons, and not changes in dissolution processes, are more likely to explain the lower abundance of diatoms in sediment cores during the LGM.

Sprenk et al. (2013) revealed that biogenic opal mass accumulation rate rose abruptly at MD07-3133 and still also the ^{230}Th -normalized biogenic opal flux record of MD07-3134 rose around 17 ka, thus representing probable increases in bioproductivity and upwelling. The rise is followed by a maximum around 15 ka in biogenic opal accumulation rate at MD07-3133, which was also detected at other core sites in the Atlantic, Indian, and Pacific sectors of the Southern Ocean (Anderson et al., 2009), and coincides with AIM 1. During the Antarctic Cold Reversal (14.54 – 12.76 ka; Putnam et al., 2010) biogenic opal mass accumulation rates at MD07-3133 and MD07-3134 are only slightly reduced and remain high. Also EDML ice core data show only a minor reduction in $\delta^{18}\text{O}$ and rise in sea-salt Na^+ flux according to regional differences. This is

slightly different from the observation of Anderson et al. (2009) showing strongly decreased biogenic opal flux indicating reduced Southern Ocean upwelling during that time. The ACR is followed by the AIM 0, an abrupt rise in temperature and CO₂, as well as sea ice decrease, also the biogenic opal content rose at both core sites during that time (Sprenk et al., 2013).

Linear sedimentation rate and biogenic opal mass accumulation rate were equivalent for both Scotia Sea sites during the LGM but increased by a factor of 1.5 to 2 at Site MD07-3133 during MIS 3, the Antarctic Cold Reversal, and MIS 1. Higher amplitudes further north could be related to an approximately 5° shift in latitude of the ACC fronts (and associated opal belt) to the north during the LGM (Gersonde et al., 2003). Allen et al. (2011) observed for the LGM a shift of the winter sea ice limit of at least 5° northwards, thus it remained north of the Scotia Sea. Accordingly, at that time, both core sites would have been within the winter sea ice limit, explaining the similarly reduced biogenic opal mass accumulation and linear sedimentation rates (Sprenk et al., 2013). Today, MD07-3133 which is located approximately 450 km northwest of MD07-3134 lies north of the winter sea ice limit with significantly elevated biogenic opal mass accumulation and linear sedimentation rates, while MD07-3134 is within the winter sea ice limit and exhibits reduced biogenic opal mass accumulation and linear sedimentation rates. Therefore, (Sprenk et al., 2013) suggested that the distribution of sea ice has a strong influence on bioproductivity and can be the reason for pronounced regional differences in the Southern Ocean.

In general, biogenic opal content and mass accumulation rates show the same trend as atmospheric CO₂ concentration; biogenic opal rises correspond well to increasing CO₂ concentration, while during low CO₂ biogenic opal is also mainly at minima. In addition, Anderson et al. (2009) also found an increase in upwelling at each phase of rising CO₂ during MIS 3, illustrated by higher biogenic opal flux in the Southern Ocean, which corresponds quite well with the ²³⁰Th normalized biogenic opal flux from MD07-3134. Sprenk et al. (2013) indicated that variations in biogenic opal flux reflect bioproductivity changes and strongly correlate to sea ice cover, summer sea surface temperature as well as atmospheric CO₂ variations.

8 Conclusions and Summary

The sediment-physical and geochemical studies on sediment cores from the Atlantic sector of the Southern Ocean provide new insights on seasonal-to-millennial-scale fluctuations during the last glacial and deglacial period. The sediment cores from channel-ridge systems on a terrace of the continental slope of the southeastern Weddell Sea, are one of very few Antarctic archives with carbonate shell preservation. However, due to the scarceness of carbonate shells only three to five AMS¹⁴C ages determined on planktonic foraminifera *Neogloboquadrina pachyderma* could be gained for each sediment core. Furthermore, no ash layers have been detected in the cores so far. The sediments mostly consist of terrigenous components and only a minor amount of biogenic material, as well as are mainly varved with only short bioturbated sections. Siliciclastic varves were counted using scanned X-radiographs and thin sections to gain new insights on the internal varve composition, thickness variations, and sedimentation process. The sediment cores were correlated among each other using varve counting results in combination with AMS¹⁴C revealing simultaneous facies changes from lamination to bioturbation and vice versa in the core site area around 25, 23, 21.5, 20, and 19 ka. The duration of the non-laminated, mainly bioturbated periods that interrupted varve accumulation, was only a couple up to a millennium, likely associated with ice-sheet retreat from the shelf, an inactive contour current on the slope, and at least partially open water conditions above the sites. Therefore, promoting multiple fluctuations of the East Antarctic Ice Sheet during the LGM. A final transition from lamination to bioturbation occurred around 16 ka, marks the final ice-sheet retreat from the shelf edge in the southeastern Weddell Sea.

Analyses of thin sections from sediment core PS1795 revealed that the varves have only small variations in grain size and no erosional or sharp surfaces occur argue against turbiditic sedimentation and favours varve formation. Also the varve counting results from PS1599, PS1789, PS1791, and PS1795 in combination with AMS¹⁴C ages support the results from earlier studies that the laminations represent true varves. High-resolution XRF-scanning every 0.2 mm and RADIUS tool measurements of PS1795 reveal seasonal changes in grain size and related changes in element and mineral composition. Lighter-coloured layers contain higher amounts of silt-sized particles, mainly Quartz grains, which is also reflected in Si count maxima. Less darkening of the X-ray film also reflects enhanced densities of the lighter-coloured layers. The finer grained layers are of a darker, brownish colour and contain mainly clay-sized particles and show maxima in K, Fe, Ti, and Rb, thus typical trace elements for clay minerals such as chlorite and illite as well as mica, e.g. biotite.

Consequently, sedimentation in the channel-ridge systems was highly dynamic during the LGM, reflecting seasonal velocity changes of the thermohaline current that transporting sediment from the upper slope downslope to the core sites. Sediments were deposited when the grounded ice sheet had advanced to the Weddell Sea shelf edge. Offshore blowing katabatic winds removed sea ice from the ice edge and coastal polynyas developed. We suggest that glacial coastal polynya processes were in general similar to today with stronger katabatic winds and enhanced coastal

polynya activity during winter season. However, that does not imply the spaces of open water may have existed for long. Following this concept, silty layers are likely glacial winter deposits, when brine release was increased leading to intensified bottom water formation and increased sediment transport. Vice versa, finer-grained clayey layers were deposited during summer, when coastal polynya activity was possibly reduced. Nonetheless, there is currently no concluding interpretation as to which season produced which layer. Coarser layers could also have been deposited during glacial summer by meltwater channels or when more sea ice melted, which might also explain the higher IRD content in silty layers. However, the density of melted freshwater would have been too low to sink down the continental slope and initiate the required thermohaline circulation.

Likely for the first time, decadal-to-centennial-scale oscillations have been detected in varved marine sediments during glacial times. Evolutionary spectra show a 50-85-year oscillation band present in all analysed varved sediment sections of the Weddell Sea cores, hence being a robust feature during the LGM. Also, 11-yr, 14-yr, 17-yr, 20-29-yr, 26-yr, 90-yr, and 116-yr cycles were detected in the bulk spectra exceeding the 96 or even the 99 % confidence level. The cycles correlate well with the periods of the Schwabe, Hale, lower and upper Gleissberg solar cycles, suggesting that solar cycles modulated sedimentation in the core sites area in the southeastern Weddell Sea during the LGM. Climate model experiments support the inference that solar-forced anomalies in atmospheric circulation over the Weddell Sea promoted coastal polynya formation during periods of high solar activity, enhancing brine formation and influencing the sedimentation process in the channel-ridge systems in the southeastern Weddell Sea. Additionally, internal atmosphere-ocean variability like the AMO, which itself might be related to solar irradiance changes, could have also influenced the sedimentation process.

Sediment cores MD07-3133 and MD07-3134 originating from the central Scotia Sea reveal centennial-to-millennial changes of dust input as well as bioproductivity. The magnetic susceptibility record of both cores shows a one-to-one coupling with the non-sea-salt Ca^{2+} flux of East Antarctic EDML ice core, a confident atmospheric dust proxy. This clearly identifies atmospheric circulation as supplier of the magnetic susceptibility signal in the Scotia Sea. Sea ice and oceanic currents thus might have operated as secondary supplier transporting atmospheric dust to the core sites. Icebergs can be presumably ruled out as dust supplier, given that IRD and magnetic susceptibility show no accordance. Atmospheric transport involves no major lead or lags, therefore correlating magnetic susceptibility with EDML non-sea-salt Ca^{2+} flux is reasonable and the detailed structure of variability allows for the establishment of a high-resolution age model for the Scotia Sea cores. The strong correlation of the signals during the last glacial period reveals that the same atmospheric circulation affected East Antarctica and the Scotia Sea. Patagonia can be identified as major dust source as the magnetic susceptibility records of Patagonian lake sediment correlates with the records from the Scotia Sea. Furthermore, shows MD07-3133, located closer to Patagonia higher magnetic susceptibility values. During glacial times, when sea level was lower, therefore shelf areas exposed, magnetic susceptibility records in the Scotia Sea cores as

well as Antarctic dust input was intensified. Highest concentrations occurred in stadials MIS 2 and MIS 4. Also colder phases between AIM indicate elevated dust concentrations, whereas reduced during most AIM. Therefore, magnetic susceptibility records of Southern Ocean deep-sea sediments can be used as reliable traces of dust as well as atmospheric circulation changes.

Additionally, biogenic opal flux of Scotia Sea cores reflects palaeoproductivity changes during the last glacial period as it is only marginally affected by preservation. Biogenic opal was determined by leaching, as well as estimated using colour b^* , wet-bulk density, Si/Ti count ratios, and FTIRS. All methods can be used to detect general biogenic opal trends, thus FTIRS provides the most reliable estimation. The biogenic opal flux record of MD07-3134 is one of the first continuous palaeoproductivity record over the last 92.5 ka for the Southern Ocean. It exhibits a relatively complicated glacial-to-interglacial pattern with large-amplitude, millennial-scale fluctuations in bioproductivity.

South of the Antarctic Polar Front, lowest bioproductivity levels deduced from biogenic opal fluxes occurred during the LGM, when upwelling of mid-depth water was reduced and sea ice cover intensified. ^{230}Th normalized biogenic opal fluxes in core MD07-3134 show a similar pattern albeit at realistic values of between 1 and 1.5 $\text{g}/\text{cm}^2/\text{kyr}$ during interglacials, whereas glacial MIS 2 and 3 were generally characterized by lower values near 0.5 $\text{g}/\text{cm}^2/\text{kyr}$. These numbers are comparable to other records in the Atlantic sector of the Southern Ocean. Around 17 ka, bioproductivity increased abruptly, corresponding to rising atmospheric CO_2 and decreasing seasonal sea ice coverage. Distribution of sea ice strongly influences bioproductivity and may be the reason for pronounced regional differences in the Southern Ocean. Also summer sea surface temperature changes are strongly correlated to the biogenic opal flux changes in the central Scotia Sea.

In summary, Southern Ocean sediments are very useful to reconstruct past climate changes. The sedimentation in the Scotia and Weddell Sea seem to have responded even to seasonal-to millennial-scale climate fluctuations during the last glacial and deglacial period. Bioproductivity was lowest during the LGM, while dust input reached maximum values. They both also record millennial-scale changes like AIM during the last glacial period. Sedimentation in the channel-ridge systems in the southeastern Weddell Sea was likely related to seasonal changes in katabatic winds and therefore coastal polynya fluctuations. Solar cycles and maybe internal atmosphere-ocean variability influenced sedimentation on decadal-to-centennial-scale time-scales. Sedimentation in the southeastern Weddell Sea possibly also indicates multiple fluctuations of East Antarctic Ice Sheet during the LGM.

9 References

- Ahn, J., Brook, E.J., 2008. Atmospheric CO₂ and Climate on Millennial Time Scales During the Last Glacial Period. *Science* 322, 83-85.
- Alfonso, J.A., Martínez, M., Flores, S., Benzo, Z., 2006. Distribution of Trace Elements in Offshore Sediments of the Orinoco Delta. *Journal of Coastal Research*, 502-510.
- Allen, C.S., Pike, J., Pudsey, C.J., 2011. Last glacial-interglacial sea-ice cover in the SW Atlantic and its potential role in global deglaciation. *Quaternary Science Reviews* 30, 2446-2458.
- Alley, A.B., 2000. The Younger Dryas cold interval as viewed from central Greenland. *Quaternary Science Reviews* 19, 213-226.
- Anderson, J.B., Andrews, J.T., 1999. Radiocarbon constraints on ice sheet advance and retreat in the Weddell Sea, Antarctica. *Geology* 27, 179-182.
- Anderson, J.B., Wright, R., Andrews, B., 1986. Weddell Fan and Associated Abyssal Plain, Antarctica: Morphology, Sediment Processes, and Factors Influencing Sediment Supply. *Geo-Marine Letters*, 121-129.
- Anderson, R.F., Ali, S., Bradtmiller, L.I., Nielsen, S.H.H., Fleisher, M.Q., Anderson, B.E., Burckle, L.H., 2009. Wind-Driven Upwelling in the Southern Ocean and the Deglacial Rise in Atmospheric CO₂. *Science* 323, 1443-1448.
- Banderas, R., Álvarez-Solas, J., Montoya, M., 2012. Role of CO₂ and Southern Ocean winds in glacial abrupt climate change. *Climate of the Past* 8, 1011-1021.
- Bard, E., Rostek, F., Turon, J.-L., Gendreau, S., 2000. Hydrological impact of Heinrich Events in the Subtropical Northeast Atlantic. *Science*, 1321-1324.
- Barker, P.F., 2001. Scotia Sea regional tectonic evolution: implications for mantle flow and palaeocirculation. *Earth-Science Reviews* 55, 1-39.
- Barker, P.F., Burrell, J., 1977. The opening of Drake Passage. *Marine Geology* 25, 15-34.
- Barker, S., Diz, P., Vautravers, M.J., Pike, J., Knorr, G., Hall, I.R., Broecker, W.S., 2009. Interhemispheric Atlantic seesaw response during the last deglaciation. *Nature* 457, 1097-1102.
- Bartoli, G., Hoenisch, B., Zeebe, R.E., 2011. Atmospheric CO₂ decline during the Pliocene intensification of Northern Hemisphere glaciations. *Paleoceanography* 26, PA4213.
- Beer, J., Mende, W., Stellmacher, R., 2000. The role of the sun in climate forcing. *Quaternary Science Reviews* 19, 403-415.
- Berger, A., Loutre, M.F., 1991. Insolation values for the climate of the last 10 million years. *Quaternary Science Reviews* 10, 297-317.
- Blunier, T., Brook, E.J., 2001. Timing of Millennial-Scale Climate Change in Antarctica and Greenland During the Last Glacial Period. *Science* 291, 109-112.
- Blunier, T., Chappellaz, J., Schwander, J., Dällenbach, A., Stauffer, B., Stocker, T.F., Raynaud, D., Jouzel, J., Clausen, H.B., C.U., H., Johnsen, S.J., 1998. Asynchrony of Antarctic and Greenland climate change during the last glacial period. *Nature* 394, 739-743.
- Bond, G., Showers, W., Cheseby, M., Lotti, R., Almasi, P., deMenocal, P., Priore, P., Cullen, H., Hajdas, I., Bonani, G., 1997. A Pervasive Millennial-Scale Cycle in North Atlantic Holocene and Glacial Climates. *Science* 278, 1257-1266.
- Boyd, P.W., Watson, A.J., Law, C.S., Abraham, E.R., Trull, T., Murdoch, R., Bakker, D.C.E., Bowie, A.R., Buesseler, K.O., Chang, H., Charette, M., Croot, P., Downing, K., Frew, R., Gall, M., Hadfield, M., Hall, J., Harvey, M., Jameson, G., LaRoche, J., Liddicoat, M., Ling, R., Maldonado, M.T., McKay, R.M., Nodder, S., Pickmere, S., Pridmore, R., Rintoul, S., Safi, K., Sutton, P., Strzpek, R., Tanneberger, K., Turner, S., Waite, A., Zeldis, J., 2000. A mesoscale phytoplankton bloom in the polar Southern Ocean stimulated by iron fertilization. *Nature* 407, 695-702.
- Bradtmiller, L.I., Anderson, R.F., Fleisher, M.Q., Burckle, L.H., 2007. Opal burial in the equatorial Atlantic Ocean over the last 30 ka: Implications for glacial-interglacial changes in the ocean silicon cycle. *Paleoceanography* 22, 15 pp.
- Breitenmoser, P., Beer, J., Broennimann, S., Frank, D., Steinhilber, F., Wanner, H., 2012. Solar and volcanic fingerprints in tree-ring chronologies over the past 2000 years. *Palaeogeography, Palaeoclimatology, Palaeoecology* 313-314, 127-139.
- Broecker, W.S., 1987. The biggest chill. *Natural History Magazine* 96, 74-82.
- Broecker, W.S., 1991. The Great Ocean Conveyor. *Oceanography* 4.

- Broecker, W.S., 1998. Paleocene circulation during the Last Deglaciation: A bipolar seesaw? *Paleoceanography* 13, 119-121.
- Burke, A., Robinson, L.F., 2012. The Southern Ocean's Role in Carbon Exchange During the Last Deglaciation. *Science* 335, 557-561.
- Carmack, E.C., Foster, T.D., 1977. Water masses and circulation in the Weddell Sea.
- Cassar, N., Bender, M.L., Barnett, B.A., Fan, S., Moxim, W.J., Levy II, H., Tilbrook, B., 2007. The Southern Ocean Biological Response to Aeolian Iron Deposition. *Science* 317, 1067-1070.
- Chase, Z., Anderson, R.F., Fleisher, M.Q., Kubik, P.W., 2003. Accumulation of biogenic and lithogenic material in the Pacific sector of the Southern Ocean during the past 40,000 years. *Deep Sea Research Part II: Topical Studies in Oceanography* 50, 799-832.
- Chylek, P., Folland, C.K., Lesins, G., Dubey, M.K., 2010. Twentieth century bipolar seesaw of the Arctic and Antarctic surface air temperatures. *Geophysical Research Letters* 37, L08703.
- Clark, P.U., Archer, D., Pollard, D., Blum, J.D., Rial, J.A., Brovkin, V., Mix, A.C., Piasias, N.G., Roy, M., 2006. The middle Pleistocene transition: characteristics, mechanisms, and implications for long-term changes in atmospheric pCO₂. *Quaternary Science Reviews* 25, 3150-3184.
- Clark, P.U., Dyke, A.S., Shakun, J.D., Carlson, A.E., Clark, J., Wohlfarth, B., Mitrovica, J.X., Hostetler, S.W., McCabe, A.M., 2009. The Last Glacial Maximum. *Science* 325, 710-714.
- Comiso, J.C., Gordon, A.L., 1998. Interannual variability in summer sea ice minimum, coastal polynyas and bottom water formation in the Weddell Sea. *Antarctic Research Series* 74, 293-315.
- Croudace, I.W., Rindby, A., Rothwell, R.G., 2006. ITRAX: description and evaluation of a new multi-function X-ray core scanner. *Geological Society, London, Special Publications* 267, 51-63.
- Dansgaard, W., Johnsen, S.J., Clausen, H.B., Dahl-Jensen, D., Gundestrup, N.S., Hammer, C.U., Hvidberg, C.S., Steffensen, J.P., Sveinbjörnsdóttir, A.E., Jouzel, J., Bond, G., 1993. Evidence for general instability of past climate from a 250-kyr ice-core record. *Nature* 364, 218-220.
- de Baar, H.J.W., Boyd, P.W., Coale, K.H., Landry, M.R., Tsuda, A., Assmy, P., Bakker, D.C.E., Bozec, Y., Barber, R.T., Brzezinski, M.A., Buesseler, K.O., Boyé, M., Croot, P.L., Gervais, F., Gorbunov, M.Y., Harrison, P.J., Hiscock, W.T., Laan, P., Lancelot, C., Law, C.S., Levasseur, M., Marchetti, A., Millero, F.J., Nishioka, J., Nojiri, Y., van Oijen, T., Riebesell, U., Rijkenberg, M.J.A., Saito, H., Takeda, S., Timmermans, K.R., Veldhuis, M.J.W., Waite, A.M., Wong, C.-S., 2005. Synthesis of iron fertilization experiments: From the Iron Age in the Age of Enlightenment. *Journal of Geophysical Research* 110, 24 pp.
- Delmonte, B., Andersson, P.S., Schöberg, H., Hansson, M., Petit, J.R., Delmas, R., Gaiero, D.M., Maggi, V., Frezzotti, M., 2010. Geographic provenance of aeolian dust in East Antarctica during Pleistocene glaciations: preliminary results from Talos Dome and comparison with East Antarctic and new Andean ice core data. *Quaternary Science Reviews* 29, 256-264.
- Delmonte, B., Petit, J.R., Andersen, K.K., Basile-Doelsch, I., Maggi, V., Ya Lipenkov, V., 2004. Dust size evidence for opposite regional atmospheric circulation changes over east Antarctica during the last climatic transition. *Climate Dynamics* 23, 427-438.
- Delworth, T.L., Mann, M.E., 2000. Observed and simulated multidecadal variability in the Northern Hemisphere. *Climate Dynamics* 16, 661-676.
- Denton, G.H., Anderson, R.F., Toggweiler, J.R., Edwards, R.L., Schaefer, J.M., Putnam, A.E., 2010. The Last Glacial Termination. *Science* 328, 1652-1656.
- Dezileau, L., Reyss, J.L., Lemoine, F., 2003. Late Quaternary changes in biogenic opal fluxes in the Southern Indian Ocean. *Marine Geology* 202, 143-158.
- Diekmann, B., Kuhn, G., Rachold, V., Abelmann, A., Brathauer, U., Fütterer, D.K., Gersonde, R., Grobe, H., 2000. Terrigenous sediment supply in the Scotia Sea (Southern Ocean): response to Late Quaternary ice dynamics in Patagonia and on the Antarctic Peninsula. *Palaeogeography, Palaeoclimatology, Palaeoecology* 162, 357-387.
- Dypvik, H., Harris, N.B., 2001. Geochemical facies analysis of fine-grained siliciclastics using Th/U, Zr/Rb and (Zr+Rb)/Sr ratios. *Chemical Geology* 181, 131-146.
- EPICA Community Members, 2004. Eight glacial cycles from an Antarctic ice core. *Nature* 429, 623-628.
- EPICA Community Members, 2006. One-to-one coupling of glacial climate variability in Greenland and Antarctica. *Nature* 444, 195-198.

- Erickson, D.J., Hernandez, J.L., Ginoux, P., Gregg, W.W., McClain, C., Christian, J., 2003. Atmospheric iron delivery and surface ocean biological activity in the Southern Ocean and Patagonian region. *Geophysical Research Letters* 30, 4 pp.
- Fischer, H., Fundel, F., Ruth, U., Twarloh, B., Wegner, A., Udisti, R., Becagli, S., Castellano, E., Morganti, A., Severi, M., Wolff, E., Littot, G., Röthlisberger, R., Mulvaney, R., Hutterli, M.A., Kaufmann, P., Federer, U., Lambert, F., Bigler, M., Hansson, M., Jonsell, U., de Angelis, M., Boutron, C., Siggaard-Andersen, M.-L., Steffensen, J.P., Barbante, C., Gaspari, V., Gabrielli, P., Wagenbach, D., 2007. Reconstruction of millennial changes in dust emission, transport and regional sea ice coverage using the deep EPICA ice cores from the Atlantic and Indian Ocean sector of Antarctica. *Earth and Planetary Science Letters* 260, 340-354.
- Foldvik, A., Gammelsrod, T., Østerhus, S., Fahrbach, E., Rohardt, G., M., S., Nicholls, K.W., Padman, L., Woodgate, R.A., 2004. Ice shelf water overflow and bottom water formation in the southern Weddell Sea. *Journal of Geophysical Research* 109.
- Francus, P., Asikainen, C.A., 2001. Sub-sampling unconsolidated sediments: A solution for the preparation of undisturbed thin-sections from clay-rich sediments. *Journal of Paleolimnology* 26, 323-326.
- Frank, M., 1996. Reconstruction of Late Quaternary environmental conditions applying the natural radionuclides ^{230}Th , ^{10}Be , ^{231}Pa and ^{238}U : A study of deep-sea sediments from the eastern sector of the Antarctic Circumpolar Current System. *Ber. Polarforsch.*
- Gabrielli, P., Wegner, A., Petit, J.R., Delmonte, B., De Deckker, P., Gaspari, V., Fischer, H., Ruth, U., Kriews, M., Boutron, C., Cescon, P., Barbante, C., 2010. A major glacial-interglacial change in aeolian dust composition inferred from Rare Earth Elements in Antarctic ice. *Quaternary Science Reviews* 29, 265-273.
- Gales, J.A., Larter, R.D., Mitchell, N.C., Hillenbrand, C.D., Østerhus, S., Shoosmith, D.R., 2012. Southern Weddell Sea shelf edge geomorphology: Implications for gully formation by the overflow of high-salinity water. *Journal of Geophysical Research* 117, F04021.
- Gersonde, R., Abelmann, A., Brathauer, U., Becquey, S., Bianchi, C., Cortese, G., Grobe, H., Kuhn, G., Niebler, H.-S., Segl, M., Sieger, R., U., Z., Fütterer, D.K., 2003. Last glacial sea surface temperatures and sea-ice extent in the Southern Ocean (Atlantic-Indian sector): A multiproxy approach *Paleoceanography* 18.
- Gleissberg, W., 1944. A table of secular variations of the solar cycle. *Terr. Magn. Atmos. Electr.* 49, 243-244.
- Gray, L.J., Beer, J., Geller, M., Haigh, J.D., Lockwood, M., Matthes, K., Cubasch, U., van Geel, B., White, W., 2010. Solar influences on climate. *Reviews of Geophysics* 48, 1-53.
- Grootes, P.M., Stuiver, M., 1997. Oxygen 18/16 variability in Greenland snow and ice with 10–3- to 105-year time resolution. *Journal of Geophysical Research: Oceans* 102, 26455-26470.
- Haberzettl, T., Anselmetti, F.S., Bowen, S.W., Fey, M., Mayr, C., Zolitschka, B., Ariztegui, D., Mauz, B., Ohlendorf, C., Kastner, S., Lücke, A., Schäbitz, F., Wille, M., 2009. Late Pleistocene dust deposition in the Patagonian steppe - extending and refining the paleoenvironmental and tephrochronological record from Laguna Potrok Aike back to 55 ka. *Quaternary Sci. Res.*, 2927-2939.
- Haid, V., Timmermann, R., 2013. Simulated heat flux and sea ice production at coastal polynyas in the southwestern Weddell Sea. *Journal of Geophysical Research: Oceans*, n/a-n/a.
- Haug, G.H., Ganopolski, A., Sigman, D.M., Rosell-Mele, A., Swann, G.E.A., Tiedemann, R., Jaccard, S.L., Bollmann, J., Maslin, M.A., Leng, M.J., Eglinton, G., 2005. North Pacific seasonality and the glaciation of North America 2.7[thinsp]million years ago. *Nature* 433, 821-825.
- Hein, A.S., Hulton, N.R.J., Dunai, T.J., Sugden, D.E., Kaplan, M.R., Xu, S., 2010. The chronology of the Last Glacial Maximum and deglacial events in central Argentine Patagonia. *Quaternary Science Reviews* 29, 1212-1227.
- Heinemann, G., Ebner, L., Haid, V., Timmermann, R., 2013. Katabatic winds and polynya dynamics in the Weddell Sea region (Antarctica). *EGU General Assembly 2013*, Vienna.
- Hillenbrand, C.-D., Melles, M., Kuhn, G., Larter, R.D., 2012. Marine geological constraints for the grounding-line position of the Antarctic Ice Sheet on the southern Weddell Sea shelf at the Last Glacial Maximum. *Quaternary Science Reviews* 32, 25-47.
- Hofmann, A., 1999. Kurzfristige Klimaschwankungen im Scotiameer und Ergebnisse zur Kalbungsgeschichte der Antarktis während der letzten 200 000 Jahre - Rapid climate

- oscillations in the Scotia Sea and results of the calving history of Antarctica during the last 200000 years, *Geosciences*. University of Bremen, Bremen, p. 178.
- Horn, M.G., Beucher, C.P., Robinson, R.S., Brzezinski, M.A., 2011. Southern ocean nitrogen and silicon dynamics during the last deglaciation. *Earth and Planetary Science Letters* 310, 334-339.
- Huber, C., Leuenberger, M., Spahni, R., Flückiger, J., Schwander, J., Stocker, T.F., Johnsen, S., Landais, A., Jouzel, J., 2006. Isotope calibrated Greenland temperature record over Marine Isotope Stage 3 and its relation to CH₄. *Earth and Planetary Science Letters* 243, 504-519.
- Huhn, O., Hellmer, H.H., Rhein, M., Rodehacke, C., Roether, W., Schodlok, M.P., Schroeder, M., 2008. Evidence of deep- and bottom-water formation in the western Weddell Sea. *Deep-Sea Research Part II* 55, 1098-1116.
- Huybrechts, P., 2002. Sea-level changes at the LGM from ice-dynamic reconstructions of the Greenland and Antarctic ice sheets during the glacial cycles. *Quaternary Science Reviews* 21, 203-231.
- Imbrie, J., Boyle, E.A., Clemens, S.C., Duffy, A., Howard, W.R., Kukla, G., Kutzbach, J., Martinson, D.G., McIntyre, A., Mix, A.C., Molfino, B., Morley, J.J., Peterson, L.C., Pisias, N.G., Prell, W.L., Raymo, M.E., Shackleton, N.J., Toggweiler, J.R., 1992. On The Structure And Origin Of Major Glaciation Cycles: 1. Linear Responses To Milankovitch Forcing. *Paleoceanography* 7, 701-738.
- IPCC, 2007. *Climate Change 2007: The Physical Science Basis*. Contribution of Working Group I to the Fourth Assessment
- Report of the Intergovernmental Panel on Climate Change, in: Solomon, S., Qin, D., Manning, M., Chen, Z., Marquis, M., Averyt, K.B., Tignor, M., Miller, H.L. (Eds.), IPCC Report, Cambridge, United Kingdom and New York, NY, USA.
- Iriondo, M., 2000. Patagonian dust in Antarctica. *Quaternary International* 68, 83-86.
- Justino, F., Peltier, W.R., 2006. Influence of present day and glacial surface conditions on the Antarctic Oscillation/Southern Annular Mode. *Geophysical Research Letters* 33, L22702.
- Kaufmann, P., Fundel, F., Fischer, H., Bigler, M., Ruth, U., Udisti, R., Hansson, M., de Angelis, M., Barbante, C., Wolff, E.W., Hutterli, M., Wagenbach, D., 2010. Ammonium and non-sea salt sulfate in the EPICA ice cores as indicator of biological activity in the Southern Ocean. *Quaternary Science Reviews* 29, 313-323.
- Kempema, E.W., Reimnitz, E., Barnes, P.W., 1989. Sea ice sediment entrainment and rafting in the Arctic. *Journal of Sedimentary Research* 59, 308-317.
- Kern, A.K., Harzhauser, M., Soliman, A., Piller, W.E., Mandic, O., 2013. High-resolution analysis of upper Miocene lake deposits: Evidence for the influence of Gleissberg-band solar forcing. *Palaeogeography, Palaeoclimatology, Palaeoecology* 370, 167-183.
- Kern, S., 2009. Wintertime Antarctic coastal polynya area: 1992-2008. *Geophysical Research Letters* 36, L14501.
- Kerr, R.A., 2000. A North Atlantic Climate Pacemaker for the Centuries. *Science* 288, 1984-1985.
- Knight, J.R., Folland, C.K., Scaife, A.A., 2006. Climate impacts of the Atlantic Multidecadal Oscillation. *Geophysical Research Letters* 33, n/a-n/a.
- Knutti, R., Flückiger, J., Stocker, T.F., Timmermann, A., 2004. Strong hemispheric coupling of glacial climate through freshwater discharge and ocean circulation. *Nature* 430, 851-856.
- Kretschmer, S., Geibert, W., Rutgers van der Loeff, M.M., Schnabel, C., Xu, S., Mollenhauer, G., 2011. Fractionation of ²³⁰Th, ²³¹Pa, and ¹⁰Be induced by particle size and composition within an opal-rich sediment of the Atlantic Southern Ocean. *Geochimica et Cosmochimica Acta* 75, 6971-6987.
- Kuhn, G., Weber, M.E., 1993. Acoustical characterization of sediments by Parasound and 3.5 kHz systems: Related sedimentary processes on the southeastern Weddell Sea continental slope, Antarctica. *Marine Geology* 113, 201-217.
- Kwon, E.Y., Hain, M.P., Sigman, D.M., Galbraith, E.D., Sarmiento, J.L., Toggweiler, J.R., 2012. North Atlantic ventilation of "southern-sourced" deep water in the glacial ocean. *Paleoceanography* 27, 12 pp.
- Lagabriele, Y., Goddérís, Y., Donnadieu, Y., Malavieille, J., Suarez, M., 2009. The tectonic history of Drake Passage and its possible impacts on global climate. *Earth and Planetary Science Letters* 279, 197-211.
- Lambeck, K., Chappell, J., 2001. Sea Level Change Through the Last Glacial Cycle. *Science* 292, 679-686.

- Lambert, F., Bigler, M., Steffensen, J.P., Hutterli, M., Fischer, H., 2011. The calcium-dust relationship in high-resolution data from Dome C, Antarctica. *Clim. Past Discuss.* 7, 1113-1137.
- Lambert, F., Delmonte, B., Petit, J.R., Bigler, M., Kaufmann, P.R., Hutterli, M.A., Stocker, T.F., Ruth, U., Steffensen, J.P., Maggi, V., 2008. Dust - climate couplings over the past 800,000 years from the EPICA Dome C ice core. *Nature* 452, 616-619.
- Lanci, L., Delmonte, B., Maggi, V., Petit, J.R., Kent, D.V., 2008. Ice magnetization in the EPICA-Dome C ice core: Implication for dust sources during glacial and interglacial periods. *J. Geophys. Res.* 113, D14207.
- Larter, R.D., Graham, A.G.C., Hillenbrand, C.-D., Smith, J.A., Gales, J.A., 2012. Late Quaternary grounded ice extent in the Filchner Trough, Weddell Sea, Antarctica: new marine geophysical evidence. *Quaternary Science Reviews* 53, 111-122.
- Lefèvre, N., Watson, A.J., 1999. Modeling the geochemical cycle of iron in the oceans and its impact on atmospheric CO₂ concentrations. *Global Biogeochemical Cycles* 13, 727-736.
- Lin, H., Rauschenberg, S., Hexel, C.R., Shaw, T.J., Twining, B.S., 2011. Free-drifting icebergs as sources of iron to the Weddell Sea. *Deep Sea Research Part II* 58, 1392-1406.
- Lisiecki, L.E., Raymo, M.E., 2005. A Pliocene-Pleistocene stack of 57 globally distributed benthic $\delta^{18}O$ records. *Paleoceanography* 20, PA1003.
- Livermore, R., Nankivell, A., Eagles, G., Morris, P., 2005. Paleogene opening of Drake Passage. *Earth and Planetary Science Letters* 236, 459-470.
- Lunt, D.J., Valdes, P.J., 2001. Dust transport to Dome C Antarctica at the Last Glacial Maximum and present day. *Geophysical Research Letters* 28, 295-298.
- Maldonado, A., Barnolas, A., Bohoyo, F., Escutia, C., Galindo-Zaldívar, J., Hernández-Molina, J., Javaloy, A., Lobo, F.J., Nelson, C.H., Rodríguez-Fernández, J., Somoza, L., Vázquez, J.-T., 2005. Miocene to Recent contourite drifts development in the northern Weddell Sea (Antarctica). *Global and Planetary Change* 45, 99-129.
- Maldonado, A., Barnolas, A., Bohoyo, F., Galindo-Zaldívar, J., Hernández-Molina, J., Lobo, F., Rodríguez-Fernández, J., Somoza, L., Vázquez, J.T., 2003. Contourite deposits in the central Scotia Sea: the importance of the Antarctic Circumpolar Current and the Weddell Gyre flows. *Palaeogeography, Palaeoclimatology, Palaeoecology* 198, 187-221.
- Martin, J.H., Gordon, R.M., Fitzwater, S.E., 1990. Iron in Antarctic waters. *Nature* 345, 156-158.
- Martínez-García, A., Rosell-Melé, A., Jaccard, S.L., Geibert, W., Sigman, D.M., Haug, G.H., 2011. Southern Ocean dust-climate coupling over the past four million years. *Nature* 476, 312-315.
- Meskhidze, N., Nenes, A., Chameides, W.L., Luo, C., Mahowald, N., 2007. Atlantic Southern Ocean productivity: Fertilization from above or below? *Global Biogeochemical Cycles* 21, 9 pp.
- Michels, K.H., Kuhn, G., Hillenbrand, C.-D., Diekmann, B., Fütterer, D.K., Grobe, H., Uenzelmann-Neben, G., 2002. The southern Weddell Sea: combined contourite-turbidite sedimentation at the southeastern margin of the Weddell Gyre. *Geological Society Memoirs* 22, 305-323.
- Milankovitch, M., 1941. *Kanon der Erdbestrahlungen und seine Anwendung auf das Eiszeitenproblem*, Belgrad.
- Monnin, E., 2006. EPICA Dome C high resolution carbon dioxide concentrations.
- Moreno, P.I., Lowell, T.V., Jacobson Jr, G.L., Denton, G.H., 1999. Abrupt Vegetation and Climate Changes During the Last Glacial Maximum and Last Termination in The Chilean Lake District: A Case Study from Canal De La Puntilla (41°S). *Geografiska Annaler: Series A, Physical Geography* 81, 285-311.
- Mudelsee, M., Raymo, M.E., 2005. Slow dynamics of the Northern Hemisphere glaciation. *Paleoceanography* 20, 1-14.
- Müller, P.J., Schneider, R., 1993. An automated leaching method for the determination of opal in sediments and particulate matter. *Deep-Sea Research I*, 425-444.
- Mursula, K., Usoskin, I.G., Kovaltsov, G.A., 2002. A 22-year cycle in sunspot activity. *Advances in Space Research* 29, 1979-1984.
- NGRIP Members, 2004. High-resolution record of Northern Hemisphere climate extending into the last interglacial period. *Nature* 431, 147-151.
- Oeschger, H., Beer, J., Siegenthaler, U., Stauffer, B., Langway, C.C., 1984. Late glacial climate history from ice cores. *Climate Processes and Climate Sensitivity* 29, 299-306.

- Ogurtsov, M.G., Nagovitsyn, Y.A., Kocharov, G.E., Jungner, H., 2002. Long-Period Cycles of the Sun's Activity Recorded in Direct Solar Data and Proxies. *Solar Physics* 211, 371-394.
- Ólafsdóttir, K.B., Geirsdóttir, A., Miller, G.H., Larsen, D.J., 2013. Evolution of NAO and AMO strength and cyclicity derived from a 3-ka varve-thickness record from Iceland. *Quaternary Science Reviews* 69, 142-154.
- Orsi, A.H., Johnson, G.C., Bullister, J.L., 1999. Circulation, mixing, and production of Antarctic Bottom Water. *Progress in Oceanography* 43, 55-109.
- Park, W., Latif, M., 2008. Multidecadal and multicentennial variability of the meridional overturning circulation. *Geophysical Research Letters* 35, L22703.
- Petty, A.A., Feltham, D.L., Holland, P.R., 2013. Impact of Atmospheric Forcing on Antarctic Continental Shelf Water Masses. *Journal of Physical Oceanography* 43, 920-940.
- Pondaven, P., Ragueneau, O., Treguer, P., Hauvespre, A., Dezileau, L., Reyss, J.L., 2000. Resolving the 'opal paradox' in the Southern Ocean. *Nature* 405, 168-172.
- Pudsey, C.J., Howe, J.A., 1998. Quaternary history of the Antarctic Circumpolar Current: evidence from the Scotia Sea. *Mar Geol* 148, 83-112.
- Pugh, R.S., McCave, I.N., Hillenbrand, C.D., Kuhn, G., 2009. Circum-Antarctic age modelling of Quaternary marine cores under the Antarctic Circumpolar Current: Ice-core dust-magnetic correlation. *Earth and Planetary Science Letters* 284, 113-123.
- Putnam, A.E., Denton, G.H., Schaefer, J.M., Barrell, D.J.A., Andersen, B.G., Finkel, R.C., Schwartz, R., Doughty, A.M., Kaplan, M.R., Schluchter, C., 2010. Glacier advance in southern middle-latitudes during the Antarctic Cold Reversal. *Nature Geoscience* 3, 700-704.
- Rahmstorf, S., 2002. Ocean circulation and climate during the past 120,000 years. *Nature* 419, 207-214.
- Raiswell, R., 2011. Iceberg-hosted nanoparticulate Fe in the Southern Ocean: Mineralogy, origin, dissolution kinetics and source of bioavailable Fe. *Deep Sea Research Part II* 58, 1364-1375.
- Raymo, M.E., Nisancioglu, K., 2003. The 41 kyr world: Milankovitch's other unsolved mystery. *Paleoceanography* 18.
- Reid, J.L., Nowlin, W.D., Patzert, W.C., 1977. On the Characteristics and Circulation of the Southwestern Atlantic Ocean. *Journal of Physical Oceanography* 7, 62-91.
- Renfrew, I.A., King, J.C., Markus, T., 2002. Coastal polynyas in the southern Weddell Sea: Variability of the surface energy budget. *J. Geophys. Res.* 107, 3063.
- Revel-Rolland, M., De Deckker, P., Delmonte, B., Hesse, P.P., Magee, J.W., Basile-Doelsch, I., Grousset, F., Bosch, D., 2006. Eastern Australia: A possible source of dust in East Antarctica interglacial ice. *Earth and Planetary Science Letters* 249, 1-13.
- Ritz, S.P., Stocker, T.F., Grimalt, J.O., Menviel, L., Timmermann, A., 2013. Estimated strength of the Atlantic overturning circulation during the last deglaciation. *Nature Geosci* 6, 208-212.
- Rosén, P., Vogel, H., Cunningham, L., Reuss, N., Conley, D., Persson, P., 2009. Fourier transform infrared spectroscopy (FTIRS): an important new technique for rapid quantitative analysis of biogeochemical properties from lake sediments. *PAGES Newsletter* 17, 98-100.
- Rosén, P., Vogel, H., Cunningham, L., Reuss, N., Conley, D.J., Persson, P., 2010. Fourier transform infrared spectroscopy, a new method for rapid determination of total organic and inorganic carbon and biogenic silica concentration in lake sediments. *Journal of Paleolimnology* 43, 247-259.
- Röthlisberger, R., Bigler, M., Wolff, E.W., Joos, F., Monnin, E., Hutterli, M.A., 2004. Ice core evidence for the extent of past atmospheric CO₂ change due to iron fertilisation. *Geophys. Res. Lett.* 31, L16207.
- Russell, J.L., Dixon, K.W., Gnanadesikan, A., Stouffer, R.J., Toggweiler, J.R., 2006. The Southern Hemisphere Westerlies in a Warming World: Propping Open the Door to the Deep Ocean. *Journal of Climate* 19, 6382-6390.
- Ruth, U., Barnola, J.-M., Beer, J., Bigler, M., Blunier, T., Castellano, E., Fischer, H., Fundel, F., Huybrechts, P., Kaufmann, P., Kipfstuhl, J., Lambrecht, A., Morganti, A., Oerter, H., Parrenin, F., Rybak, O., Severi, M., Udisti, R., Wilhelms, F., Wolff, E., 2007. "EDML1": a chronology for the EPICA deep ice core from Dronning Maud Land, Antarctica, over the last 150 000 years. *Climate of the Past* 3, 475-484.
- Schlüter, M., Rickert, D., 1998. Effect of pH on the measurement of biogenic silica. *Marine Chemistry* 63, 81-93.
- Schulz, M., 2002. On the 1470-year pacing of Dansgaard-Oeschger warm events. *Paleoceanography* 17.

- Schulz, M., Mudelsee, M., 2002. REDFIT: estimation red-noise spectra directly from unevenly spaced paleoclimatic time series. *Computer & Geosciences* 28, 421-426.
- Schwabe, H., 1844. Sonnen-Beobachtungen im Jahre 1843. *Astronomische Nachrichten* 495, 233-236.
- Seelos, K., Sirocko, F., 2005. RADIUS – rapid particle analysis of digital images by ultra-high-resolution scanning of thin sections. *Sedimentology* 52, 669-681.
- Seidenglanz, A., Prange, M., Varma, V., Schulz, M., 2012. Ocean temperature response to idealized Gleissberg and de Vries solar cycles in a comprehensive climate model. *Geophysical Research Letters* 39, 1-6.
- Seidov, D., Barron, E., Haupt, B.J., 2001. Meltwater and the global ocean conveyor: northern versus southern connections. *Global and Planetary Change* 30, 257-270.
- Shackleton, N.J., Hall, M.A., Vincent, E., 2000. Phase relationships between millennial-scale events 64,000-24,000 years ago. *Paleoceanography*, 565-569.
- Shin, S.-I., Liu, Z., Otto-Bliesner, B.L., Kutzbach, J.E., Vavrus, S.J., 2003. Southern Ocean sea-ice control of the glacial North Atlantic thermohaline circulation. *Geophysical Research Letters* 30, 68:61-68:64.
- Siddall, M., Rohling, E.J., Blunier, T., Spahni, R., 2010. Patterns of millennial variability over the last 500 ka. *Climate of the Past* 6, 295-303.
- Smith, J.A., Hillenbrand, C.-D., Pudsey, C.J., Allen, C.S., Graham, A.G.C., 2010. The presence of polynyas in the Weddell Sea during the Last Glacial Period with implications for the reconstruction of sea-ice limits and ice sheet history. *Earth and Planetary Science Letters* 296, 287-298.
- Sprenk, D., Lohmann, G., unpublished.
- Sprenk, D., Weber, M.E., Kuhn, G., Prange, M., Varma, V., Schulz, M., in review-a. Decadal- to millennial-scale oscillations in the Weddell Sea during the Last Glacial Maximum. *Quaternary Science Reviews*.
- Sprenk, D., Weber, M.E., Kuhn, G., Rosén, P., Frank, M., Molina-Kescher, M., Liebetrau, V., Röhling, H.-G., 2013. Southern Ocean bioproductivity during the last glacial cycle – new decadal-scale insight from the Scotia Sea. *Geological Society, London, Special Publications* 381.
- Sprenk, D., Weber, M.E., Kuhn, G., Wennrich, V., Hartmann, T., Seelos, K., in review-b. Seasonal changes in glacial polynya activity inferred from Weddell Sea varves. *Climate of the past discussions*.
- Steinhilber, F., Abreu, J.A., Beer, J., Brunner, I., Christl, M., Fischer, H., Heikkilä, U., Kubik, P.W., Mann, M., McCracken, K.G., Miller, H., Miyahara, H., Oerter, H., Wilhelms, F., 2012. 9,400 years of cosmic radiation and solar activity from ice cores and tree rings. *Proceedings of the National Academy of Sciences* 109, 5967-5971.
- Stocker, T.F., Johnson, S.J., 2003. A minimum thermodynamic model for the bipolar seesaw. *Paleoceanography* 18, 1087-1095.
- Stuart, K.M., Long, D.G., 2011. Tracking large tabular icebergs using the SeaWinds Ku-band microwave scatterometer. *Deep Sea Research Part II: Topical Studies in Oceanography* 58, 1285-1300.
- Sugden, D.E., McCulloch, R.D., Bory, A.J.-M., Hein, A.S., 2009. Influence of Patagonian glaciers on Antarctic dust deposition during the last glacial period. *Nature Geoscience* 2, 281-285.
- Swann, G., 2010. A comparison of the Si/Al and Si/time wet-alkaline digestion methods for measurement of biogenic silica in lake sediments. *Journal of Paleolimnology* 44, 375-385.
- Tamura, T., Ohshima, K.I., Nihashi, S., 2008. Mapping of sea ice production for Antarctic coastal polynyas. *Geophysical Research Letters* 35, L07606.
- Thompson, D.W.J., Wallace, J.M., 2000. Annular Modes in the Extratropical Circulation. Part I: Month-to-Month Variability*. *Journal of Climate* 13, 1000-1016.
- Toggweiler, J.R., Lea, D.W., 2010. Temperature differences between the hemispheres and ice age climate variability. *Paleoceanography* 25, PA2212.
- Toggweiler, J.R., Russell, J., 2008. Ocean circulation in a warming climate. *Nature* 451, 286-288.
- Toggweiler, J.R., Russell, J.L., Carson, S.R., 2006. Midlatitude westerlies, atmospheric CO₂, and climate change during the ice ages. *Paleoceanography* 21, PA2005.
- Varma, V., Prange, M., Lamy, F., Merkel, U., Schulz, M., 2011. Solar-forced shifts of the Southern Hemisphere Westerlies during the Holocene. *Climate of the Past* 7, 339-347.

- Vital, H., Statterger, K., 2000. Major and trace elements of stream sediments from the lowermost Amazon River. *Chemical Geology* 168, 151-168.
- Vogel, H., Rosén, P., Wagner, B., Melles, M., Persson, P., 2008. Fourier transform infrared spectroscopy, a new cost-effective tool for quantitative analysis of biogeochemical properties in long sediment records. *Journal of Paleolimnology* 40, 689-702.
- Waelbroeck, C., Labeyrie, L., Michel, E., Duplessy, J.C., McManus, J.F., Lambeck, K., Balbon, E., Labracherie, M., 2002. Sea-level and deep water temperature changes derived from benthic foraminifera isotopic records. *Quaternary Science Reviews* 21, 295-305.
- Wayne Nesbitt, H., Markovics, G., 1997. Weathering of granodioritic crust, long-term storage of elements in weathering profiles, and petrogenesis of siliciclastic sediments. *Geochimica et Cosmochimica Acta* 61, 1653-1670.
- Weber, M.E., 1998. Estimation of biogenic carbonate and opal by continuous non-destructive measurements in deep-sea sediments: application to the eastern Equatorial Pacific. *Deep-Sea Research* 1 45, 1955-1975.
- Weber, M.E., Bonani, G., Fütterer, K.D., 1994. Sedimentation processes within channel-ridge systems, southeastern Wedell Sea, Antarctica. *Paleoceanography* 9, 1027-1048.
- Weber, M.E., Clark, P.U., Kuhn, G., Timmermann, A., Spreng, D., Gladstone, R., Zhang, X., Lohmann, G., Menviel, L., Chikamoto, M., Friedrich, T., in review. Millennial-scale variability in Antarctic ice-sheet discharge throughout the last deglaciation. *Nature*.
- Weber, M.E., Clark, P.U., Ricken, W., Mitrovica, J.X., Hostetler, S.W., Kuhn, G., 2011. Interhemispheric Ice-Sheet Synchronicity During the Last Glacial Maximum. *Science* 334, 1265-1269.
- Weber, M.E., Kuhn, G., Spreng, D., Rolf, C., Ohlwein, C., Ricken, W., 2012. Dust transport from Patagonia to Antarctica - A new stratigraphic approach from the Scotia Sea and its implications for the last glacial cycle. *Quaternary Science Reviews* 36, 177-188.
- Weber, M.E., Reichelt, L., Kuhn, G., Pfeiffer, M., Korff, B., Thurow, J., Ricken, W., 2010a. BMPix and PEAK tools: New methods for automated laminae recognition and counting—Application to glacial varves from Antarctic marine sediment. *Geochemistry Geophysics Geosystems* 11, 1-18.
- Weber, M.E., Tougiannidis, N., Kleineder, M., Bertram, N., Ricken, W., Rolf, C., Reinsch, T., Antoniadis, P., 2010b. Lacustrine sediments document millennial-scale climate variability in northern Greece prior to the onset of the northern hemisphere glaciation. *Palaeogeography, Palaeoclimatology, Palaeoecology* 291, 360-370.
- Whitworth, T., Peterson, R.G., 1985. Volume Transport of the Antarctic Circumpolar Current from Bottom Pressure Measurements. *Journal of Physical Oceanography* 15, 810-816.
- Williams, W.J., Carmack, E.C., Ingram, R.G., 2007. Chapter 2 Physical Oceanography of Polynyas, in: Smith, W.O., Barber, D.G. (Eds.), *Elsevier Oceanography Series*. Elsevier, pp. 55-85.
- Wyatt, M.G., Kravtsov, S., Tsonis, A.A., 2012. Atlantic Multidecadal Oscillation and Northern Hemisphere's climate variability. *Climate Dynamics* 38, 929-949.
- Zachos, J.C., Dickens, G.R., Zeebe, R.E., 2008. An early Cenozoic perspective on greenhouse warming and carbon-cycle dynamics. *Nature* 451, 279-283.
- Zachos, J.C., Pagani, M., Sloan, L., Thomas, E., Billups, K., 2001. Trends, Rhythms, and Aberrations in Global Climate 65 Ma to Present. *Science* 292, 686-693.

10 Paper contributions

D. Sprenk, M. E. Weber, G. Kuhn, M. Prange, V. Varma, and M. Schulz (in review): Decadal- and millennial scale oscillations in the Weddell Sea during the Last Glacial Maximum. *Quaternary Science Reviews*.

D. Sprenk conducted the varve counting and varve thickness variation for PS1599, PS1789, and PS1791. Varve counting error estimation was accomplished by D. Sprenk and M. E. Weber. D. Sprenk also did all spectral analysis presented in the paper. M. Schulz, M. Prange, and V. Varma conducted the atmosphere-ocean model simulations and their interpretations. D. Sprenk wrote the text with contributions from M. E. Weber and G. Kuhn. Overall D. Sprenk's contribution to the paper was 70 %.

D. Sprenk, M. E. Weber, G. Kuhn, V. Wennrich, T. Hartmann, and K. Seelos (in review): Seasonal changes of glacial polynya activity inferred from Weddell Sea varves. *Climate of the Past Discussions Special Issue: The Past: A Compass for Future Earth - PAGES Young Scientists Meeting 2013*.

D. Sprenk did the core description and sampling of PS1795. Sediment-physical measurements were done at Alfred Wegener Institute Helmholtz-Centre for Polar and Marine Research in Bremerhaven in Bremerhaven supervised by G. Kuhn. High-Resolution XRF-data and radiographs were measured by V. Wennrich at the University of Cologne. K. Seelos did the RADIUS tool measurements. D. Sprenk and diploma student T. Hartmann did the sieving of the coarse size fraction. D. Sprenk collected foraminifera for AMS 14C measurements and produced the age-depth model. D. Sprenk counted ice-rafted debris and partly prepared the thin sections. D. Sprenk also analysed and counted varves. D. Sprenk wrote the manuscript with contributions from M. E. Weber and G. Kuhn. D. Sprenk contributed about 80 % to the manuscript.

D. Sprenk, M. E. Weber, G. Kuhn, P. Rosén, M. Frank, M. Molina-Kescher, V. Liebetrau, and H.-G. Röhlting (2013): Southern Ocean bioproductivity during the last glacial cycle - new detection method and decadal-scale insight from the Scotia Sea. *Antarctic Palaeoenvironments and Earth-Surface Processes*. Geological Society of London, Special Publication series, volume 381.

D. Sprenk conducted all sample preparations for FTIRS measurements and assisted the measurements at the Umeå University in Sweden. P. Rosén did the statistical evaluation of the FTIRS data. The 230Th normalization was done by M. Frank, M. Molina-Kescher, and V. Liebetrau. D. Sprenk wrote the text with contributions from M. E. Weber, P. Rosén, M. Frank, and G. Kuhn. Overall D. Sprenk contributed 80 % to the paper.

M. E. Weber, G. Kuhn, D. Sprenk, C. Rolf, C. Ohlwein, and W. Ricken (2012): Dust transport from Patagonia to Antarctica – a new stratigraphic approach from the Scotia Sea and its

implications for the last glacial cycle. *Quaternary Science Reviews*, 36, 177-188, doi: 10.1016/j.quascirev.2012.01.016.

D. Sprenk conducted the correlation of magnetic susceptibility from MD07-3133 and MD07-3134 with the EDML dust record. D Sprenk also helped establishing high-resolution age-depth models for MD07-3133 and MD07-3134. D. Sprenk also produced the figures. M. E. Weber wrote the text with contributions from D. Sprenk, G. Kuhn, C. Rolf, C. Ohlwein, and W. Ricken. Overall D. Sprenk contributed about 35 % to the paper.

11 Erklärung

Ich versichere, dass ich die von mir vorgelegte Dissertation selbständig angefertigt, die benutzten Quellen und Hilfsmittel vollständig angegeben und die Stellen der Arbeit – einschließlich Tabellen, Karten, und Abbildungen –, die anderen Werken im Wortlaut oder dem Sinn nach entnommen sind, in jedem Einzelfall als Entlehnung kenntlich gemacht habe; dass diese Dissertation noch keiner anderen Fakultät oder Universität zur Prüfung vorgelegen hat; dass sie – abgesehen von unten angegebenen Teilpublikationen – noch nicht veröffentlicht worden ist, sowie, dass ich eine solche Veröffentlichung vor Abschluss des Promotionsverfahrens nicht vornehmen werde. Die Bestimmungen der Promotionsordnung sind mir bekannt. Die von mir vorgelegte Dissertation ist von PD Dr. Michael E. Weber betreut worden.

Nachfolgend genannte Teilpublikationen liegen vor:

D. Sprenk, M. E. Weber, G. Kuhn, M. Prange, V. Varma, and M. Schulz (in review): Decadal- and millennial scale oscillations in the Weddell Sea during the Last Glacial Maximum. *Quaternary Science Reviews*.

D. Sprenk, M. E. Weber, G. Kuhn, V. Wennrich, T. Hartmann, and K. Seelos (in review): Seasonal changes in glacial polynya activity inferred from Weddell Sea varves. *Climate of the Past Discussions Special Issue: The Past: A Compass for Future Earth - PAGES Young Scientists Meeting 2013*.

D. Sprenk, M. E. Weber, G. Kuhn, P. Rosén, M. Frank, M. Molina-Kescher, V. Liebetrau, and H.-G. Röhlhling (2013): Southern Ocean bioproductivity during the last glacial cycle - new detection method and decadal-scale insight from the Scotia Sea. *Antarctic Palaeoenvironments and Earth-Surface Processes*. Geological Society of London, Special Publication series, volume 381.

M. E. Weber, G. Kuhn, D. Sprenk, C. Rolf, C. Ohlwein, and W. Ricken (2012): Dust transport from Patagonia to Antarctica – a new stratigraphic approach from the Scotia Sea and its implications for the last glacial cycle. *Quaternary Science Reviews*, 36, 177-188

Köln, den 28.10.2013

Daniela Sprenk

12 Curriculum Vitae

Dipl.-Geol. Daniela Sprenk

Work Experience

- 09.2010 – 08.2013** *Research assistant at the Institute of Geology at the University of Cologne: interpreted sediment-physical data, core chronologies and correlations, analysed sediment varves, spectral analysis, reconstructed palaeoclimate, wrote scientific articles, attended international conferences, supervised diploma student*
- 05.2011** Prepared sediment samples for Fourier-transform Infrared Spectroscopy (FTIRS) measurements at the University of Umea in Sweden
- 04.2011** Opened, described, and sampled sediment cores at the laboratory at the Alfred Wegener Institute for Polar and Marine Research, Bremerhaven
- 01. – 03.2011** *Participated in the scientific cruise JR244 with British Antarctic Survey (BAS) to the Southern Weddell Sea and the South Orkney continental shelf on RRS James Clark Ross: deep-sea sediment core site survey, collected multibeam bathymetric and TOPAS sub-bottom acoustic profiler data; assisted drilling gravity and box cores; opened/described and sampled sediment cores; measured magnetic susceptibility*
- 01.2011** Personal Safety Techniques Course at Warsash Maritime Academy
- 04.2009 – 06.2010** *Student research assistant at the department of Sedimentology at the University of Cologne: collected foraminifera shells for AMS ¹⁴C dating, assisted operating the Multi-Sensor Core Logger, produced scientific figures using Adobe Illustrator and Photoshop, counted ice-rafted debris*

- 06. – 07.2009** Four weeks work experience (at the geochemical laboratory) at Alfred Wegener Institute for Polar and Marine Research, Bremerhaven: analysed grain-size distribution, leached biogenic opal
- 07. – 08.2008** Four weeks work experience at the Messel Pit (Senckenbergische Naturforschende Gesellschaft) near Darmstadt: splitted shales to reveal Eocene fossils
- 04.2006 – 03-2009** *Student assistant in the industrial sales department at Krüger GmbH in Bergisch Gladbach: e.g. wrote letters/invoices to customers, managed incoming orders using SAP software, filing of records*
- 2004 and 2005** Four and two weeks long student holiday job at the Federal Highway Research Institute in Bergisch Gladbach
- 2001** Two weeks work experience at Acorn Veterinary Centres in Birmingham (UK)

Scholarships

- 03.2013** GESEP School 2013 “Basics of Drilling Technology in Continental and Marine Earth Science, Freiberg (German Science Foundation scholarship)
- 02.2013** PAGES Young & Open Science Meeting in Goa (PAGES scholarship)
- 07.2012** Participated in the Urbino Summer School in Paleoclimate 2012 (ECORD and ESF Scholarships awardee): focus on climate dynamics, long-term carbon cycling, paleoceanography, reconstructing and modelling of past climates

Education

- 09.2010 – present** *PhD study at the University of Cologne: Palaeoclimate and ice-sheet dynamics in the Southern Ocean deduced from Scotia and Weddell Sea sediment cores*

- 2005 – 2010** *Study of Geology/Palaeontology at the University of Cologne:*
Geologie Diplom (degree: 1.71; equivalent to M.Sc. in Geology)
in 08.2010 with Diploma thesis on the reconstruction of Scotia
Sea dust input during the Last Glacial
Geologie Vordiplom (Pre-Diploma in Geology) in 12.2007:
degree: 1,83
- 1996 – 2005** *Otto-Hahn-Gymnasium (equivalent to Grammar School) in
Bergisch Gladbach with mathematical/natural scientific focus:*
Allgemeine Hochschulreife (equivalent to A level) in 06.2005:
degree: 2.8

Further skills and personal details

- Computer skills** Very good knowledge of Microsoft Office (Word, Excel,
PowerPoint), Mac OS X, Adobe Illustrator and Photoshop,
Origin, Surfer, AnalySeries, PanPlot, and ImageJ
- Languages** German: native speaker
English: Excellent conversational and written English
French and Spanish: basic knowledge
- Interests** running, playing the piano, reading, travelling, scuba diving,
playing board games with family and friends

Publications

1. Sprenk, D., Weber, M. E., Kuhn, G., Rosén, P., Frank, M., Molina-Kescher, M., Liebetrau, V., and Röhling, H.-G. (2013): Southern Ocean bioproductivity during the last glacial cycle - new detection method and decadal-scale insight from the Scotia Sea. Antarctic Palaeoenvironments and Earth-Surface Processes. Geological Society, London, Special Publications, 381. doi: 10.1144/SP381.17
2. Weber, M. E., Kuhn, G., Sprenk, D., Rolf, C., Ohlwein, C., and Ricken, W. (2012): Dust transport from Patagonia to Antarctica – a new stratigraphic approach from the Scotia Sea and its implications for the last glacial cycle. Quaternary Science Reviews, 36, 177-188, doi: 10.1016/j.quascirev.2012.01.016.

3. Sprenk, D., Weber, M. E., Kuhn, G., Prange, M., Varma, V., and Schulz, M. (in review): Decadal- and millennial-scale oscillations in the Weddell Sea during the Last Glacial Maximum. *Quaternary Science Reviews*.
4. Sprenk, D., Weber, M. E., Kuhn, G., Wennrich, V., Hartmann, T., and Seelos, K., (in review): Seasonal changes in glacial polynya activity inferred from Weddell Sea varves. *Climate of the Past Discussions Special Issue: The Past: A Compass for Future Earth - PAGES Young Scientists Meeting 2013*.
5. Weber, M. E., Clark, P. U., Kuhn, G., Timmermann, A., Sprenk, D., Gladstone, R., Zhang, X., Lohmann, G., Menviel, L., Chikamoto, M., and Friedrich, T. (in review): Millennial-scale variability in Antarctic ice-sheet discharge throughout the last deglaciation. *Nature*.

Conference abstracts

1. **Sprenk, D.**, Weber, M. E., and Kuhn, G. (2013): Last Glacial Maximum decadal- to millennial-scale ice-sheet fluctuations recorded in southeastern Weddell Sea sediment. – Joint ICDP/IODP colloquium, Freiberg.
2. Weber, M. E., Kuhn, G., Clark, P. U., Timmermann, A., Lohmann, G., Gladstone, R., and Sprenk, D. (2013): Antarctic Ice Sheet deglaciation revised – the dynamic record of Iceberg Alley. – Joint ICDP/IODP colloquium, Freiberg.
3. **Sprenk, D.**, Weber, M. E., and Kuhn, G. (2013): Decadal-to millennial-scale ice-sheet oscillations in southeastern Weddell Sea during the Last Glacial Maximum. – 25th International Symposium on Polar Research, abstract volume, Hamburg.
4. Weber, M. E., Kuhn, G., Clark, P. U., Timmermann, A., Lohmann, G., Gladstone, R., and **Sprenk, D.** (2013): Iceberg Alley – Antarctic gateway to lower latitudes. – 25th International Symposium on Polar Research, abstract volume, Hamburg.
5. Weber, M. E., Clark, P. U., Gladstone, R., Timmermann, A., Lohmann, G., Kuhn, G., and **Sprenk, D.** (2013): Dynamic Antarctic ice-sheet behavior during the last deglaciation – implications to past and future sea-level rise. – Davos Atmosphere and Cryosphere Assembly DACA-13, Davos
6. Weber, M. E., Kuhn, G., Clark, P. U., Timmermann, A., Lohmann, G., **Sprenk, D.**, and Gladstone, R. (2013): The Scotia Sea Iceberg Alley - Antarctic Gateway to lower latitudes and its history of ice-sheet instability. – Scotia Arc Symposium, Granada.
7. Weber, M. E., Clark, P. U., Timmermann, A., Lohmann, G., Kuhn, G., Sprenk, D., and Gladstone, R. (2013): Dynamic Antarctic ice-sheet response to deglacial meltwater pulses. – European Geoscience Union, General Assembly, Vienna.
8. Sprenk, D., Weber, M. E., and Kuhn, G. (2013): New Insights on Last Glacial Ice-sheet dynamics deduced from Weddell Sea sediment. – PAGES Young & Open Science Meeting, Goa.

9. Weber, M. E., Clark, P. U., Gladstone, R., Timmermann, A., Lohmann, G., Mitrovica, Kuhn, G., and Sprenk, D. (2013): Antarctic deglaciation rewritten - highly dynamic ice-sheet disintegration during meltwater pulses and contribution to sea-level rise. – PAGES Open Science Meeting, Goa.
10. Sprenk, D., Weber, M. E., and Kuhn, G. (2012): Glacial ice-sheet dynamics and retreat deduced from southeastern Weddell Sea sediment. – SPP 1158 Antarctica workshop, Jena.
11. Sprenk, D., Weber, M. E., Kuhn, G., Rosén, P., and Röhling, H.-G. (2012): Bioproductivity in the Southern Ocean since the last interglacial - new high-resolution biogenic opal flux records from the Scotia Sea. – European Geosciences Union, General Assembly, Vienna.
12. Weber, M. E., Clark, P. U., Gladstone, R., Timmermann, A., Lohmann, G., Kuhn, G., and Sprenk, D. (2012): Dynamic Antarctic ice-sheet disintegration during the last deglaciation – contribution to meltwater pulse 1a. – AGU Fall Meeting, EOS, Transactions, AGU, San Francisco.
13. Weber, M. E., Kuhn, G., Clark, P. U., and Sprenk, D. (2012): Antarctic contribution to meltwater pulses during the last deglaciation. – XXXII Scientific Committee on Antarctic Research (SCAR) and Open Science Conference, Portland.
14. Weber, M. E., Clark, P. U., Ricken, W., Mitrovica, J. X., Hostetler, S. W., Sprenk, D., and Kuhn, G. (2012): Bipolar synchronicity for the termination of the Last Glacial Maximum. – Joint ICDP/IODP colloquium, Kiel.
15. Weber, M. E., Clark, P. U., Kuhn, G., Ricken, W., and Sprenk, D. (2011): Interhemispheric Ice-Sheet Synchronicity During the Last Glacial Maximum. – AGU Fall Meeting, EOS, Transactions, AGU, San Francisco.
16. Sprenk, D., Weber, M. E., and Kuhn, G. (2011): Glacial ice-sheet dynamics and retreat deduced from southeastern Weddell Sea sediment. – SPP 1158 Antarctica workshop, Bad Münster am Stein.
17. Sprenk, D., Weber, M. E., Kuhn, G., and Rosén, P. (2011): Glacial and Deglacial Trends in the Atlantic Sector of Antarctica during the last 25 ka. - XVIII. INQUA Congress, Bern.
18. Weber, M. E., Kuhn, G., Clark, P. U., and Sprenk, D. (2011): Late Quaternary paleoclimate and paleoenvironmental change from high latitude Southern Hemisphere regions including Antarctica. - XVIII. INQUA Congress, Bern.
19. Weber, M. E., Kuhn, G., Clark, P. U., and Sprenk, D. (2011): Antarctic Ice Sheet Retreat since the LGM - relation to Southern Hemisphere temperature and global sea-level rise. Joint ICDP/IODP colloquium, abstract volume. Münster.
20. Weber, M. E., Kuhn, G., Clark, P. U., and Sprenk, D. (2011): Southern Hemisphere temperature and global sea-level rise since the Last Glacial Maximum. - Annual meeting of the Working Group for Polar Regions abstract volume. Bremen.
21. Weber, M. E., Kuhn, G., Clark, P. U., and Sprenk, D. (2011): Antarctic ice-sheet retreat and sea-level rise during the last deglaciation. European Geoscience Union, General Assembly, Vienna.

22. Larter, R. D., Graham, A. G. C., Hillenbrand, C.-D., Smith, J. A. and JR244 Scientific Party (2011): Late Quaternary grounded ice extent in the Filchner Trough, Weddell Sea: new marine evidence. - 11th International Symposium on Antarctic Earth Sciences, Edinburgh.
23. Sprenk, D., Weber, M. E., and Kuhn, G. (2010): Dust Input to the Scotia Sea – Chronostratigraphic Implications. Sediment 2010, 25th Sediment meeting, abstract volume, Potsdam.
24. Weber, M. E., Kuhn, G., Clark, P., and Sprenk, D. (2010): New insights into Antarctic ice-sheet retreat during the last sea-level rise. – AGU Fall Meeting, EOS, Transactions, AGU, San Francisco.
25. Weber, M. E., Sprenk, D., and Kuhn, G. (2010): Dust transport from Patagonia to Antarctica – a perspective from the Scotia Sea for the last glacial cycle. – Joint ICDP/IODP colloquium, abstract volume, Frankfurt.
26. Weber, M. E., Sprenk, D., Kuhn, G., and Ricken, W. (2010): Dust record from the Scotia Sea during the last glacial cycle. – European Geoscience Union, General Assembly, Vienna.
27. Weber, M. E., Clark, P., Kuhn, G., and Sprenk, D. (2010): Antarctic ice-sheet retreat during the last sea-level rise – new insights from the Weddell Sea and the Scotia Sea. – 10th International Conference on Paleoceanography (ICP X), abstract volume, San Diego.